CLIMATOLOGY OF LAKE ONTARIO AND LAKE ERIE SURFACE HEAT EXCHANGES 1953-1983

by

A.M. Sawchuk[1] and W.M. Schertzer[2]

NWRI Contribution No. 88-37

[1] Department of Geography
University of Toronto at Scarborough
Scarborough, Ontario M1C 1A4

[2] Project Leader: NWRI Climate Studies
National Water Research Institute
Canada Centre for Inland Waters
Burlington, Ontario L7R 4A6

EXECUTIVE SUMMARY

As part of the NWRI commitment to the Canada Climate Program a major research effort was undertaken to examine the long-term heat balance for the Lower Great Lakes. Prior to this initiative, detailed investigations on Lake Ontario were limited to the IFYGL program and on Lake Erie previous results were reported primarily as monthly means. In this investigation, a new model of the surface heat flux is developed and verified with IFYGL data. The verified model is applied over a 30-year data base for each lake. The model is used to simulate the daily surface heat flux components and time series are developed from which annual and interannual variability of the hydrometeorological and limnological parameters are assessed. The results form a reliable baseline of the climatology of Lake Erie and Lake Ontario from which climate change scenarios can be initiated.

MANAGEMENT PERSPECTIVE

This study is concerned with establishing the climatology of surface heat excahnges on Lake Erie and Lake Ontario for the NWRI Climate Studies on the Lower Great Lakes. Accurate representation of the air-water interactions at the water surface is essential for simulation of the complex lake responses to climate change. The present verified model is capable of producing good correspondence between calculations and observations in both Lake Ontario and Lake Erie largely due to improvements in modelling of the solar flux. Additional development is required for climate applications in the latent heat flux and atmospheric longwave sub-models to accommodate the influence of atmospheric 'green-house' gases.

This investigation has produced an enormous hydrometeorological data base for Lake Ontario and Lake Erie spanning the period 1953 to 1983. This data base of hourly and daily parameters will be invaluable for future long-term studies on these lakes.

ABSTRACT

A new model for evaluating radiation and surface energy balance components for Lake Ontario and Lake Erie is described and illustrated with calculations for the period 1953-1983. Radiation and turbulent fluxes are evaluated directly while the surface heat flux is determined as a residual from the surface energy balance equation. The model performs calculations on a daily basis, however, results may be combined into weekly, or longer, time periods.

The model contains many improvements on previous energy balance studies. Shortwave radiation receipts are evaluated from a true radiative transfer model that treats multiple scattering effects explicitly. Estimates of incoming longwave radiation incorporate effects of aerosols and clouds. Root mean square errors for differences between estimates and measured net radiation over Lake Ontario during the International Field Year for the Great Lakes (IFYGL) are approximately 3.2 MJ m^{-2} day^{-1}, an improvement of approximately 25 percent over previous studies.

Estimates of overlake meteorological data incorporate effects of atmospheric stability, while evaporation estimates are derived from a mass transfer formulation that includes a dependency on wind speed and atmospheric stability. Comparison of evaporation estimates with weekly and monthly values tabulated by the IFYGL Energy Balance Panel shows excellent agreement.

The model includes a method for estimating surface water temperatures based on lake heat content. This relationship represents a strong negative feedback mechanism and provides a constraint that prevents numerical instabilities from amplifying. The model includes a simple relationship based on cumulative freezing degree days for estimating ice concentrations. Comparison of predicted ice concentrations shows excellent agreement with values tabulated by Assel *et.al.* (1983) for both Lake Ontario and Lake Erie. Extensive comparisons with measured data and previous estimates suggest the model can simulate daily radiation and surface energy

balance components accurately and efficiently.

The model was applied to estimate daily surface radiation and energy balance components for Lake Erie and Lake Ontario for the period 1953-1983. Comparison of estimated lake heat content shows good agreement with heat contents determined from bathymetric measurements. Calculations demonstrate that, on an annual basis, surface heat flux is balanced over periods ranging from three to six years for Lake Erie while Lake Ontario appears to be gaining heat over the 31 year period. The gain, however, is small and within the uncertainty of the heat content measurements. These results may be compared to air temperature climatology at shoreline meteorological stations which indicate decreasing air temperatures from 1953 to the late 1970's with a small increase since that time.

The results contained herein describe NWRI Climate Studies conducted from 1984 to 1987 with respect to modelling the air-water interactions of surface heat exchanges. This final report synthesizes results from heat modelling conducted in DSS Contracts KW405-4-1340, KW405-5-0531, and KW405-50532.

RÉSUMÉ POUR LA DIRECTION

Dans le cadre de la participation de l'INRE au Programme climatologique canadien, d'importantes recherches ont été entreprises pour étudier le bilan thermique à long terme des Grands lacs inférieurs. Avant cette initiative, les études détaillées sur le lac Ontario se limitaient au programme IFYGL, et les résultats antérieurs relatifs au lac Érié ont été principalement communiqués sous forme de moyennes mensuelles. Au cours des présentes recherches, un nouveau modèle de flux thermique de surface a été mis au point et vérifié à l'aide des données IFYGL. Le modèle vérifié est appliqué à chaque lac selon une base de données s'étalant sur 30 ans. Le modèle simule les constituants journaliers du flux thermique de surface; des séries temporelles sont élaborées à partir desquelles on évalue la variabilité annuelle et interannuelle des paramètres hydrométéorologiques et limnologiques. Les résultats donnent une ligne de base fiable de la climatologie du lac Érié et du lac Ontario, à partir de laquelle des scénarios de variation climatologique peuvent être préparés.

PERSPECTIVES DE GESTION

La présente étude vise à caractériser la climatologie relative aux échanges thermiques en surface sur le lac Érié et le lac Ontario, dans le cadre des Études climatologiques INRE sur les Grands lacs inférieurs. Une représentation exacte des interactions air-eau à la surface de l'eau est primordiale pour la simulation des réactions complexes du lac aux variations climatiques. L'actuel modèle vérifié permet une bonne correspondance entre les calculs et les observations aussi bien pour le lac Ontario que pour le lac Érié, grâce surtout à l'amélioration du modèle de flux solaire. D'autres travaux sont nécessaires pour les applications climatologiques aux sous-modèles de flux de chaleur totale et de rayonnement atmosphérique de grande longueur d'onde, de façon à pouvoir tenir compte de l'influence des gaz atmosphériques à effet de "serre".

Ces recherches ont permis d'obtenir une énorme base de données hydrométéréologiques pour le lac Ontario et le lac Érié, couvrant la période de 1953 à 1983. Les paramètres horaires et quotidiens de la base de données seront précieux pour les études futures à long terme de ces lacs.

RÉSUMÉ

Un nouveau modèle pour l'évaluation des constituants du bilan énergétique de surface et radiatif dans le lac Ontario et le lac Érié est décrit et illustré, avec les calculs pour la période 1953-1983. Les flux de rayonnement et de turbulence sont évalués directement, alors que le flux thermique de surface est déterminé sous forme de fraction résiduelle à partir de l'équation du bilan énergétique de surface. Le modèle effectue les calculs selon une base quotidienne, mais les résultats peuvent être combinés en périodes hebdomadaires ou plus longues.

Le modèle comporte beaucoup d'améliorations si on le compare aux études antérieures du bilan énergétique. L'apport de rayonnement à onde courte est évalué à partir d'un modèle vrai de transfert radiatif, qui traite explicitement les effets de dispersion multiple. Les estimations du rayonnement incident de grande longueur d'onde incorporent les effets des aérosols et des nuages. Les erreurs de moyenne quadratique pour les différences entre les estimations et le rayonnement net mesuré au-dessus du lac Ontario pendant l'Année internationale d'étude des Grands lacs (IFYGL) sont de l'ordre de 3.2 $MJm^{-2}jour^{-1}$, soit une amélioration d'environ 25 pour cent par rapport aux études précédentes.

Les estimations des données météorologiques au-dessus des lacs tiennent compte des effets de la stabilité atmosphérique, alors que les estimations relatives à l'évaporation sont dérivées d'une formulation de transfert massique, qui inclut une dépendance de la vitesse du vent et de la stabilité atmosphérique. Une comparaison des estimations d'évaporation avec les valeurs hebdomadaires et mensuelles du tableau de bilan énergétique IFYGL révèlent une excellente corrélation.

Le modèle comprend une méthode permettant d'évaluer la température de l'eau de surface d'après la chaleur totale du lac. Cette relation représente un mécanisme de rétro-action fortement négative, et donne une contrainte qui empêche l'amplification des instabilités numériques. Pour l'évaluation des concentrations de glace, le modèle inclut aussi une relation simple, fondée sur le nombre cumulatif de degrés-jours de gel. Une comparaison des concentrations de glace prévues montre une excellente corrélation avec les valeurs de tabulation d'Assel et al (1983) pour le lac Ontario et le lac Érié. Une comparaison poussée avec des valeurs mesurées et des estimations antérieures montre que le modèle peut simuler exactement et efficacement le rayonnement quotidien et le bilan énergétique de surface.

Le modèle a été utilisé pour évaluer le bilan énergétique et le rayonnement de surface quotidiens du lac Erié et du lac Ontario pendant la période 1953-1983. Une étude comparative montre qu'il existe une bonne corrélation entre la chaleur totale estimative des lacs, et la chaleur totale déterminée grâce à des mesures bathymétriques. Les calculs montrent qu'annuellement le flux thermique de surface s'équilibre sur une période variant de trois à six ans pour le lac Érié, alors que le lac Ontario semble faire un gain de chaleur pendant la période de 31 ans. Mais, ce gain est faible, et il se situe dans les limites d'incertitude des mesures de la chaleur totale. Les résultats obtenus peuvent se comparer à la climatologie des températures de l'air aux stations météorologiques littorales, qui révèle une diminution de ces températures de 1953 jusqu'à la fin des années 70, avec une faible augmentation depuis cette époque.

Les résultats présentés ici décrivent les études climatologiques INRE, effectuées de 1984 à 1987, et plus précisément la modélisation des interactions air-eau au niveau des échanges thermiques de surface. Ce rapport final présente la synthèse des résultats de la modélisation thermique, effectuée en vertu des contrats MAS KW405-4-1340, KW405-5-0531 et KW405-50532.

ACKNOWLEDGEMENTS

The authors would like to express their appreciation to the following people: Mike Fellowes, for assistance in developing the meteorological data base; Craig McCrimmon, for providing ice extent data for Lake Ontario; the programming assistants at the Canada Centre for Inland Waters; and Alan Rosselet, University of Toronto at Scarborough.

TABLE OF CONTENTS

ABSTRACT ii

ACKNOWLEDGEMENTS iv

TABLE OF CONTENTS v

LIST OF ILLUSTRATIONS viii

LIST OF TABLES xi

1 INTRODUCTION 1

Study Objectives 2

2 MODELLING THE ENERGY BALANCE AT A LAKE SURFACE 4

2.1 Net Radiation 4

2.1.1 Shortwave Radiation 5

2.1.1.1 *Delta–D_2* Model for a Homogeneous Atmosphere 6

2.1.1.2 Application of the Delta-*M* Method 12

2.1.1.3 The Multi-Layer Component 13

2.1.1.4 The Multi-Spectral Component 18

2.1.2 Longwave Radiation 21

2.1.2.1 Clear-Sky Formulation 22

2.1.2.2 Effects of Clouds and Aerosols 25

2.2 Turbulent (Latent and Sensible Heat) Fluxes 28

2.3 Ice Heat Flux 31

2.4 Minor Energy Fluxes 34

3 MODEL IMPLEMENTATION 35

3.1 Meteorological Data Base 35

3.2 Model Atmosphere 39

3.2.1 Vertical Profiles of Temperature and Humidity 39

3.2.2 Optical Properties of Clouds and Aerosols 42
3.3 *Delta–D*$_2$ for Daily Totals of Shortwave Radiation 44
3.4 Boundary Conditions 47
3.4.1 Incident Top-of-the-Atmosphere Radiation 47
3.4.2 Surface Water Temperature 49

4 MODEL VERIFICATION TESTS 57
4.1 Overlake Meteorological Data 58
4.2 Surface Water Temperature 65
4.3 Surface Radiation Fluxes 68
4.3.1 Incoming Shortwave Radiation 68
4.3.2 Incoming Longwave Radiation 74
4.3.3 Net Radiation 80
4.4 Turbulent Fluxes 83
4.5 Ice Heat Flux 92
4.6 Surface Heat Flux and Lake Heat Content 92

5 ENERGY BALANCE CLIMATOLOGY OF THE LOWER GREAT LAKES 1953-1983 97
5.1 Energy Balance Components 97
5.2 Lake Heat Content 116
5.3 Long-Term Variations 119
5.4 Comparison with Previous Studies 133

6 SUMMARY AND CONCLUSIONS 145

APPENDIX A - List of Symbols 149
APPENDIX B - Spectral Data for *Delta–D*$_2$ Model 155
APPENDIX C - Coefficients for Estimating Saturation Vapour Pressure 156
APPENDIX D - Optical Properties of Clouds and Aerosols 157

APPENDIX E - Coefficients for Estimating Astronomical Parameters 159
APPENDIX F - Coefficients for Estimating Surface Water Temperature 160
APPENDIX G - Mean Daily Surface Water Temperature 162
APPENDIX H - Ice Concentration Data 163
APPENDIX I - Minor Energy Balance Terms 164
REFERENCES 165

LIST OF ILLUSTRATIONS

Figure	Title	Page
2.1	Definition of the Scattering Angle.	8
2.2	The Multi-Layer Atmosphere.	14
3.1	Meteorological Stations for Lake Ontario and Lake Erie.	36
3.2	Comparison of Paired Surface Water Temperatures (Ship and *ART*) for Lake Ontario, 1966-1983.	50
3.3	Relationship between Surface Water Temperature T_w and Total Lake Heat Content Q for Lake Ontario, Lake Erie, and Lake Erie Basins.	52
3.4	Mean Daily Surface Water Temperatures for Lake Ontario, Lake Erie, and Basins of Lake Erie, 1966-1983.	55
4.1	Comparison of Estimated Three-Day Mean Air Temperatures with Measured Values over Lake Ontario, 1 May to 30 November, 1972.	59
4.2	Comparison of Estimated Monthly Mean Air Temperature (a), Dew Point Temperature (b), Lake-Averaged Wind Speeds (c), and Central Basin Wind Speeds (d) over Lake Ontario, May, 1972, - March, 1973.	61
4.3	Comparison of Estimated Daily Overlake Total Cloudiness with Values Reported by Atwater and Ball (1974) over Lake Ontario during IFYGL.	64
4.4	Comparison of Estimated Daily Surface Water Temperature with Measured Values for Lake Ontario during IFYGL.	67
4.5	Deviations of Estimates of Daily Incoming Shortwave Radiation from Mean Measured Values over Lake Ontario, 1 May, 1972, to 31 March, 1973.	70
4.6	Frequency Distribution of Absolute Errors of Estimates of Daily Incoming Shortwave Radiation from Mean Measured Values (a) and Range of Daily Measured Values (b).	71
4.7	Comparison of Estimates of Daily Incoming Shortwave Radiation as a Function of Cloudiness over Lake Ontario, 1 May, 1972, to 31 March, 1973.	72
4.8	Comparison of Root Mean Square Errors and *D*-statistics of Estimates of Incoming Shortwave Radiation over Lake Ontario, 1 May, 1972, to 31 March, 1973, as a Function of Averaging Period.	73
4.9	Deviations of Estimates of Daily Incoming Longwave Radiation from Mean Measured Values over Lake Ontario, 1 May, 1972, to 31 March, 1973.	76

4.10	Frequency Distribution of Absolute Errors of Estimates of Daily Incoming Longwave Radiation from Mean Measured Values (a) and Range of Daily Measured Values (b).	77
4.11	Comparison of Estimates of Daily Incoming Longwave Radiation as a Function of Cloudiness over Lake Ontario, 1 May, 1972, to 31 March, 1973.	78
4.12	Comparison of Root Mean Square Errors and *D*-statistics of Estimates of Incoming Longwave Radiation over Lake Ontario, 1 May, 1972, to 31 March,	79
4.13	Deviations of Estimates of Daily Net Radiation from Mean Measured Values over Lake Ontario, 1 May, 1972, to 31 March, 1973.	81
4.14	Comparison of Root Mean Square Errors and *D*-statistics of Estimates of Net Radiation over Lake Ontario, 1 May, 1972, to 31 March, 1973, as a Function of Averaging Period.	82
4.15	Comparison of Estimates of Daily-Averaged Bowen Ratio over Lake Ontario, 1 May to 16 December, 1972.	84
4.16	Comparison of Estimates of Weekly-Averaged Sensible Heat and Latent Heat Fluxes with Values from Objective Analyses over Lake Ontario, 1 May to 26 October, 1972.	85
4.17	Comparison of Estimates of Weekly Evaporation Totals with Values Tabulated by the IFYGL Energy Balance Panel for Lake Ontario, 4 May, 1972, to 28 March, 1973.	87
4.18	Comparison of Estimated Weekly Evaporation Totals for Lake Ontario, 7 May, 1972, - 30 March, 1973, with Estimates from Phillips (1978) and Quinn (1978).	89
4.19	Comparison of Estimated Monthly Evaporation with Values Recommended by the IFYGL Energy Balance Panel for Lake Ontario, May, 1972, to March, 1973.	90
4.20	Comparison of Estimates of Monthly Evaporation with Values Recommended by the IFYGL Energy Balance Panel for Lake Ontario, May, 1972, to March, 1973.	91
4.21	Comparison of Estimates of Weekly-Averaged Ice Heat Flux with Values Tabulated by the IFYGL Energy Balance Panel for Lake Ontario, 1 November, 1972, - 26 March, 1973.	93
4.22	Comparison of Estimates of Weekly, Bi-weekly, and Monthly Average Surface Heat Fluxes with Values Interpolated from Heat Content Measurements for Lake Ontario, 3 May, 1972, - 28 March, 1973.	94
4.23	Comaprison of Estimates of Daily Lake Heat Contents with Measured Values for Lake Ontario, 1 May, 1972, - 31 March, 1973.	95

5.1	Maximum, Mean, and Minimum Five-Day Hydrometeorological Variables, Radiation, and Energy Balance Components for Lake Erie, 1953-1983.	98
5.2	Maximum, Mean, and Minimum Five-Day Hydrometeorological Variables, Radiation, and Energy Balance Components for Lake Ontario, 1953-1983.	105
5.3	Comparison of Mean Monthly Values for Selected Hydrometeorological Variables, Radiation, and Energy Balance Components for Lake Erie and Lake Ontario, 1953-1983.	112
5.4	Daily Heat Contents, Mean Daily Heat Contents, and Measured Heat Contents for Lake Erie, 1953-1983.	117
5.5	Annual Variation of Hydrometeorological Variables, Radiation, and Energy Balance Components for Lake Erie, 1953-1983.	121
5.6	Annual Variation of Hydrometeorological Variables, Radiation, and Energy Balance Components for Lake Ontario, 1953-1983.	123
5.7	Mean Five-Day Air Temperatures, Dew Point Temperatures, Surface Water Temperatures, Wind Speed, Cloudiness, Net Radiation, Latent, Sensible, and Surface Heat Flux, for Lake Erie, 1 June, 1983, - 31 October, 1983 and Corresponding Long-Term (1953-1983) Values.	128
5.8	Mean Five-Day Air Temperatures, Dew Point Temperatures, Surface Water Temperatures, Wind Speed, Cloudiness, Net Radiation, Latent, Sensible, and Surface Heat Flux, for Lake Erie, 1 November, 1982, - 30 April, 1983 and Corresponding Long-Term (1953-1983) Values.	129
5.9	Mean Five-Day Air Temperatures, Dew Point Temperatures, Surface Water Temperatures, Wind Speed, Cloudiness, Net Radiation, Latent, Sensible, and Surface Heat Flux, for Lake Erie, 1 June, 1972, - 30 September, 1972, and Corresponding Long-Term (1953-1983) Values.	132
5.10	Comparison of Monthly Evaporation Estimates from Present Study with Derecki's (1975) *MT*-II Approach for Lake Erie, 1953-1968.	135
5.11	Comparison of Monthly Evaporation Estimates from Present Study with Derecki's (1975) *MT*-I Approach for Lake Erie, 1953-1968.	136
5.12	Comparison of Monthly Evaporation Estimates from Present Study with Estimates from Yu and Brutsaert (1969) for Lake Ontario, 1953-1965.	140
5.13	Comparison of Mean Monthly Evaporation Estimates from the Present Study with Estimates from Derecki (1975) for Lake Erie, 1953-1968, (a) [*MT*-I] and (b) [*MT*-II], Yu and Brutsaert (1969) for Lake Ontario, 1953-1965, (c), and Schertzer (1987) for Lake Erie, 1967-1982, (d).	142

LIST OF TABLES

Table	Title	Page
3.1	Definition of Scaling Functions for Overlake Variables	37
3.2	Definition of Stability and Scaling Functions	38
3.3	Root Mean Square Errors of Differences between Predicted and Observed Surface Water Temperatures.	51
B.1	Band Limits, Incident Radiation, and Absorbers for the *Delta–D*$_2$ Model.	155
B.2	Spectral Weights and Absorption Coefficients for Water Vapour and Ozone in the *Delta–D*$_2$ Model.	155
C.1	Coefficients for Estimating Saturation Vapour Pressure.	156
D.1	Band-Average Values of Single Scattering Albedo and Asymmetry Factor for Clouds and Normalized Rayleigh Scattering Optical Depths.	157
D.2	Coefficients for Estimating Aerosol Emissivity at 11 μm as a Function of Relative Humidity.	157
D.3	Coefficients for Estimating Fraction of Planck Function at Window Wavelengths.	158
D.4	Coefficients for Estimating Asymmetry Factor at Infrared Wavelengths.	158
D.5	Monthly Values of Thickness of Aerosol Layer and Cloud Depths.	158
E.1	Coefficients for Estimating Astronomical Parameters Normalized Radius Vector, Equation of Time, and Solar Declination.	159
F.1	Coefficients for Estimating Surface Water Temperature from Total Lake Heat Content.	160
F.2	Coefficients for Estimating Total Lake Heat Content from Daily Mean Surface Water Temperature.	161
G.1	Coefficients for Estimating Mean Daily Surface Water Temperatures from Julian Day for Lake Ontario, Lake Erie, and Basins of Lake Erie.	162
H.1	Maximum, Mean, and Minimum Cumulative Freezing Degree Days and Corresponding Ice Concentrations for Selected Days of the Winter Season for Lake Ontario.	163
H.2	Maximum, Mean, and Minimum Cumulative Freezing Degree Days and Corresponding Ice Concentrations for Selected Days of the Winter Season for Lake Erie.	163

I.1 Average Daily Values of Minor Energy Balance Terms for Lake Ontario and Lake Erie. 164

1. INTRODUCTION

The exchange of energy across an air-water interface is a fundamental mechanism in the formation and decay of thermal stratification of a water body and in knowledge of how water bodies moderate climate. Modelling this exchange may be accomplished by evaluating components of the surface energy balance equation. Neglecting minor energy gains and losses, such as from chemical and biological sources, the energy balance equation at the lake surface may be given as (Lam et.al., 1983):

$$Q^* - Q_H - Q_{LE} - Q_t - Q_I - Q_M = 0 \qquad [1]$$

where Q^* is net radiation, Q_H is sensible heat flux, Q_{LE} is latent heat flux, Q_t is the surface heat flux, Q_I is ice heat flux, and Q_M represents minor heat flux terms such as exchanges resulting from inflow and outflow of water into the lake and from precipitation over the lake. Surface heat flux may then be evaluated as a residual term in eq.(1).

Evaluation of energy balance components for a large lake ideally requires measurement of individual components at representative locations at the lake surface. This is seldom possible except during specialized experiments such as the International Field Year for the Great Lakes (IFYGL). One must therefore model mean meteorological conditions at the lake surface by averaging meteorological data from adjacent shoreline stations. Computational techniques may then be applied to estimate radiation and energy balance components of eq.(1).

This approach was applied by Derecki (1975) for estimating monthly evaporation totals for Lake Erie (1950-1968) and, with some modifications, by Lam et.al. (1983) and Scherzter (1987) for Lake Erie (lakewide and individual basins) for 1967-1982. The winter months of November to March were excluded in the two latter studies. Such studies indicate the magnitude and variability of monthly energy balance components as well as some differences. It is difficult to determine,

however, whether these differences are due to differences in how radiation and energy balance components were parameterized , or to differences in time period for which computations were performed, or to some combination therein.

Few comparable long-term studies exist for Lake Ontario, although intensive measurements and calculations of energy balance components were performed during IFYGL from April, 1972 to March .1973 (Pinsak and Rodgers, 1981). Quinn and den Hartog (1983) compared latent and sensible heat fluxes evaluated from solving the energy balance components with other methods, such as estimates from the water balance equation and mass transfer models, with values recommended by the IFYGL Energy Balance Panel. These authors observed that evaporation estimates varied widely during the April to June period, but with only minor differences thereafter. These analyses indicate the potential sensitivity of some computational techniques during certain portions of the year, although specific causes remain to be identified.

It is also important to note that the energy balance comparisons performed with IFYGL data were based on an extensive data base comprised of detailed over-lake measurements. Such detailed measurements are not likely to be available on a routine basis. Thus, studies of the long-term behaviour of surface energy balance components will have to rely on modelling techniques that perform accurately for all times of the year and utilize crude, but routinely measured, meteorological data.

Objectives of the Study

This study has two major objectives. The first objective is to develop a model for evaluating daily values of surface radiation and energy balance components. Many of the models appearing in the literature (some of which are described in Section 2 and 3) contain empirical and site-specific parameterizations that render general application difficult. The thrust of the present modelling effort has been to replace empirical and site-specific formulations with physical models (where

possible) thus leading to a numerical algorithm with general application. Considerable effort has been expended in ensuring the algorithm is numerically stable, provides accurate flux estimates, requires little computer time, and performs in all environmental conditions. Sections 2 and 3 describe model development. Section 4 describes model performance.

The second objective is to apply the model to surface heat flux calculations for Lake Ontario and Lake Erie (lakewide and individual basins) for the period 1953 to 1983 to evaluate the magnitude and variability of surface energy balance components and to compare these estimates, where possible, with estimates from other long-term studies.

2. MODELLING THE ENERGY BALANCE AT A LAKE SURFACE

The model to evaluate energy balance components consists of component algorithms to estimate each term of eq.(1). This section describes the defining equations for each component. Section 3 describes how the model was implemented for calculations and the required data sources.

2.1. Net Radiation

Net radiation is a dominant term of the surface energy balance of large midlatitude lakes such as Ontario and Erie (Pinsak and Rodgers, 1981). It is also the most difficult term to model because it is strongly dependent on the state of the atmosphere and the underlying surface. It will seldom be possible to prescribe these conditions, especially cloudiness, precisely.

Models of net radiation are derived by partitioning net radiation Q^* into its components:

$$Q^* = (1-\alpha_S)K_D + L_D - L_r - \epsilon_S \sigma T_S^4 \qquad [2]$$

where α_S is the albedo for shortwave radiation, K_D is the incoming shortwave radiation at the ground surface, L_D is the incoming longwave radiation, L_r is the (upward) reflected longwave radiation, ϵ_S is the surface emissivity, σ is the Stefan-Boltzmann constant (5.67×10^{-8} $Wm^{-2}K^{-4}$), and T_S is the surface temperature (K). The first term on the right hand side of eq.(2) represents the net shortwave radiation ($0.3\,\mu m \leq \lambda \leq 4.0\,\mu m$). The remaining terms represent the net longwave radiation ($4.0\mu m \leq \lambda \leq 100\mu m$). K_D is the sum of a direct-beam component S and the downward diffuse flux D. Eq.(2) may then be restated as:

$$Q^* = (1-\alpha_S)(S+D) + L_D - L_r - \epsilon_S \sigma T_S^4 \qquad [3]$$

Evaluation of Q^* was based on a term-by-term evaluation of eq.(3).

2.1.1. Shortwave Radiation

Shortwave radiation-atmosphere interactions are complex: they include spectral absorption by atmospheric gases, multiple scattering by air molecules, aerosols, and clouds, and spectral reflection at the Earth's surface. A variety of models have been proposed to evaluate radiative fluxes incorporating these processes. They range in complexity from detailed numerical solutions of the radiative transfer equation (Bergstrom and Viskanta, 1972; Braslau and Dave, 1972; Liou, 1973, 1980) to simple statistical relationships based on one or two parameters such as relative sunshine duration (Angstrom, 1924, 1956; Mateer, 1955; Davies, 1965; Driedger and Catchpole, 1970) or cloudiness (Laevastu, 1960; Kimura and Stephenson, 1969).

Models based on detailed numerical solutions of the radiative transfer equation have the advantage of incorporating all processes affecting the radiative transfer process. The primary disadvantages are the requirements of: (i) extensive computing resources and (ii) detailed knowledge of vertical profiles of atmospheric composition. Radiative transfer algorithms have, for the most part, found application to theoretical studies of changes in the radiation balance of the Earth-Atmosphere system when it experiences a change in composition. Application to studies where radiation fluxes must be repeatedly evaluated remains largely untested.

Simple statistical models, on the other hand, require little computation but are generally suited to monthly time periods (Davies, 1980) and involve coefficients that are site-specific. Little confidence can be placed in these models for providing accurate flux estimates over short time periods such as a day.

The shortwave radiation model developed in this study (the *Delta–D_2* model) is a blend of these two extremes. It represents a modification of the more general *Delta – D_M* model of Sawchuk (1983) to evaluate daily totals of shortwave fluxes (direct-beam, upward and downward diffuse fluxes) at the ground surface accurately and efficiently. Multiple scattering by air molecules, clouds, and aerosols is accounted

for, as is spectral absorption by ozone and water vapour. The model includes partial cloudiness and provides a realistic treatment of boundary layer aerosols.

The *Delta* – D_2 algorithm represents a two-term discrete ordinate solution to the radiative transfer equation for diffuse shortwave radiation in a scattering and absorbing atmosphere. The heart of the *Delta* – D_2 algorithm is an algorithm termed the homogeneous *Delta* – D_2 for evaluating radiative fluxes in a homogeneous atmosphere. Evaluation of shortwave fluxes in a vertically inhomogeneous atmosphere containing multi-layer clouds and one or more aerosol species may be evaluated by resolving vertical profiles of atmospheric composition into layers that are homogeneous with respect to composition and into spectral intervals across which gaseous absorption is effectively constant. Spectrally integrated fluxes are then obtained by applying the homogeneous *Delta* – D_2 algorithm to each layer-spectral interval combination and suming the results.

2.1.1.1. The *Delta*–D_2 Model for a Homogeneous Atmosphere

Model description may be simplified by first considering radiative transfer in a homogeneous atmosphere where atmospheric composition is everywhere identical. The solar beam is assumed to be incident at the top of the atmosphere from an angle θ from the local vertical.

The radiative transfer equation defining the diffuse intensity in a homogeneous atmosphere is then (Chandrasekhar, 1950):

$$\mu \frac{\partial I(\tau,\mu,\phi)}{\partial \tau} = -I(\tau,\mu,\phi) + \frac{\tilde{\omega}_o}{4\pi} \int_0^{2\pi} \int_{-1}^{+1} p(\mu,\phi;\mu',\phi') I(\tau,\mu',\phi') d\mu' d\phi' \qquad [4]$$

$$+ \frac{\tilde{\omega}_o}{4\pi} p(\mu,\phi;\mu_o,\phi_o) \exp(-\tau/\mu_o)$$

where $I(\tau,\mu,\phi)$ is the diffuse intensity along direction (μ,ϕ) where $\mu = \cos\theta$ and ϕ is the azimuth angle, τ is the optical depth, $\tilde{\omega}_o$ is the single scattering albedo, and $p(\mu,\phi;\mu',\phi')$

is the scattering phase function describing the angular distribution of radiation scattered by an elemental volume of atmosphere. The optical depth, single scattering albedo, and scattering phase function are the optical properties of the atmosphere and are determined from, e.g. Mie theory, when the physical characteristics of the atmosphere, e.g. aerosol number density, complex index of refraction, are specified.

Physically, the first term on the right hand side of eq.(4) represents the attenuation due to scattering and absorption along direction (μ,ϕ). The second term accounts for the contribution of multiple scattering of photons into $I(\tau,\mu,\phi)$ from all directions (μ',ϕ') while the third term accounts for those photons scattered directly from the solar beam at direction (μ_o,ϕ_o). Equation (4) therefore describes the net gain in diffuse intensity along direction (μ,ϕ).

Equation (4) may be simplified for flux computations. First, the scattering phase function may be approximated as an M-term series of Legendre polynomials:

$$p(\mu,\phi;\mu',\phi') = \sum_{k=0}^{M} \omega_k P_k(\cos\psi_S) \qquad [5]$$

where $P_k(\cos\psi_S)$ is the Legendre polynomial of order k, ψ_S is the scattering angle (Fig. 2.1) between (μ,ϕ) and (μ',ϕ'), and ω_k are the phase function moments of $p(\mu,\phi;\mu',\phi')$ with respect to P_k.

Second, when the scattering phase function is approximated by eq.(5), $I(\tau,\mu,\phi)$ can be expanded as an M-term Fourier cosine series (Chandrasekhar, 1950):

$$I(\tau,\mu,\phi) \equiv \sum_{k=0}^{M} I_k(\tau,\mu,\phi)\cos[k(\phi'-\phi)] \qquad [6]$$

Only the I_o term of eq.(6) contributes to the flux. Substituting eqs.(5) and (6) into eq.(4), and integrating over azimuth yields the azimuthally-averaged radiative transfer equation for the diffuse intensity:

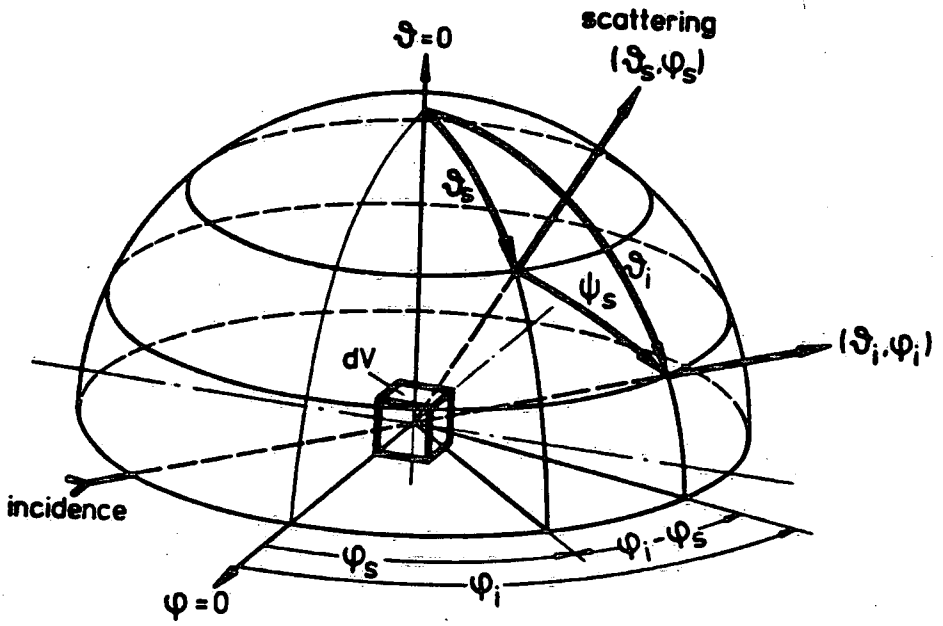

Figure 2.1 - Definition of the scattering angle (Raschke, 1978). Angles ϑ and φ denote zenith and azimuth angles, respectively, while subscripts *i* and *s* denote incident and scattering directions, respectively.

$$\mu\frac{\partial I(\tau,\mu)}{\partial\tau} = -I(\tau,\mu) + \frac{\tilde{\omega}_o}{2}\int_{-1}^{+1} I(\tau,\mu)\sum_{k=0}^{M-1}\omega_k P_k(\mu)P_k(\mu')d\mu' \qquad [7]$$

$$+\frac{\tilde{\omega}_o(\pi F_o)}{4\pi}\exp(-\tau/\mu_o)\sum_{k=0}^{M-1}\omega_k P_k(\mu)P_k(\mu_o)$$

where the subscript *o* has been omitted for clarity.

A variety of techniques have been proposed to solve eq.(7) (Lenoble, 1977). One technique that has been extensively analysed and shown to possess several advantages from the point of view of both accuracy and computational efficiency, is the discrete ordinate method (Sawchuk, 1983). This method consists of approximating the integral term of eq.(7) by a Gaussian integration formula:

$$\int_{-1}^{+1} f(\mu)d\mu \approx \sum_{k=0}^{M-1} w_k f(\mu_k) \qquad [8]$$

where the w_k are weight functions and the μ_k are the abscissas, or points of division on

[0,1] (with symmetric points on [-1,0]), at which the function is to be evaluated. The value chosen for M is a balance between accuracy (obtained with large values of M) and computational efficiency (obtained with small values of M). In general, the amount of computation is proportional to M^3, and for this reason it is desireable to keep the value of M as small as possible. Sawchuk (1983) has shown that the two-point integration formula has an accuracy of better than ten percent compared to higher values of M, e.g. $M = 16$. In this study, M is chosen to be 2 leading to a two-point, or 'two-stream', formula. Section 2.1.1.2 describes how two-stream formulae may be modified to perform well for all conditions. For the two-point formula, $w_{+1} = w_{-1} = 1$, while $\mu_{+1} = \frac{1}{2}$ and $\mu_{-1} = -\frac{1}{2}$ (Abramowitz and Stegun, 1972).

Repeated application of eq.(8) to eq.(7) by setting μ in eq.(7) equal to each abscissa yields a pair of coupled linear differential equations defining downward (μ_1) and upward (μ_{-1}) diffuse intensities:

$$\frac{dI(\tau,\mu_1)}{d\tau} = UI(\tau,\mu_1) + VI(\tau,\mu_{-1}) + P\exp(-\tau/\mu_o) \qquad [9]$$

$$\frac{dI(\tau,\mu_{-1})}{d\tau} = -UI(\tau,\mu_1) - VI(\tau,\mu_{-1}) - Q\exp(-\tau/\mu_o) \qquad [10]$$

where

$$U = \tilde{\omega}_o(1 + \frac{3g}{4}) - 2$$

$$V = \tilde{\omega}_o(1 - \frac{3g}{4})$$

$$P = \tilde{\omega}_o f(1 + \frac{3g\mu_o}{2})$$

$$Q = \tilde{\omega}_o f(1 - \frac{3g\mu_o}{2})$$

$$f = (\pi F_o)/2\pi$$

and where $g = \frac{\omega_1}{3}$ is the asymmetry factor.

Solution of equations (9)-(10) is straightforward. Application of matrix techniques, for example, yields:

$$I(\tau,\mu_1) = c_1 R_1 e^{\lambda\tau} + c_2 R_2 e^{-\lambda\tau} + \alpha \exp(-\tau/\mu_o) \quad [11]$$

$$I(\tau,\mu_{-1}) = c_1 R_2 e^{\lambda\tau} + c_2 R_1 e^{-\lambda\tau} + \beta \exp(-\tau/\mu_o) \quad [12]$$

where

$$\lambda = \sqrt{U^2 - V^2}$$

$$R_1 = \tfrac{1}{2}(1 + (U+V)\lambda^{-1})$$

$$R_2 = \tfrac{1}{2}(1 - (U+V)\lambda^{-1})$$

$$\alpha = [-P(\mu_o^{-1} - U) - VQ]/D$$

$$\beta = [Q(\mu_o^{-1} + U) - VP]/D$$

$$D = V^2 - U^2 + \mu_o^{-2}$$

and c_1, c_2 are constants.

For the two-stream approximation considered in this study, $\pm\lambda$ are the two eigenvalues and the columns of the (2×2) matrix R:

$$R = \begin{bmatrix} R_1 & R_2 \\ R_2 & R_1 \end{bmatrix}$$

are the corresponding eigenvectors. Letting Λ be the diagonal matrix

$$\Lambda = \begin{bmatrix} \exp(\lambda\tau) & 0 \\ 0 & \exp(-\lambda\tau) \end{bmatrix}$$

and c a column vector with elements c_1 and c_2, eqs. (11) and (12) can be expressed as a matrix equation:

$$I(\tau,\mu) = R\Lambda c + \exp(-\tau/\mu_o)p$$

where p is a column vector with elements α and β. The first term on the right-hand side then represents the homogeneous solution and the second term represents the particular solution. Mathematically, c_1, c_2 arise because eigenvectors can only be determined up to some arbitrary constant.

Since there are two constants, a pair of linear equations defining c_1 and c_2 are required to solve for them. The equations defining these constants are obtained from boundary conditions for diffuse fluxes at the top and base of the atmosphere.

At the base of the atmosphere, the upward diffuse intensity is assumed to be proportional to the total incoming (direct + diffuse) intensity and surface albedo:

$$I(\tau,\mu_{-1}) = \frac{\alpha_S}{\pi}(F_D + S) \qquad [13]$$

where F_D is the incoming diffuse flux at the base of the atmosphere (eq.[15]) and S is the incoming direct beam solar radiation at the base of the atmosphere (eq.[17]).

At the top of the atmosphere, the direct beam radiation is assumed to be the only incident radiation:

$$I(\tau = 0,\mu_1) = 0 \qquad [14]$$

Equations (13) and (14) constitute a system of linear equations defining c_1 and c_2 and may be solved by conventional Gaussian elimination methods.

Upward F_U and downward F_D diffuse fluxes are obtained by integrating intensities over zenith and azimuth directions:

$$F_D = \int_0^{2\pi}\int_0^{+1} I(\tau,\mu_1)\mu\, d\mu\, d\phi = \pi I(\tau,\mu_1) \qquad [15]$$

$$F_U = \int_0^{2\pi}\int_{-1}^{0} I(\tau,\mu_{-1})\mu\, d\mu\, d\phi = -\pi I(\tau,\mu_{-1}) \qquad [16]$$

The extinction of the direct beam radiation is described by the Beer-Bouger- Lambert law and is given by:

$$S = \mu_o(\pi F_o)\exp(-\tau/\mu_o) \qquad [17]$$

2.1.1.2. Application of the *Delta–M* Method

Extensive numerical testing of several low order (e.g. $M=2$ or 4) radiative transfer models indicates that all algorithms experience numerical difficulties when $\tilde{\omega}_o \rightarrow 1$ (quasi-conservative scattering), $g \rightarrow 1$ (increasing forward scattering) and/or some combination of these two cases. One expression of these numerical difficulties are negative fluxes for some combinations of optical depth and solar zenith angle (e.g. Liou, 1973). These observations would appear to preclude application of low-order radiative transfer algorithms to real atmospheres, which would be the most useful from the viewpoint of computing times.

Joseph et.al. (1976) and Wiscombe (1977b) have demonstrated, however, that it is possible to extend the range of the Eddington approximation (a two-term spherical harmonics solution to the radiative transfer equation), and thus *any* radiative transfer algorithm to all $(\tilde{\omega}_o, g)$ combinations, even to non-absorbing, highly asymmetric, scatter such as by cloud droplets at visible wavelengths. This extension to all $(\tilde{\omega}_o, g)$ combinations was made with the *Delta–M* method (Wiscombe, 1977b).

The *Delta–M* method provides a rational basis for transforming a highly asymmetric scattering problem to an equivalent transfer problem with reduced values of $\tilde{\omega}_o$ and g for which most radiative transfer algorithms, including two-term approximations, perform well. The essence of the *Delta–M* method is that the large forward peak in the scattering phase function associated with large particle (e.g. aerosols, and cloud droplets) is truncated by an amount f_S which depends on both the order of approximation M and the scattering phase function used to represent the scattering process. For the Henyey-Greenstein phase function, which has been shown to simulate Mie scattering well (Hansen, 1969) (and which is used in this study) and the $M=2$ discrete ordinate solution described above, $f_S = g^2$.

In application, the *Delta–M* method consists of simply scaling the optical properties describing the transfer problem and applying these scaled parameters in place of

the unscaled parameters in the radiative transfer equation. The scaling relationships for two term solutions to the radiative transfer equation are:

$$g' = g/(1+g) \quad [18]$$

$$\tilde{\omega}_o' = (1-f_s)\tilde{\omega}_o/(1-\tilde{\omega}_o f_s) \quad [19]$$

$$\tau' = (1-\tilde{\omega}_o f_s)\tau \quad [20]$$

where g' is the scaled asymmetry factor, $\tilde{\omega}_o'$ is the scaled single scattering albedo, and τ' is the scaled optical depth.

Extensive numerical testing by Joseph et.al. (1976), Schaller (1979), and Sawchuk (1983) indicates inclusion of the *Delta–M* method can lead to (often) dramatic improvements in flux estimates. When the *Delta–M* method is combined with the two-term discrete ordinate approximation of Section 2.1.1.1 (thus leading to the *Delta–D_2* approximation), where one can take advantage of numerous symmetries, one obtains both accuracy and computational efficiency.

2.1.1.3. The Multi-Layer Component

The real atmosphere is characterized by vertical inhomogeneities such as aerosols, clouds (possibly at several altitudes), and varying concentrations of spectrally absorbing gases. The *Delta–D_2* model may be applied to this vertically inhomogeneous atmosphere by first resolving the solar spectrum into spectral intervals across which the gaseous absorption coefficient is effectively constant and second, by resolving the vertical profile of atmospheric composition into layers within which atmospheric composition is effectively constant. Spectrally integrated fluxes are then obtained by applying the *Delta–D_2* model to each layer within a spectral interval to obtain spectral fluxes (in practice, quasi-monochromatic fluxes). Spectral fluxes are then summed to obtain diffuse fluxes integrated over the solar spectrum. This procedure entails two distinct sub-algorithms: calculating shortwave fluxes for a single spectral interval (the 'multi-layer formulation'), and subdividing the solar spectrum into spectral intervals (the 'multi-spectral formulation').

The multi-layered atmosphere is shown in Figure 2.2.

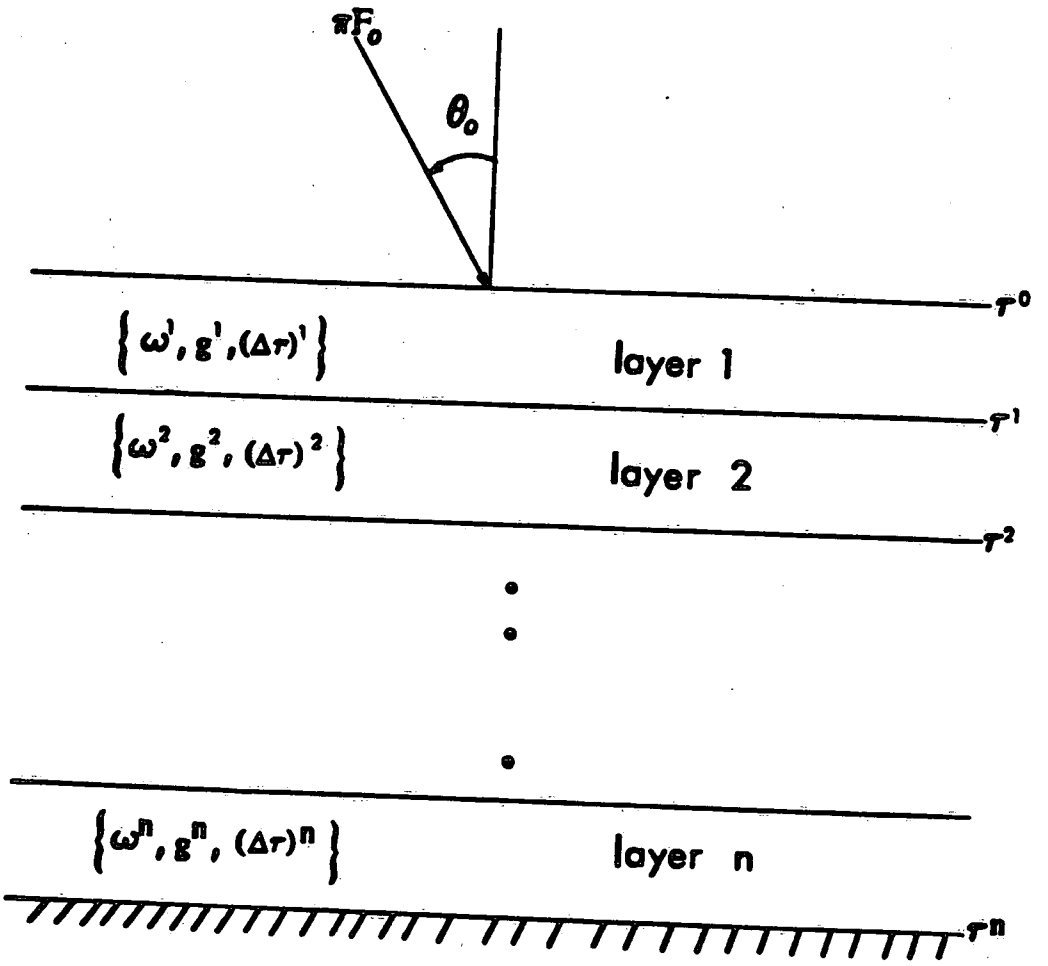

Figure 2.2 - The multi-layer atmosphere (Sawchuk, 1983).

It has been subdivided into homogeneous layers across which $\tilde{\omega}_o$ and g are constant. The solar beam, with incident flux density equal to πF_o enters the atmosphere at an angle θ_o from the local vertical. The ground surface is assumed to reflect radiation isotropically with albedo α_S. Layer numbering begins at the top of the atmosphere while layer quantities are indicated by superscripts within parentheses. For example, $\tau^{(k)}$

indicates total optical depth from the top of the atmosphere to the base of the k-th layer while $\Delta\tau^{(k)}$ represents the optical depth of the k-th layer. The homogeneous *Delta–D*$_2$ is applied to each layer to obtain the homogeneous solution ($\lambda^{(k)}$, $R_1^{(k)}$, $R_2^{(k)}$) and the particular solution ($\alpha^{(k)}$,$\beta^{(k)}$).

The system of equations defining the c_k for each layer are obtained from boundary conditions for diffuse intensity at the top and base of the atmosphere and conservation of energy at layer boundaries. A two-layer atmosphere will illustrate the process. There are four constants in all. Therefore, four equations defining the c_k are required.

The first equation states that the direct beam solar radiation is the only radiation incident at the top of the atmosphere, i.e., there is no diffuse radiation incident at the top of the atmosphere:

$$I(\tau=0,\mu_1) = 0 \qquad [21]$$

The second equation states that the downwelling diffuse flux at the base of the first layer equals the downwelling diffuse flux at the top of the second layer:

$$I^{(1)}(\tau^{(1)},\mu_1) = I^{(2)}(\tau^{(2)},\mu_1) \qquad [22]$$

while the third equation states that the upwelling diffuse flux at the top base of the first layer equals the upwelling diffuse flux at the top of the second layer:

$$I^{(1)}(\tau^{(1)},\mu_{-1}) = I^{(2)}(\tau^{(1)},\mu_{-1}) \qquad [23]$$

The last equation specifies the upward diffuse intensity at the base of the atmosphere:

$$I^{(2)}(\tau^{(2)},\mu_{-1}) = \frac{\alpha_S}{\pi}\left[I^{(2)}(\tau^{(2)},\mu_1) + \mu_o(\pi F_o)e^{-\tau^{(2)}/\mu_o}\right] \qquad [24]$$

Substituting expressions for $I(\tau,\mu_1)$ and $I(\tau,\mu_{-1})$ (eqs.[11] and [12]) yields a system of linear equations defining the c_k:

$$\boldsymbol{A}\cdot\boldsymbol{c}=\boldsymbol{b} \qquad [25]$$

where

$$\boldsymbol{A}\equiv\begin{bmatrix} R_1^{(1)} & R_2^{(1)} & 0 & 0 \\ R_1^{(1)}e_1 & R_2^{(1)}e_{-1} & -R_1^{(2)}e_2 & -R_2^{(2)}e_{-2} \\ R_2^{(1)}e_1 & R_1^{(1)}e_{-1} & -R_2^{(2)}e_2 & -R_1^{(2)}e_{-2} \\ 0 & 0 & (R_2^{(2)}-\alpha_S R_1^{(2)})e_2 & (R_1^{(2)}-\alpha_S R_2^{(2)})e_2 \end{bmatrix}$$

$$\boldsymbol{b}\equiv\begin{bmatrix} \alpha^{(1)} \\ \exp(-\tau^{(1)}/\mu_o)\left[\alpha^{(2)}-\alpha^{(1)}\right] \\ \exp(-\tau/\mu_o)\left[\beta^{(2)}-\beta^{(1)}\right] \\ \exp(-\tau/\mu_o)\left[\alpha_S\left[\alpha^{(2)}+\dfrac{\mu_o\pi F_o}{\pi}\right]-\beta^{(2)}\right] \end{bmatrix}$$

$\boldsymbol{c}\equiv\left[c_1^{(1)}, c_2^{(1)}, c_1^{(2)}, c_2^{(2)}\right]^T$, $e_{\pm j}\equiv\exp(\pm\lambda^{(j)}\tau)$, and the superscript T denotes the transpose.

The order of the system of equations defined by eq.(25) can become large even when the number of layers is kept to a minimum. The coefficient matrix $\boldsymbol{A}$, however, has a special structure: it is a banded matrix. For the two-stream approximation used in this study, the number of non-zero diagonals is five, leading to a penta-diagonal system of equations. Sparse systems of equations may be solved efficiently and accurately with well-written subroutines, e.g. the International Mathematical and Statistical Library (IMSL), that take advantage of the sparse structure (e.g. Wiscombe, 1977a). A similar method, but one which reduces the computations much further, is applied in this study. It makes use of a block-tridiagonal solution to eq.(25). It is essential that eq.(25) be solved accurately and efficiently, because integrated fluxes for one solar zenith angle are obtained from solving eq.(25) for each spectral interval that the solar spectrum has been subdivided into (Section 2.1.1.4).

The block-tridiagonal solution evaluates the LU decomposition of A by organising A as a tridiagonal matrix where each element is an $M \times M$ matix (block):

$$A = \begin{bmatrix} A_1 & C_1 & & & \\ B_2 & A_2 & C_2 & & \\ & \cdot & \cdot & \cdot & \\ & & \cdot & \cdot & \cdot \\ & & & B_n & A_n \end{bmatrix}; b = \begin{bmatrix} b^{(1)} \\ b^{(2)} \\ \cdot \\ \cdot \\ b^{(n)} \end{bmatrix}$$

where the A_i, B_i and C_i are square matrices of order M, and the $b^{(i)}$ are column vectors each with M elements. The vector of unknowns $c^{(i)}$ is assumed to have this same partitioned form. The LU decomposition of A has the form (Isaccson and Keller, 1966):

$$A = L \cdot U$$

$$= \begin{bmatrix} \hat{A}_1 & & & & \\ B_2 & \hat{A}_2 & & & \\ & B_3 & \hat{A}_3 & & \\ & & \cdot & \cdot & \\ & & & B_n & \hat{A}_n \end{bmatrix} \cdot \begin{bmatrix} I_1 & \Gamma_1 & & & \\ & I_2 & \Gamma_2 & & \\ & & \cdot & \cdot & \\ & & & \cdot & \Gamma_{(n-1)} \\ & & & & I_n \end{bmatrix}$$

where the I_i are identity matrices of order M, and the $\hat{A}_i$ and Γ_i are square matrices of order M. The definition of A, L, and U provides a recursion relation for evaluating the $\hat{A}_i$ and Γ_i:

$$A_1 = A_1, \quad \Gamma_1 = \hat{A}_1^{-1} \cdot C_1 \qquad [26]$$

$$\hat{A}_k = A_k - B_k \Gamma_{(k-1)}, \quad k = 2, 3, \cdots, n \qquad [27]$$

$$\Gamma_k = \hat{A}_k^{-1} \cdot C_k, \quad k = 2, 3, \cdots, (n-1) \qquad [28]$$

The solution stage involves two steps: (i) first solving:

$$L \cdot y = b \qquad [29]$$

by forward substitution. The vector y has the partitioned form of b and c. The recursion relation is:

$$y^{(1)} = \hat{A}_1^{-1} \cdot b^{(1)} \qquad [30]$$

$$y^{(k)} = \hat{A}_k^{-1}\left[b^{(k)} - B_k \cdot y^{(k-1)}\right] \qquad [31]$$

The second step involves solving

$$U \cdot c = y \qquad [32]$$

Equation (32) is normally solved by recursion, although the important observation is that $c^{(n)} = y^{(n)}$. When only surface fluxes are required, as in this study, the c_i required for evaluation of surface fluxes are available when the last layer has been processed. Thus, the back substitution step (eq.[32]) can be obviated entirely (this step normally entails approximately one quarter of the time required to solve a system of linear equations).

Equations (26)-(32) highlight other advantages of the block-tridiagonal solution. First, the B_i are lower-half zero, while the C_i are upper-half zero. This reduces matrix products by a factor of two, in effect saving a matix-matrix product for each layer. Equations (26)-(32) can be coded in a form that avoids calculating inverses explicitly. For example, eq.(28) can be re-written as:

$$\hat{A}_k \Gamma_k = C_k$$

Evaluating Γ_k by solving this system of equations is both quicker and more accurate than finding $\hat{A}_k^{-1}$ and performing an additional matrix-matrix product. In addition, by computing the *LU* decomposition of $\hat{A}_k$ one obtains a rapid solution for the $y^{(k)}$, since eq.(30) may be re-written as eq.(28) was. Thus, both eq.(28) and (30) may be solved by computing the *LU* decomposition of $\hat{A}_k$ once and only once. Sawchuk (1983) list several other advantages of the block-tridiagonal solution. One important further advantage is described in Section 3.3.

2.1.1.4. The Multi-Spectral Component

It is crucial to compute spectral fluxes efficiently, because spectrally integrated fluxes entail solving eq.(25) for as many spectral intervals as the solar spectrum has

been subdivided. Because of the highly oscillatory nature of gaseous absorption coefficients, a sufficiently detailed subdivision would require on the order of several thousand spectral intervals. Clearly, processing thousands of spectral intervals to evaluate (integrated) fluxes for one solar zenith angle would lead to prohibitive computing times. Therefore, a method for reducing the number of spectral intervals must be implemented to render computations feasible. The 'multi-spectral' component identifies the precise manner in which the solar spectrum is subdivided.

In the solar spectrum, water vapour and ozone are the principal absorbing gases. These gases are also spectrally separate and this observation leads to a major subdivision of the solar spectrum into two major bands at 0.83 μm. Wavelengths less than 0.83 μm will be referred to as the visible band, while wavelengths greater than 0.83 μm will be referred to as the near infrared band.

For the near infrared band, this study has applied the wing scaling approximation of Chou and Arking (1981) to reduce the number of spectral intervals to a minimum (≈9) while retaining high accuracy.

Briefly, the wing scaling approximation seeks to approximate the spectrally dependent gaseous absorption coefficient $k_\nu(p,T)$, where p is pressure and T is temperature, as a function of some (ideal) reference pressure p_r and reference temperature T_r. That is:

$$k_\nu(p,T) = k_\nu(p_r,T_r)\left(\frac{p}{p_r}\right)^t \qquad [33]$$

where t is a scaling parameter ($0 \leq t \leq 1$) to account for the non-saturation at the line centre. T_r, p_r, and t are empirically chosen to minimize the difference $k_\nu(p,T)$ and $k_\nu(p_r,T_r)$. Chou and Arking choose $p_r = 300$mb, $T_r = 240$K, and $t = 0.8$ on the basis of sensitivity tests.

Molecular line data of McClatchey et.al. (1972) were then used to compute $k_\nu(p_r = 300$ mb, $T_r = 240$K) at 472,000 wavelengths between 0.83 μm and 4.0 μm. This

wavelength range includes the five major water vapour bands centred at 0.94 μm, 1.14 μm, 1.38 μm, 1.87 μm, and 2.7 μm. Distribution of absorption coefficients were then tabulated for each absorption band and the entire near infrared band at equal intervals of $\Delta\log(k_\nu)=0.3$ for $\log(k_\nu)=-5.0$ to $\log(k_\nu)=3.7$. By noting the incident shortwave flux associated with each $\Delta\log(k_\nu)$, and by dividing the shortwave flux contained within $\Delta\log(k_\nu)$ by the shortwave radiation incident over the entire absorption band, a set (i.e. distribution) of weights (fractions) and absorption coefficients k_ν is obtained for both individual absorption bands and the entire near infrared spectrum is obtained. Sawchuk (1983) applied these tabulated data of Chou and Arking (1981) to reduce the number of spectral intervals within the near infrared spectrum to only nine.

Sawchuk (1983) applied a similar technique using low resolution (20 cm^{-1}) transmittance model LOWTRAN 4 (McClatchey et.al., 1974) to parameterize ozone absorption across the visible spectrum 0.2 μm to 0.82 μm with only nine spectral intervals. Weights and absorption coefficients for each of the 18 spectrals are given in TABLE B.2 (Appendix B).

Chou and Arking (1981) have demonstrated excellent agreement between the wing scaling approximation and line-by-line calculations, which may be considered the most accurate that may be performed within the limits of uncertainty of line parameter data. In addition, Sawchuk (1983) demonstrated that the nine spectral interval bands described above were superior to other methods of representing the distribution of absorption coefficients.

Reflected shortwave radiation is evaluated from the product of the incoming shortwave radiation and the surface albedo. The albedo of the water surface is assumed constant at 0.08 for both visible and near-infrared bands. The albedo of ice is set at 0.75 for the visible band and 0.45 for the near infrared band. These values were determined from spectral values of albedo for snow tabulated by McClatchey

et.al. (1972). Reflected radiation integrated over the solar spectrum were then obtained by areally weighting water and ice surfaces.

2.1.2. Longwave Radiation

Evaluation of longwave radiative fluxes is simpler than for the shortwave case because multiple scattering effects are small and may be neglected. In addition, infrared transfer is dominated by absorption and emission processes and these are easily parameterized in terms of the Stefan- Boltzmann law.

Incoming longwave radiation at the ground surface L_D may be viewed as being comprised of two terms: a clear-sky component L_o originating from emission by water vapour, carbon dioxide, ozone, and other trace gases, and a cloud-aerosol component $L_{C,H}$:

$$L_D = L_o + L_{C,H} \qquad [34]$$

The clear-sky component is easiest to model and a variety of empirical expressions for L_o have appeared in the literature (Brunt, 1932; Swinbank, 1963; Idso and Jackson, 1969; Brutsaert, 1975; Satterland, 1979; Idso, 1981). These statistical models represent L_o as simple functions of surface air temperature and vapour pressure, except the Swinbank and Idso and Jackson formulae where L_o is a function of air temperature only. Swinbank's relationship, for example, is:

$$L_o = 5.31\times10^{-14}\, T_S^6 \quad (\mathrm{Wm^{-2}}) \qquad [35]$$

Paltridge and Platt (1976) observe that eq.(35) was derived by Swinbank from predominantly nighttime conditions which are likely to be associated with inversion conditions. During daytime, when lapse conditions predominate, the actual centre of gravity temperature is lower relative to screen temperature and eq.(35) overestimates observed radiative fluxes by approximately 20 $\mathrm{Wm^{-2}}$ (winter) to 30 $\mathrm{Wm^{-2}}$ (summer) for midlatitude stations such as Aspendale, Australia. Paltridge and Platt (1976) con-

clude that eq.(35) provides good estimates of L_o if daytime estimates are reduced by an average of 20 Wm^{-2}. Unfortunately, these authors do not indicate the correction factor to be applied when daily values of L_o are computed from the daily mean T_S, as in this study.

There are other problems associated with application of simple statistical models for longwave fluxes. For example, most expressions, as eq.(35) illustrates, are power functions or polynomials that perform well near the centre of gravity of the data from which the relationship was determined but may deteriorate at higher or lower temperatures. Most authors simply do not state the range of validity appropriate for their model. Some models, e.g. Brunt (1932) and Idso and Jackson (1969), contain constants that are site-specific and thus not strictly applicable to locations other than that for which they were developed. Finally, none of these simple models attempt to incorporate the effects of aerosols. Aerosol effects on L_o may be small in some circumstances, but there is a growing body of experimental (Rouse et.al., 1973; Dalrymple and Unsworth, 1978) and theoretical (Welch and Zdunkowski, 1976) evidence which indicates that these effects are not insignificant. These studies suggest aerosols may contribute from 30 to 60 W m^{-2} to L_o. The lower Great Lakes straddle the industrial heartland of Canada and the United States; aerosol effects on both the shortwave and longwave spectrums must be significant.

These problems frustrate attempts to apply simple models for L_o generally and lead to the development of a physically-based model for L_o for this study, although it may be applicable to other geographical regions.

2.1.2.1. Clear-Sky Formulation

The physical basis for the model of L_o developed in this study is that the atmosphere radiates as a blackbody outside the window region (8.3 $\mu m \leq \lambda \leq$ 12.8 μm) (Paltridge and Platt, 1976). Then,

$$L_o = (1 - f_P)\sigma T_A^4 \quad (\mathrm{Wm}^{-2}) \qquad [36]$$

where T_A is the radiating temperature (K) of the atmosphere, and f_P is the fraction of the Planck curve within the atmospheric window at temperature T_A. f_P, a function of temperature, is routinely required for evaluation of L_o and $L_{C,H}$. An efficient evaluation of f_P was developed by first integrating the Planck function between 8.3 and 12.8 μm from $T_A = -100$ °C to $T_A = 100$ °C in steps of $\Delta T_A = 5$ °C (Houghton, 1986 (p.236-237)). These values of $f_P = f(T_A)$ were then fit to a combination of Legendre polynomials of order 0 to 3 inclusive to obtain a third order polynomial:

$$f_P = A_0 + T'(A_1 + T'(A_2 + A_3 T')) \qquad [37]$$

where T' is the scaled temperature:

$$T' = \frac{T_A}{100} \qquad [38]$$

Equation (38) scales T_A to the interval [-1,+1], as required for evaluation of Legendre polynomials, which are the basis functions of eq.(37). The value of T_A applied in eq.(38) must be representative of the centre of gravity temperature of the radiating atmosphere. Following Paltridge and Platt (1976), these altitudes are assumed constant at 300 m in summer and 200 m in winter.

Comparison of values of f_P computed from eq.(37) and numerical integration of the Planck curve reveals root mean square errors of 0.0012 over the temperature range [-100°C,100°C]; the root mean square error decreases to 0.00087 over the temperature range [-40°C, +40°C] where the majority of f_P evaluations will be made. Increasing the order of approximation in eq.(37) does not appreciably reduce root mean square errors.

Equation (36) will underestimate L_o because f_P includes emission by ozone at 9.1 μm and 9.65 μm. The 9.1 μm band is only partially absorbing. Kondratyev (1965, p.130) suggests this band extends from approximately 8.97 μm to 9.17 μm with a mean

transmission of approximately 0.55. The 9.65 μm band is much more intense. It extends from 9.4 μm to 9.9 μm with a mean transmission of 0.05. Legendre Polynomial approximations were developed for both bands, as in eq.(37). Coefficients for estimating each of the three portions of Planck curve are given in Table D.3 (Appendix D).

In the presence of aerosols, radiation emitted by gases will be scattered by aerosols. To a first approximation, it was assumed that the asymmetry factor could adequately describe the transfer to the ground surface. The asymmetry factor depends critically on the *type* of aerosol and relative humidity. The urban aerosol model proposed by Shettle and Fenn (1979) was assumed to best represent aerosol conditions over the lower Great Lakes. These authors surveyed amd merged direct measurements of aerosols from several different environments to obtain models of physical and chemical properties for several aerosol species, e.g. urban, marine, continental, in the atmospheric boundary layer. These authors then applied Mie theory to evaluate optical properties for each aerosol model as a function of relative humidity and wavelength for both solar and infrared spectrums.

In the infrared spectrum, the spectrally-averaged asymmetry factor might be assumed to be heavily weighted to the value near 11 μm, as the bulk of emitted radiation will be at these wavelengths, as Wien's law demonstrates. It was therefore assumed that the asymmetry factor at 11 μm best described the average asymmetry factor in the infrared spectrum. A Legendre Polynomial approximation for the infrared-averaged asymmetry factor g_{IR} as a function of surface relative humidity was determined as:

$$g_{IR} = a_0 + U'_R(a_1 + U'_R(a_2 + a_3 U'_R)) \qquad [39]$$

where U'_R is the scaled relative humidity,

$$U'_R = \frac{2U_R - 99}{99} \qquad [40]$$

where U_R is the relative humidity (percent), and the a_i are tabulated in TABLE D.4 (Appendix D).

2.1.2.2. Effects of Clouds and Aerosols

Evaluation of longwave emission from clouds and aerosols is more difficult because fluxes depend explicitly on cloud-base temperature and liquid water content of cloud and on aerosol species.

For aerosols, spectral values of optical properties tabulated by Shettle and Fenn were applied to approximate radiative transfer. To a first approximation, it was assumed that aerosols contribute to L_D through emission at window wavelengths:

$$L_H = f_F \epsilon_H \sigma T_H^4 \qquad [41]$$

where ϵ_H is the aerosol emissivity averaged across the atmospheric window, and T_H is the mean temperature (K) of the aerosol layer. Radiation emitted outside window wavelengths may be assumed to be completely absorbed by atmospheric gases.

Since the single scattering albedo defines the ratio of scattered radiation to total radiation attenuated for an individual scattering event,

$$\epsilon_H = 1 - \tilde{\omega}_o \qquad [42]$$

Following Hunt (1973), it was assumed that the value of $\tilde{\omega}_o$ at $\lambda = 11\ \mu$m was representative of the entire window region. Values of $\tilde{\omega}_o$ at 11 μm for relative humidities ranging from 0 to 99 percent (Shettle and Fenn, 1979) were used to derive a Legendre Polynomial approximation relating $(1 - \tilde{\omega}_o)$ to relative humidity, as in eq.(39). Coefficients are given in TABLE D.2 (Appendix D).

Clouds are often assumed to radiate as blackbodies, although this is not likely to be true for thin clouds such as Cirrus or, more generally, for clouds with low liquid water contents (Stephens, 1978a). Stephens (1978a) has demonstrated that cloud

emissivity ϵ_C is approximately an exponential function of cloud liquid water content. Stephens (1978a) has parameterized ϵ_C at window wavelengths for downward emission as:

$$\epsilon_C = 1 - \exp(-0.116\, W) \qquad [43]$$

where W is the total liquid water content (g m^{-2}). Assuming the cloud contribution to L_D to be that emitted at window wavelengths, cloud emission may be approximated as:

$$L_C = f_p \epsilon_C \sigma T_B^4 \qquad [44]$$

where T_B is cloud base temperature (K). Evaluation of W is described in section 3.2.1.

The net effect of cloud and aerosol emission $L_{C,H}$ will be less than the sum of L_H and L_C because some of the radiation emitted by the cloud will be attenuated by the aerosol layer. Short of developing a radiative transfer algorithm to determine the joint effect, it was assumed that $L_{C,H}$ could be modelled as the sum of radiation emitted by the aerosol layer plus cloud-emitted radiation transmitted by the aerosol layer. The small optical depths of the haze layer at window wavelengths suggested the transmission of cloud emitted radiation through the aerosol layer could be approximated by Beer's law:

$$I(\tau_H) = I_o \exp(-\tau_H/\mu_o) \qquad [45]$$

where τ_H is the optical depth of the aerosol layer averaged across window wavelengths, I_o is the radiation emitted by cloud, and μ_o is the cosine of the zenith angle of incident radiation. Clouds will emit radiation in all directions so that incoming radiation at the top of the aerosol layer cannot be strictly considered a collimated beam as, for example, the solar beam. Therefore, μ_o^{-1} was assumed constant and set equal to 1.66, which is approximately the mean value of the cosine of the zenith angle over the range [0, 90].

Aerosol optical depth was computed from data for the urban aerosol model of Shettle and Fenn (1979). By definition, optical depth is given by an integration over

altitude of the extinction coefficient. When the extinction coefficient is constant with respect to altitude, as assumed in this study, optical depth may be determined from:

$$\tau_H = (E_{xt})_{ND} \times D_H \qquad [46]$$

where D_H is the depth of the aerosol layer (km), and $(E_{xt})_{ND}$ is the extinction coefficient at 11 μm corresponding to an aerosol particle density of ND particles cm^{-3}.

Shettle and Fenn (1979) provide extinction coefficients for a number density of 20,000 cm^{-3} and tables with particle number density as a function of visibility and relative humidity. The number density tables are set as a bi-cubic spline function which estimates particle number density ND as a function of ambient visibility (km) and relative humidity. The corresponding extinction coefficient is then computed from:

$$(E_{xt})_{ND} = \frac{ND}{20{,}000} \cdot (E_{xt})_{ND=20{,}000} \qquad [47]$$

Incoming longwave radiation from clouds and aerosols is then given by:

$$L_{C,H} = \epsilon_H \sigma T_H^4 + (f_P \epsilon_C \sigma T_B^4 C)\exp(-1.66\tau_H) \qquad [48]$$

The radiation flux density emitted by the ground surface L_U is assumed to follow grey-body emission:

$$L_U = \epsilon_S \sigma T_S^4 \qquad [49]$$

where ϵ_S is the surface emissivity and T_S is the ground surface temperature. There appears to be little difference in spectrally integrated values of snow/ice and water emissivities. Therefore, ϵ_S was assumed constant at 0.985 (Davies et.al., 1971). In the presence of ice, the ice-covered surface is assumed to have a temperature of 0 °C. T_S is then modelled as:

$$T_S = T_w \cdot (1 - p_i) + T_K \cdot p_i \qquad [50]$$

where T_w is the surface water temperature (K), T_K is 273.15 K, and p_i is the fraction of

lake surface covered by ice.

2.2. Turbulent (Latent and Sensible Heat) Fluxes

Latent Q_{LE} and sensible Q_H heat fluxes were evaluated by application of the Bowen ratio method:

$$\beta_R = \frac{Q_H}{Q_{LE}} \qquad [51]$$

Expressing Q_H and Q_{LE} in terms of the turbulent transfer mechanisms and assuming equality of eddy diffusivities for heat and water vapour, β_R may be expressed as (Quinn and den Hartog, 1981):

$$\beta_R = kP\frac{(T_w - T_a)}{(e_s - e_a)} \qquad [52]$$

where k is a constant ($=6.1\times10^{-4}$), P is atmospheric pressure (mb), T_w is surface water temperature (°C), T_a is air temperature (°C) at a level a above the water surface, e_s is the saturation vapour pressure (mb) at T_w, and e_a is the vapour pressure (mb) at level a.

k is often assumed to be a constant (e.g. Elder et.al., 1974; Pinsak and Rodgers, 1981), although it may be evaluated directly from (Monteith, 1973):

$$k = \frac{c_P P}{L\epsilon} \qquad [53]$$

where c_P is the specific heat of air:

$$c_P = (1 + 0.9q)c_{P_a} \qquad [54]$$

where q is the specific humidity (kg kg^{-1}) and c_{P_a} is the specific heat of dry air (1005J kg^{-1}) K^{-1}, P is pressure, L is the latent heat of vapourization, and ϵ is the ratio of gas constants for dry air to that of water vapour (0.622)

Vapour pressures were determined from (Pruppacher and Klett, 1980):

$$e_s = a_o + T(a_1 + T(a_2 + T(a_3 + T(a_4 + T(a_5 + Ta_6)))))) \quad [55]$$

where e_s is in mb and T in °C. Equation (55) is valid over the temperature range -50 °C $\leq T \leq$ 50°C. Values of the a_i are given in TABLE C.1 (Appendix C). Actual vapour pressures are obtained by substituting the dew point temperature T_d in eq.(55).

With β_R determined from eq.(51), either Q_H or Q_{LE} must be independently evaluated. In this study, Q_{LE} is evaluated from a variant of the mass transfer approach. Sensible heat flux is then obtained from:

$$Q_H = \beta_R Q_{LE} \quad [56]$$

In the mass transfer approach, evaporation is modelled as a function of wind speed and vapour pressure difference between the lake surface and the overlying air (Quinn and den Hartog, 1981):

$$E = M(e_s - e_a)U_a t_D \quad [57]$$

where E is the evaporation rate mm day^{-1}, M is the mass transfer coefficient, e_s and e_a are defined by eq.(55), and U_a is the wind speed at level a (defined below). Alternatively, evaporation may be computed from a bulk transfer (aerodynamic) equation as:

$$E = C_E \rho (q_s - q_a) U_a t_D \quad [58]$$

where C_E is the bulk evaporation coefficient at level a, ρ is air density (kgm^{-3}), q is specific humidity (kg kg^{-1}), and t_D is the number of seconds in a day. Specific humidity is defined as:

$$q = \frac{0.622 e_a}{P - 0.378 e_a}$$

Since $0.378 e_a \ll P$, $q \approx 0.622 e_a / P$ and substituting this expression for q in eq.(58) yields:

$$E = C_E \rho (e_s - e_a) U_a t_D' \quad [59]$$

where t_D' is the product of 0.622 and t_D.

Comparison of like terms in eqs.(57) and (58) shows that the mass transfer coefficient M is proportional to the bulk evaporation coefficient C_E, air density, and surface pressure:

$$M = \frac{\rho C_E}{P} \qquad [60]$$

In application, ρ and P will be given while C_E will have to be evaluated. Quinn and den Hartog (1981) examined three methods of evaluating C_E from data collected over Lake Ontario during IFYGL, each of which employed a different method for assessing atmospheric stability. For given values of T_a, e_s, e_a, and U_a, it may be shown that these methods predict different stability measures.

Quinn and den Hartog (1981) concluded that, for most Great Lake studies, inclusion of variation of C_E with stability was not warranted. These authors then regressed C_E against U_a for neutral conditions and obtained:

$$C_E \times 10^3 = 0.713 + 0.07 U_8 \qquad [61]$$

where U_8 is windspeed at $Z = 8$ m. Equation (61) includes the significant variation of C_E with windspeed. Stability effects were incorporated indirectly by scaling overlake wind speeds as a function of stability criteria established by Phillips and Irbe (1976) (see Section 3.1).

Some insight into the evaporation behaviour of large lakes may be obtained by prescribing values of U_8, vapour pressure difference between lake surface and overlying air, and air density in eq.(57) with M evaluated from eq.(60). For $U_8 = 11 \text{ms}^{-1}$, $M_8 = 0.0971$, which is identical to that determined for Lake Hefner and used by many investigators (e.g. Derecki, 1975).

Over Lake Ontario during IFYGL, average wind speeds were 4 to 5 ms^{-1}, with maximum average daily wind speeds of 7 ms^{-1} during November (Quinn and den Hartog, 1981). Assuming the Lake Hefner value for M would result in substantial overestimates of Lake Ontario evaporation rates. It is therefore expected that evaluation of M

by eq.(60), rather than assigning it a constant (in particular, the Lake Hefner) value, will result in improved evaporation estimates.

With evaporation rates computed from eq.(57), corresponding energy flux densities are obtained from:

$$Q_{LE} = \rho_S L E \qquad [62]$$

where ρ_S is the density of water (assumed constant at 1,000 kg m^{-3}) and L is the latent heat of vapourization at surface water temperature T_w. L is a weak (linear) function of temperature and the following simple linear regression equation is sufficiently accurate:

$$L = 2.5003571 - 0.0023571\,T_w \quad (\text{MJ kg}^{-1}) \qquad [63]$$

2.3. Ice Heat Flux

Ice formation and decay are significant events in the thermal regime of a midlatitude lake because of both the thermal exchange between ice and water (release of latent heat of fusion during ice formation and heat loss in melting) and the large reflectivity of the ice surface to shortwave radiation. From data collected over Lake Ontario during IFYGL, Pinsak and Rodgers (1981) observe average daily values of ≈ 0.5 W m^{-2}. Largest daily values, $25 - 50 \text{Wm}^{-2}$, were observed during late February and early March when ice concentrations began rapidly decreasing. By comparison, these maximum values amounted to $\approx \frac{2}{3} Q^*$ at this time of year.

Previous studies either affix a constant value for Q_I (e.g. Derecki, 1975) or neglect it altogether (e.g. Henderson-Sellers, 1986). Indeed, Pinsak and Rodgers (1981) observe that, for Lake Ontario during IFYGL, a 15 percent difference between observed and predicted ice concentrations amounted to a heat flux difference of ≈ 1 W m^{-2}, which is not significant at any time of the year. These results suggest that the thermal exchange between ice and water may be relatively insensitive to accuracy of predicted

ice concentrations. Net radiation, however, will be much more sensitive to ice concentrations and this was the motivation for modelling ice concentrations in this study.

The ice concentration model developed in this study may be described as a statistical-physical model. The statistical part of the model relates to characterizing ice concentrations (fraction of lake surface covered by ice) as a function of time of year t. This relationship will clearly be unique for a given lake because this will depend on lake depth as well as topographical controls. The relationships developed in this study for Lake Ontario and Lake Erie are derived from ice data prepared by Assel et.al. (1983). These authors, using several data sources ranging from historical ice-chart to satellite imagery, quantified maximum, normal, and minimum ice concentrations for each of the Great Lakes for each half of winter months from the second half of December to the end of April.

Assel et.al. (1983) related limiting ice concentrations to an easily computed quantity, the cumulative freezing degree days Σf_D. The freezing degree day f_D is defined as the difference between the mean daily temperature and 0°C, e.g. $f_D = 4$ if mean daily air temperature is −4°C. In addition, Σf_D is a non-negative function of time of year. Bi-monthly ice concentrations for both lakes are given in TABLE H.1 (Appendix H). These data were used to establish six spline functions for each lake:

$$I_{max} = f(t) \quad [64]$$

$$I_n = f(t) \quad [65]$$

$$I_{min} = f(t) \quad [66]$$

$$(\Sigma f_D)_{max} = f(t) \quad [67]$$

$$(\Sigma f_D)_n = f(t) \quad [68]$$

$$(\Sigma f_D)_{min} = f(t) \quad [69]$$

where I is ice concentration and the subscript n refers to normal ice concentrations.

Spline functions [64] through [69] estimate ice concentrations for an arbitrary day D_o with corresponding cummulative freezing degree days Σf_{D_o} as follows. First, two arrays (x and y) each containing three elements are evaluated. x_1 contains $(\Sigma f_D)_{min}$

for D_o, x_2 contains $(\Sigma f_D)_n$ for this day, while x_3 contains maximum ice concentrations for this day. These x_i are computed from splines [69] to [67] respectively. The y_i are the corresponding ice concentrations determined from cubic splines [64] to [66].

The arrays x and y define a new relationship for this day D_o where Σf_{D_o} (i.e. x_i) is the independent variable and I (i.e. y_i) is the dependent variable. A new spline function is determined using the x and y arrays. This allows estimation of I_{D_o} corresponding to Σf_{D_o}.

This procedure may appear time consuming, but the computational effort is actually quite small. This is because the first step (evaluating spline functions [64] to [69]) need only be performed once, before any other ice concentration computations. Computations are further economized by noting that the spline functions will remain constant for a given day. Therefore, this information may be stored as a (2×3) matrix, one for each day of the winter season. Then, estimation of I_{D_o} for any day requires only one function evaluation.

One disadvantage of this procedure is that for any day D_o estimated ice concentrations will be constrained to the interval $(I_{min}, I_{max})_{D_o}$. Thus the model cannot simulate a new minimum or maximum ice concentrations for a given day D_o. However, there are likely to be few such instances since the original data base spans almost a century of ice observations.

Ice heat fluxes Q_i are evaluated from:

$$Q_i = \Delta I_v L_f \rho_i \qquad [70]$$

where ΔI_v is the change in ice volume, L_f is the latent heat of fusion (0.335 MJ kg^{-1}), and ρ_i is the density of ice, assumed constant at 916 kgm^{-3}. The computer code keeps a running counter of daily total ice volume. The change in ice volume is determined from the product of fractional lake surface area covered by ice (eqs.[64]-[69]) and the estimated depth of ice, I_d, which is assumed to be a simple function of the ice concen-

tration:

$$l_d = 0.2 l_{D_o} \quad \text{(m)} \qquad [71]$$

$$l_d = 0.4 \exp(l_{D_o}{}^5 - 1) \quad \text{(m)} \qquad [72]$$

Equation (71) is applied when ice concentration is less than 50 percent; eq.(72) when l_{D_o} is greater than or equal to 50 percent. Equations (71) and (72) are approximate fits to ice depth and concentration data for Lake Ontario during IFYGL (Pinsak and Rodgers, 1981).

2.4. Minor Energy Heat Fluxes

Minor heat fluxes include exchanges resulting from inflow and outflow of water of differing temperature to and from the lake, precipitation, and waste heat from industrial and power plants. Detailed analyses of these energy exchanges by Boyce *et.al.* (1977) for Lake Ontario during IFYGL reveal that these exchanges are small, approximately one percent of the daily surface heat flux or less. These results agree well with values given by Derecki (1975) for Lake Erie.

In this study, daily values for minor heat fluxes were set according to monthly values. Values for Lake Ontario are based on values reported by Pinsak and Rodgers (1981), while values for Lake Erie are taken from Derecki (1975). The values are given in TABLE I.1 (Appendix I). These estimates of Q_M may not be very accurate, however, they are probably correct in order of magnitude.

3. MODEL IMPLEMENTATION

The equations defining energy balance components of Section 2 require several data sources for implementation. These include: overlake meteorological data, vertical profiles of atmospheric temperature and humidity, and specification of boundary conditions: incoming shortwave radiation at the top of the atmosphere and surface water temperature. This section describes how these quantities were evaluated.

3.1. Meteorological Data Base

The model equations implicitly assume input meteorological data representative of overlake conditions. In the absence of direct measurement, overlake meteorological data must be modelled from a knowledge of mean conditions at the lake perimeter. The procedure applied in this study consists of two steps. The first step involved construction of a data base consisting of mean hourly data from stations at or near the lake perimeter for each day of the study period (1 January, 1953 - 31 December, 1983) for Lake Ontario, Lake Erie, and the three basins of Lake Erie. Meteorological stations are shown in Fig. 3.1. Hourly station data included: wind speed (ms^{-1}), pressure (mb), air temperature (°C), dew point temperature (°C), relative humidity (percent), visibility (km), and total cloudiness (percent).

The second step involved application of scaling relationships to overland data to estimate overlake values. Previous Great Lake heat balance studies (e.g. Derecki, 1975; Lam *et.al.*, 1983; Schertzer, 1987) have applied scaling ratios derived for monthly time scales (e.g. Richards and Fortin, 1962). Extensive statistical analyses of paired overland-overwater measurements of wind speed, air and dew point temperatures, reveals that the difference between overland and overwater values depends on fetch, duration of air over water, and atmospheric stability over the lake (Phillips and Irbe, 1976, 1978; Phillips and Almazan, 1981).

Phillips and Almazan (1981) summarized these comparisons according to (i)

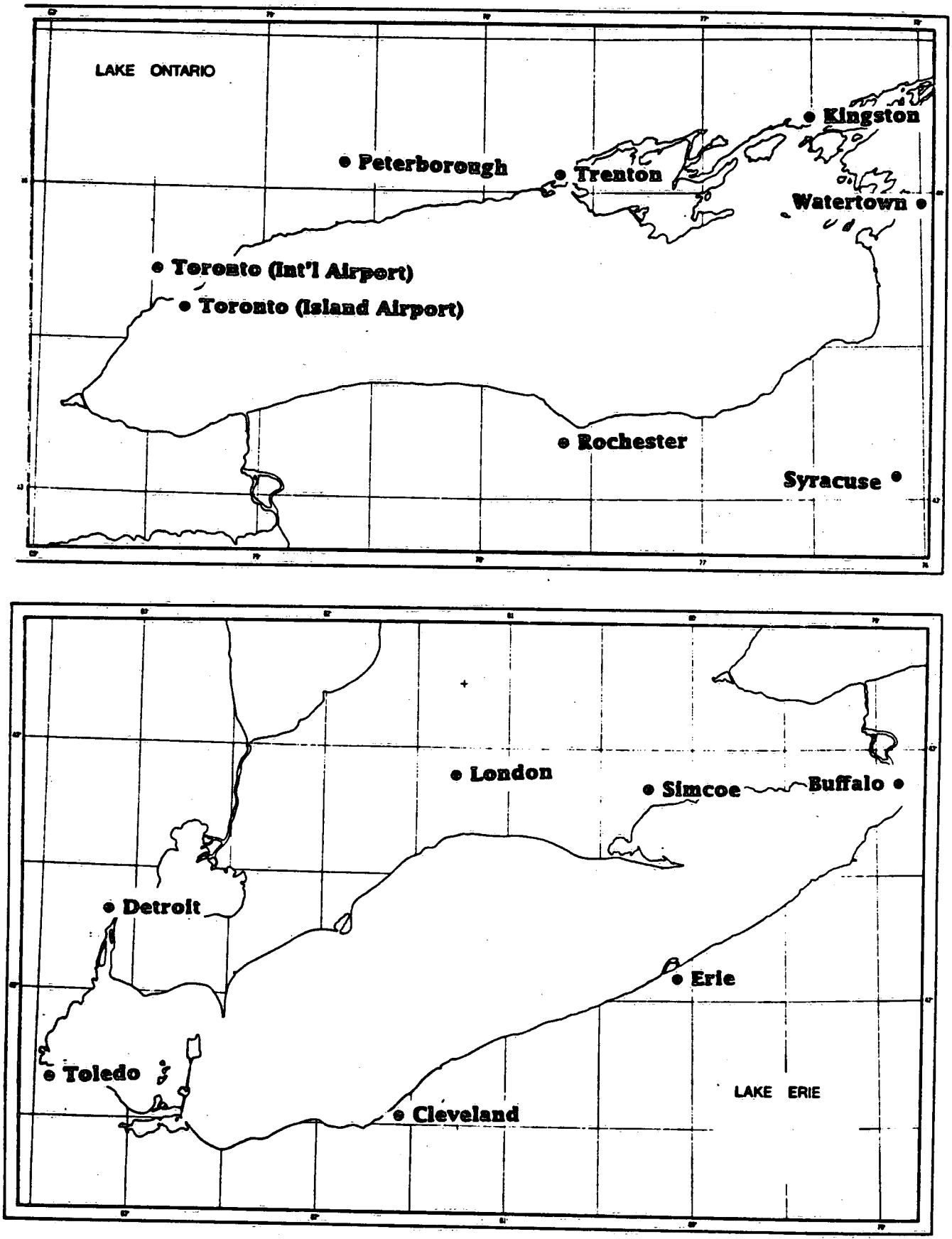

Figure 3.1 - Meteorological stations for Lake Ontario and Lake Erie.

fetch, (ii) overland wind speed, (iii) atmospheric stability, and (iv) stepwise multiple regression equations for estimating overlake values in terms of overland values and other statistically significant variables (e.g. duration of air over water, surface water temperature). Analyses in terms of atmospheric stability included classifications ranging from very stable to very unstable and averages over all stability classifications. Unfortunately, Phillips and Almazan did not compare overlake values predicted by these methods with direct measurements. Thus, there is no indication which method best simulates overlake meteorological conditions.

As part of the model verification process, this study examined methods (i), (ii), and (iii). Method (iv) could not be examined because required data were either lacking or could not be adequately evaluated.

The scaling functions for simulating overlake data from overland data are defined in TABLE 3.1.

TABLE 3.1 - Definition of Scaling Functions for Overlake Variables.

Parameter	Scaling Function	Definition
U_a	R_W	$\frac{U_{a,\,lake}}{U_{a,\,land}}$
T_a	ΔT_a	$T_{a,\,land} - T_{a,\,lake}$
T_d	ΔT_d	$T_{d,\,land} - T_{d,\,lake}$

Analyses of predicted evaporation totals and modelled lake heat content (Section 4) during IFYGL indicates that evaporation rates are sensitive to how overland values of U_a, T_a and T_d are scaled. In general, all methods were found to perform similarly during the heating portion of the year (early March to late August), especially when wind speeds are low, say < 5 ms^{-1}. Major differences were observed during high evaporation episodes in autumn and winter, particularly with high wind speeds (say,

$U_a > 8 ms^{-1}$). In these circumstances, method (ii) underestimated evaporation rates (and thus sensible heat fluxes), in some cases quite dramatically. Method (iii) was found to predict evaporation totals that were too large compared with values recommended by the IFYGL Energy Balance Panel (Quinn and den Hartog, 1981). Method (i) was found to perform best in these circumstances (in fact, at all times of the year) and was therefore chosen as the scaling method.

Method (i) represents scaling functions in terms of fetch and overlake atmospheric stability (ΔT), which is defined as the difference between the overland air temperature $T_{a,\,land}$ and the surface water temperature T_w. Stability classifications and corresponding scaling ratios are shown in TABLE 3.2.

TABLE 3.2 - Definition of Stability and Scaling Functions.

Stability Class	Definition	R_W	ΔT_A	ΔT_d
very stable	$\Delta T \geq 10.4°C$	1.1	8.78	4.38
stable	$3.5°C \leq \Delta T < 10.4°C$	1.1	3.74	0.50
neutral	$-3.4°C \leq \Delta T < 3.5°C$	1.4	-0.17	-1.08
unstable	$-10.4°C \leq \Delta T < -3.4°C$	1.7	-2.81	-1.63
very unstable	$\Delta T < -10.4°C$	1.8	-5.26	-3.08

Values for R_W are given by Phillips and Irbe (1976); scaling ratios for air and dew point temperatures are given by Phillips and Irbe (1978).

Overlake relative humidity U_R must be re-evaluated on the basis of these scaled temperatures. U_R was evaluated from the definition of relative humidity (Barry and Chorely, 1976):

$$U_R = \frac{e}{e_s} \times 100\% \qquad [73]$$

where e_s is saturation vapour pressure (mb) at T_w and e is the actual vapour pressure (mb) evaluated as saturation vapour pressure at temperature T_d.

Values of surface atmospheric pressure obtained from the data base are equivalent sea-level pressure. These values were adjusted to surface values by application of the hypsometric equation:

$$P(z) = P_o \exp(-gz/RT_{av}) \qquad [74]$$

where P_o is sea-level pressure (mb), g is gravitational acceleration, z is surface elevation (m), R is the gas constant for air (287 $Jkg^{-1}K^{-1}$), and T_{av} is the average air temperature (K) of the layer midpoint between surface and sea-level, obtained by applying the (average) environmental lapse rate $\gamma = -6.5°C\ km^{-1}$ from the surface to the layer midpoint.

No transformations were applied to values of visibility or cloudiness.

3.2. Model Atmosphere

3.2.1. Vertical Profiles of Temperature and Humidity

Application of radiative transfer models for estimating surface fluxes requires a knowledge of vertical profiles of temperature, humidity, and atmospheric composition. These quantities were not measured in this study and therefore had to be modelled. In this study, the atmosphere was modelled as a six-layer atmosphere with three layers above 5 km and three layers below 5 km.

Temperature and humidity profiles above 5 km may be viewed as slowly varying functions of time of year. For these layers it was assumed that climatological temperature and humidity profiles for a model midlatitude atmosphere (McClatchey *et.al.*, 1972) were applicable. These authors provide climatological data for winter and sum-

mer seasons, although seasons are not defined by dates. For this study, it was assumed that summer lasted from 1 May to 31 October, while winter lasted from 1 November to 30 April.

Day to day variations in temperature, humidity, and atmospheric composition will be much greater in the lower troposphere. Vertical profiles of these quantities were generated from a knowledge of surface conditions. The lowest layer (the sub-cloud layer) was initialized first. The environmental lapse rate is assumed to be $-7.6\ ^{\circ}C\ km^{-1}$ (summer) and $-8.1\ ^{\circ}C\ km^{-1}$ during winter (Matveev, 1965). The depth of the sub-cloud layer then becomes:

$$D_6 = 300 + Z_p \quad (m) \qquad [75]$$

where D_6 is the depth of sub-cloud layer (m) and Z_p is given by (Matveev, 1968):

$$Z_p = D\Delta T_{a,d} \quad (m) \qquad [76]$$

where $\Delta T_{a,d}$ is the difference between surface air and dew point temperatures, and D is given by:

$$D = \frac{b}{b|\gamma| - H^{-1} - H_1^{-1}} \quad (mK^{-1}) \qquad [77]$$

where $b = L/R_v T_d^2$ with L being the latent heat of vaporization, R_v the gas constant for water vapour, and T_d the dew point temperature (K), $|\gamma|$ is the absolute value of the environmental lapse rate ($^{\circ}Cm^{-1}$), H_1 is the alititude of the tropopause (m) (12 km in summer, 10 km in winter), and $H = RT_d/g$, where R is the gas constant for dry air, is the scale height (m). The factor 300 (eq.[75]) is included to ensure that the depth of the first layer is not equal to zero when the air-dew point temperature difference is zero. A depth of 300 m may be considered as the approximate cloud-base altitude under completely overcast, precipitating clouds for mid-latitudes (Matveev, 1984). Pressure at the top of the sub-cloud layer is determined from the hypsometric equation where the appropriate temperature is the mean temperature of the sub-cloud layer.

Cloud, if present, is assumed to occupy layer number 5. The saturated adiabatic lapse rate is assumed to adequately describe the temperature lapse rate within cloud (McIntosh and Thom, 1979) at cloud-base temperature T_B. The corresponding saturated adiabatic lapse rate Γ_s is approximated from Rodgers (1976):

$$\Gamma_s = \frac{\Gamma[1 + (Lw_s/RT_B)]}{[1 + (L^2\epsilon w_s)/(Rc_pT_B^2)]} \quad (^{\circ}C\ km^{-1}) \qquad [78]$$

where L is the latent heat of vapourization, w_s is the saturation mixing ratio for pressure and temperature at the cloud base, R is the gas constant for air, ϵ is a constant (= 0.622), c_p is the specific heat of air (1,005 $Jkg^{-1}K^{-1}$), and Γ is the dry adiabatic lapse rate (-9.8 $^{\circ}C\ km^{-1}$).

There is no way of adequately assessing cloud depths, and since the model assumes that all cloudiness is contained within the cloud layer, cloud depths were specified as a function of time of year (TABLE D.5 Appendix D). The cloud depths given in TABLE D.5 are smaller than those frequently considered in numerical radiative transfer studies but are more representative of low stratified clouds encountered in experimental radiative transfer studies (e.g. Neiburger, 1949, Slingo *et.al.* 1982, Schmetz *et.al.* 1981).

The cloud liquid water content W is estimated from (McIntosh and Thom, 1969):

$$W = W_c\rho_a D_c \quad (gm^{-2}) \qquad [79]$$

where W_c is the equivalent condensed water:

$$W_c = \frac{\Delta T_{B-T}}{2.5} \quad (g\ kg^{-1}) \qquad [80]$$

where ΔT_{B-T} is the temperature difference between cloud-top and cloud-base, ρ_a is the average air density ($kg\ m^{-3}$) within cloud, and D_C is the cloud depth (m).

Aircraft observations of cloud liquid water contents (e.g. Slingo *et.al.*, 1982) often indicate measured values of W less than that computed from following the saturated adiabat to cloud top. The difference is accounted for by entrainment of drier air from

above cloud. Accordingly, cloud liquid water contents determined from eq.(78) were reduced by 25 percent of those estimated from eq.(78). This scaling is approximately the reduction observed from aircraft traverses through midlatitude cloud decks.

Vertical profiles in the above-cloud layer are determined once pressure and temperature at the cloud-top are determined. Layer water vapour P_W and ozone P_O amounts are evaluated from from:

$$P_W = \rho_{H_2O} f_{H_2O} D_L \quad (\text{g cm}^{-2}) \qquad [81]$$

$$P_O = \rho_{O_3} f_{O_3} D_L \quad (\text{cm–atm}) \qquad [82]$$

where ρ_{H_2O} is the water vapour density (gm^{-3}) at layer midpoint (Selby and McClatchey, 1975):

$$\rho_{H_2O} = U_R\left[A\exp(18.9766 - 14.9595A - 2.4388A^2)\right]$$

where $A = 273.15/(T_{av} + 273.15)$, T_{av} is the mean temperature of the layer (°C), U_R is the fractional relative humidity, ρ_{O_3} is ozone density (g m^{-3}) at the layer midpoint, f_{H_2O} (= 0.1) and f_{O_3} (= 46.667) are constants to convert water vapour and ozone densities to mass densities per unit altitude (Braslau and Dave, 1972), and D_L is layer thickness (km).

Layer water vapour amounts calculated from eq.(81) were then scaled for the wing-scaling approximation:

$$P_W' = P_W(\bar{P}/P_r)^{0.8} \qquad [83]$$

where $\bar{P}$ is the pressure at the layer midpoint (mb) and P_r is the reference pressure level (300 mb).

3.2.2. Optical Properties of Clouds and Aerosols

Optical properties of clouds and aerosols were evaluated from the physical properties of individual layers. Bulk layer optical depths, single scattering albedo, and

asymmetry factor must be defined when two or more atmospheric species contribute to layer attenuation of radiation. Cloud effects are restricted to layer number 5, while effects of boundary layer aerosols are incorporated in the sub-cloud layer (layer number 6).

Incorporation of aerosol effects for estimation of longwave radiative fluxes was described in Section 2.1.2.2. Shortwave radiation calculations required spectral band averages of τ, $\tilde{\omega}_o$, and g, i.e. over the visible and near infrared spectral bands defined in TABLE D.1. Average values of E_{xt}, $\tilde{\omega}_o$, and g were computed for both bands and for each value of relative humidity considered by Shettle and Fenn (1979). Because of the wide spectral limits, band-average quantities were determined as weighted averages of the spectral shortwave flux incident at the top of the atmosphere. Incident spectral interval fluxes were taken from the Labs and Neckel (1968) solar spectrum. Aerosol optical depths are determined by first estimating the particle number density as a function of surface visibility and relative humidity as described in Section 2.1.2.2. Assuming the extinction coefficient does not vary with altitude, band-average values of aerosol optical depth τ_A are given by:

$$\tau_A = \frac{E_{xt}(\lambda)_{N_D = f(V,U_R)}}{E_{xt}(\lambda)_{N_D = 20,000}} \times D_L \qquad [84]$$

Cloud optical thickness was determined from empirical relationships of cloud optical depth and cloud liquid water path (Stephens, 1978b):

$$\log(\tau_{C,V}) = 0.2633 + 1.7095 \ln[\log(W)] \qquad [85]$$

$$\log(\tau_{C,IR}) = 0.3492 + 1.6518 \ln[\log(W)] \qquad [86]$$

where $\tau_{C,V}$ is cloud optical depth in the visible band and $\tau_{C,IR}$ is cloud optical depth for the near infrared band. Stephens (1978b) has demonstrated that eqs.(85) and (86) provide excellent approximations for cloud optical thickness and that all cloud types lie on, or deviate only slightly from, these curves. This observation suggests that, for

radiative transfer calculations, cloud liquid water path is the important parameter, not necessarily cloud type per se. Band-average values of single scattering albedo and asymmetry factor for clouds are given in TABLE D.1 (Appendix D).

Bulk layer optical depth τ_B, single scattering albedo $\tilde{\omega}_{oB}$, and asymmetry factor g_B are then computed from (Leighton, 1978):

$$\tau_B = \tau_C + \tau_A + \tau_R + \tau_G \qquad [87]$$

$$\tilde{\omega}_{oB} = (\tau_R + \tilde{\omega}_{oC}\tau_C + \tilde{\omega}_{oA})/\tau_B \qquad [88]$$

$$g_B = (g_C\tilde{\omega}_{oC}\tau_C + g_A\tilde{\omega}_{oA}\tau_A)/(\tilde{\omega}_{oB}\tau_B) \qquad [89]$$

Values of Rayleigh scattering optical depth τ_R for a layer ΔP (mb) in thickness is given by:

$$\tau_R = \tau_o \Delta P/P_o \qquad [90]$$

where P_o is surface pressure (mb) and τ_o is given by (Hansen and Travis, 1974):

$$\tau_o = 0.008569\lambda^{-4}(1 + 0.0113\lambda^{-2} + 0.00013\lambda^{-4}) \qquad [91]$$

where λ is wavelength of radiation (μm). Values of τ_o for visible and near infrared bands are given in TABLE D.1 (Appendix D).

Optical depths due to gaseous absorption τ_G are given by:

$$\tau_G = \overline{k_\nu} \cdot U_G \qquad [92]$$

where $\overline{k_\nu}$ is the gaseous absorption coefficient averaged over the spectral interval (TABLE B.2) and U_G is the mass of gas in a given layer (eqs.[81] and [82]).

3.3. *Delta–D*$_2$ for Daily Totals of Shortwave Radiation

The equations describing the *Delta–D*$_2$ model describe the procedure for evaluating shortwave radiation for a single solar zenith angle. For partial cloudiness, the shortwave calculations must be performed twice: once for the clear-sky portion and once for the overcast portion of the sky. Total radiative income is then the weighted sum of the clear- and cloudy-sky radiation fluxes. Previous studies (e.g.

Fouquart and Bonnel, 1980) weight radiation fluxes according to fractional cloudiness , while calculations are often performed on an hourly basis (e.g. Atwater and Ball, 1974) to account for diurnal variations in cloudiness.

This procedure was initially implemented in this study. The results were not encouraging from the viewpoint of computing times. The reasons lie in the large number of times the radiation code was called: from 18 times per day in December to approximately 32 times per day in June for days in which partial cloudiness was recorded in each hour. The number of calls to the shortwave routine was reduced when an hour was either clear or completely overcast, although these occasions form a small portion of distribution of hourly cloudiness.

A procedure for reducing the number of calls to the shortwave radiation routine was therefore established to reduce computer time requirements. This procedure proved almost as accurate as performing calculations on an hourly basis and reduced the number of calls to the radiation to a maximum of two calls per day, independent of time of year.

The procedure partitions the day into two periods: a bright sunshine period and an equivalent overcast period. Prior to calls to the shortwave radiation routine, each daylight hour was examined to evaluate the fraction of the hour that was in bright sunshine and the fraction of the hour that was overcast. Each portion of the hour is then weighted by the cosine of the solar zenith angle at the mid-hour. This process yields four quantities:

$$C_o = \sum_{sunrise}^{sunset} f_{C_i} \qquad [93]$$

$$S_o = \sum_{sunrise}^{sunset} f_{S_i} \qquad [94]$$

$$\overline{\mu_{oC}} = \frac{1}{C_o} \sum_{sunrise}^{sunset} \cos Z_i f_{C_i} \qquad [95]$$

$$\overline{\mu_{oS}} = \frac{1}{S_o} \sum_{sunrise}^{sunset} \cos Z_i f_{S_i} \qquad [96]$$

where C_o is the duration of overcast sky, and S_o is the duration of bright sunshine, N is the duration of daylight for the day in question ($N = S_o + C_o$), f_{S_i} is the fraction of the i-th hour that is in bright sunshine, f_{C_i} is the fraction of the i-th hour that is overcast, $\overline{\mu_{oS}}$ is the mean zenith angle for the bright sunshine portion of the day, and $\overline{\mu_{oC}}$ is the mean cosine of the solar zenith angle for the overcast portion of the day. Part hours at the beginning and end of the daylight period are not considered, as radiative fluxes at these times are negligible.

Duration of overcast and bright sunshine is obtained from a knowledge of total cloudiness. The duration of bright sunshine is often assumed to have the form:

$$S_o = 1 - C \qquad [97]$$

Equation (97) can only be true at the maximum and minimum values of C, assuming the values do not change during the hour. Moreover, eq.(97) cannot be true for high-altitude clouds, such as Cirrus clouds, which transmit most of the shortwave radiation incident on them.

Analyses of the relationship between duration of bright sunshine and total cloudiness (e.g. Timanovskaya and Feygel'son, 1972) often reveals a curvlinear relationship between S_o and C where S_o is much larger for $0.2 \leq C \leq 0.6$ than predicted from eq.(97). An approximate fit to the S_o–C data given by Timanovskaya and Feygel'son (1972) is:

$$S_o = 1 - C^{(2.0 + C)} \qquad [98]$$

where C is the total fractional cloudiness. Equation (98) was applied to partition each daylight hour into bright sunshine and overcast. C_o is then determined from

$C_o = 1 - S_o$

The shortwave radiation routine is then called twice per day, once to process the clear sky portion of the day, and once to process the overcast portion of the day. Daily totals were then obtained from a weighted average of duration of clear sky and duration of overcast. For example, the direct beam radiation S is given by:

$$S = (S_o \cdot R_o + C_o \cdot R_C)/N \qquad [99]$$

where R_o is the direct beam flux for the bright sunshine period of the day and R_C is the direct beam radiation for the overcast portion of the day. Only one call to the shortwave radiation routine is required when S_o or C_o equals zero.

The majority of days over the Great Lakes will be classified as partial cloudiness which, by virtue of eq.(99), means that the shortwave calculations will have to be performed twice. The computational advantage of the block tridiagonal solution of the *Delta–D*$_2$ model is that calculations for the clear-sky are performed first. The γ and Γ matrices (eqs.[28] and [31]) will be identical for the cloud-sky case, except for the cloud layer. Thus, if these results are saved from the clear-sky calculations, as they are in this study, *only* the cloud layer needs to be processed. This greatly reduces the computation, and effectively reduces the total shortwave calculations by a factor of two. Shortwave radiation codes which solve eq.(25) with library subroutines must solve this system of equations for the clear-sky and overcast sky cases separately.

3.4. Boundary Conditions

3.4.1. Incident Top-of-the-Atmosphere Shortwave Radiation

Instantaneous incident shortwave radiation at the top of the atmosphere is given by Lambert's Law:

$$I = I_o \cdot \cos Z \cdot R^{*2} \qquad [100]$$

where R^{*2} is the (normalized) radius vector, Z is the solar zenith angle, and I_o is the solar constant (1370 W m^{-2}). The zenith angle depends on the latitude l, time of year δ

(solar

declination), and the time of day h (hour angle) according to:

$$\cos Z = \sin I \sin\delta + \cos I \cos\delta \cos h \qquad [101]$$

Mid-hourly values of $\cos Z$ are required for evaluating $\overline{\mu_{os}}$ and $\overline{\mu_{oc}}$, while daily values of R^* are required for evaluating incident shortwave radiation for each spectral interval.

Hour angle was evaluated from:

$$h = 15(12 - LAT) \quad \text{(degrees)} \qquad [102]$$

where LAT (hours) is the local apparent time (true sun time) and evaluated from (Latimer, 1971):

$$LAT = CT + \Delta L + E_t \qquad [103]$$

where ΔL is the longitudinal difference between the station longitude L_s and the standard longitude for the time zone of the station L_p (75 °W for this study)

$$\Delta L = (L_p - L_s)/15 \quad \text{(hours)} \qquad [104]$$

and CT is clock time (hours).

Spencer's (1971) approximations for R^*, δ (radians), and E_t (radians) were applied:

$$R^* = a_0 + a_1\cos\theta_o + a_2\sin\theta_o + a_3\cos 2\theta_o + a_4\sin 2\theta_o \qquad [105]$$

where θ_o is the Julian day of the year expressed in radians:

$$\theta_o = \frac{2\pi d_n}{365} \qquad [106]$$

where d_n is the day of the year (0 on 1 January, 364 on 31 December). The solar declination and equation of time are determined from:

$$\delta = a_0 - a_1\cos\theta_o + a_2\sin\theta_o - a_3\cos 2\theta_o + a_4\sin 2\theta_o - a_5\cos 3\theta_o + a_6\sin 3\theta_o \qquad [107]$$

$$E_t = a_0 + a_1\cos\theta_o - a_2\sin\theta_o - a_3\cos 2\theta_o - a_4\sin 2\theta_o \qquad [108]$$

Values of the coefficients a_i are given TABLE E.1 (Appendix E).

3.4.2. Surface Water Temperature

Surface water temperatures were modelled in this study, as measured values were unavailable prior to 1966. Schertzer and Sawchuk (1985) summarized all available surface water temperature measurements (bucket measurements from ship surveys, airborne radiometer thermometer (ART) surveys, and satellite measurements) for the lower Great Lakes for the period 1966-1983.

Figure 3.2 compares available paired surface water temperature measurements (bucket measurements from ship surveys and ART measurements) for Lake Ontario for this time period. The comparison includes paired measurements taken within 24 hours of each measurement. This time delay is not considered significant as diurnal variations in surface water temperatures are believed to be small. Strong upwelling events are an obvious exception.

Agreement between the two methods appears good. Temperatures measured from ship surveys are almost always less than corresponding temperatures from ART surveys. This may result from the the nature of bucket measurements which are usually made a few centimetres below the surface. Evaporation at the surface would account for a lower temperature.

The dashed line in Fig.3.2 represents ± 1 °C limits from the 1:1 line. The majority of comparisons fall within these limits. The root mean square error of the difference between paired measurements is 0.75 °C. This value serves as a benchmark comparison for the algorithm to estimate surface water temperatures described below.

The algorithm to estimate surface water temperature is based on the relationship between surface water temperature and the total heat content of the lake (Fig.3.3). The relationships were derived by using paired surface water temperatures and heat content values obtained from (vertical) temperature surveys conducted from vessels by personnel from the National Water Research Institute at the Canada Centre for Inland Waters. Surface water temperatures included temperatures obtained from both

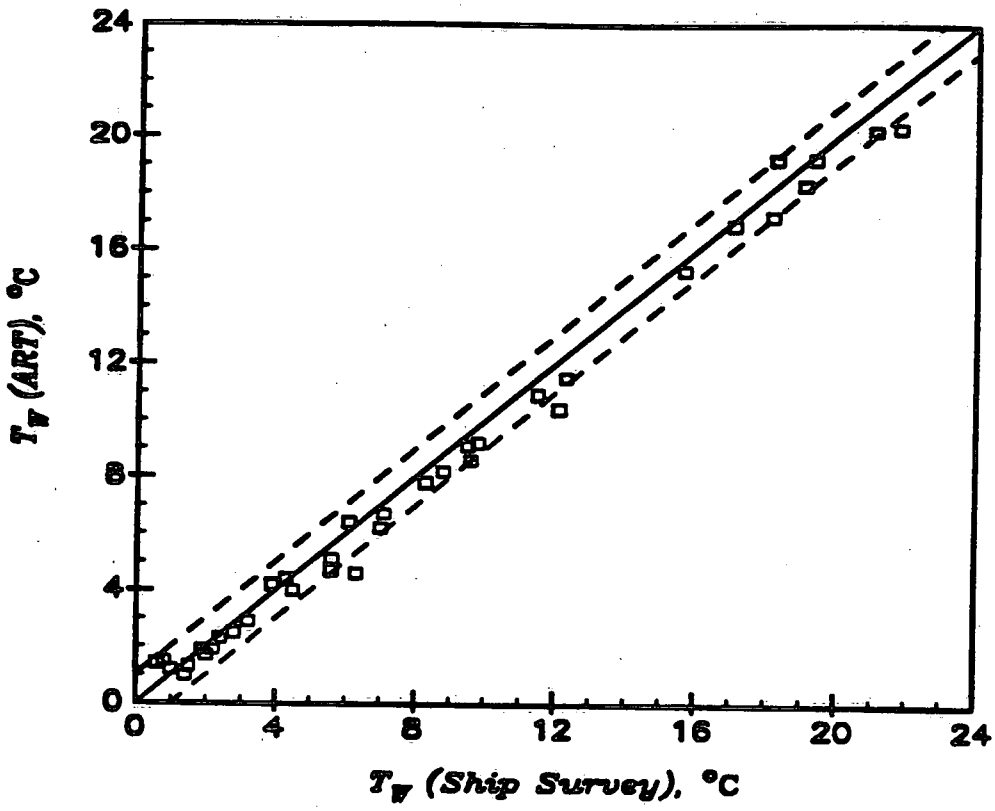

Figure 3.2 - Comparison of Paired Surface Water Temperatures (Ship and ART) for Lake Ontario, 1966-1983.

ship and *ART* surveys, so that some of the variability is accounted for by the variability between these types of measurements.

Figure 3.3 illustrates this relationship for two periods of the year: a warming phase (15 March to 10 September) and a cooling phase (11 September to 14 March). Separation of the relationship into two periods became necessary because of the large thermal inertia of the lakes. This is especially apparent for Lake Ontario where the relationship is very different for heating and cooling periods. The difference between heating and cooling periods are much less for Lake Erie because it is much shallower than Lake Ontario. For both lakes there is a much larger variability during the warming period of the year, especially during late summer when heat contents are at, or near, their maximum values. Some of this variability can be accounted for by

differences in lake levels, while much of the variability is probably accounted for by upwelling of colder water to the surface.

The relationship between T_w and Q was approximated by a linear combination of Legendre Polynomials of order 0 to 5 inclusive. These are shown as the solid and dashed curves in Fig. 3.3. Higher-order approximations were attempted but they did not appreciably reduce the root mean square error of the estimates or improve statistics of the fit. In addition, higher-order approximations displayed erratic behaviour (e.g. oscillations) near the upper and lower limits of Q. The relationship has the form:

$$T_w = \sum_{l=0}^{5} a_l Q'_l \qquad [109]$$

where the coefficients are tabulated in TABLE F.1 (Appendix F), and Q' is the scaled lake heat content to the interval $[Q_l, Q_u]$, where Q_l is the smallest measured heat content, and Q_u is the largest measured heat content. The scaling relationship is:

$$Q' = (2Q - Q_l - Q_u)/(Q_u - Q_l) \qquad [110]$$

Equation (110) converts Q to the interval [-1, 1] as required for the evaluation of the Legendre Polynomials implicit in eq.(109). Values of Q_u and Q_l are given in TABLE F.1 (Appendix F).

Statistics of the approximation (eq.[109]) are shown in TABLE 3.3, which summarizes root mean square errors of the difference between predicted and observed surface water temperatures for data given in Figure 3.3.

TABLE 3.3 - Root Mean Square Errors of Differences between Predicted (eq.[109]) and Observed Surface Water Temperatures (°C).

	Lake Ontario	Lake Erie	Lake Erie	Lake Erie	Lake Erie
Warming Phase	1.32	1.19	1.14	1.12	1.09
Cooling Phase	1.05	0.98	0.87	0.82	1.11

TABLE 3.3 illustrates that, in almost all cases, the approximations perform better dur-

Figure 3.3 - Relationship between Surface Water Temperature T_w and Total Lake Heat Content Q for Lake Ontario, Lake Erie, and Lake Erie Basins (upper half). Relationship between Q and T_w is shown in the lower half. Full line represents warming period; dashed line represents cooling period.

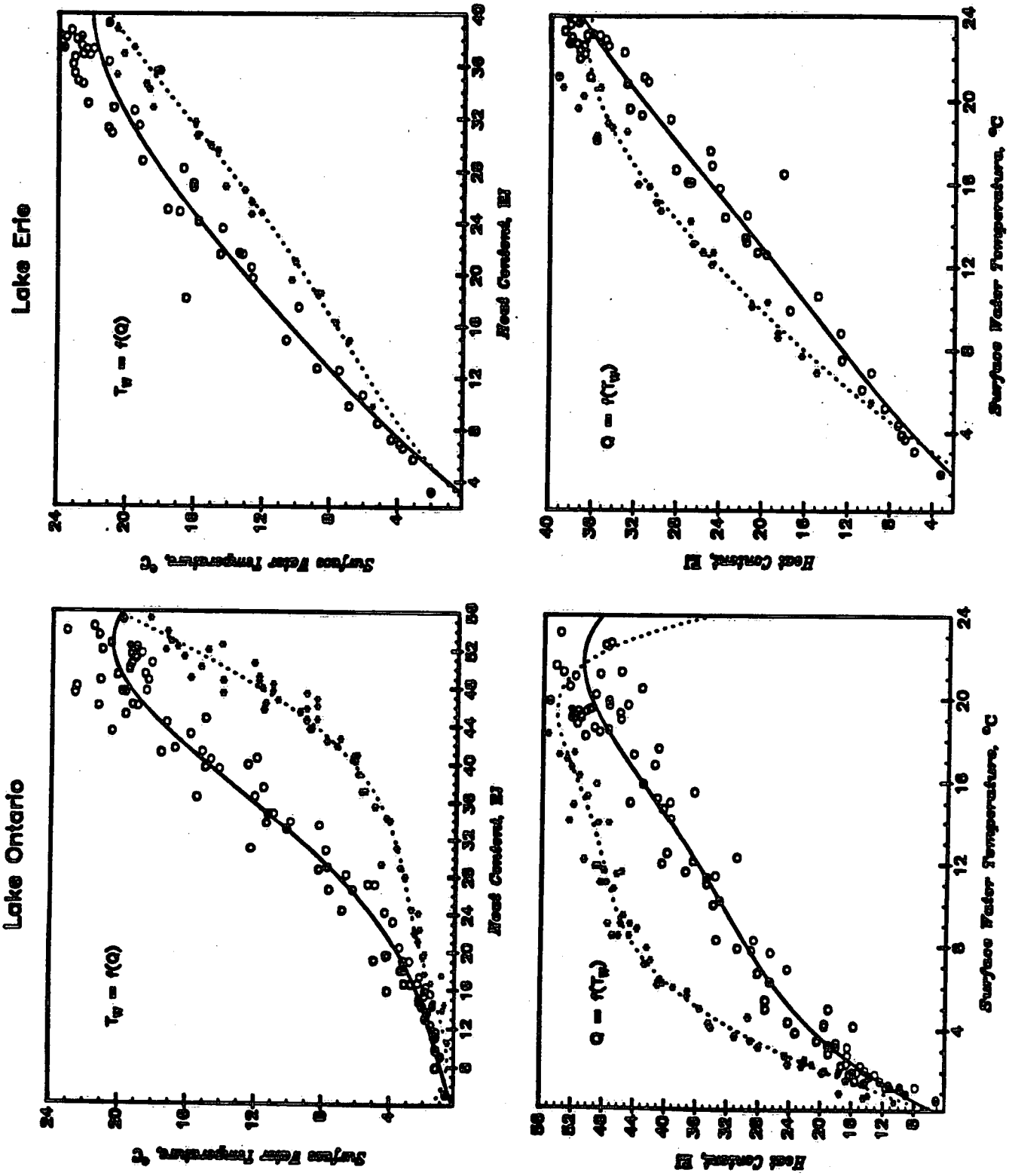

Figure 3.3 - continued.

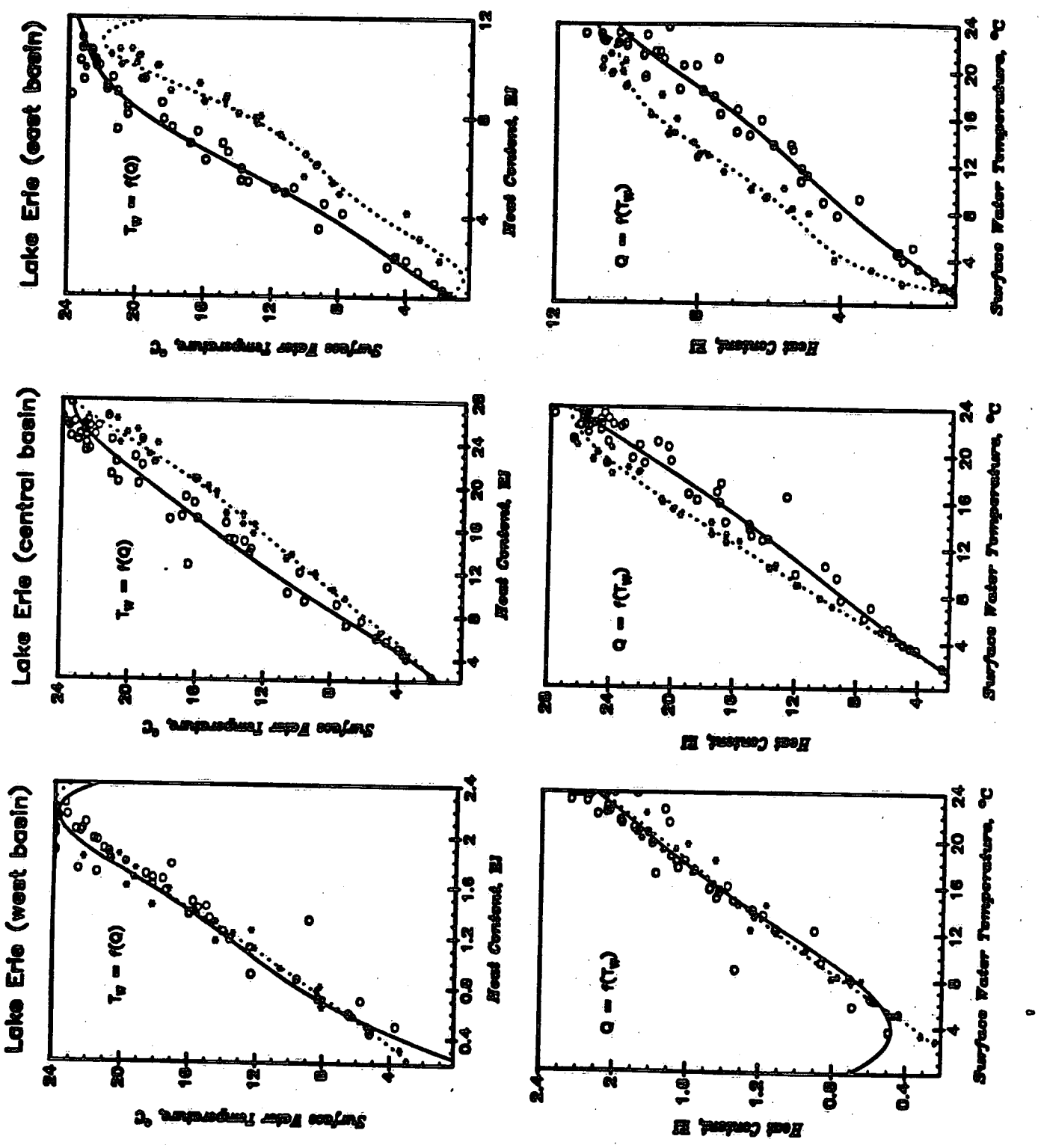

ing

the cooling period than the warming period.

Root mean square errors are slightly larger than the root mean square error of the difference between bucket and *ART* surface water temperatures during the cooling period. Root mean square errors average 0.97 °C during the cooling phase and 1.15 °C during the warming phase, reflecting the effects of upwelling of cold water. This effect is most evident for Lake Ontario, which is the deepest of the water bodies considered.

The lower half of Fig. 3.3 shows the inverse relationship $Q = f(T_w)$. This relationship, derived in exactly the same manner as eq.(109), is applied once and only once at the start of the simulation. Surface water temperature is initialized either by specifying a known value for T_w or estimating the mean daily surface water temperature (described below). The inverse relationship is then called to estimate the lake heat content on the day immediately prior to first day of the simulation. For each day of the simulation, Q_t is evaluated from the energy balance equation. Lake heat content is then updated by adding the surface- integrated surface heat flux to the lake heat content. Surface water temperature for the following day is then evaluated from the direct relationship $T_w = f(Q)$ (eq.[109]). In the event of missing data for a day, the process is modified to estimate daily T_w from a function for mean daily T_w. Lake heat content is then updated with this value of T_w.

Daily mean T_w was estimated from linear combinations of Legendre Polynomial functions (order 0 to 15, inclusive) using all available surface water temperature measurements (Schertzer and Sawchuk, 1985) for each of the water bodies examined in this study. These approximations are similar to those developed for eq.(109), except that the dependent variable is Julian day. Coefficients and scaling functions are provided in TABLE G.1 (Appendix G), while the resulting functions are plotted in Figure 3.4.

Figure 3.4 - Mean Daily Surface Water Temperature for Lake Ontario, Lake Erie, and the Basins of Lake Erie, 1966-1983. From Schertzer and Sawchuk (1985). Symbols represent surface water temperature collected by ship survey (open squares), *ART* (open circles), and satellite imagery (open diamonds).

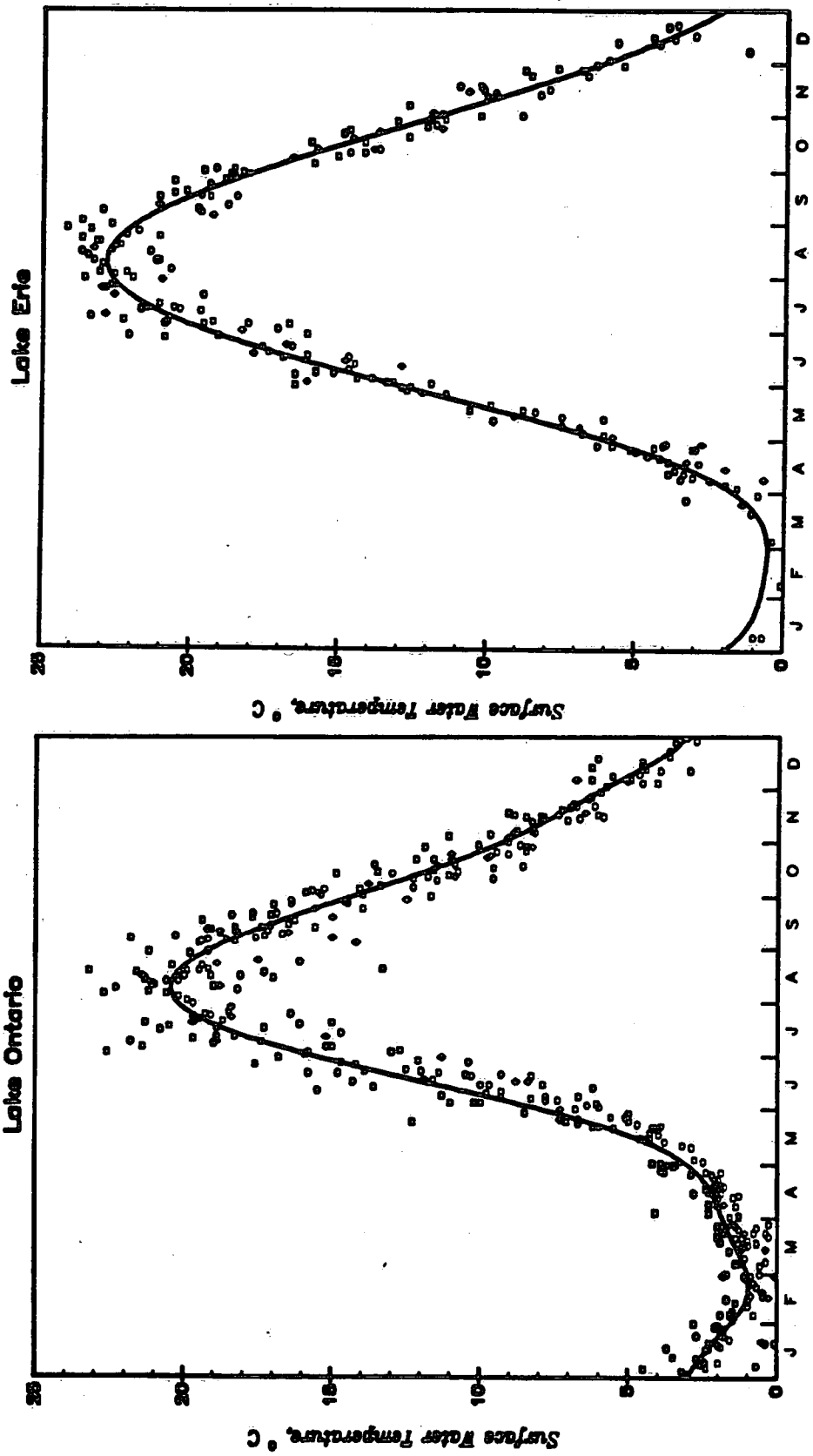

Figure 3.4 - continued.

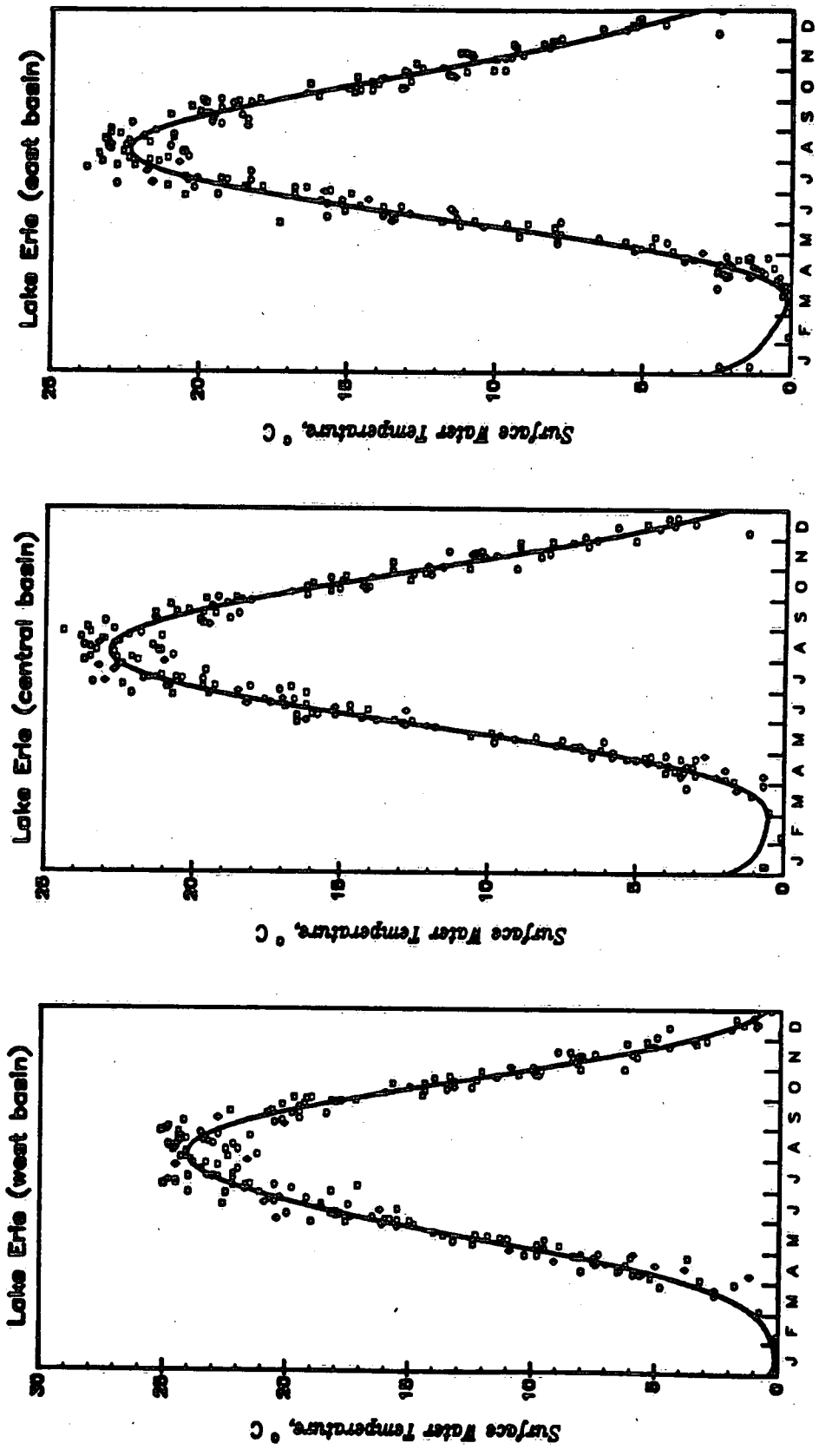

4. MODEL VERIFICATION TESTS

Individual model components were tested with data for Lake Ontario for the period May, 1972, to March, 1973 (IFYGL). Lake Ontario was intensively monitored during this period and the resulting data base has served as the basis for model verification of many radiation (e.g. Atwater and Ball, 1974; Davies *et.al.*, 1975) and energy balance studies (e.g. Elder *et.al.*, 1974; Phillips, 1978; Quinn, 1978), since that time. This study adheres to this practice. Model verification included assessment of overlake meteorological conditions, radiative fluxes, turbulent fluxes, ice concentrations, surface heat flux, and estimated lake heat contents.

Many of the comparisons between model estimates and measured values are presented in graphical form. Numerical measures of goodness-of-fit include root mean square error E_{rms}, mean bias error E_{mb}, and the index of agreement D. The root mean square error,

$$E_{rms} = \left[\frac{1}{N}\sum_{j=1}^{N}(x_e - x_o)^2\right]^{1/2} \qquad [111]$$

where x_e is the estimated variate, x_o is the observed or measured value, N is the total number of observations, indicates the size of the difference between model estimates and measured values (defined as error in this study). The mean bias error is defined as:

$$E_{mb} = \frac{1}{N}\sum_{j=1}^{N} d_j \qquad [112]$$

where d_j is the j-th deviation. The mean bias error describes the tendency of the model to overestimate or underestimate over the entire data set.

The index of agreement (Willmott, 1981) is defined as:

$$D = 1 - \frac{\sum_{j=1}^{N}(x_{ej} - x_{oj})^2}{\sum_{j=1}^{N}\left[|x'_{ej}| + |x'_{oj}|\right]^2} \qquad [113]$$

where $x'_{ej} = x_{ej} - \bar{x}_e$ and $x'_{oj} = x_{oj} - \bar{x}_o$, where the overbar denotes the mean. The *D*–statistic estimates the overall agreement between model estimates and measured values. As described by Willmott (1981), "*D* specifies the degree to which the observed deviations [about $\bar{x}_o$] correspond, both in magnitude and sign, to predicted deviations [about $\bar{x}_o$]". The numerator in the second term on the right-hand side of eq.(113) can be shown to represent the portion of unexplained error, while the denominator represents the total potential error. Physically, *D* represents the fraction of explained error accounted for by the model and ranges from 0 (little or no agreement) to 1 (perfect agreement). The advantage of this *D*–statistic, as opposed to the correlation coefficient, is that assumptions regarding the underlying distribution of the independent variable are not required. Moreover, "unlike the correlation coefficient, the *D*–statistic is sensitive to differences between the observed and predicted means as well as other changes in proportionality" (Willmott, 1981).

4.1. Overlake Meteorological Data

Comparison of model estimates of overlake air temperature, dew point temperature, wind speed, and cloudiness, are shown in Figs. 4.1 - 4.3.

Figure 4.1 compares mean three-day air overlake temperatures (thin line) with buoy measurements (thick line) compiled by Almazan (1980). This was the smallest time interval for which comparisons could be made. Deviations are shown in more detail in Fig. 4.1(b). The root mean square error of the deviations is 2.2 °C, while the mean bias error is -0.2 °C. Figure 4.1(b) illustrates that the model both overestimates and underestimates overlake air temperature. In general, model underestimates are larger in magnitude than overestimates, accounting for a negative mean bais error.

Figure 4.1 - Comparison of Estimated Three-Day Mean Air Temperatures (thin line) with Measured Values (thick lines) over Lake Ontario, 1 May to 30 November, 1972. From Almazan (1980).

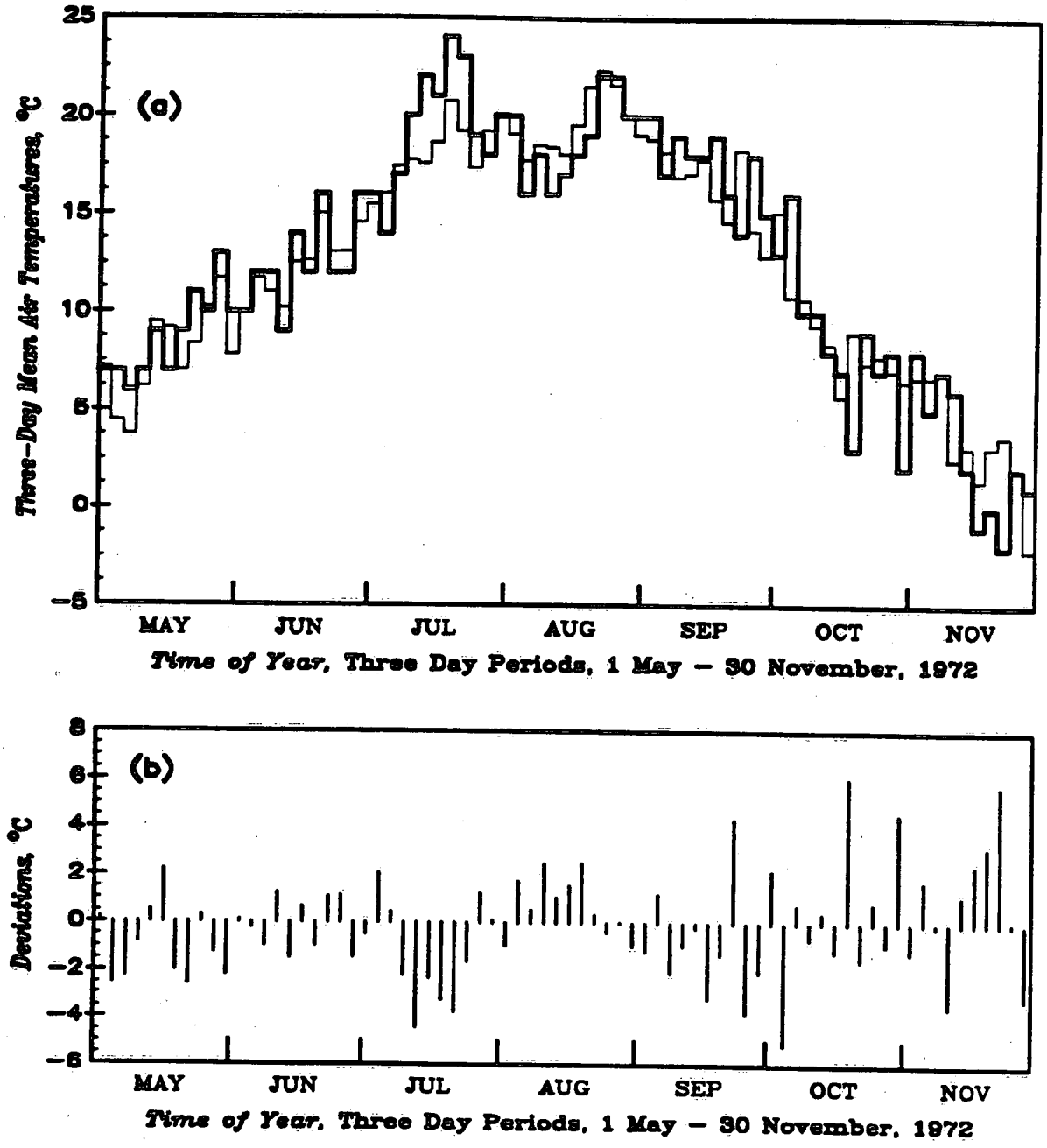

Model estimates are generally in phase with measured values and show best agreement from May through early July. The magnitude of errors appears to increase thereafter. Part of the explanation must lie with errors in surface water temperature (Section 4.2), because the scaling functions for overlake meteorological variables are

functions of the difference between overland values and surface water temperature. Figure 4.4 illustrates that surface water temperature was overestimated during July. This would decrease ΔT, thereby decreasing the scaling for overlake air temperature, thus accounting for the large underestimates shown for July.

Largest model overestimates occur during October and November. These overestimates appear to be associated with the first outbreaks of true Arctic air over the lake. Although errors in surface water temperature may be a contributing factor, the analysis seems to suggest that the open-ended nature of the scaling functions (Table 3.2) for very stable and very unstable classes may be contributing to these overestimates. This seems particularly true for overestimates during November, when surface water temperature is well estimated.

Figure 4.2(a) compares mean monthly overlake air temperature estimates (thin line) with buoy measurements averaged over the lake (thick line) tabulated by Almazan (1980). The root mean square error (1.1 °C) and mean bias error (0.09 °C) both decrease with the increase in averaging period. Figure 4.2(a) suggests that air temperatures are generally underestimated during the summer months by approximately 1 °C and overestimated during the winter months, although the sample size (= 8) is small.

Figure 4.2(b) compares mean monthly dew point temperature estimates (thin line) with values tabulated by Quinn and den Hartog, (1981) (thick line). The root mean square error (1.1 °C) is similar to that for air temperature while the mean bias error (–0.8 °C) indicates an overall underestimate. Nine of the 11 months have underestimated dew point temperatures, with the largest errors occurring during the months of September to November when the difference amounts to approximately 1.6 °C.

Figure 4.2(c) compares mean monthly wind speed estimates (thin line) with measured values (thick lines) from towers (8 m) and buoys (3 m and 4 m) (Almazan, 1980).

Figure 4.2 - Comparison of Estimated Monthly Mean Air Temperature (a), Dew Point Temperature (b), Wind Speed (c), and Wind Speed over Central Basin of Lake Ontario (d) with Observed Values during IFYGL. Dew point temperatures given by Quinn and den Hartog (1981); values of wind speed and air temperature are from Almazan (1980).

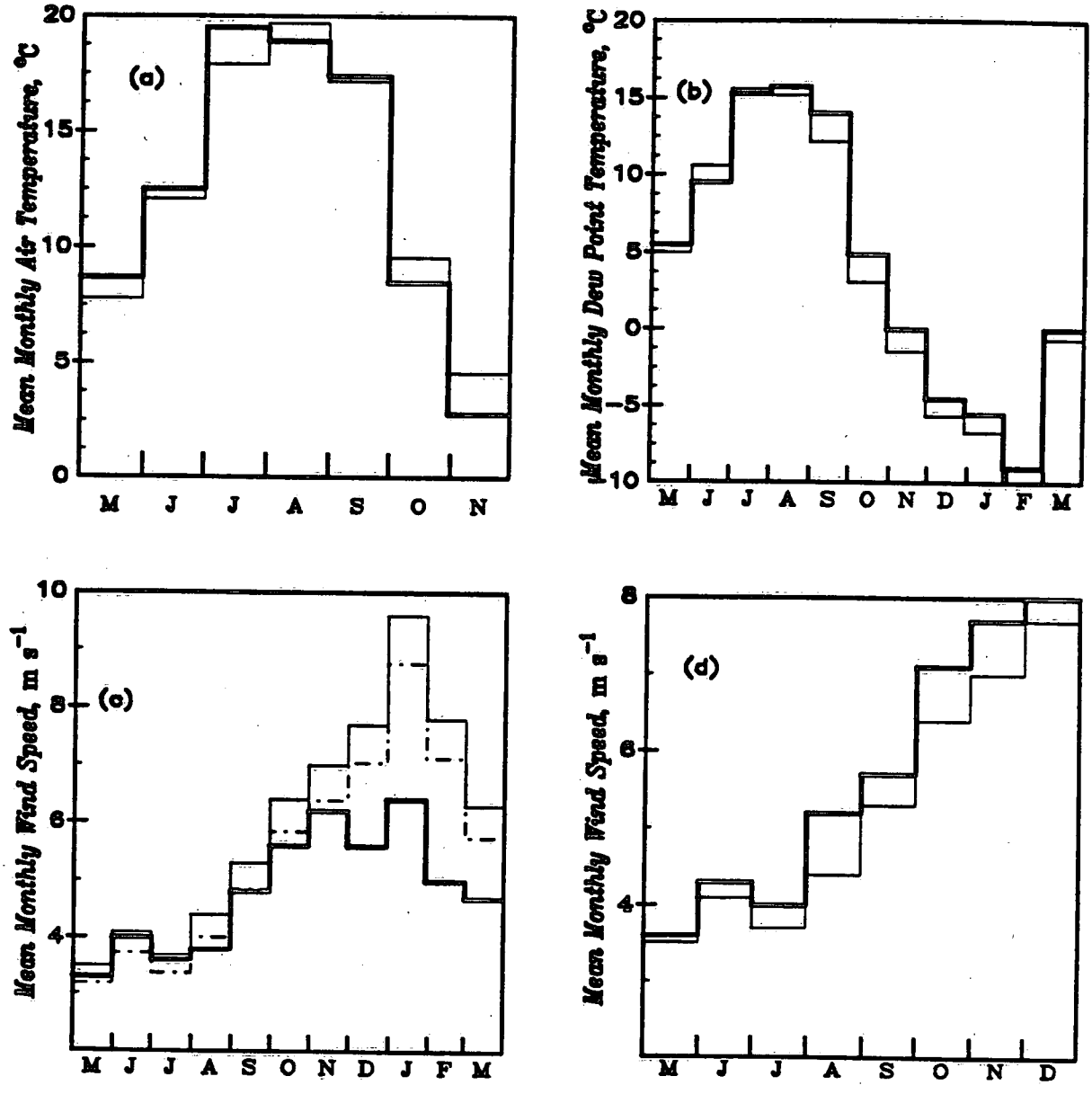

Average wind speeds tabulated by Almazan (1980) refer to a reference height of 3 m and were obtained by assuming neutral stability and the logarithmic wind profile. Wind speeds in this study refer to a height of 8 m. There is generally good agreement between estimated and measured wind speeds, especially in the spring and early

summer months when the differences are less than 0.1 m s^{-1}. The errors are much larger from December to March when the difference averages more than 2 m s^{-1}. The large differences at this time of year account for a root mean square error of 1.6 m s^{-1} and a mean bias error of 1.16 m s^{-1} for the entire study period. Part of the disagreement arises from the uncertainty of wind speed values during the winter months tabulated by Almazan. Many of the buoys stationed in Lake Ontario became inoperative in early December. Almazan does not indicate how wind speeds from December to March were determined.

Part of the disagreement is also due to differences in reference levels. This difference can be (partially) removed by transforming estimated wind speeds to 3 m. Assuming neutral stability and the logarithmic wind profile:

$$\frac{U_8}{U_3} = \frac{\ln z_8 - \ln z_o}{\ln z_3 - \ln z_o} \qquad [114]$$

where z is height (m), U are wind speeds, and z_o is the roughness height (0.01 cm (IFYGL Atmospheric Boundary Layer Panel)), $U_3 = 0.913 U_8$. These values are shown as the dash-dot lines in Figure 4.2(c). The agreement has improved, with the root mean square error at 1.1 m s^{-1} and mean bias error of 0.6 m s^{-1}. The maximum difference is 2.4 m s^{-1} in January.

A more instructive comparison is Figure 4.2(d) where estimated wind speeds (thin line) are compared with average wind speeds derived from buoys in central basin of Lake Ontario, which is what the model is attempting to simulate. The agreement over this time period appears quite good. The root mean square error is 0.5 m s^{-1} and the mean bias error is –0.4 m s^{-1}, which as Figure 4.2(d) demonstrates, represents a consistent underestimate. These differences must be larger on a daily basis. Unfortunately, there are no published tabulations of average daily wind speeds. Such tabulations would provide a better verification of scaling functions applied in this study.

Atwater and Ball (1974) performed extensive analyses of cloudiness over Lake Ontario during IFYGL. These authors combined cloud data from land stations, ship surveys, and satellite imagery, to form a cloud data-base for IFYGL. In addition, regression equations were developed to account for lake effects on cloudiness. Two effects were considered. First, during springtime, it was assumed that the lake surface was much colder than the overlying air. This condition strongly suppresses cloudiness over the lake in comparison to values reported at land stations. The second effect occurred during autumn when the lake surface was warmer than the overlying air. These circumstances would enhance convective activity over the lake surface, so that cloudiness, especially low level cloudiness, could be expected to be greater over the lake compared to values at land stations. The correlation coefficients for these statistical relationships were on the order of 0.25, corresponding to a coefficient of determination (percentage of explained variation) of approximately 6 percent. The low degree of explanation attests to the difficulty of quantifying lake effects on cloudiness.

Figure 4.3 illustrates the deviations between estimates of daily total cloudiness and values tabulated by Atwater and Ball (1974). Deviations are positive when values from the present study exceed values given by Atwater and Ball, and negative otherwise. The root mean square error of these deviations is 0.13, which is close to the estimated uncertainty of cloudiness observations. The largest discrepancy between the two cloudiness values occurs during May, when differences reach 0.92. The difference may arise from Atwater and Ball's fog model, which predicts almost complete overcast on these days. There is some evidence (Section 4.3.1) that Atwater and Ball's cloudiness values on these days are much too large. Their estimated incoming shortwave radiation on these days are underestimated by over 20 MJ m^{-2} day^{-1}. Their cloudiness values must therefore be seriously in error.

Differences between the two data sets are much less for the remainder of the

Figure 4.3 - Comparison of Estimated Daily Overlake Total Cloudiness with Values Reported by Atwater and Ball (1974) over Lake Ontario during IFYGL. Deviations are defined as the difference of Atwater and Ball's values from values in the present study.

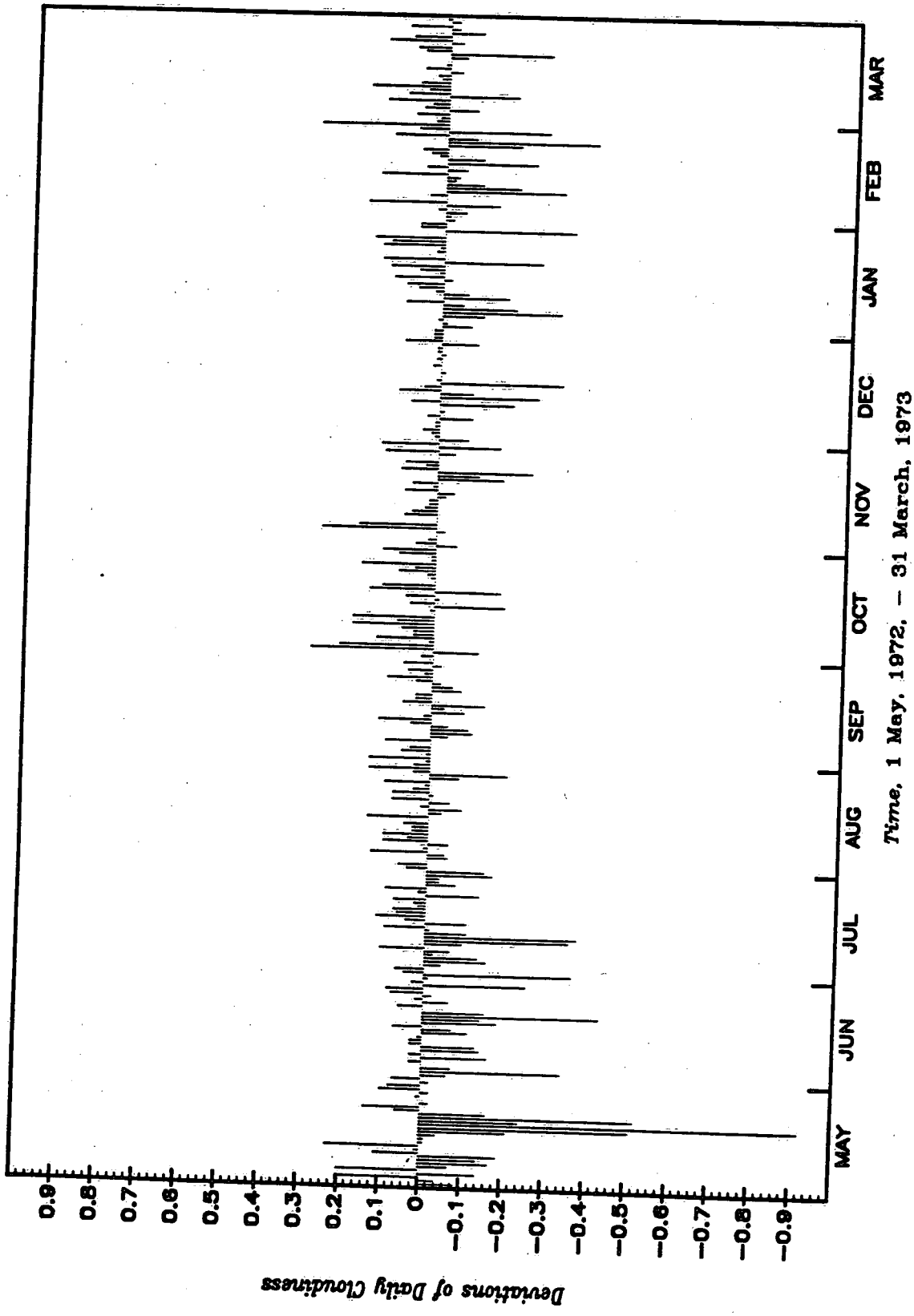

study period. Values for the present study appear as positive deviations on most days from September to March, although the differences are not much greater than could be expected from the uncertainty of cloud observations. Mean monthly estimates of incoming shortwave radiation (Section 4.3.1) are underestimated by amounts of order 0.1 MJ m^{-2} day^{-1}, however, these differences could easily arise from assumed cloud depths. Cloudiness values also appear overestimated during September and October. These months are also months in which incoming shortwave radiation is overestimated. There is thus little evidence to suggest cloudiness values in the present study are in serious error.

4.2. Surface Water Temperatures

Comparison of estimated and measured surface water temperatures during IFYGL are illustrated in Figure 4.4. The full line shows estimated daily surface water temperatures while symbols represent measured values. The measured values include both ship and *ART* surface water temperatures. For this reason error bars, representing 0.75 °C, have been included on measured values. Deviations between estimated and measured values are shown in more detail in Figure 4.4(b).

Figure 4.4 demonstrates generally good agreement with measured values. The root mean square error of the deviations is 1.24 °C which is within the range of root mean square errors for the temperature-heat content relationship for the lower Great Lakes (Section 3.4.2). The mean bias error is positive, as is evident from Figure 4.4(b).

Largest errors occur on a few selected dates. These dates correspond to major upwelling and hydrodynamical events in Lake Ontario. The large overestimates during the latter half of June, 1972, for example, are associated with Hurricane Agnes (Boyce *et.al.*, 1977), while colder upwelled water near the middle of August was associated with the "Betty" storm. Boyce *et.al.* noted other major upwelling events on 19 September, 18 October, and 1 to 7 November. Overestimated surface water temperature on these dates are clearly shown in Figure 4.4(b). These results were not

anticipated when the temperature-heat content relationship was developed. The effects, however, do not appear long-lasting, because the temperature- heat content relationship is a strong negative feedback mechanism. There appears to be a rapid adjustment in most instances. October seems to be a general exception, although, as shown later, evaporation totals for October are in excellent agreement with recommended values (IFYGL Energy Balance Panel).

There are two discontinuities in the estimated surface water temperatures. These occur on 10 September, when surface water temperature decreases from approximately 20.5 °C to 16 °C, and on 15 March, when temperature increases from approximately 1.5 °C to 2.5 °C. These discontinuities arise from the switchover of the temperature-heat content relationship from heating to cooling phase and cooling to warming phase, respectively. Both functions predict nearly the same surface water temperature in mid-March and the resulting temperature discontinuity is small, usually less than 1 °C.

The resulting temperature discontinuity in mid-September, however, *can* be large. Only if the position on the warming phase function is close to the intersection of the warming and cooling phase functions will the resulting discontinuity be small. One method of avoiding potentially large temperature discontinuities is to rescale the problem as follows. One first estimates the heat content for the first day of the cooling phase and the heat content from the cooling phase relationship assuming temperature continuity and average these two values. Surface water temperature is then re-initialized, using the $T_w = f(Q)$ relationship. This value of T_W is then used as the surface water temperature for the first day of the cooling phase. This procedure produces an error in T_W of less than 2 °C, which is less than errors resulting from the inability to simulate upwelling of colder sub-surface water.

Figure 4.4 - Comparison of Estimated Daily Surface Water Temperature with Measured Values (Schertzer and Sawchuk,1985) during IFYGL.

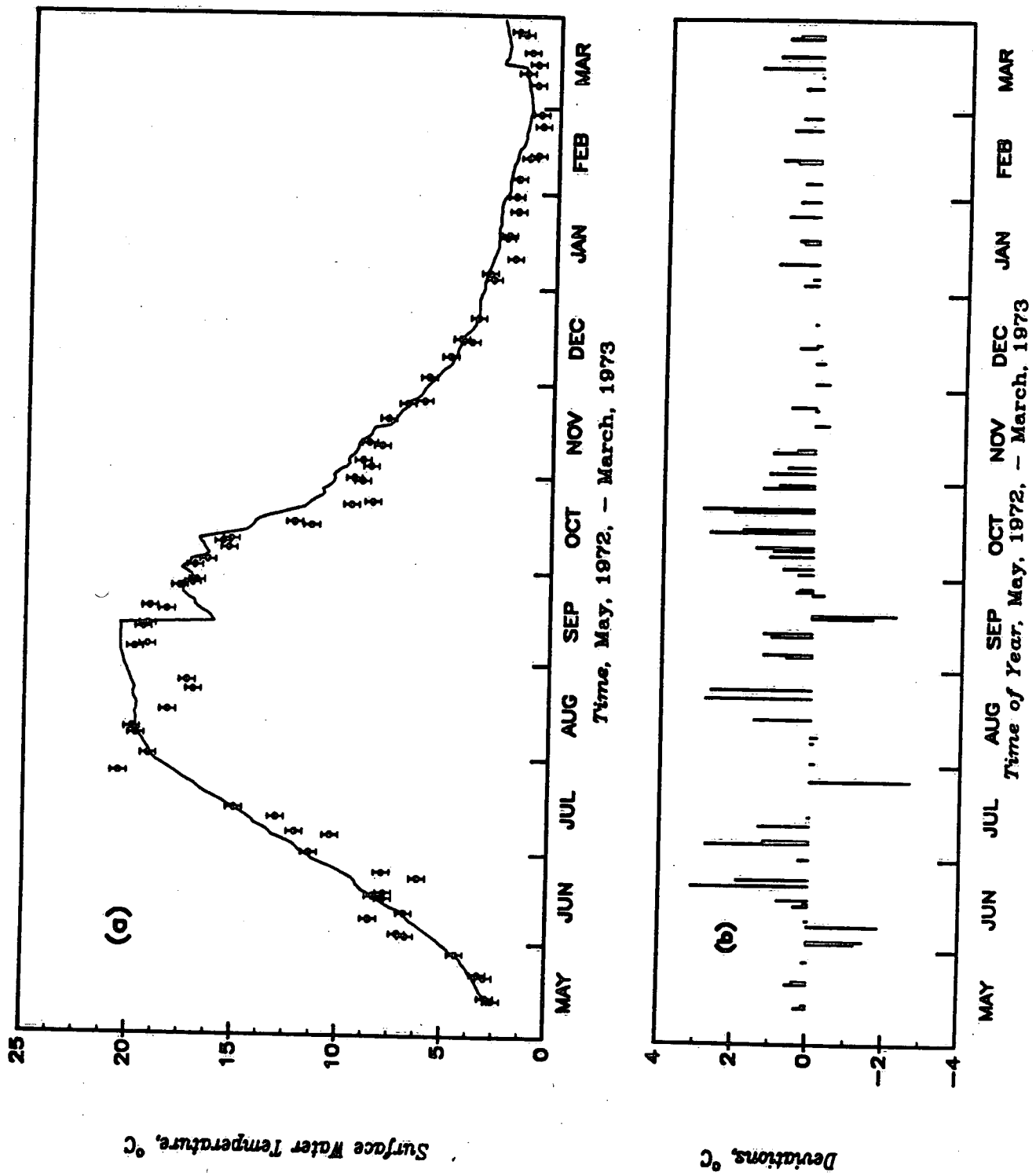

4.3. Surface Radiation Fluxes

This section summarizes comparisons of estimated and measured surface radiation values. Davies and Schertzer (1974) compiled measured surface radiation totals for a number of stations in and around Lake Ontario during IFYGL. Values included all components of the surface radiation balance for each of 13 zones comprising Lake Ontario. These data have been used to derive maximum and minimum daily flux densities and a mean daily value by areally weighting values recorded for each zone.

The comparisons presented in this section include estimates of radiation fluxes by Atwater and Ball (1974). These authors performed radiation calculations at a number of grid points over Lake Ontario to describe spatial and temporal variations of surface radiation fluxes over the Lake Ontario. These radiation values were applied by the IFYGL Energy Balance Panel to estimate evaporation totals, as well as other parameters.

Incoming shortwave, incoming longwave, and net radiation, are considered in this section. The first two fluxes represent the largest components of the surface radiation balance and are the most difficult to model, as they are strong functions of the state of the atmosphere and ground surface. Errors in reflected shortwave and longwave fluxes are much smaller; analysis of net radiation will include effects of errors in these fluxes.

4.3.1. Incoming Shortwave Radiation

Incoming shortwave radiation comparisons are shown in Figures 4.5 - 4.8. Figure 4.5 illustrates the range and estimates from the present study (upper half) and Atwater and Ball (lower half) expressed as deviations from mean measured values. Vertical scales for graphs are not the same. Figure 4.5 illustrates that the shortwave radiation model developed in this study is capable of estimating incoming shortwave radiation quite well. Daily estimates are almost always within the range of measured values.

Largest errors occur during the spring and early summer months, as is the case with Atwater and Ball's model. The *Delta–D*$_2$ model, however, both overestimates and underestimates. This contrasts with results from the Atwater and Ball model, where errors of the same sign tend to occur for several consecutive days. Moreover, these errors are large, amounting to 10 to 20 MJ m^{-2} day^{-1}. Averaged over the surface area of the lake, this must seriously underestimate surface heat flux. It seems likely that cloudiness values employed by Atwater and Ball for these days were seriously overestimated.

Averaged over the study period, the root mean square error of estimates from the *Delta–D*$_2$ model are 2.46 MJ m^{-2} day^{-1}. This is a large improvement from the corresponding value from the Atwater and Ball model of 3.6 MJ m^{-2} day^{-1}. Both models provide acceptable estimates during the winter months, although estimates from the Atwater and Ball model are consistent underestimates. This may stem from their model which neglects multiple scattering effects.

The distribution of radiation estimate errors are illustrated in Fig. 4.6. Figure 4.6 illustrates that errors from mean measured values (Fig. 4.6(a)) and from the range (Fig. 4.6(b)) are more evenly distributed for the *Delta–D*$_2$ model. Errors from the Atwater and Ball model tend to be negative, demonstrating that, overall, the Atwater and Ball model tends to underestimate incoming shortwave radiation. This may be the result of both model formulation and cloud input data, which, however, was more detailed than available for this study.

Figure 4.7 compares incoming shortwave radiation estimates from both models as a function of cloudiness. The intervals represent 0.1 total cloudiness. Figure 4.7 shows that there is not a large difference in estimates for $C>0.6$ (*Delta–D*$_2$ estimates have a lower E_{rms} in all cases). The major difference between model estimates occurs when the sky is partially overcast with small cloud amounts. *Delta–D*$_2$ estimates are superior in these circumstances, which is important because these conditions are

Figure 4.5 - Deviations of Estimates (present study - upper half; Atwater and Ball (1974) - lower half) of Daily Incoming Shortwave Radiation from Mean Measured Values (Davies and Schertzer, 1974) over Lake Ontario, 1 May, 1972, to 31 March, 1973.

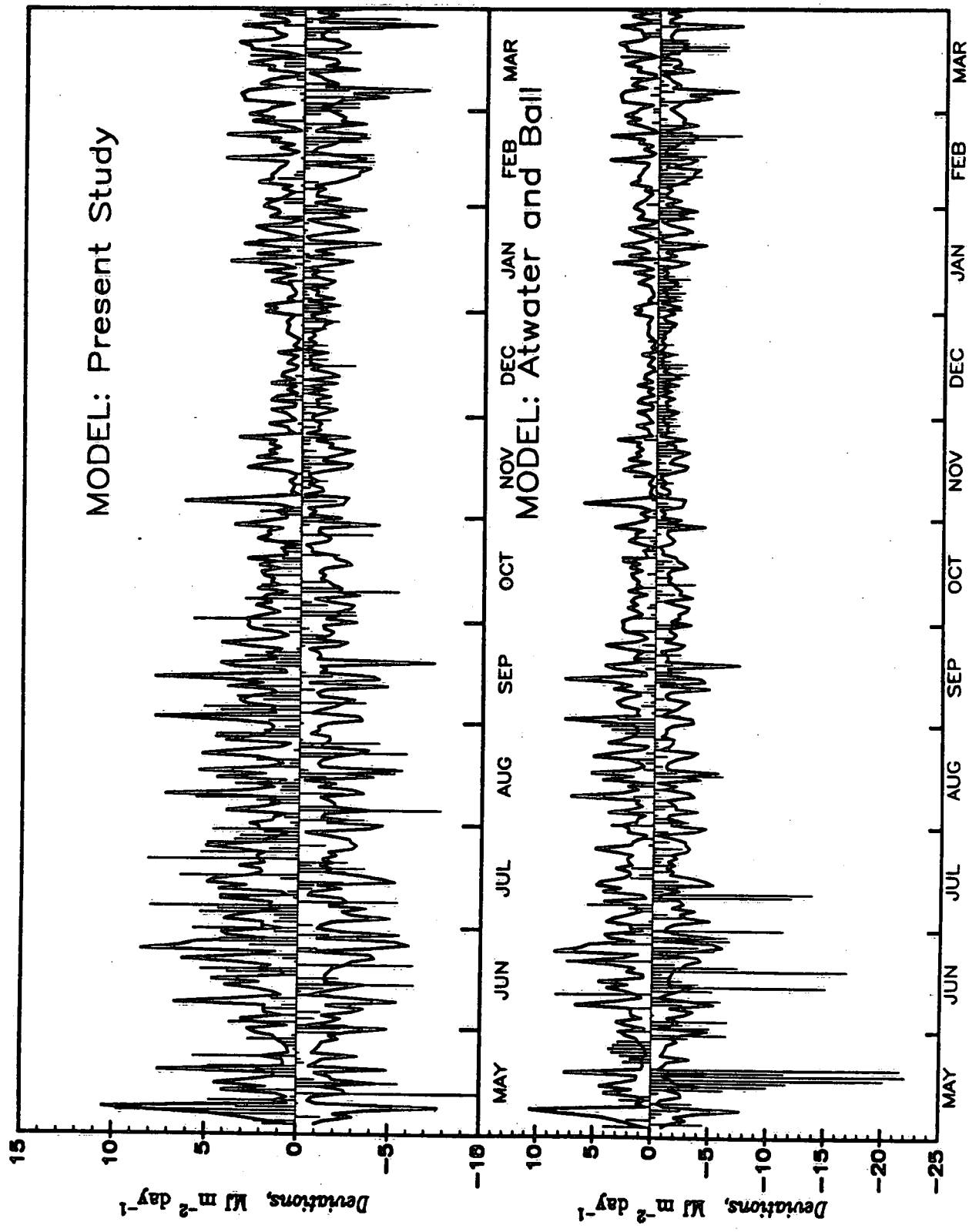

Figure 4.6 - Frequency Distribution of Absolute Errors (Difference of Mean Measured Values from Estimated Values) of Estimates of Daily Incoming Shortwave Radiation. Solid line refers to results from present study; dashed line for Atwater and Ball's (1974) results. (a) refers to deviations from mean measured values; (b) refers to deviations from the range.

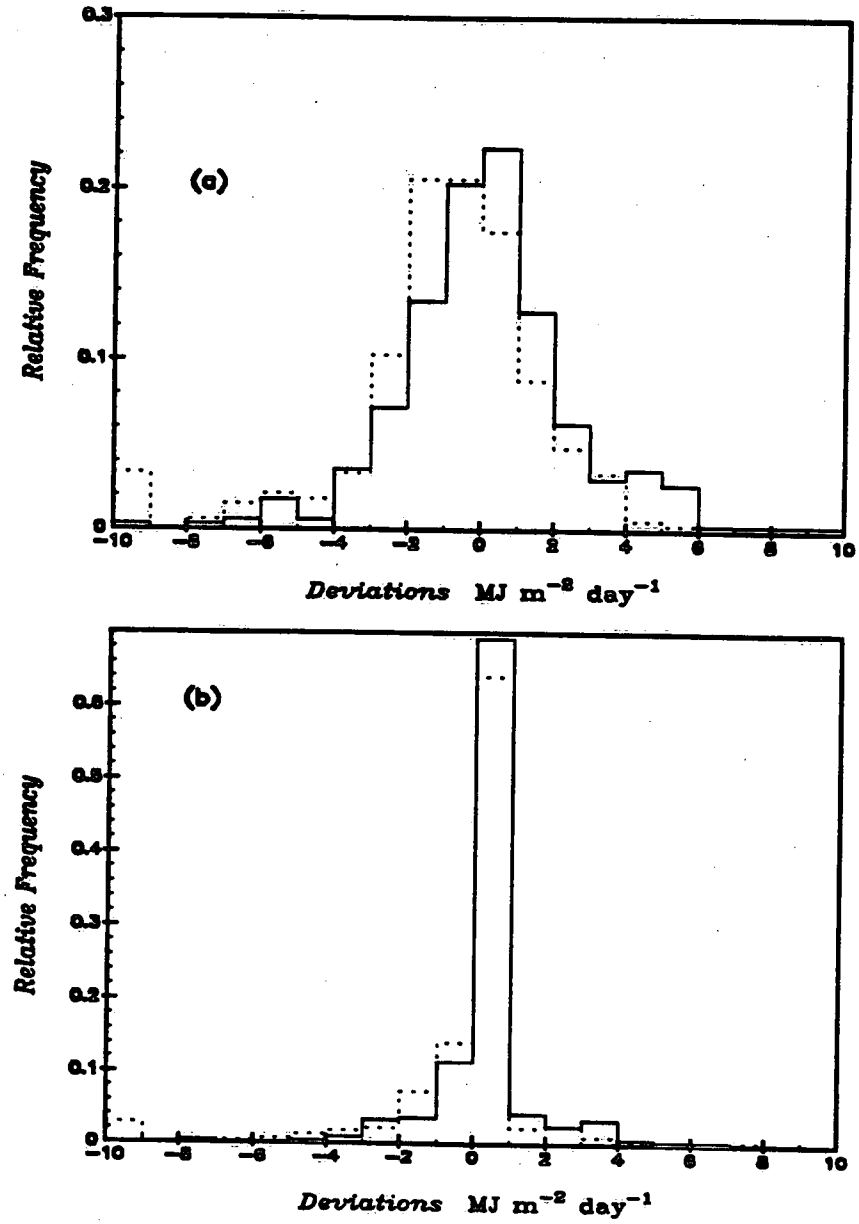

associated with large radiative gains at the surface, especially during spring and early summer months.

Figure 4.8 illsutrates the effect of averaging period on root mean square errors and *D*–statistic for periods ranging from 1 to 10 days. Root mean square errors for *Delta*–D_2 estimates decrease almost exponentially with increase in averaging period.

Figure 4.7 - Comparison of Estimates of Daily Incoming Shortwave Radiation as a Function of Cloudiness over Lake Ontario, 1 May, 1972, to 31 March, 1973. Symbols represent results from present study (full circles) and Atwater and Ball (1974) (open circles). Diagonal lines represent the 1:1 line.

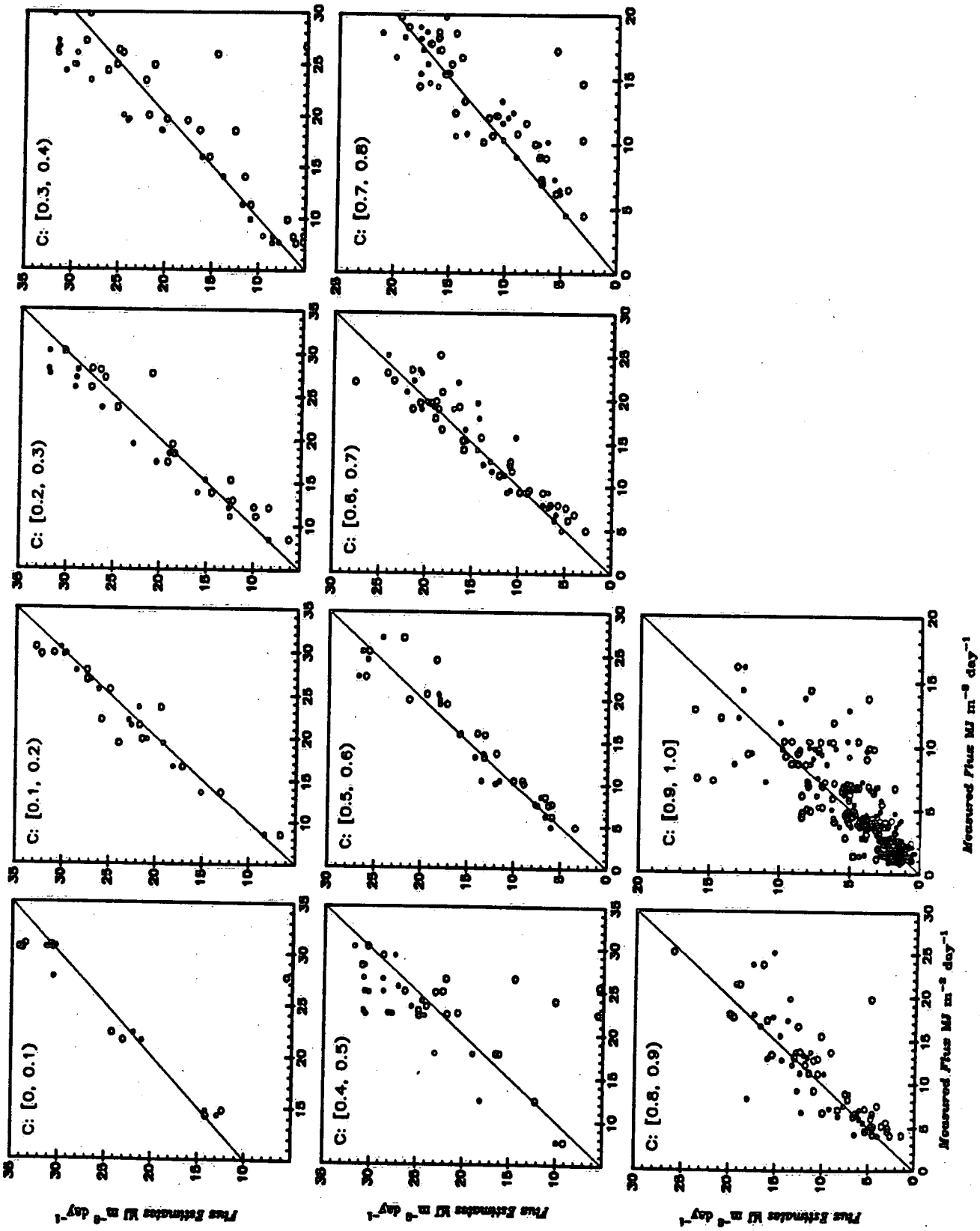

Figure 4.8 - Comparison of Root Mean Square Errors and D-Statistics of Estimates of Daily Incoming Shortwave Radiation over Lake Ontario, 1 May, 1972, to 31 March, 1973, as a Function of Averaging Period. Symbols represent results from present study (*) and Atwater and Ball (1974) (open circle).

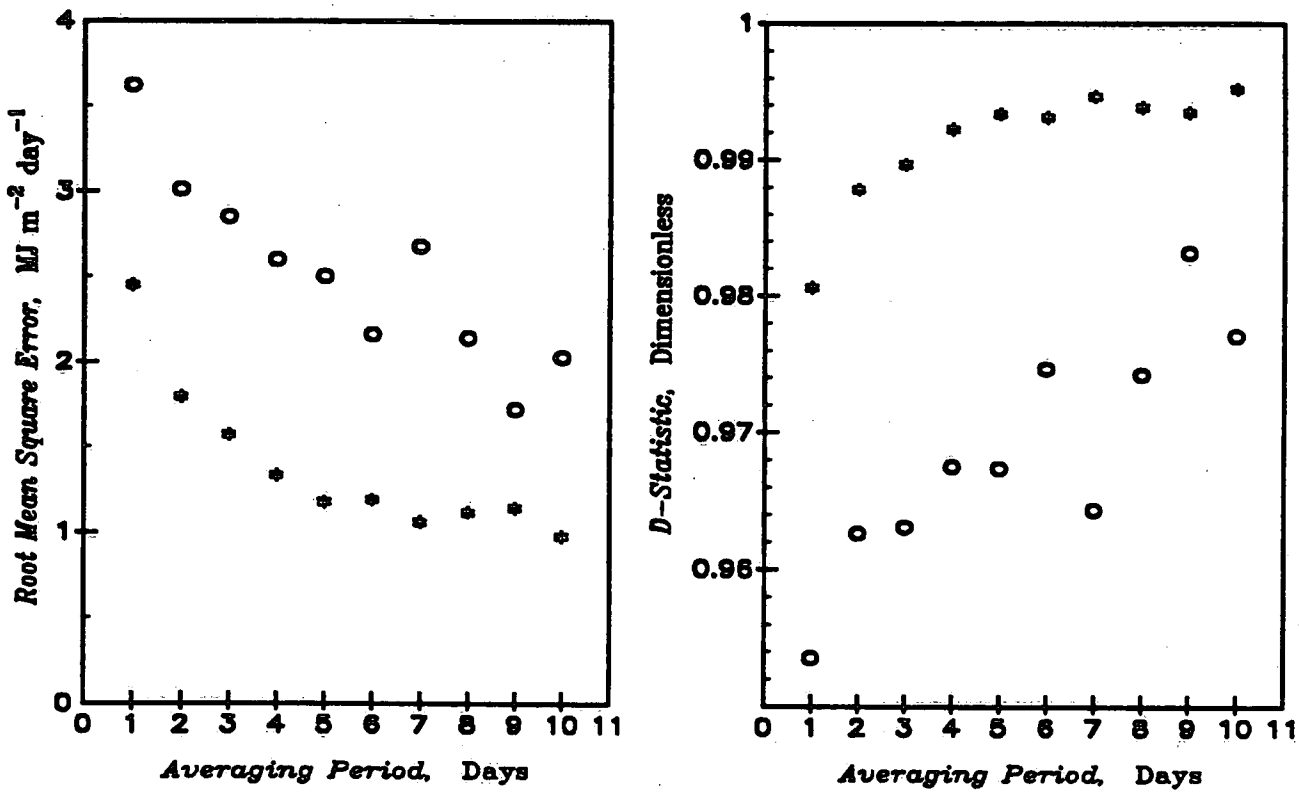

Five-day estimates are almost as good as 10 day estimates. Estimates from the Atwater and Ball model decrease more slowly with averaging period; 10 day estimates are only marginally better than 5 day means. The 7 day mean estimates, which were used by the IFYGL Energy Balance Panel, have an error that is comparable to 3 and 4 day mean estimates from the present study. Beyond five day periods, E_{rms} begins to oscillate by approximately 0.5 MJ m^{-2} day^{-1}, illustrating the effect of large errors occurring on consecutive days. Root mean square errors for *Delta–D*$_2$ also display this

behaviour, but in this case oscillations are strongly damped. On a monthly basis, root mean square errors for *Delta–D*$_2$ are 0.69 MJ m^{-2} day^{-1} compared to 1.43 MJ m^{-2} day^{-1} for estimates from the Atwater and Ball model. These results attest to the dramatic improvement in flux estimates possible with radiative transfer models.

4.3.2. Incoming Longwave Radiation

Comparison of estimates of incoming longwave radiation are shown in Figs. 4.9 to 4.12. Figure 4.9 illustrates daily estimates of incoming longwave radiation during IFYGL. It demonstrates that while estimates from the present study both overestimate and underestimate, incoming longwave radiation is generally underestimated as confirmed by Fig. 4.10. The majority of deviations lie in the range -4 to 1 MJ m^{-2} day^{-1}, as compared to results from the Atwater and Ball model, where most of the deviations are in the range -2 to 3 MJ m^{-2} day^{-1}. These deviations are within, or close to, the uncertainty of incoming longwave radiation measurements (approximately 10 percent, Latimer (1971)) for the majority of days for both models.

These comparisons emphasize the importance of accurate overlake air temperatures which were available for Atwater and Ball's calculations. Figs. 4.1 and 4.2 both suggest that overlake air temperatures are underestimated in the present study. The largest underestimates occur during the spring and early summer months, which is also the period when errors in estimates of incoming longwave radiation are largest. There may be another source of error. The present study assumes the altitude of the centre of gravity temperature for emission varies from 200 m (winter) to 300 m (summer). With the assumed environmental lapse rates used in this study, this reduces the radiating temperature by a further 2 to 3 °C. This height may be too great, e.g. an altitude of 100 m may be more appropriate.

On a daily basis, the root mean square error of model estimates is approximately 3.2 MJ m^{-2} day^{-1} for the present study and 2.5 MJ m^{-2} day^{-1} for the Atwater and Ball model. Figure 4.11 compares estimates of incoming longwave radiation as a function

of cloudiness. Figure 4.11 shows that there is very little difference between flux estimates for the two models for $C > 0.5$. The striking difference is for low values of cloudiness, where estimates from the present model consistently underestimate measured values. One possibility that was not considered during the model development stage was the possbility of temperature inversions. Although the strength and location of temperature inversions will depend on both time of day and season, one might reasonably assume that the diurnally-averaged environmental lapse rate in these circumstances might be quite small, say, close to zero. Even small differences in the assumed environmental lapse rate could lead to large differences in flux estimates, especially during summertime, because of the fourth power nature of the Stefan-Boltzmann law. This seems to be evident in Fig. 4.11, where the largest underestimates occur when the measured fluxes are greater than 25 MJ m^{-2} day^{-1}, i.e., summer. These results emphasize the sensitivity of longwave fluxes to air temperatures, in contrast to shortwave fluxes which are somewhat insensitive to the exact composition-temperature profile.

Figure 4.12 illustrates root mean square errors and *D*–statistic for flux estimates as a function of averaging period. Flux estimates from both models improve with increase in averaging period. There is little difference between estimates from either model for 10 day periods. One interesting result is that the *D*–statistic for estimates from the present model continue to increase with averaging period. Analysis suggests that estimates from the present study are in better agreement for averaging periods greater than 5 days. One possible explanation for this result is the distribution of errors as a function of time. Figure 4.9 shows that estimates from the Atwater and Ball model are almost consistently less than mean measured values from May through September. Thereafter, model estimates are almost consistently greater than mean measured values. Average flux estimates do not appreciably improve with averaging period because improvement depends on *both* overestimates and underestimates

Figure 4.9 - Deviations of Estimates (present study - upper half; Atwater and Ball (1974) - lower half) of Daily Longwave Incoming Radiation from Mean Measured Values (Davies and Schertzer, 1974) over Lake Ontario, 1 May, 1972, to 31 March, 1973.

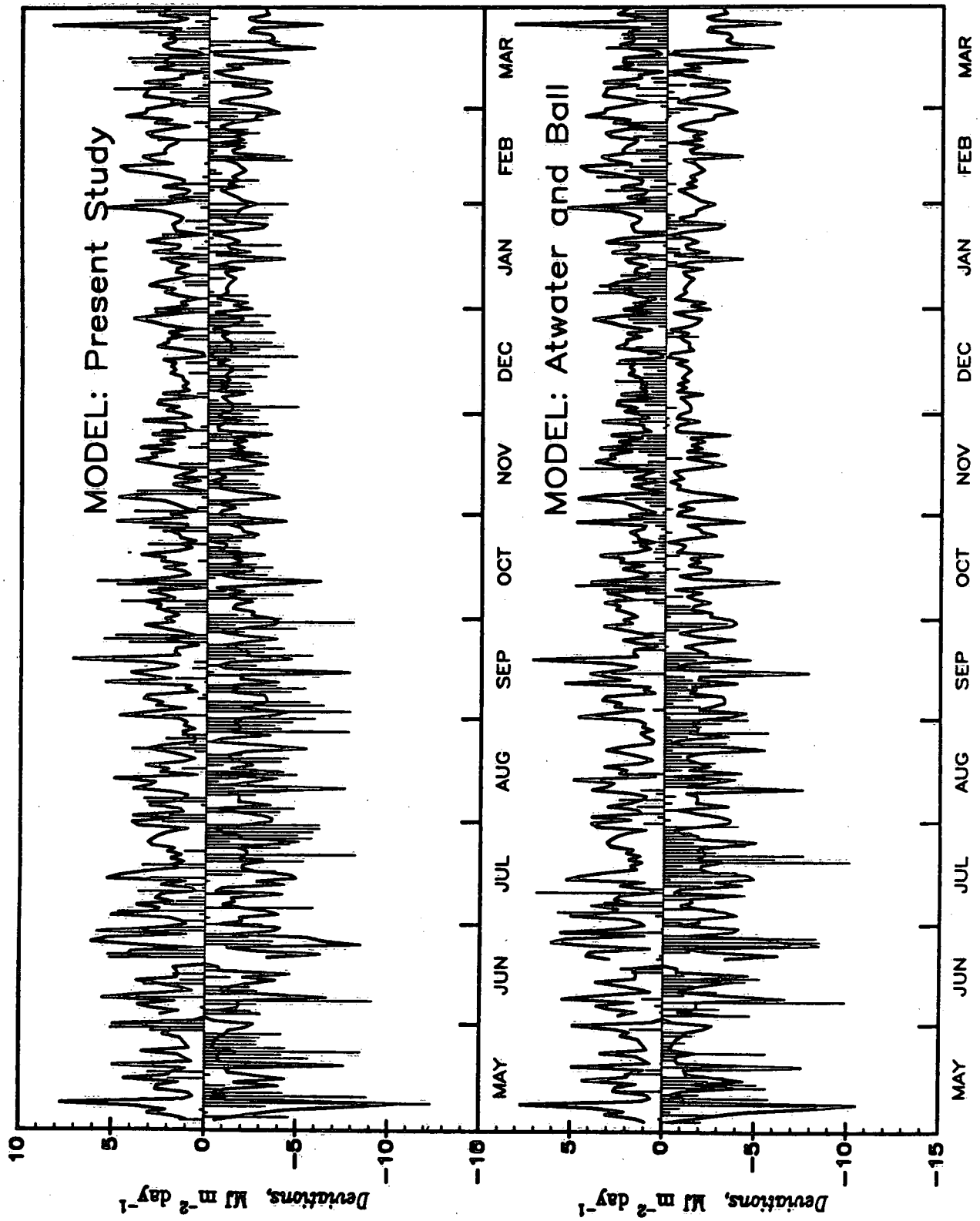

Figure 4.10 - Frequency Distribution of Absolute Errors (Difference of Mean Measured Values from Estimated Values) of Estimates of Daily Incoming Longwave Radiation. Solid line refers to results from present study; dashed line for Atwater and Ball's (1974) results. (a) refers to deviations from mean measured values; (b) refers to deviations from the range.

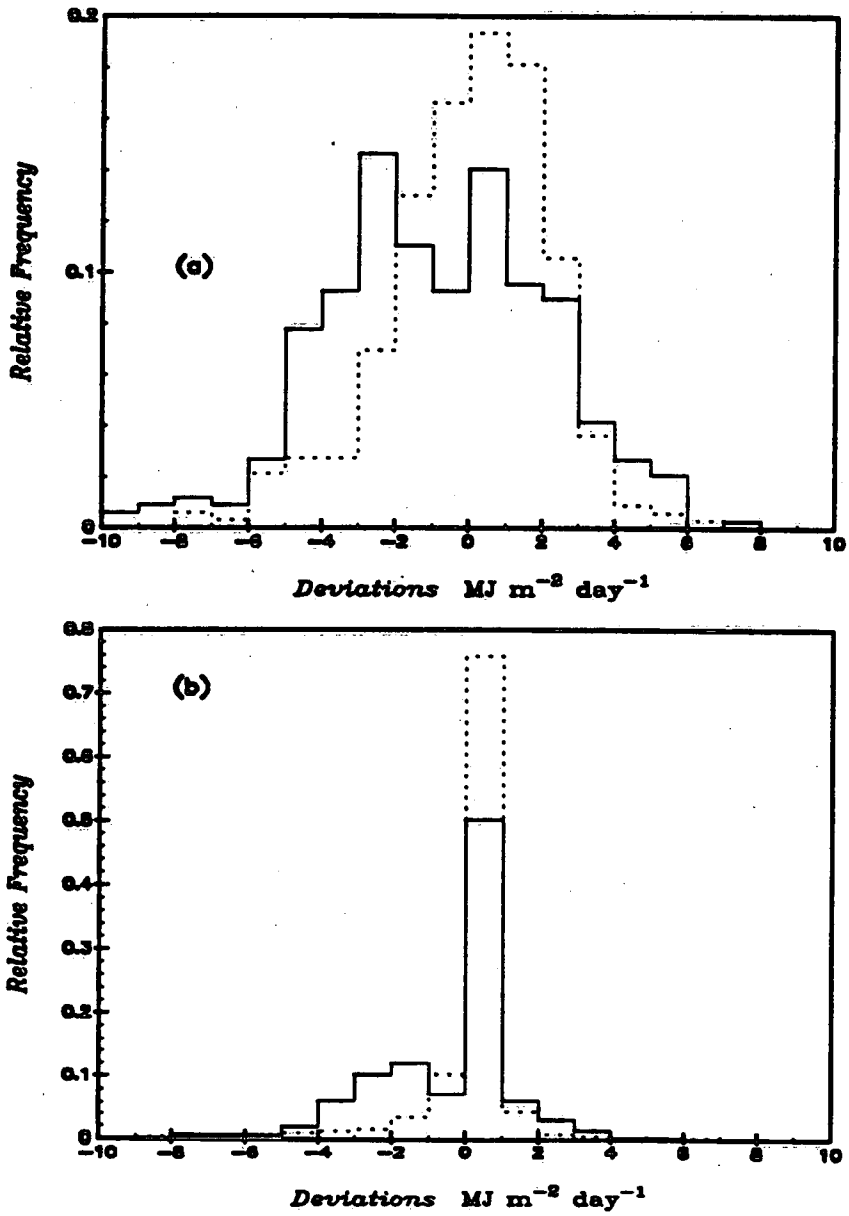

occurring within the averaging interval. The present model both overestimates and underestimates and this leads to a better agreement with increase in averaging period. On a monthly basis, root mean square error of flux estimates is 1.31 MJ m^{-2} day^{-1} for the present model and 1.38 MJ m^{-2} day^{-1} for Atwater and Ball's model.

Figure 4.11 - Comparison of Estimates of Daily Incoming Longwave Radiation as a Function of Cloudiness over Lake Ontario, 1 May, 1972, to 31 March, 1973. Symbols represent results from present study (full circles) and Atwater and Ball (1974) (open circles). Diagonal lines represent the 1:1 line.

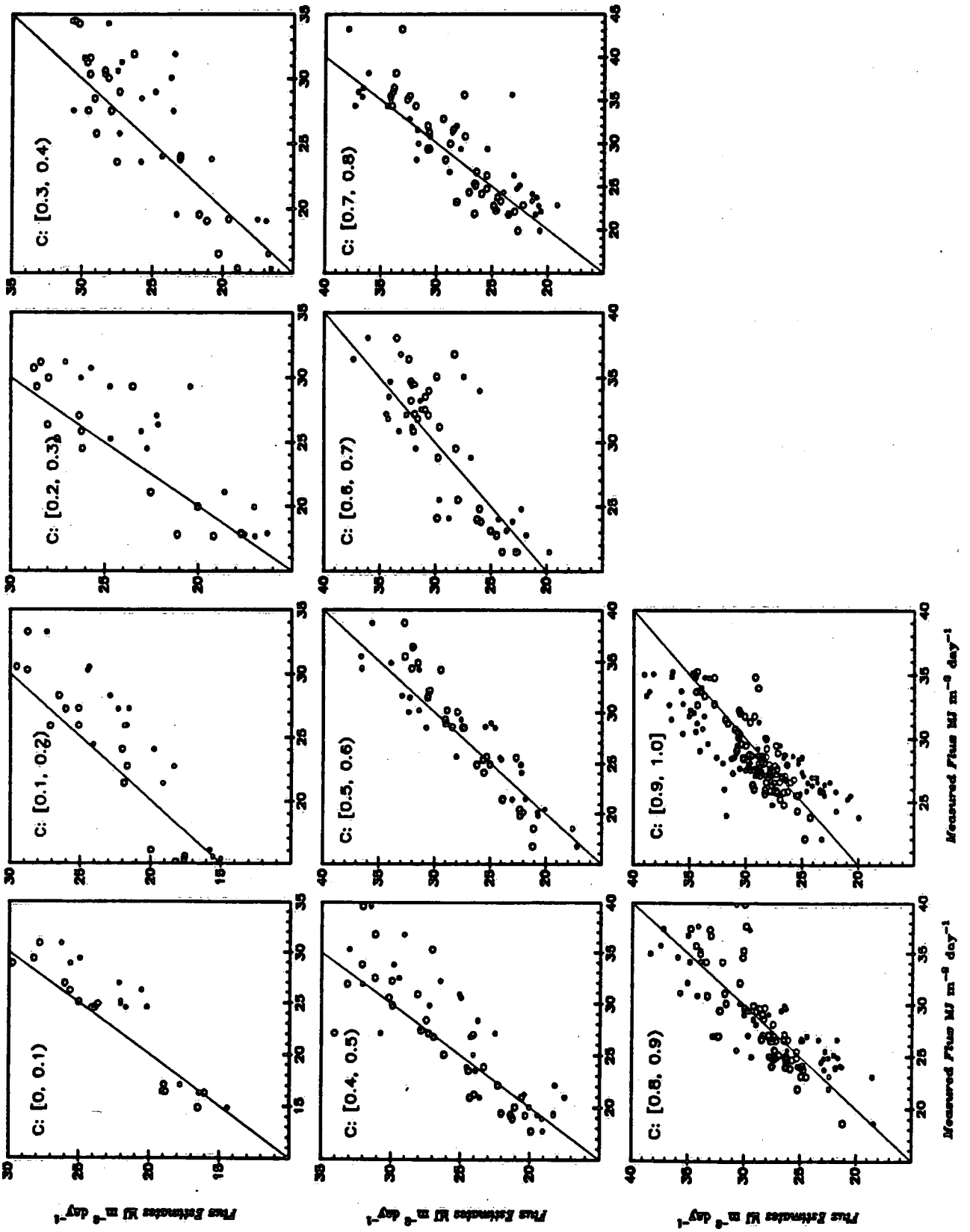

Figure 4.12 - Comparison of Root Mean Square Errors and D-Statistics of Estimates of Daily Incoming Longwave Radiation over Lake Ontario, 1 May, 1972, to 31 March, 1973, as a Function of Averaging Period. Symbols represent results from present study (*) and Atwater and Ball (1974) (open circle).

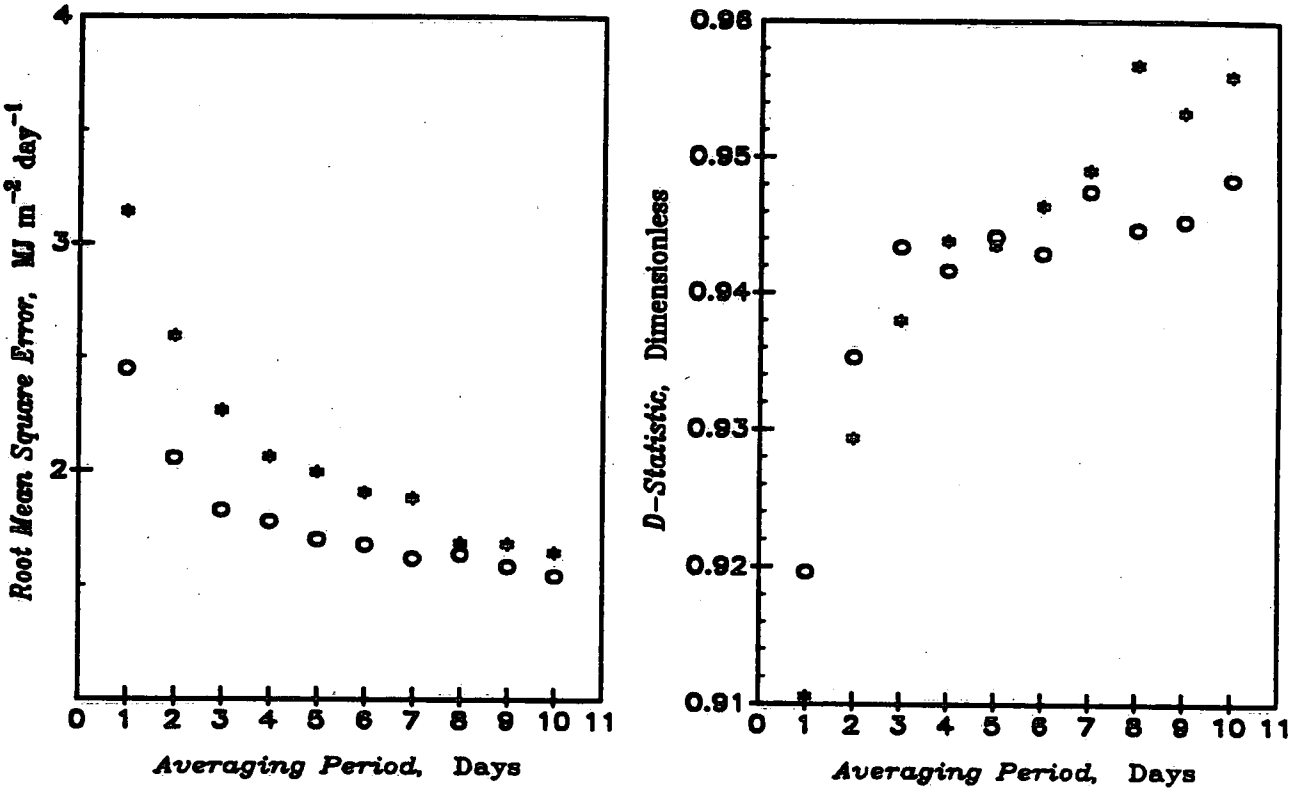

It is difficult to explain why both models underestimate incoming longwave fluxes. Atwater and Ball had temperature and humidity profiles from radiosonde ascents. Therefore, boundary conditions for solving the radiative transfer equation were known, as opposed to modelled. There is the possibility that these profile data were not applicable or representative of conditions over the lake. Or, their treatment of aerosols on infrared radiation transfer, e.g. assumed physical properties of the aerosol model, may be inappropriate.

Flux estimates from the present model are known to be sensitive to small temperature changes. For example, the root mean square error for monthly flux estimates decreases from 1.31 MJ m^{-2} day^{-1} to approximately 1.07 MJ m^{-2} day^{-1} when the step function for scaling functions (Table 3.2) is replaced by a polynomial approximation.

Thus, only small temperature changes may be required to bring flux estimates into better agreement with measured values. This might result if surface water temperatures could be more accurately modelled.

There is one other possibility that is relevant to both models. Neither model treats multiple scattering effects in the infrared region in a credible manner. The Atwater and Ball model relies on what is essentially a transmittance model derived from the radiative transfer equation, while the present model relies on elementary concepts from radiative transfer theory. Neglect of multiple scattering effects was assumed on the basis that such effects are small in the infrared spectrum, since optical depths are likely to be small. This assumption may not in fact be valid, and consistent flux underestimates may simply be reflecting the neglect of multiple scattering effects. The previous section demonstrated that even simple two-term radiative transfer models can greatly improve shortwave flux estimates compared to conventional transmittance models. This possibility should be investigated in future research.

4.3.3. Net Radiation

Net radiation estimates include errors from each component term. Improvement in flux estimates will depend on simultaneous improvement in each term, or on compensating errors. Comparisons of net radiation estimates with measured values are summarized in Figs. 4.13 and 4.14.

Figure 4.13 illustrates deviations of daily estimates from mean measured values and range of daily values for both the present study and Atwater and Ball's model. Vertical scales in Fig. 4.13 are not identical. Figure 4.13 is similar to Fig. 4.5 for shortwave estimates. Root mean square error of daily flux estimates is 3.2 $MJ\,m^{-2}\,day^{-1}$ for the present model and 4.1 $MJ\,m^{-2}\,day^{-1}$ for the Atwater and Ball model. These root mean square errors decrease with averaging period for both models, although the decrease is much greater for estimates from the present study. The *D*–statistic increases with averaging period, as both shortwave and longwave

Figure 4.13 - Deviations of Estimates (present study - upper half; Atwater and Ball (1974) - lower half) of Daily Net Radiation from Mean Measured Values (Davies and Schertzer, 1974) over Lake Ontario, 1 May, 1972, to 31 March, 1973.

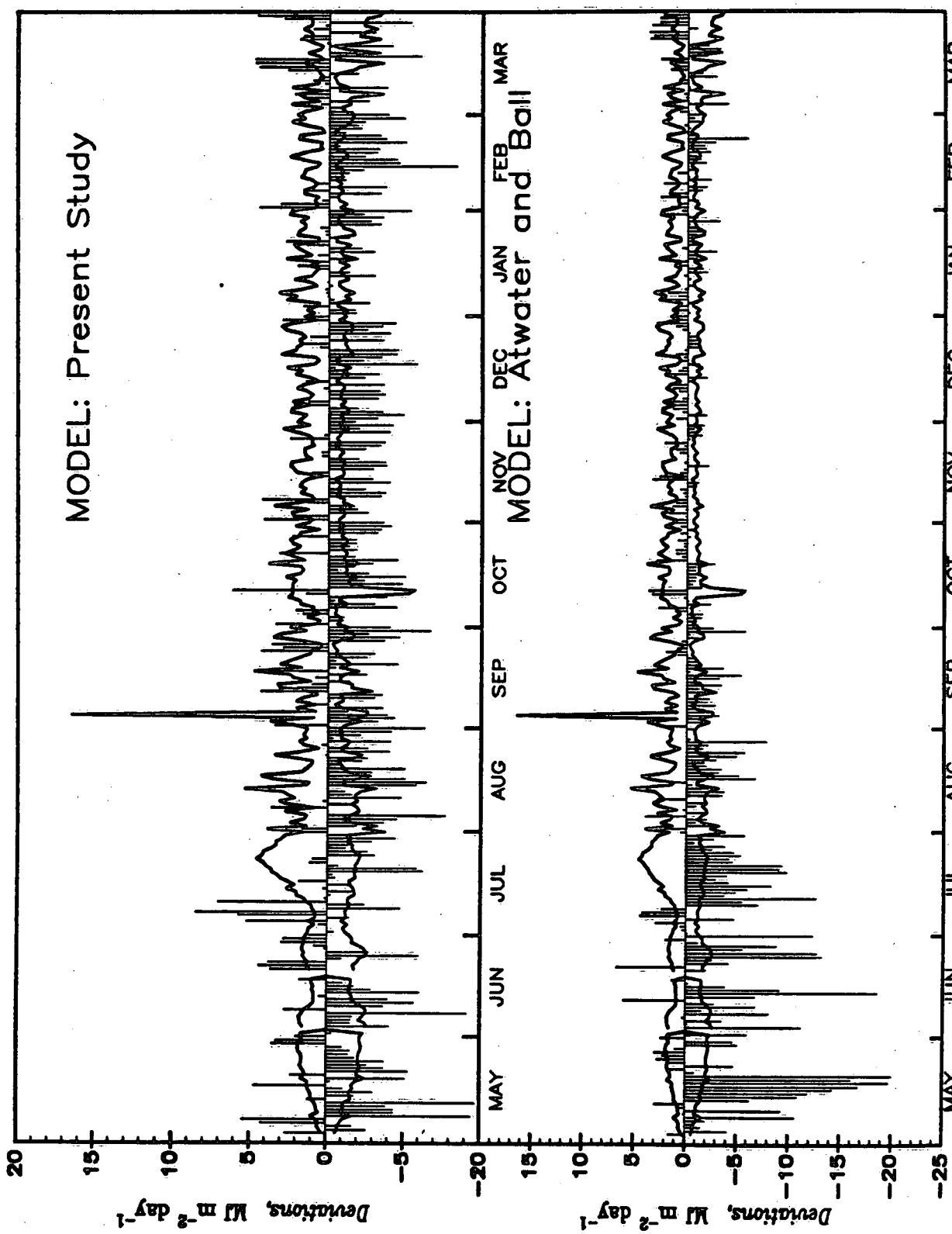

Figure 4.14 - Comparison of Root Mean Square Errors and D-Statistics of Estimates of Daily Net Radiation over Lake Ontario, 1 May, 1972, to 31 March, 1973, as a Function of Averaging Period. Symbols represent results from present study (*) and Atwater and Ball (1974) (open circle).

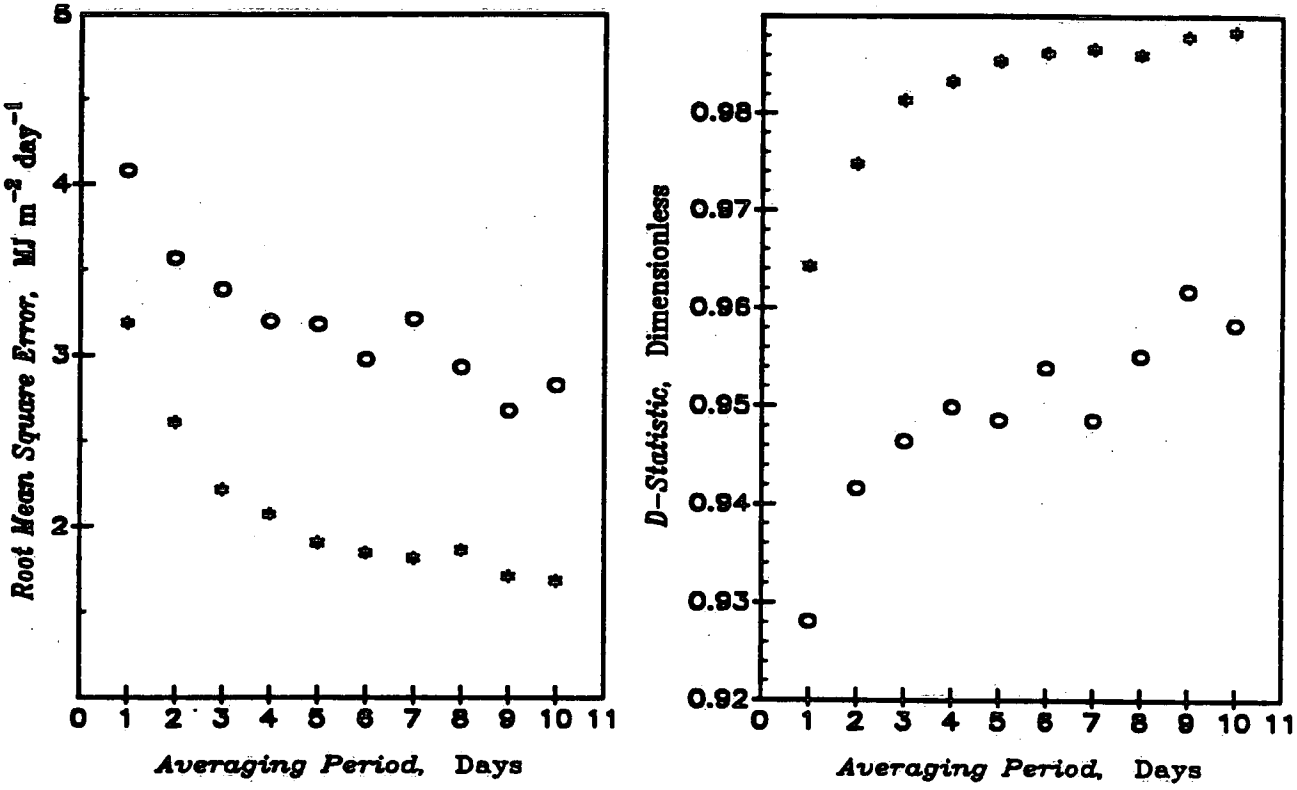

estimates improve with averaging period.

Both models yield acceptable estimates during the winter months, although the present model yields estimates that exceed the range by 1 to 2 MJ m^{-2} day^{-1}. Estimates from the present model during the spring and summer months are clearly superior to those from the Atwater and Ball model, both in terms of magnitude and frequency. This is significant from the surface energy balance point of view: this is the time of maximum energy gain at the lake surface. It is important, therefore, that radiation models perform well at this time of year. The present model for estimating net radiation performs well in this respect.

4.4. Turbulent Fluxes

Estimates of turbulent energy fluxes depends upon values of the Bowen ratio, wind speed and the mass transfer coefficient. Figure 4.15 compares estimates of daily Bowen ratio (thin line) with values tabulated by Pinsak and Rodgers (1981) for Lake Ontario for the period 1 May, 1972, to 11 December, 1972. Values tabulated by Pinsak and Rodgers are considered to be exact in this analysis, as values were derived from overlake values of air and dew point temperature, as well as known values of surface water temperatures. They assumed a constant value for the psychrometric constant (eq.[53]), whereas k was evaluated directly from the definition of this parameter in this study. In addition, values from the present study incorporate the effect of humidity on values of specific heat of air. While the net effect is likely to be small, some of the variation between Bowen ratios shown in Fig. 4.15 will arise from this difference in evaluation of k.

Figure 4.15 illustrates essentially two regimes of agreement. Estimated daily Bowen ratios fluctuate considerably from May to August , a time when overlake stability can be generally classified as stable. Largest disagreement between model estimates and observed values occur at this time of year, although individual deviations tend to be isolated. Figure 4.15 suggests that estimates are generally in phase with observed values, while absolute differences may be large. Much of the error in estimated values can be traced to errors in surface water temperature. The large deviations occurring in early June and late July result from overestimated surface water temperature. The impact of underestimated surface water temperatures from mid June to early July results in underestimated Bowen ratios.

Figure 4.15 illustrates a second Bowen ratio regime beginning in September. Estimates and observed values are in virtual agreement. An exception occurs near the middle of September, when estimates of surface temperature changes from the heating to cooling period functions. This agreement is encouraging because evaporation

Figure 4.15 - Comparison of Estimates of Daily-Averaged Bowen Ratio over Lake Ontario, 1 May to 16 December, 1972. Values tabulated by Pinsak and Rodgers (1981) shown by thick line. Results from the present study shown by thin line.

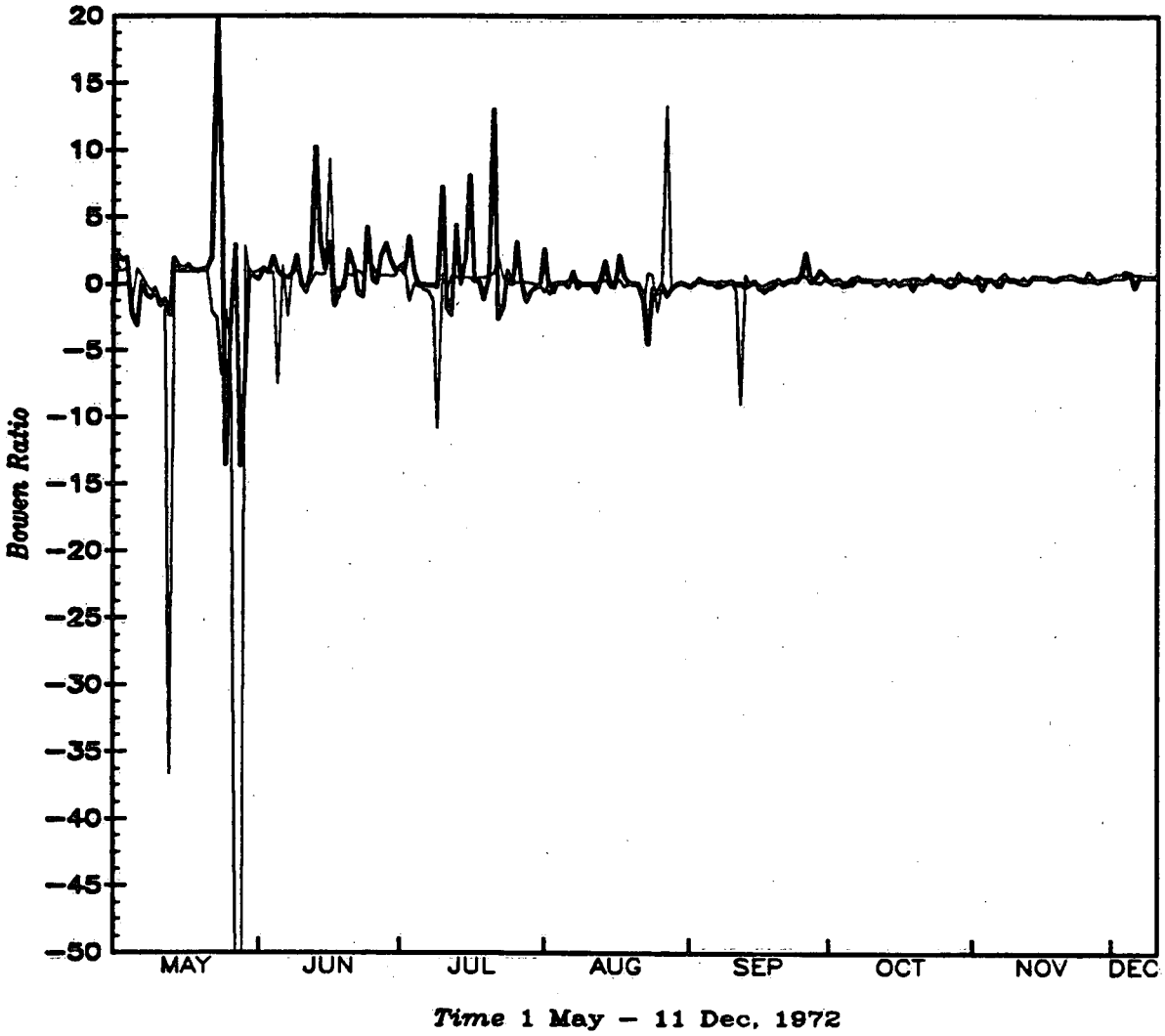

rates are greatest during the autumn and winter months. The agreement is also somewhat surprising during October, where surface water temperatures are overestimated by approximately 2 °C. This suggests that the joint effect of errors in estimates of air

Figure 4.16 - Comparison of Estimates of Weekly-Averaged Sensible Heat (upper half) and Latent Heat Fluxes (lower half) with Values Determined from Objective Analyses (Holland et.al., 1981) over Lake Ontario, 1 May to 26 October, 1972.

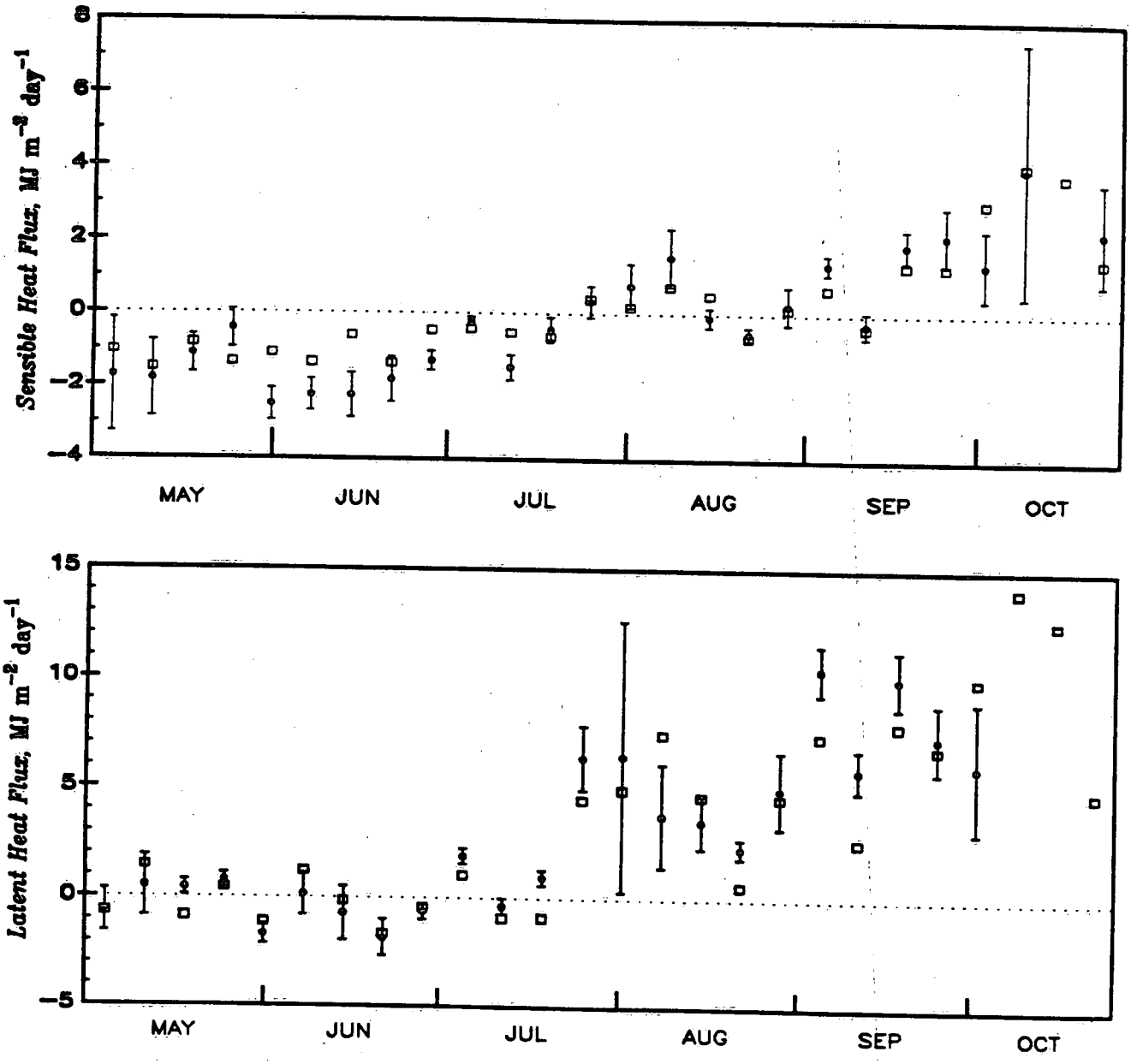

and dew point temperatures and surface water temperature are largely compensating. The good agreement between estimated and observed Bowen ratios indicates that errors in evaporation must therefore derive from errors in estimates of wind speed

and/or the bulk evaporation coefficient C_E.

Figure 4.16 compares estimated latent and sensible heat fluxes with values obtained by objective analyses (Holland *et.al.*, 1981). These values are considered as the measured values in the following discussion. The utility of these values lies in the fact that it is possible to attach confidence limits to (mean) values. Ninety-five percent confidence limits are implied in values shown in Fig. 4.16. Estimated latent and sensible heat fluxes are shown by open squares in Fig. 4.16.

The root mean square error of the difference between mean measured values and flux estimates is 0.78 MJ m^{-2} day^{-1} for sensible heat flux and 1.77 MJ m^{-2} day^{-1} for latent heat flux over this time period. These values may be compared with the root mean square of the range of measured values in Fig. 4.16: 1.91 MJ m^{-2} day^{-1} for sensible heat and 3.53 MJ m^{-2} day^{-1} for latent heat flux. These comparisons indicate excellent agreement over the period considered, which includes stability classifications ranging from very stable to very unstable.

Estimates are within the range of measured values for almost every week. The major disagreements for sensible heat flux (approximately 1 MJ m^{-2} day^{-1}) occurs during June when surface water temperatures are overestimated. These overestimated surface water temperatures apparently have little or no effect on latent heat flux estimates, however. A similar situation occurs in September, however, the effect is quite different. Sensible heat flux is reasonably well estimated while latent fluxes are underestimated. These underestimates may be related to the underestimated wind speed (Fig. 4.2 (d)) and/or the mass transfer coefficient which is essentially a function of the bulk evaporation coefficient C_E. This question cannot be resolved at the weekly time scale. Accurate knowledge of atmospheric stability and wind speed on a daily basis will be required to resolve this question.

Figure 4.17 compares estimated weekly evaporation totals with values tabulated by the IFYGL Energy Balance Panel for the period 4 May, 1972, to 28 March, 1973. The

Figure 4.17 - Comparison of Estimates of Weekly Evaporation Totals (thin line) with Values Tabulated by the IFYGL Energy Balance Panel (Quinn and den Hartog, 1981) for Lake Ontario, 4 May, 1972, to 26 March, 1973.

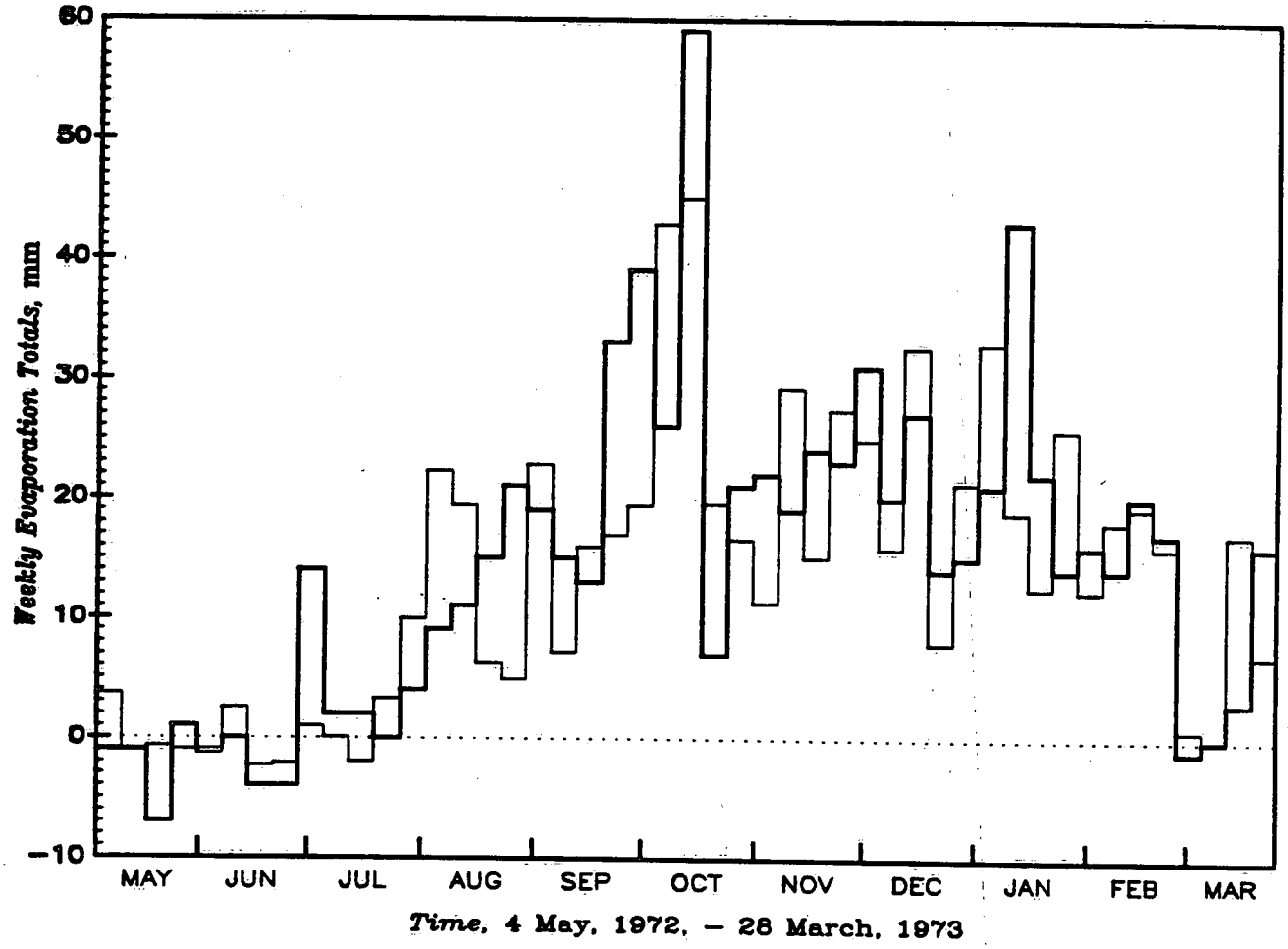

values tabulated by the IFYGL Energy Balance Panel employed Atwater and Ball's net radiation values and surface heat fluxes determined from vertical temperature profiles on Lake Ontario. Evaporation may then be evaluated from:

$$E = \frac{Q^* - Q_t + Q_M + Q_i}{\rho(1+\beta)L}$$

The largest differences occur during August, September, and October, when

evaporation rates are approaching maximum values. The effect of errors in surface water temperature appears ambiguous. During the latter half of June, surface water temperatures are overestimated. This appears to have little effect on evaporation totals. Surface water temperatures are also overestimated during early July, when the difference between the two evaporation totals is 13 mm. During the August to September period, relative errors range from 5 to 50 percent, with overestimates and underestimates being approximately equal in magnitude. From November onwards, deviations from measured values range from -6 mm to 8 mm on a weekly basis. The root mean square error of the difference between estimated and measured weekly evaporation totals is 9.3 mm $week^{-1}$ with a mean bias error of -0.8 mm $week^{-1}$, suggesting an overall underestimate of evaporation totals.

Figure 4.18 compares weekly evaporation totals from the present study with estimates by Phillips (1978) (heavy line) and Quinn (1978) (dash-dot line). Phillips performed evaporation calculations by applying multiple regression equations to estimate overlake wind speed, air, and dew point temperatures (as described in Section 3) for a grid over Lake Ontario. Fetch and surface water temperatures were known exactly. Aerodynamic equations were applied to estimate latent and sensible heat fluxes, where C_E was allowed to vary with atmospheric stability, although this was specified as a step function. Phillips' approach is thus similar to the present study in form, except that many variables are modelled in this present study.

Quinn's approach is similar in that aerodynamic equations were applied to estimate daily evaporation totals. The major difference was that C_E was determined as an explicit function of atmospheric stability through the nondimensional wind speed gradient, potential temperature gradient, and the Monin-Obukhov length. Input meteorological data was derived from buoys stationed in Lake Ontario. The buoys became inoperative in early December. Quinn's results therefore end at this time.

Figure 4.18 demonstrates that all three methods yield nearly identical results

Figure 4.18 - Comparison of Weekly Evaporation Totals for Lake Ontario, 7 May, 1972, - 30 March, 1973. Thick line represents estimates from Phillips (1978); dash-dot line represents estimates from Quinn (1978); estimates from present study shown by thin line.

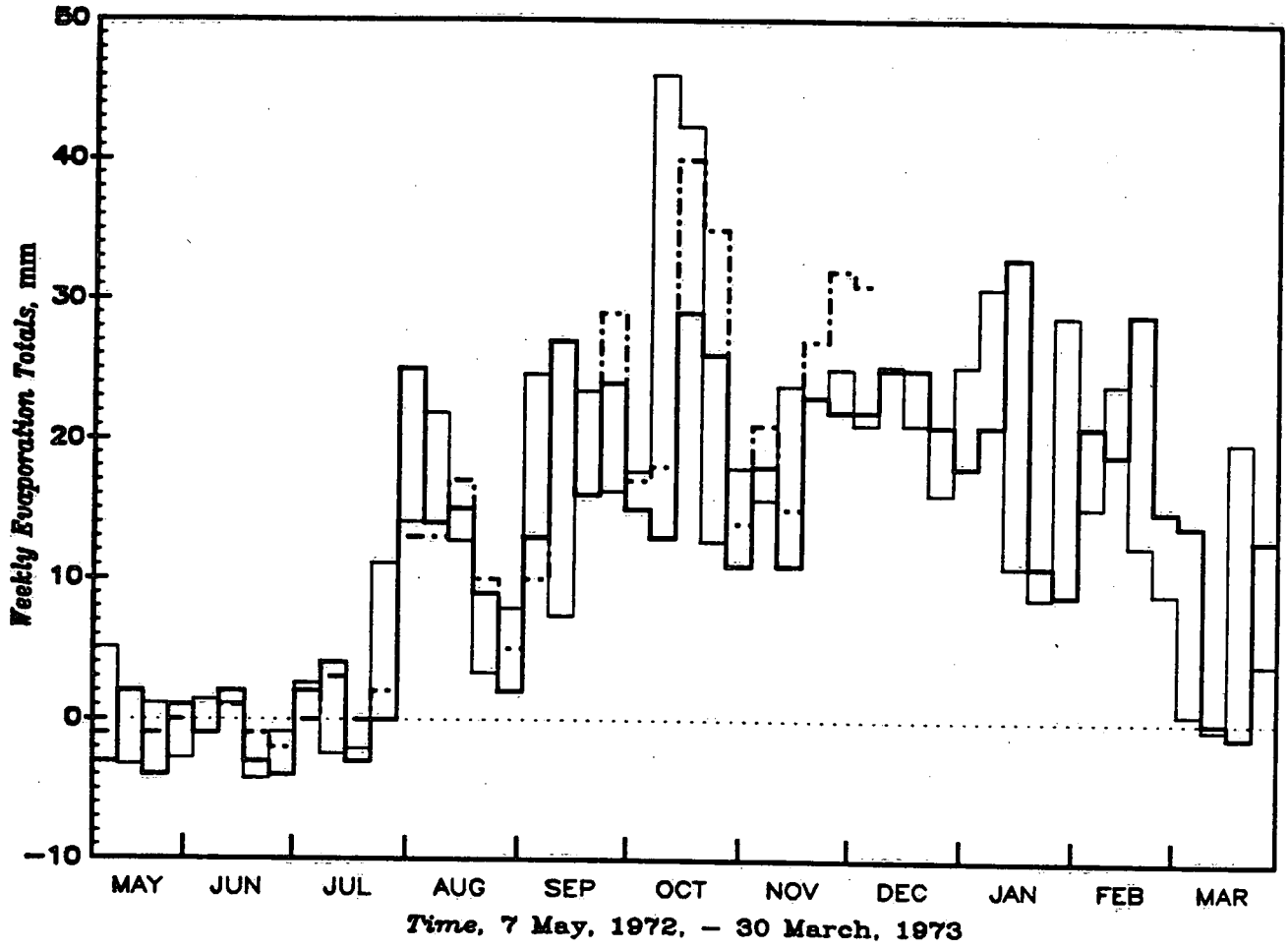

from the beginning of the study period (7 May, 1972) to early September. The largest disagreement occurs in September and October with more minor variations thereafter. Accepting Phillips' values as the measured values yields a root mean square error of 10.3 mm week^{-1} for estimates for the present study and a mean bias error of +0.8 mm week^{-1}. Accepting Quinn's values as the measured values yields a

Figure 4.19 - Comparison of Estimated Monthly Evaporation (thin line) with Values recommended by the IFYGL Energy Balance Panel (Quinn and den Hartog, 1981) for Lake Ontario, May, 1972, to March, 1973.

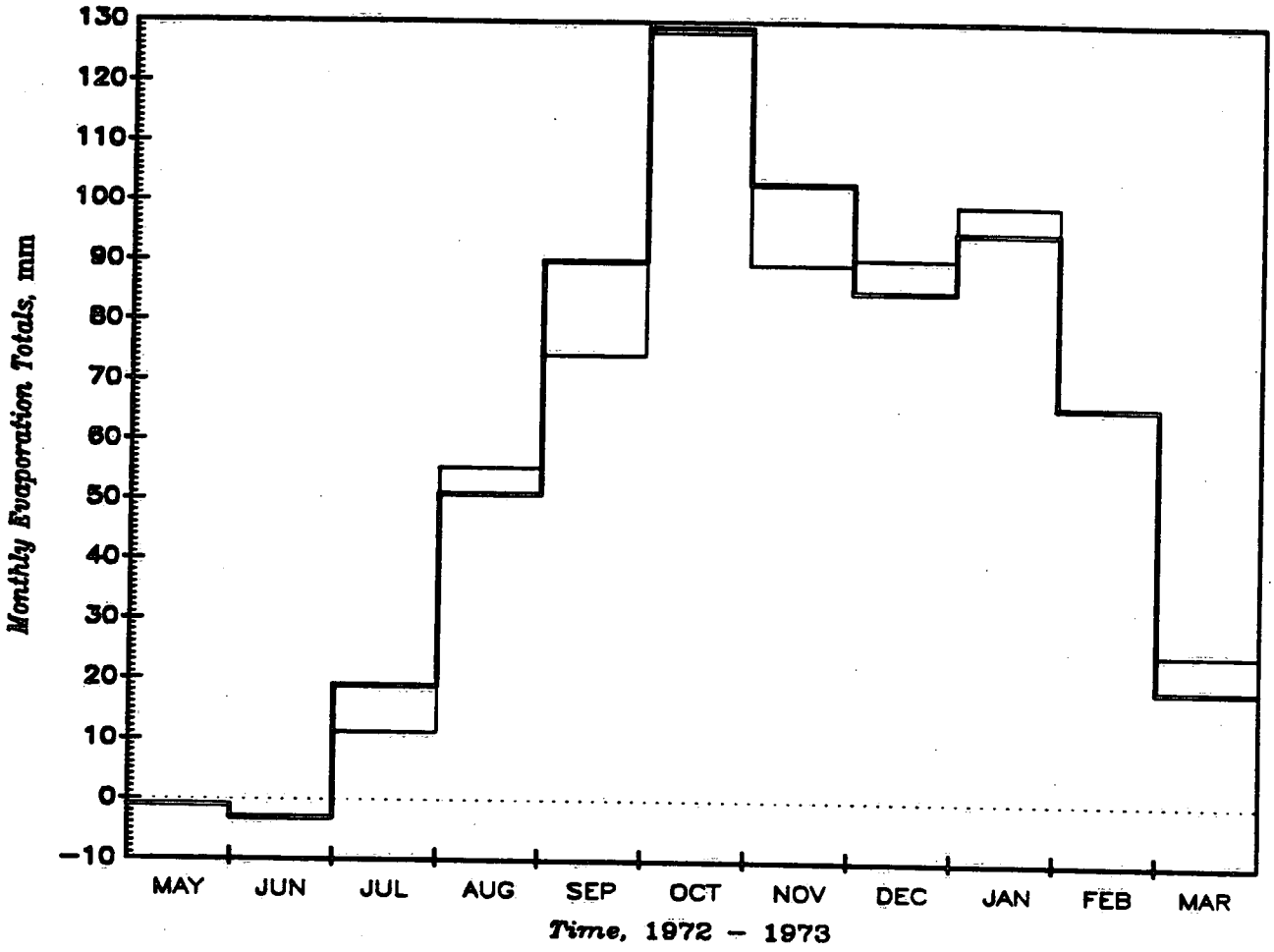

root mean square error of 9.4 mm week^{-1} and a mean bias error of -0.2 mm week^{-1}. These results are similar to those obtained for evaporation totals recommended by the IFYGL Energy Balance Panel, although the mean bias error is much closer to zero, suggesting a better overall estimate. There are clear differences in weekly evaporation totals between the four sets. It is encouraging, however, that results from the

Figure 4.20 - Comparison of Estimates of Monthly Evaporation with Values Recommended by the IFYGL Energy Balance Panel for Lake Ontario, May, 1972, to March, 1973 (Quinn and den Hartog, 1981). Symbols represent present study (full circle), aerodynamic method (open circle), energy balance (diamond), and water balance (square).

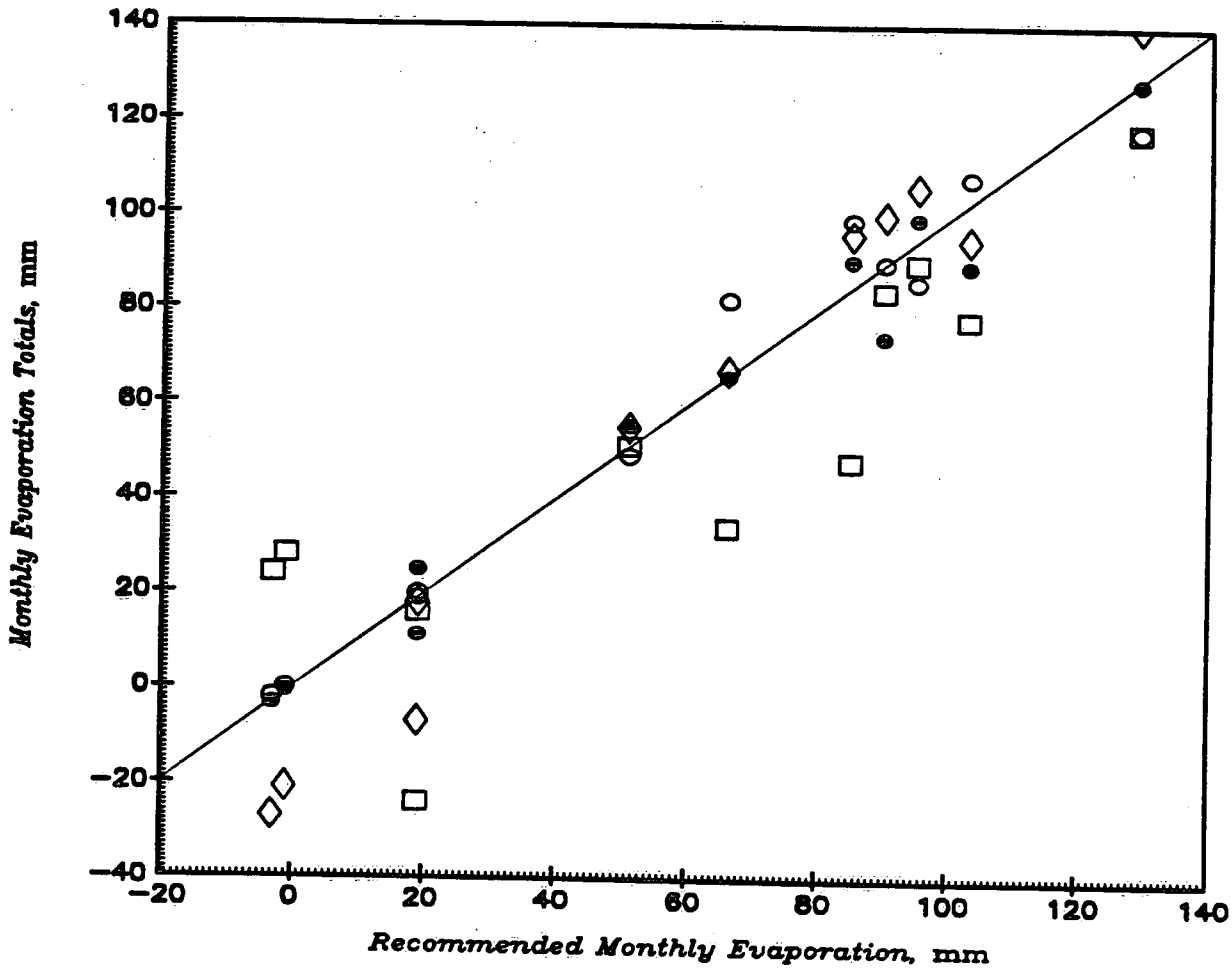

present study are comparable with recommended values since the present study uses input data collected at land stations.

Figure 4.19 compares estimated monthly evaporation totals (mm) from the present study (thin line) with recommended values (Quinn and den Hartog, 1981). Figure 4.20 compares monthly evaporation totals from this study with values determined from the mass transfer method, energy balance approach, and water balance methods.

The largest difference in the present study occurs during September when the difference amounts to 15 mm, or 15 percent of the recommended value. Estimated evaporation is essentially exact in all months except September and November. In no other month does the relative error exceed 5 percent of recommended values.

Figure 4.20 demonstrates that, on a monthly basis, estimates from the present study compare very favourably with other methods surveyed by Quinn and den Hartog (1981). Monthly estimates are on or near the 1:1 line for both low and high evaporation rates.

4.5. Ice Heat Flux

Figure 4.21 compares estimated weekly ice heat flux over Lake Ontario for the period 2 November, 1972, to 28 March, 1973, with estimates tabulated by the IFYGL Energy Balance Panel. The agreement between the two estimates is generally excellent throughout the study period. This suggests that the fractional ice concentrations predicted by the ice model are correct, at least in order of magnitude. The largest differences occur over a four week period from mid-February to mid-March, when the error ranges from 1 to 3 MJ m^{-2} day^{-1}, which is similar to errors in incoming longwave radiation. Errors at other times are insignificant.

Ice heat fluxes presented by the IFYGL Energy Balance Panel for these four weeks may be overestimated. Boyce *et.al.* (1977) estimated minor energy fluxes, including ice heat flux, and found ice heat flux values of approximately 1 MJ m^{-2} day^{-1} from mid-February to mid-March. Estimates from the present study agree with these values closely.

4.6. Surface Heat Flux and Lake Heat Content

Figure 4.22 compares estimated weekly surface heat flux with values derived from vertical temperature profiles from ship surveys in Lake Ontario during IFYGL (Boyce *et.al.*, 1977). Figure 4.22 demonstrates that weekly surface heat fluxes fluctuate

Figure 4.21 - Comparison of Estimates of Weekly-Averaged Ice Heat Flux with Values Tabulated by the IFYGL Energy Balance Panel (Quinn and den Hartog, 1981) for Lake Ontario, 1 November, 1972, to 26 March, 1973. Modelled values are shown by thin line; tabulated values shown by thick line.

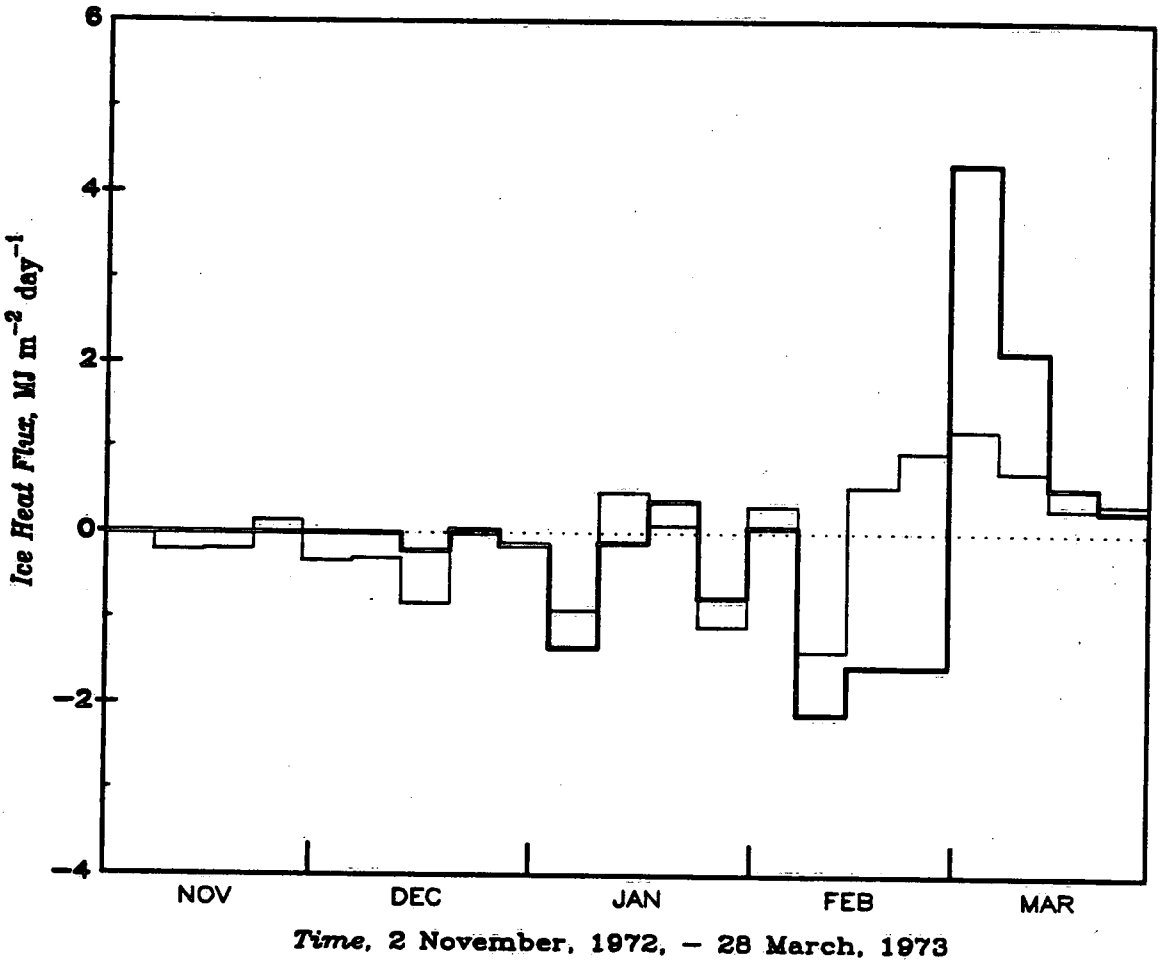

about measured values by within the 5 MJ m^{-2} day^{-1}, which is within the uncertainty of the heat content measurements. Errors in flux estimates are evenly distributed with respect to sign and time of year. Root mean square errors are 4.8 MJ m^{-2} day^{-1}, 2.2 MJ m^{-2} day^{-1}, and 1.0 MJ m^{-2} day^{-1} for weekly, biweekly, and monthly periods, respectively.

Accurate surface heat fluxes are required for evaluation of lake heat content, which, in turn, is required in estimating surface water temperature. Comparison of

Figure 4.22 - Comparison of Estimates of Weekly-, Biweekly-, and Monthly-Averaged Surface Heat Flux with Values Interpolated from Heat Content Measurements (Boyce et.al., 1977) for Lake Ontario, 3 May, 1972, to 28 March, 1973. Model estimates shown by thin line; values inferred from heat content measurements by thick line.

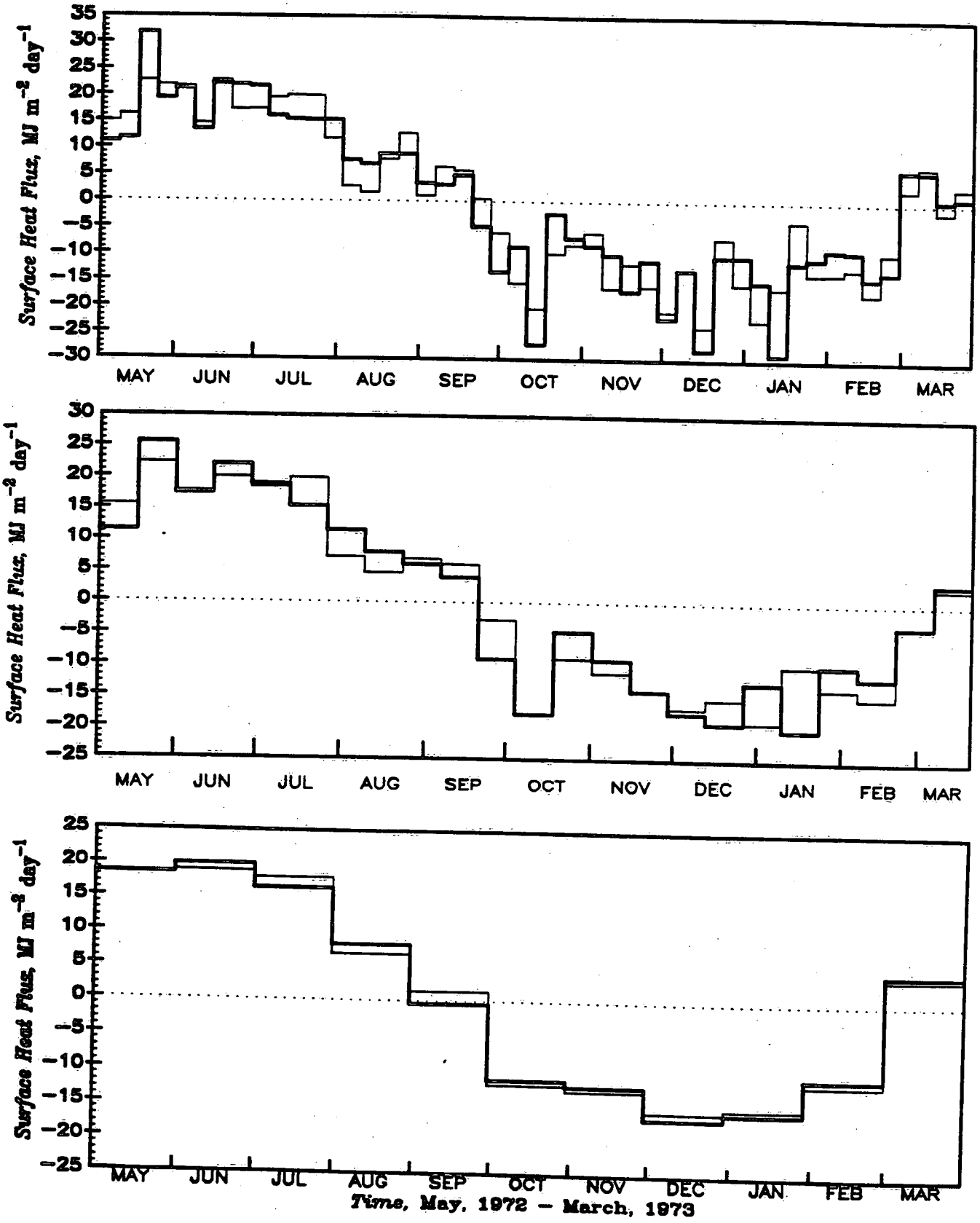

Figure 4.23 - Comparison of Estimates of Daily Lake Heat Contents with Measured Values (Boyce et.al., 1977) for Lake Ontario, 1 May, 1972, to 31 March, 1973. Model estimates shown by full line; measured values given by error bars.

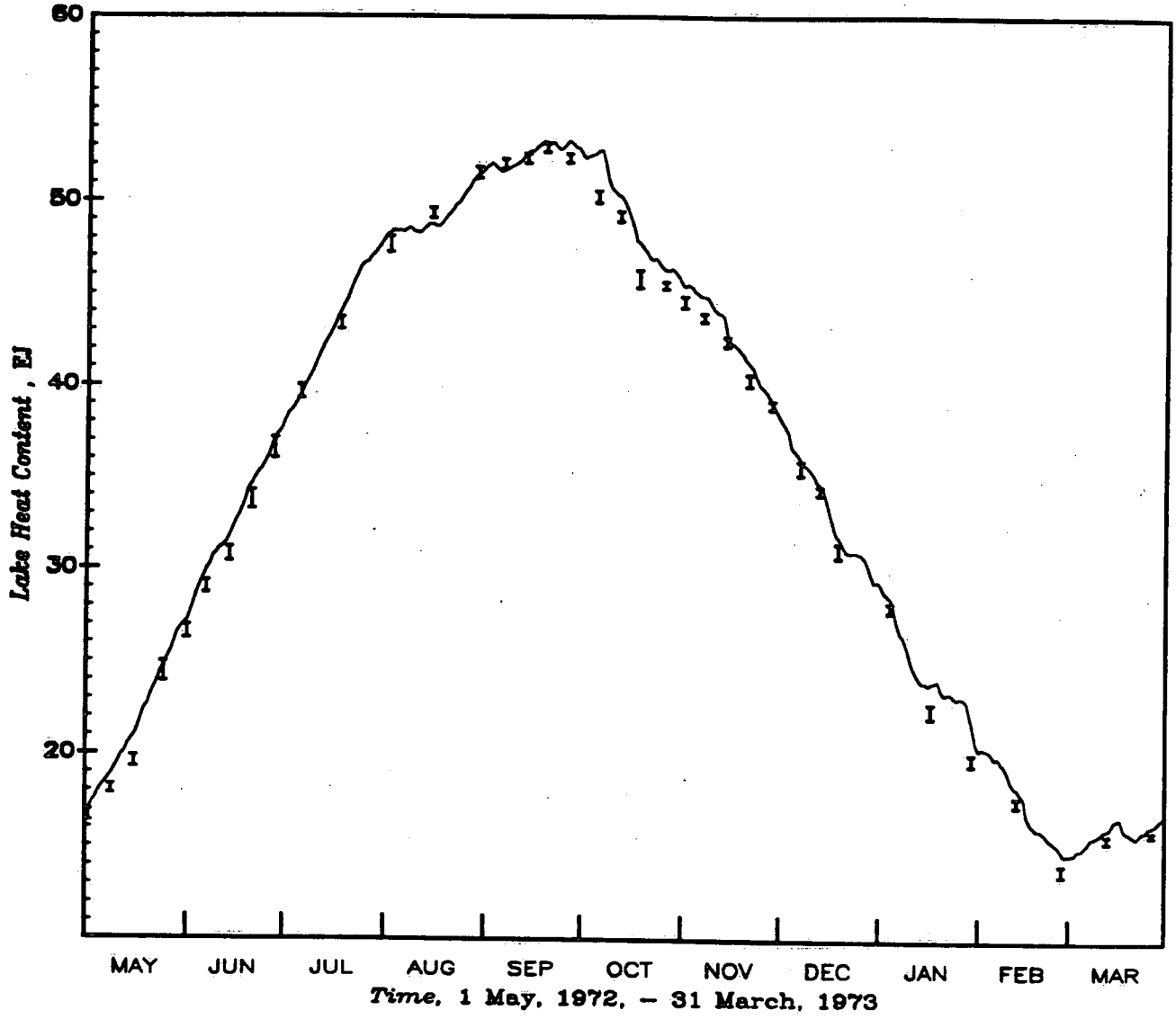

estimated daily heat contents with measured values (Boyce *et.al.* 1977) are illustrated in Figure 4.23. The full line represents the modelled heat content, while symbols represent measured values. Boyce *et.al.* estimated the magnitude of several sources

of error affecting heat content measurements. The error bars represent these measurement errors. In general, measurement errors vary from approximately 1 to 10 percent of heat content values.

Figure 4.23 illustrates excellent agreement between estimated and measured heat contents. The largest disgreement occurs in the September-October period, when surface water temperature must be estimated from the cooling phase function. Errors in surface water temperature at this time of year are therefore critical. During the rest of the year, heat contents are accurately estimated. Estimates are within, or close to, uncertainty limits of measured values. Part of this good agreement arises from the negative feedback nature of the surface water temperature-heat content relationship. Errors are never allowed to amplify. The agreement is also good because major components are estimated well at the times that it is important to estimate accurately, i.e., net radiation during the spring and early summer months and latent and sensible heat fluxes during autumn and early winter months.

5. ENERGY BALANCE CLIMATOLOGY OF THE LOWER GREAT LAKES

The model for evaluating radiation and energy balance components described in Sections 2 and 3 was applied to estimate daily values for the lower Great Lakes for the period 1953-1983. This Section describes the results of this simulation.

Figure 3.1 illustrates shoreline stations from which meteorological data were merged to form a meteorological data base for each lake. Meteorological stations are not equally distributed: the data base is biased to data from Canadian stations for Lake Ontario and to the American stations for Lake Erie. No sensitivity analyses have been performed to estimate the impact of station bias to the data base, but it is believed to be small as prevailing winds are from the west to southwest, which is nearly coincident with the major axis for both lakes.

5.1. ENERGY BALANCE COMPONENTS

Figures 5.1 and 5.2 illustrate maximum, mean, and minimum five-day values for selected hydrometeorological variables, radiation and energy balance components for Lake Erie and Lake Ontario, 1953-1983, respectively. Comparison of mean monthly values is shown in Fig. 5.3. In general, maximum and minimum values represent approximately two standard deviations from estimated mean values.

Air and dew point temperatures are similar for both lakes. The largest difference occurs from April to July, when Lake Erie air temperatures are greater than for Lake Ontario. The difference in air temperatures is approximately 4 °C, and approximately 1 to 2 °C for dew point temperatures. Part of this difference arises from Lake Erie's more southerly position, while much of the difference is accounted for by low surface water temperature of Lake Ontario at this time of year. This pattern is reversed during late autumn and early winter months when Lake Ontario is warmer than Lake Erie, although the differences are small.

Maximum wind speeds are observed during December and January, when they

Figure 5.1 - Maximum, Mean, and Minimum Five-Day Hydrometeorological, Radiation, and Energy Balance Components for Lake Erie, 1953-1983.

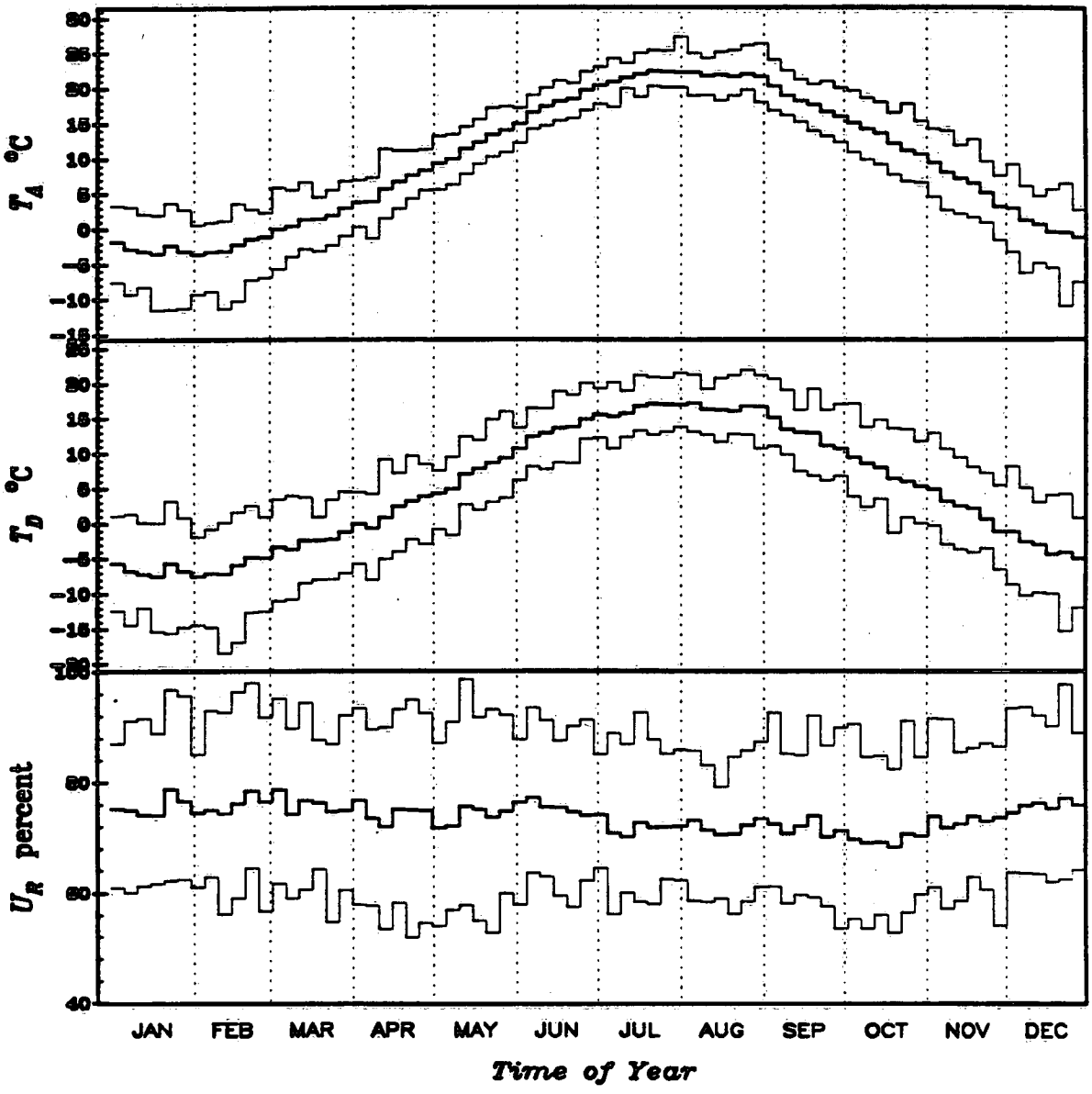

average approximately 11 m s^{-1} for Lake Ontario and 8 m s^{-1} for Lake Erie. Lowest wind speeds are observed during May and June when they average approximately 4 to 5 m s^{-1}. There is little difference in wind speeds during early summer months. The difference is much larger, however, during the winter months when it amounts to approximately 3 m s^{-1}. The difference arises from the greater scaling for wind speeds over Lake Ontario that arise from the larger difference between overland air

Figure 5.1 - Maximum, Mean, and Minimum Five-Day Hydrometeorological, Radiation, and Energy Balance Components for Lake Erie, 1953-1983.

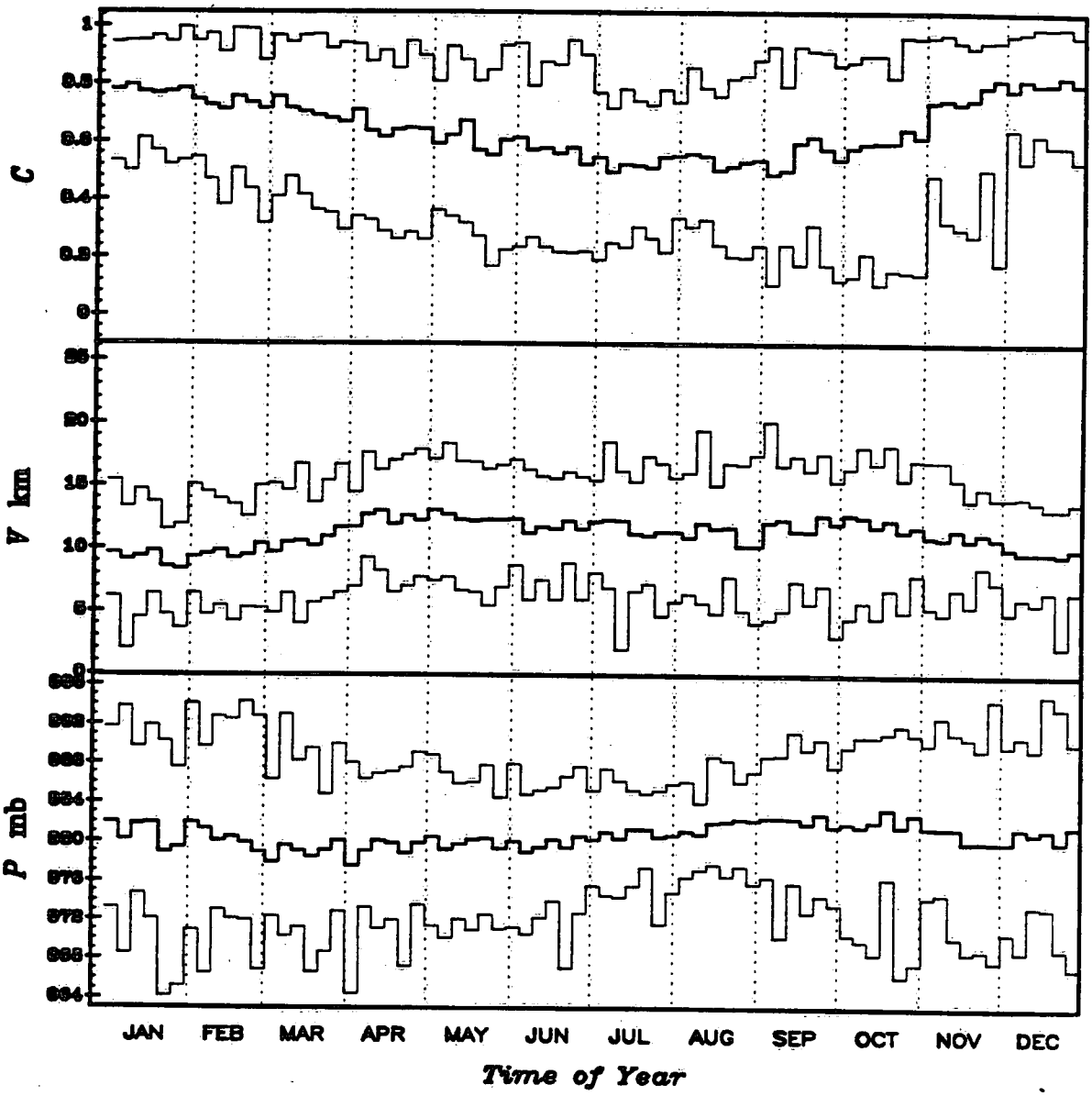

temperatures and surface water temperatures at this time of year.

Cloudiness is slightly greater over Lake Erie than over Lake Ontario during winter and early spring, although these differences are slight. Cloudiness is nearly identical for both lakes from May to November. Maximum cloudiness for both lakes occurs during November and December (approximately 80 percent) and is least during July, August, and September (approximately 50 percent) when surface pressure

Figure 5.1 - Maximum, Mean, and Minimum Five-Day Hydrometeorological, Radiation, and Energy Balance Components for Lake Erie, 1953-1983.

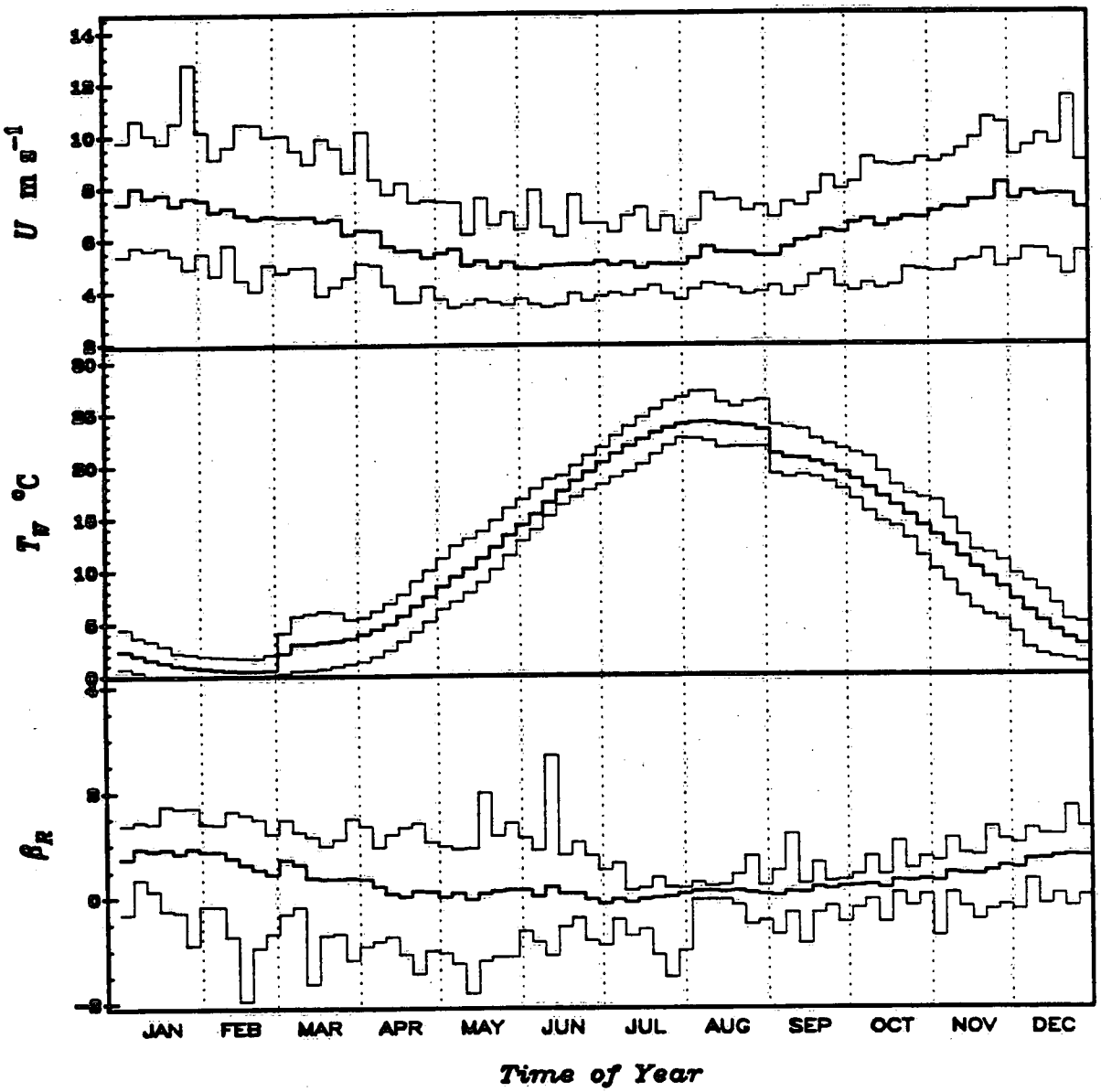

is greatest over both lakes. Largest surface pressure at this time of year occurs in association with maximum poleward displacement of the Bermuda anticyclone.

Seasonal variation of surface visibility is similar for both lakes. The data reveal a primary maximum during April and October, when cyclonic activity is greatest. Minimum values are observed during the winter months when migratory anticyclones stagnate over the Great Lakes basin. This is also the time when indus-

Figure 5.1 - Maximum, Mean, and Minimum Five-Day Hydrometeorological, Radiation, and Energy Balance Components for Lake Erie, 1953-1983.

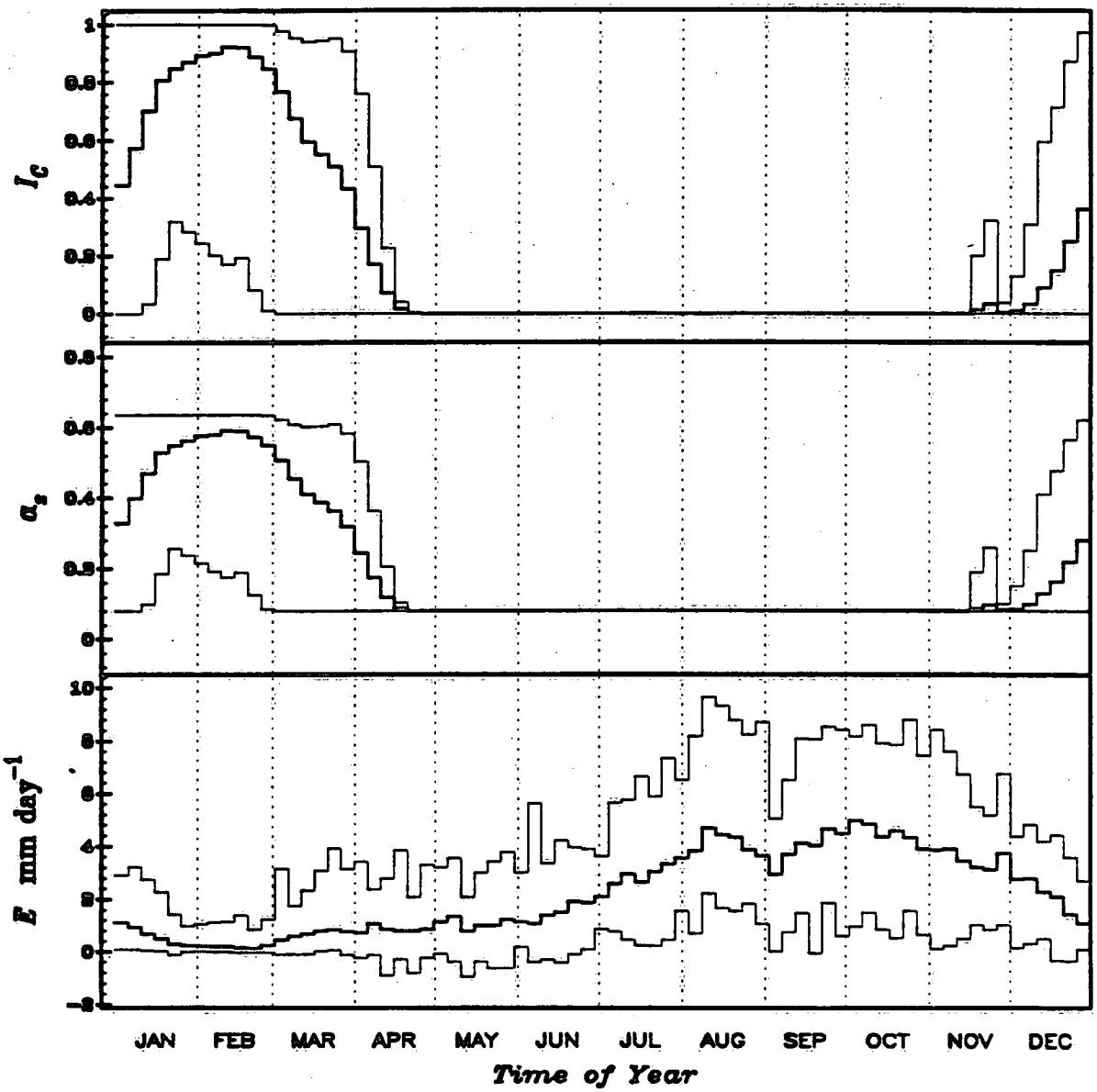

trial activity is greatest and convective motions are least. A weaker, secondary minimum occurs during August when the Bermuda anticyclone is displaced poleward. Visibility is consistently greater over Lake Ontario than over Lake Erie. This difference averages approximately 4 km.

Monthly estimates of ice concentration are in excellent agreement with tabluated values of Assel *et.al.* (1983). It is therefore anticipated that estimates of

Figure 5.1 - Maximum, Mean, and Minimum Five-Day Hydrometeorological, Radiation, and Energy Balance Components for Lake Erie, 1953-1983.

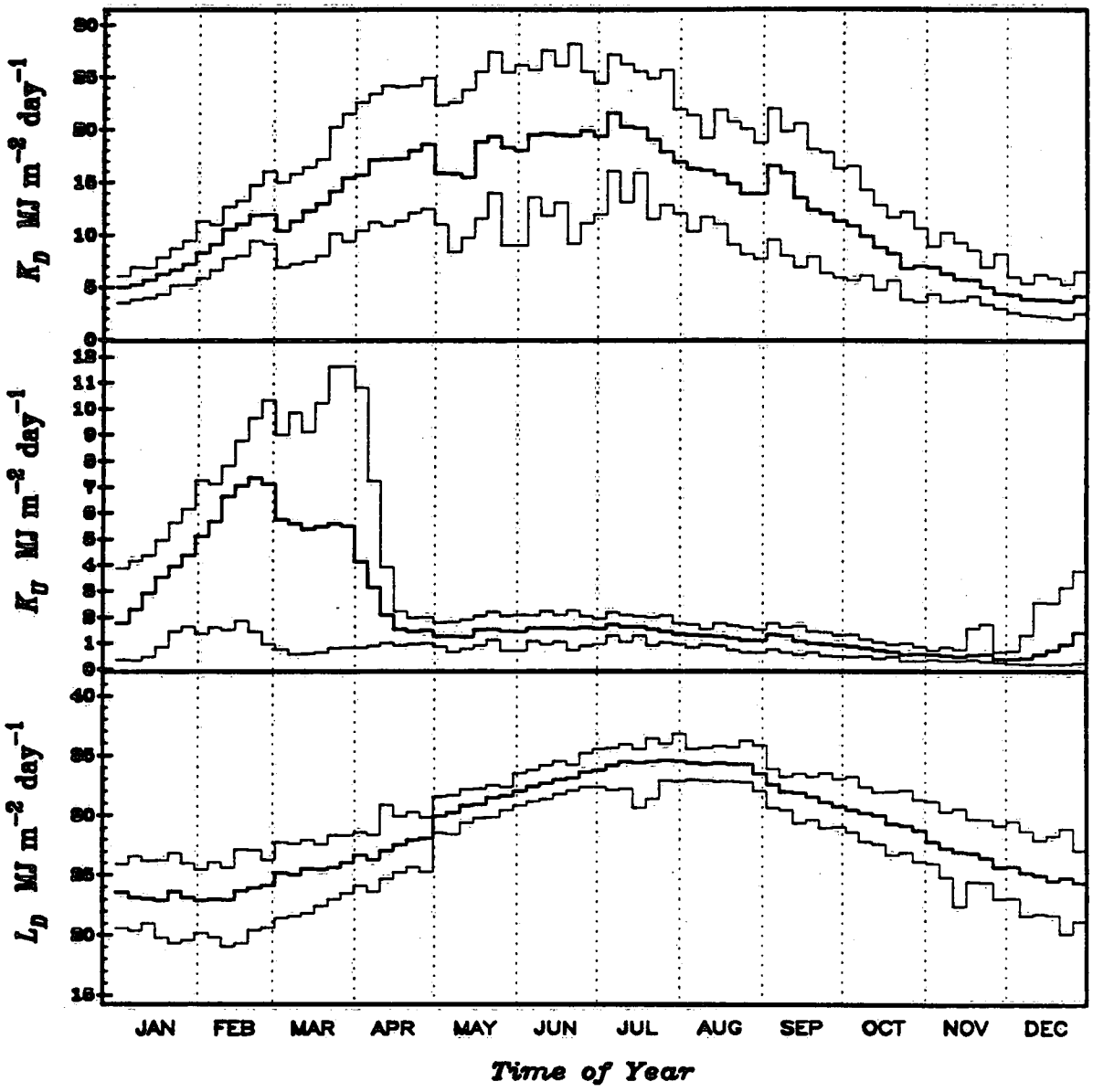

surface albedo are correct. Bowen ratios are similar for both lakes. Largest values are observed during the winter months. Minimum values are found during the late spring and early summer months, when β_R is approximately zero. Bowen ratios are, however, most variable at this time of year. They fluctuate within a much narrower range during the winter.

Shortwave radiation K_D is greatest during June and July and least during

Figure 5.1 - Maximum, Mean, and Minimum Five-Day Hydrometeorological, Radiation, and Energy Balance Components for Lake Erie, 1953-1983.

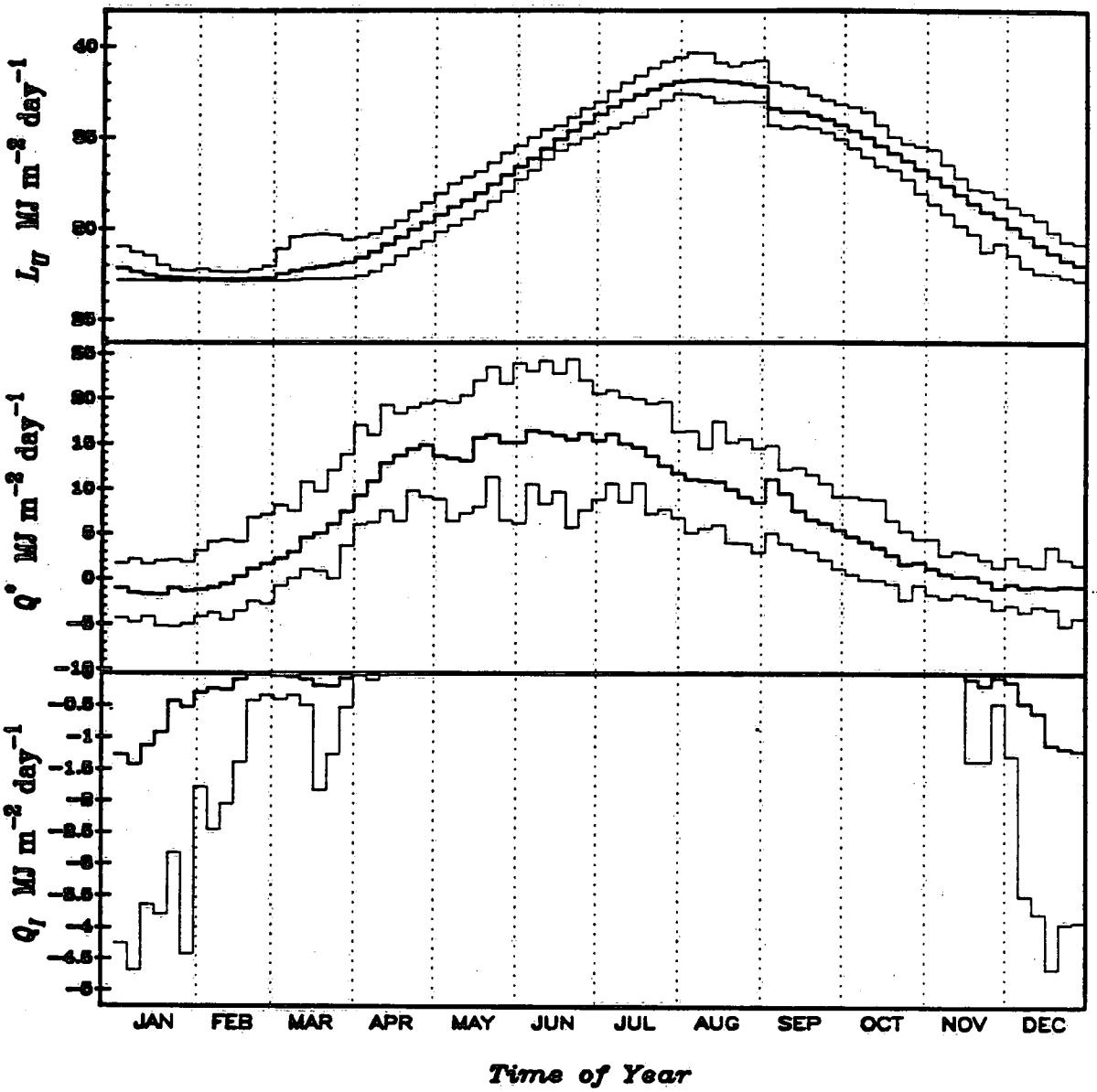

December, when the intensity of the incoming solar beam at the top of the atmosphere is least and cloudiness is generally greatest. Shortwave radiative income is very similar for both lakes from September to December. Incoming shortwave radiation is greater over Lake Erie from January to March, while Lake Ontario has a larger receipt from May to July. Both lakes have similar geographical position. Therefore, differences in daylight period are minor. These differences in shortwave

Figure 5.1 - Maximum, Mean, and Minimum Five-Day Hydrometeorological, Radiation, and Energy Balance Components for Lake Erie, 1953-1983.

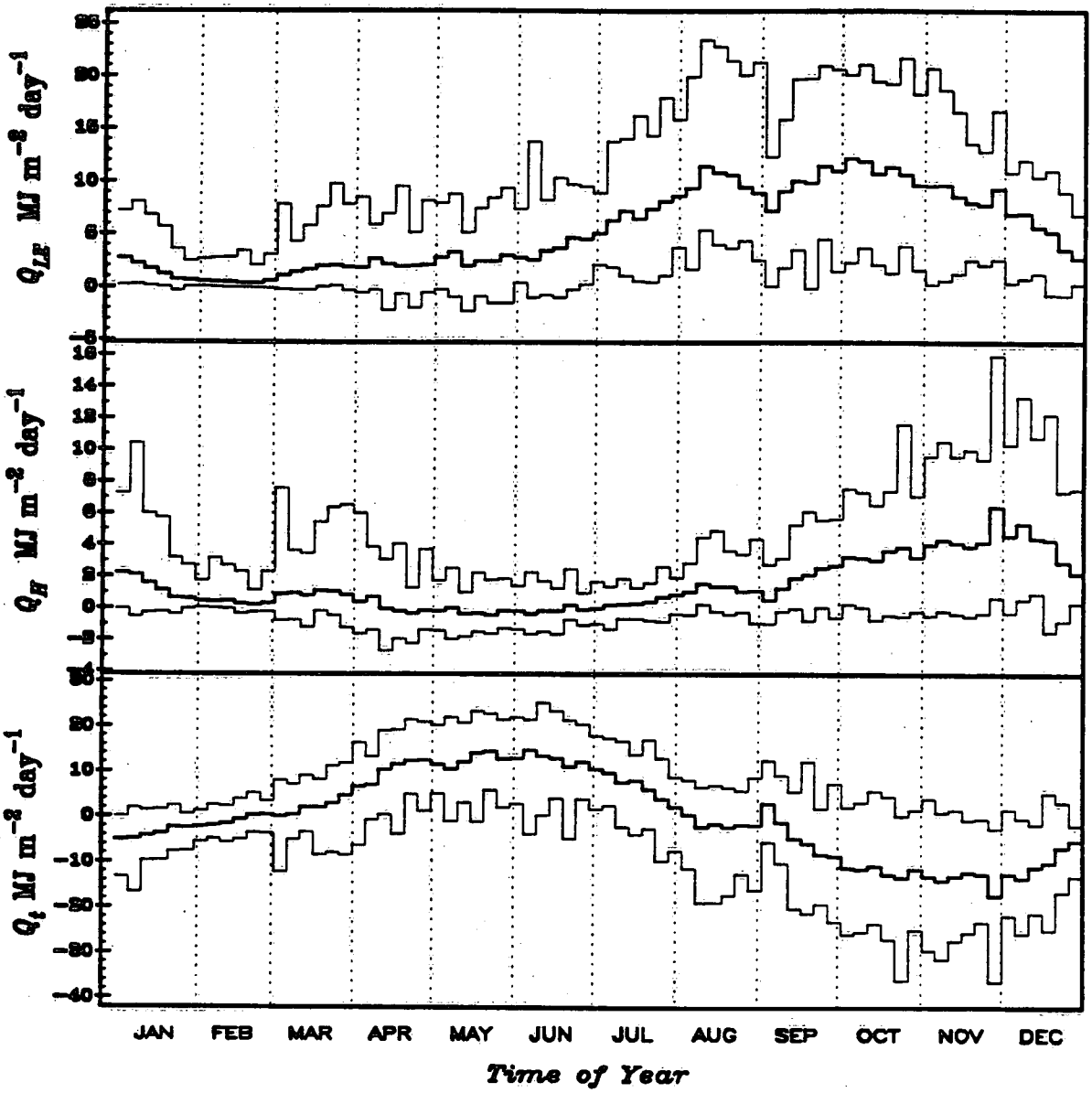

income arise for two quite different reasons. During the winter months, Lake Erie is largely ice-covered. Ice-cover greatly enhances multiple scattering of shortwave radiation and is responsible for the larger shortwave radiative income over Lake Erie. Lake Ontario experiences relatively little ice-cover during the winter and multiple scattering effects are therefore reduced.

Cloudiness is similar for both lakes at all times of the year, however, visibility

Figure 5.2 - Maximum, Mean, and Minimum Five-Day Hydrometeorological, Radiation, and Energy Balance Components for Lake Ontario, 1953-1983.

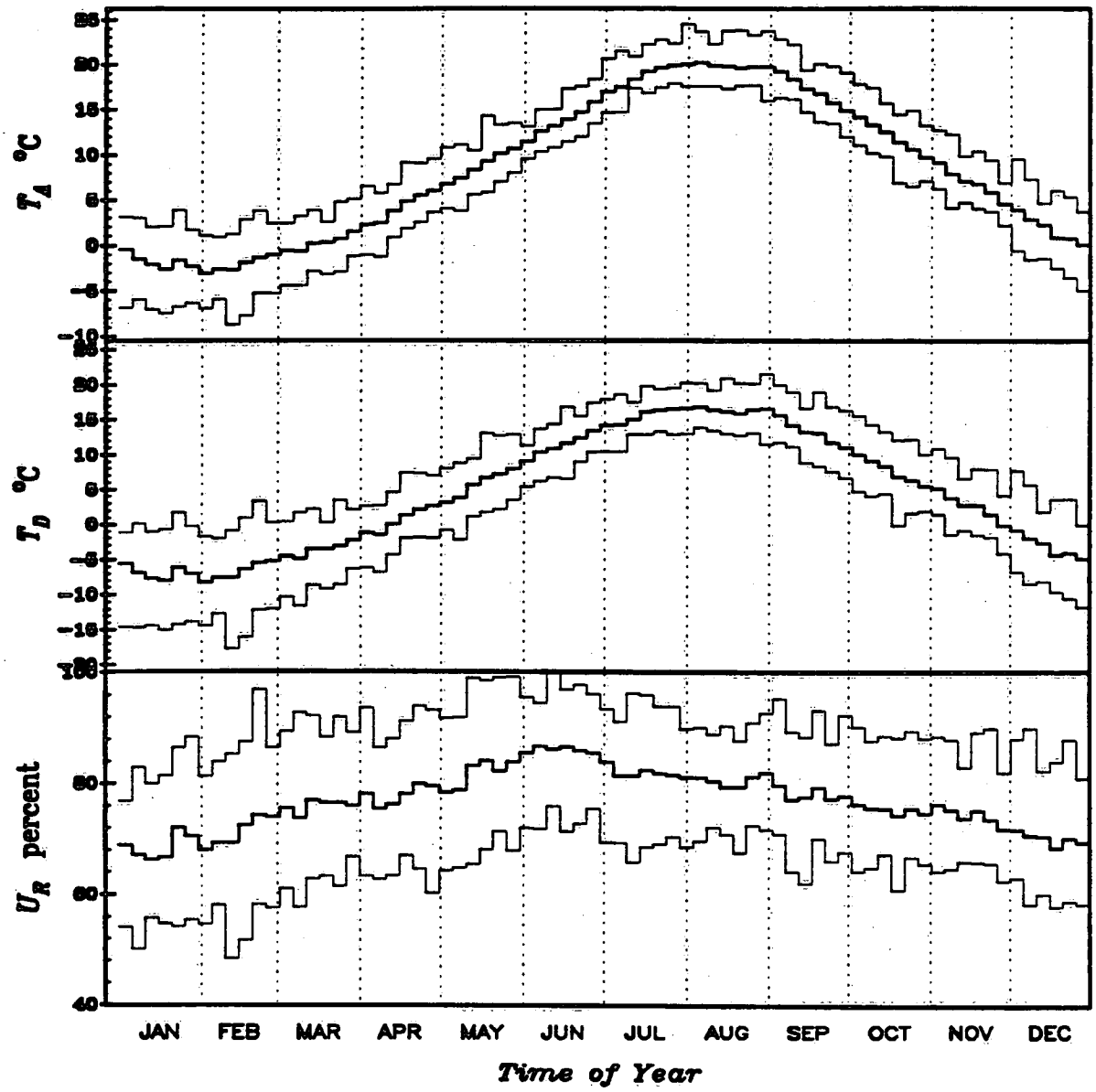

is greater over Lake Ontario than over Lake Erie. This results in a greater shortwave radiative income over Lake Ontario for the May through July period. The difference, approximately 2 to 4 MJ m^{-2} day^{-1}, is not insignificant and emphasizes the importance of incorporating aerosol effects on radiative transfer.

The reflected shortwave radiation, being directly proportional to K_D and the surface albedo α_s, is largest over Lake Erie during February and March when ice con-

Figure 5.2 - Maximum, Mean, and Minimum Five-Day Hydrometeorological, Radiation, and Energy Balance Components for Lake Ontario, 1953-1983.

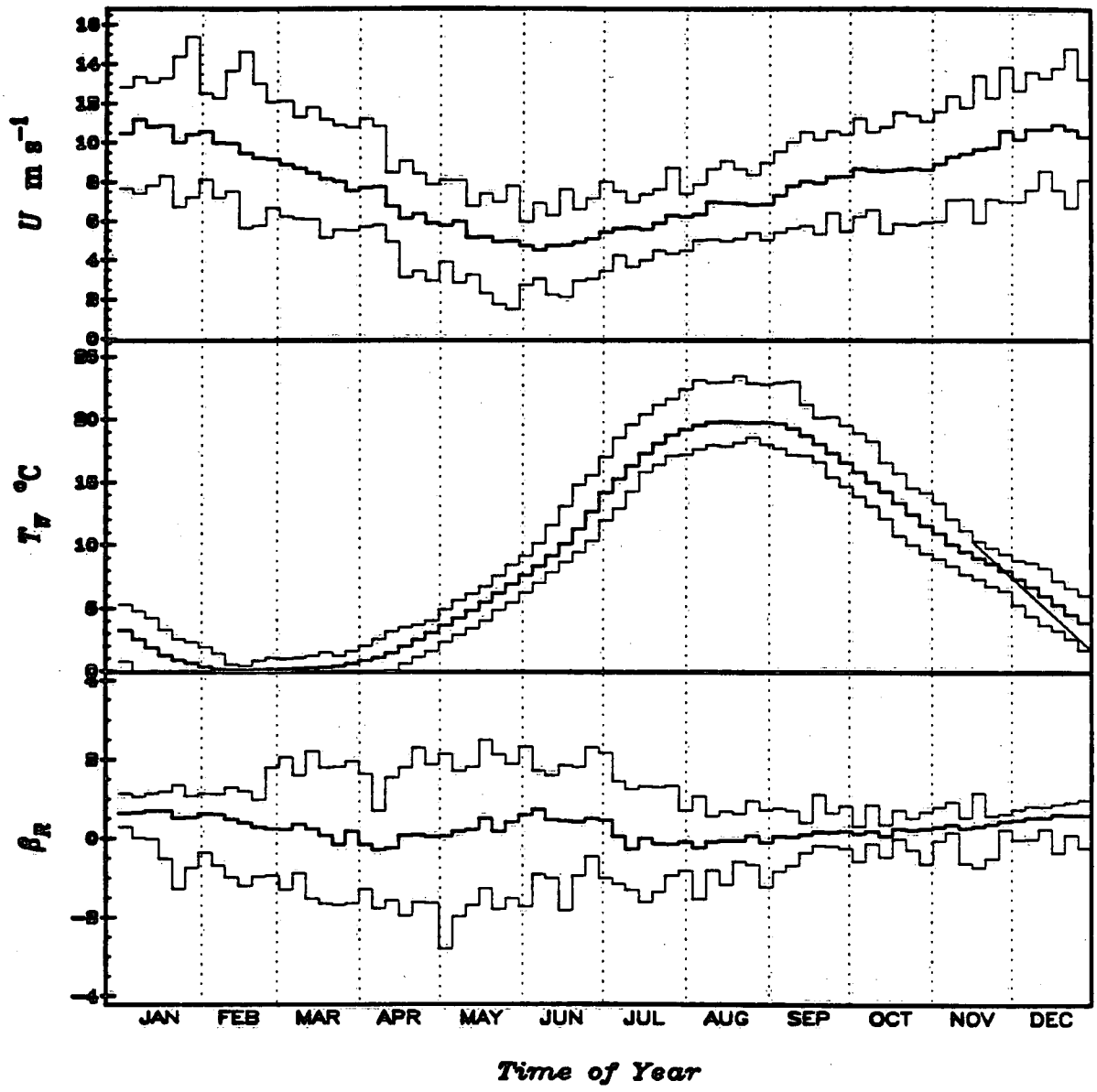

centrations are greatest. Reflected shortwave radiation is approximately one half of the incoming shortwave radiation at this time of year. The small ice concentrations over Lake Ontario have little impact on reflected radiation as the incoming shortwave radiation at this time of year is also small. Thus, annual variation of reflected shortwave radiation over Lake Ontario is very similar to that for incoming shortwave radiation.

Figure 5.2 - Maximum, Mean, and Minimum Five-Day Hydrometeorological, Radiation, and Energy Balance Components for Lake Ontario, 1953-1983.

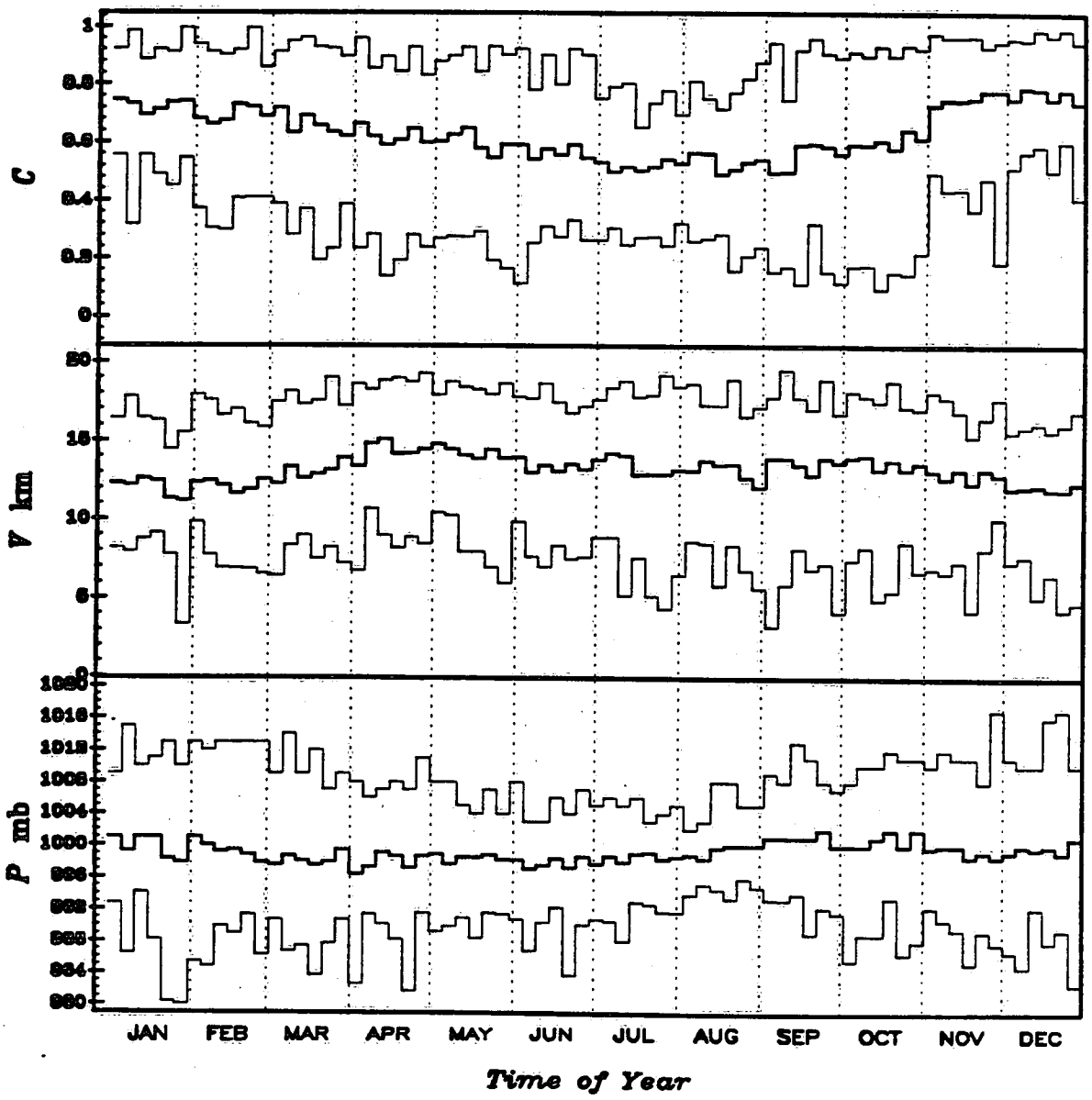

Incoming longwave radiation is largest during July and August and least in January and February. This pattern strongly mirrors the seasonal variation in air temperature. Longwave fluxes are greater over Lake Erie than over Lake Ontario at all times of the year except during November, December, and January, when they are approximately equal. During May and June, incoming longwave over Lake Erie exceeds that for Lake Ontario by 2 to 4 MJ m^{-2} day^{-1}. This difference results from

Figure 5.2 - Maximum, Mean, and Minimum Five-Day Hydrometeorological, Radiation, and Energy Balance Components for Lake Ontario, 1953-1983.

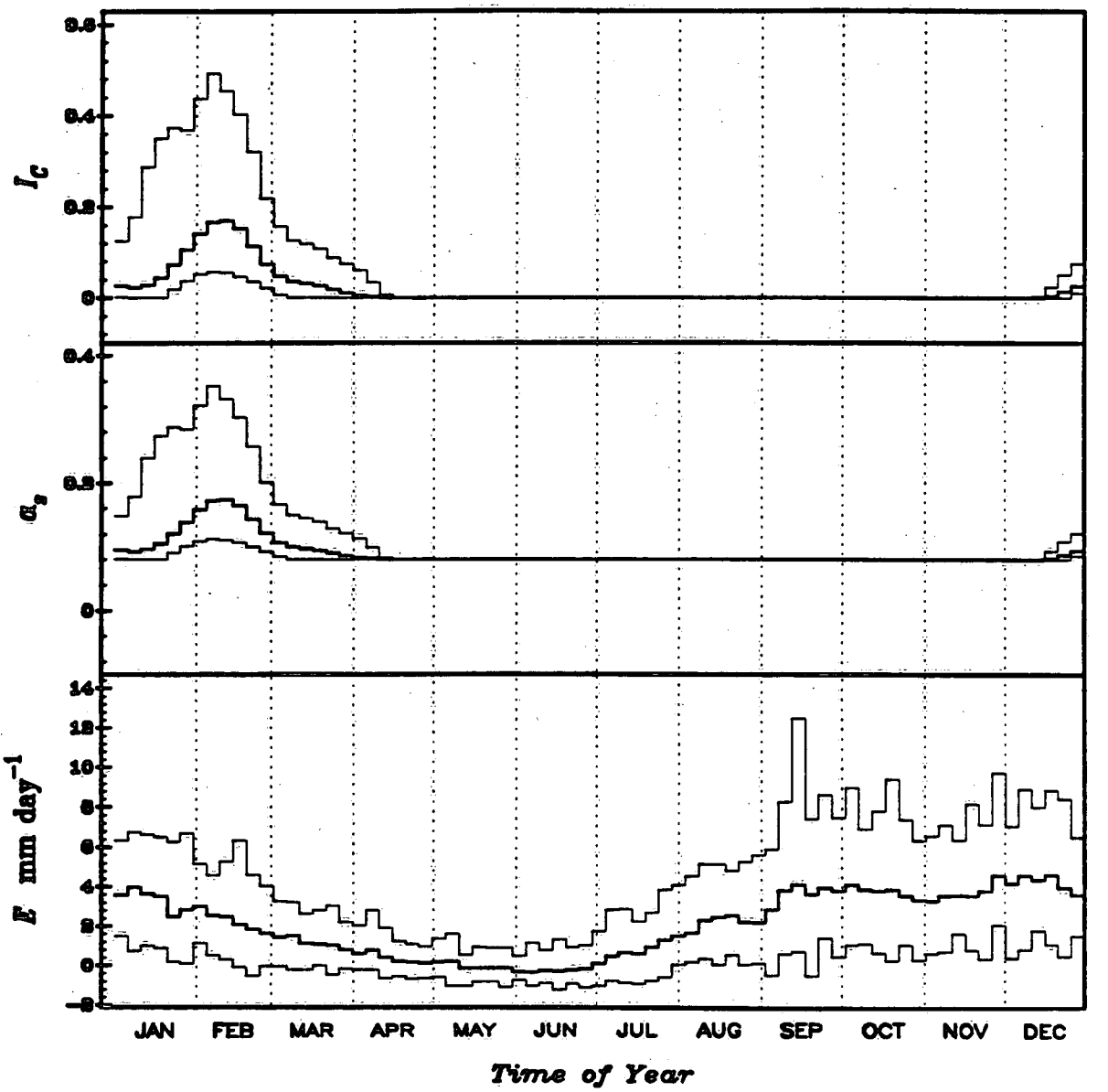

greater air temperatures over Lake Erie at these times, but may also reflect a greater radiative income from greater aerosol concentrations.

On an annual basis, incoming longwave radiation ranges from approximately 23 MJ m^{-2} day^{-1} in January to 34 MJ m^{-2} day^{-1} in July for Lake Erie and 22 MJ m^{-2} day^{-1} in January to 33 MJ m^{-2} day^{-1} in August for Lake Ontario. This is a range of approximately 11 MJ m^{-2} day^{-1} for both lakes and is approximately one

Figure 5.2 - Maximum, Mean, and Minimum Five-Day Hydrometeorological, Radiation, and Energy Balance Components for Lake Ontario, 1953-1983.

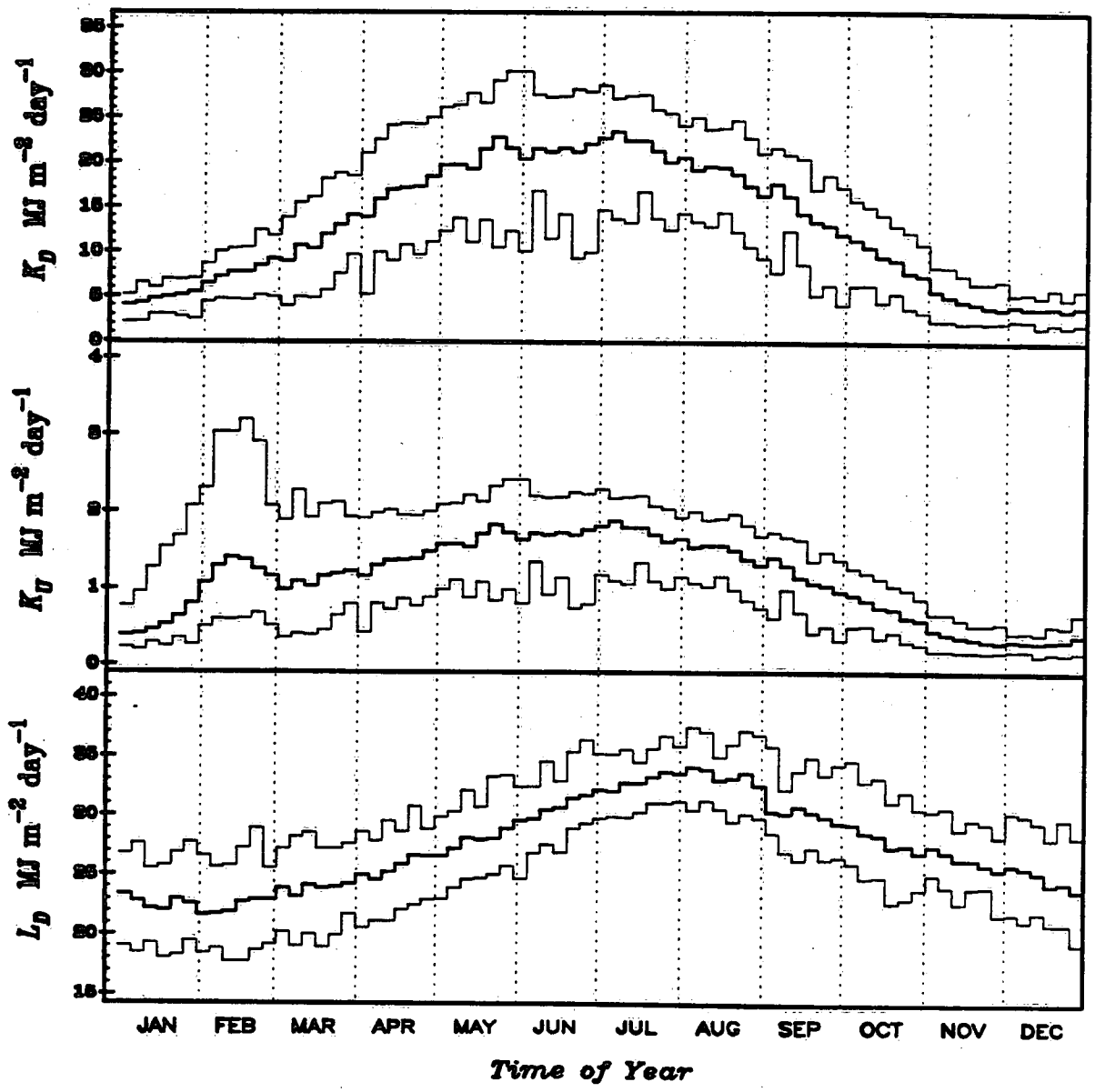

half the annual range for incoming shortwave radiation. This is a consequence of cloudiness which affects longwave radiation income differently from shortwave radiation receipt. During winter months, when cloudiness is greatest, incoming longwave radiation is greater than would be observed if there less cloud. The opposite effect occurs during summer months when cloudiness is less. In these months, incoming longwave radiation is less than would be observed if cloudiness

Figure 5.2 - Maximum, Mean, and Minimum Five-Day Hydrometeorological, Radiation, and Energy Balance Components for Lake Ontario, 1953-1983.

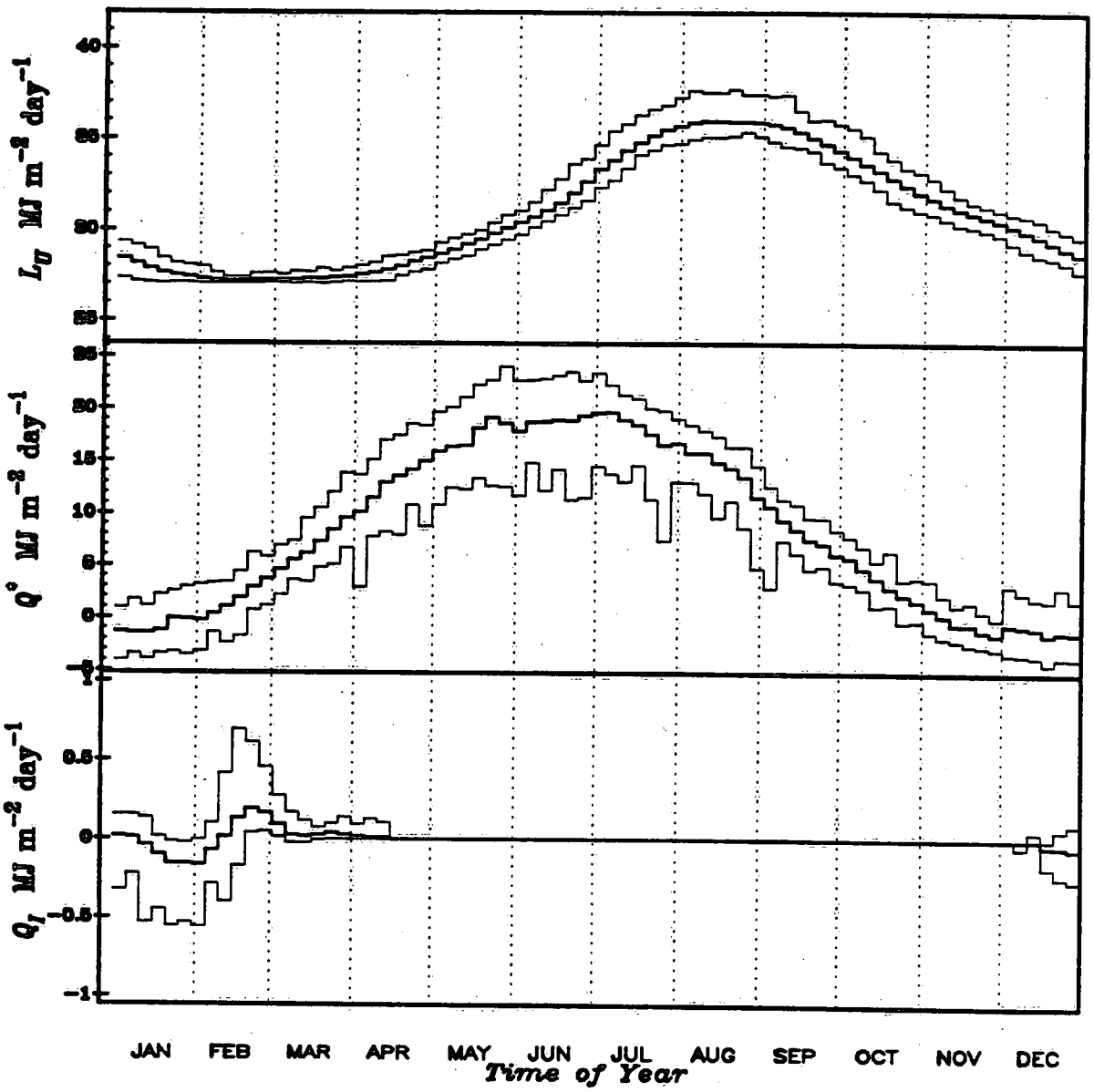

were greater. The net result is that the seasonal variation of cloudiness reduces the annual range of incoming longwave radiation. Shortwave radiation is directly proportional to cloudiness. In wintertime, cloudiness reduces an incoming solar beam that is initially low in intensity. During the summer months, the incoming solar beam is much more intense while small cloud amounts result in large radiative gains at the surface.

Figure 5.2 - Maximum, Mean, and Minimum Five-Day Hydrometeorological, Radiation, and Energy Balance Components for Lake Ontario, 1953-1983.

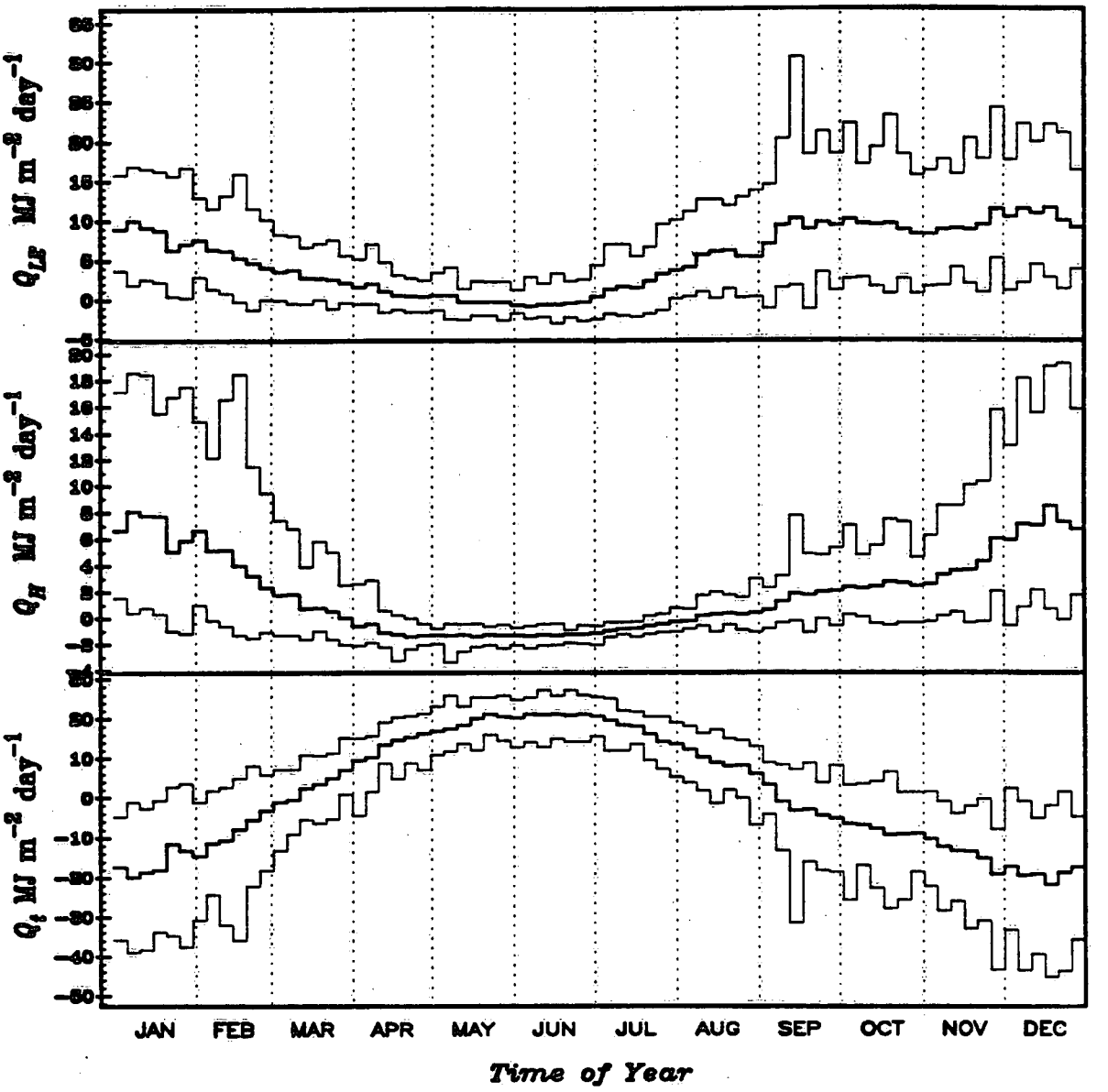

The upward emitted longwave radiation L_U, being directly proportional to surface water temperature, displays the same seasonal variation as the latter. Outgoing longwave radiation is largest during August for both lakes and least in February when surface water temperatures are at, or near, minimum values. Outgoing longwave radiation is slightly larger for Lake Ontario from December to February when Lake Ontario is slightly warmer than Lake Erie. The largest difference occurs

Figure 5.3 - Comparison of Mean Monthly Values for Selected Hydrometeorological Variables, Radiation, and Energy Balance Components for Lake Erie (thin line) and Lake Ontario (thick line), 1953-1983.

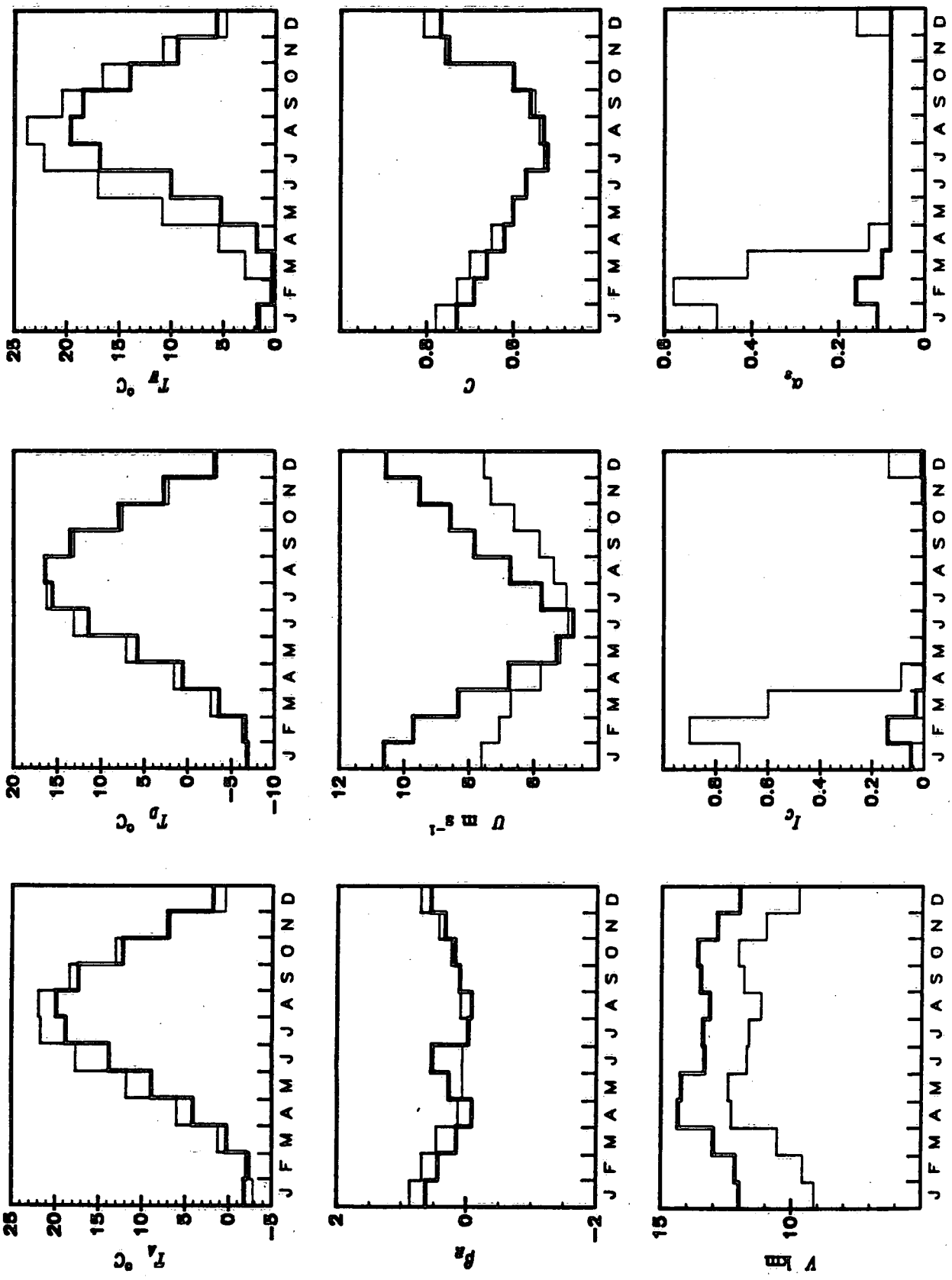

Figure 5.3 - Continued.

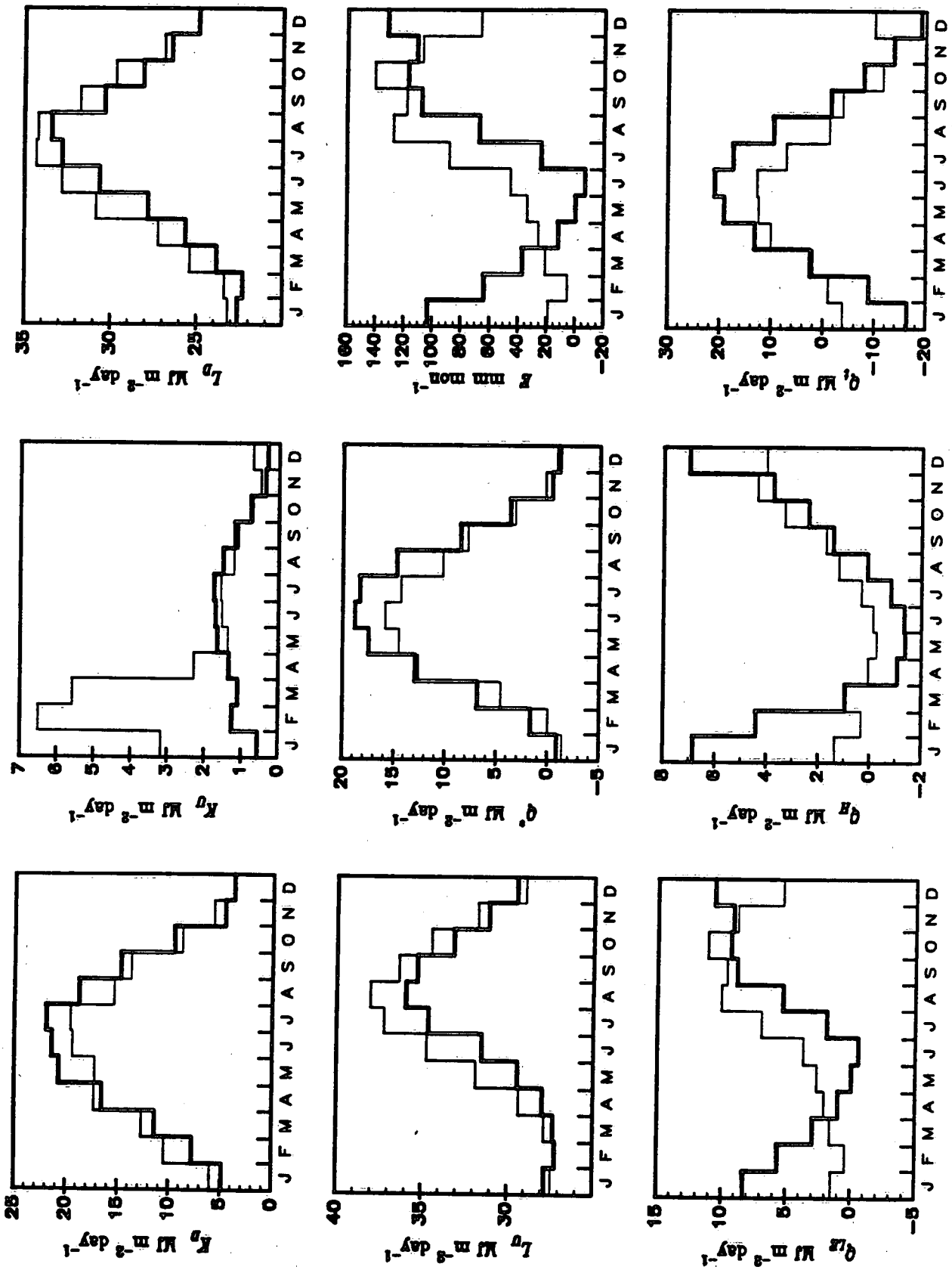

during the May through August period when Lake Erie is significantly warmer than Lake Ontario.

Net radiation balance is the joint effect of the net shortwave and net longwave balances. For both lakes, net radiation is a slowly varying function of time of year. It is approximately zero from late November to early February. It has a broad, rather featureless, maximum in summer when it averages approximately 15 MJ m^{-2} day^{-1} (Lake Erie) to 18 MJ m^{-2} day^{-1} (Lake Ontario) from mid- May to late July and then begins decreasing rapidly thereafter. Net radiation income is very similar for both lakes and strongly mirrors the shortwave income, except that values are reduced by approximately 4 MJ m^{-2} day^{-1}, which is approximately the amount outgoing longwave radiation exceeds the incoming longwave radiation. Net radiation is greater over Lake Ontario (approximately 3 to 4 MJ m^{-2} day^{-1}) from May to August. This result largely reflects the increased shortwave radiative income arising from reduced aerosol concentrations.

Seasonal variation of latent and sensible heat fluxes is opposite to that of net radiation. Largest latent heat fluxes occur during autumn and winter months while smallest values are observed during late winter and spring months. Figure 5.3 shows, however, that times of maximum and minimum values for Lake Ontario lag behind those for Lake Erie by approximately two to three months. Largest latent heat fluxes occur during October for Lake Erie and December for Lake Ontario. These differences arise from the differences in timing of occurrences of maximum temperature and vapour pressure gradients between lake surface and overlying air. The larger heat content of Lake Ontario ensures that surface water temperatures decrease at a slower rate, while Arctic air masses generally appear in late November and early December. The magnitude of latent heat fluxes during the high evaporation months is similar for both lakes, approximately 10 MJ m^{-2} day^{-1}.

Latent heat fluxes decrease during the winter months, although the decrease is

much more rapid over Lake Erie because of seasonal ice-cover. Lake Ontario, with little ice cover, averages 5 MJ m^{-2} day^{-1} during these months. During the spring months, latent heat fluxes over Lake Erie are small, but positive, and become large by July and August as surface water temperature rapidly increases. Lake Ontario heats up much more slowly. During May and June, ambient dew point temperatures are approximately equal to, or greater than, surface water temperature of Lake Ontario. The result is that latent fluxes are frequently close to zero or negative (condensation) for these months. Surface water temperatures begin increasing rapidly during July and August, and latent heat fluxes begin increasing.

Seasonal variation of sensible heat fluxes mirrors that of latent heat fluxes, since sensible heat flux is directly proportional to the latent heat flux by the Bowen ratio. Sensible heat fluxes are less than latent heat fluxes, as the average Bowen ratio is less than one. Largest differences between the lakes occurs from December to March, when the difference is approximately 5 MJ m^{-2} day^{-1}. Differences are much smaller at other times of the year. Lake Ontario sensible heat fluxes average -1 to -2 MJ m^{-2} day^{-1} from April to July, indicating a heat gain at the surface. Sensible heat fluxes over Lake Erie during these months is approximately zero or slightly negative. On a annual basis, maximum sensible heat fluxes lag behind maximum latent heat fluxes for both lakes. This effect arises from the difference in seasonal variation of latent heat flux and Bowen ratios. The latter lags behind the former in such a way that the increase in Bowen ratio is larger than the decrease in latent heat flux. The difference is usually small, but large enough to yield maximum sensible heat fluxes after largest latent heat fluxes have occurred.

The surface heat flux is the joint effect of net radiation and turbulent heat fluxes. Seasonal variation for both lakes is very similar: maximum heat gain occurs during June for both lakes, while largest losses occur in November for Lake Erie and December for Lake Ontario. Maximum and minimum heat fluxes are approximately

20 MJ m^{-2} day^{-1} for Lake Ontario and approximately 12 MJ m^{-2} day^{-1} for Lake Erie. Annual net surface heat flux is not zero, however. It is close to zero for Lake Erie over periods ranging from three to six years. Lake Ontario appears to be gaining heat on an annual basis, although the gain over the 31 year period is small, amounting to approximately 0.4 percent of average annual minimum heat content. This value is well within the estimated measurement error for heat contents.

5.2. LAKE HEAT CONTENT

Accurate evaluation of lake heat content is a crucial step in model calculations because surface water temperature, upon which estimates of several other variables are made, is directly proportional to heat content. On the other hand, lake heat content serves as an important constraint on estimated surface heat fluxes and, in turn, on estimated turbulent heat fluxes. Heat content measurements afford an independent verification of surface heat estimates and provide some insight into the stability of the numerical algorithm. This section describes the comparison of daily estimates of heat content with measured values for Lake Erie. Similar comparisons have been performed for Lake Ontario, however, they are not very different from those presented in Figure 5.4 for Lake Erie.

Figure 5.4 illustrates daily estimates of heat content for Lake Erie for 1953 to 1983. Measured heat contents, obtained from vertical temperature profiles from ship surveys, are available for the period 1967 to 1980. These are shown as filled circles on the appropriate dates. Mean daily heat contents, obtained by averaging over the 31 year period, are shown by the dotted line.

The estimated daily heat contents were obtained with a single run of the computer programme. The results are encouraging. Agreement between estimated and measured values are generally quite good, especially between 1967 and 1973 when estimated values are in virtual agreement with measured values. Estimated heat contents appear consistently overestimated during 1978 and 1979, while the

Figure 5.4 - Daily Heat Contents (thin line), Mean Daily Heat Contents (dotted line), and Measured Heat Contents (filled circles) for Lake Erie, 1953-1983. Heat contents are expressed in exa (10^{18}) Joules.

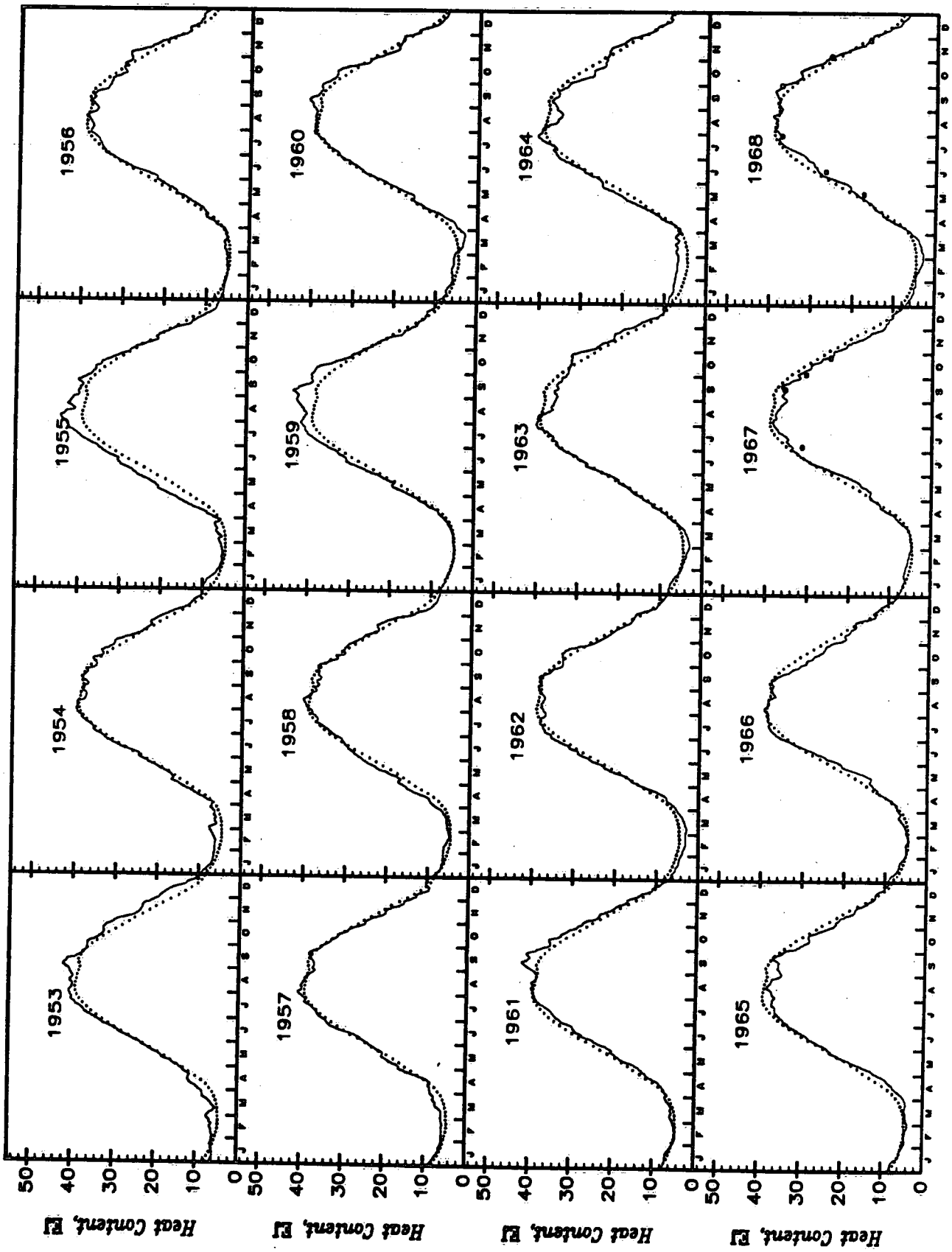

Figure 5.4 - Continued.

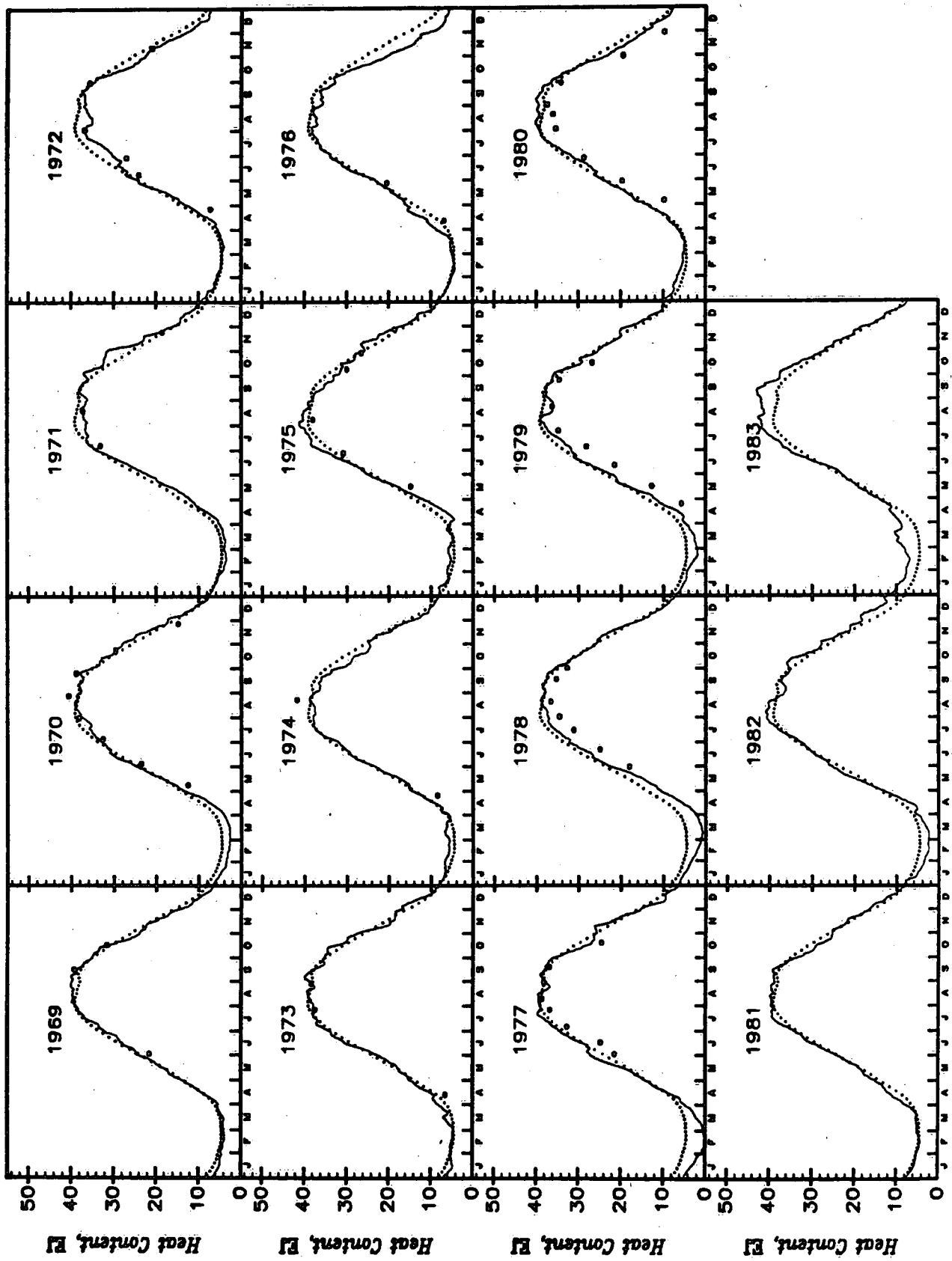

agreement improves during 1980. The overall agreement is thus seen to be good, especially since the model had been simulating daily heat contents for 14 years before the first measured values became available.

The good agreement suggests that the model representation of the physics of the surface heat transfer is correct. The major uncertainty are heat contents during the winter months, when ice conditions preclude ship surveys. No "run-away" situations (e.g. negative heat contents which arise in frequent large heat losses during winter) were ever witnessed during the 31 year period, however, and this suggests that wintertime heat contents are reasonably well estimated.

There is one source of uncertainty in these results. This is the effect of lake levels on heat content values. Lake surface area is assumed constant in this study, which implies a constant lake level. Lake levels vary seasonally, e.g. snowmelt during March and April, and with heavy precipitation events. The good agreement between estimated and measured heat contents between 1967 and 1973 suggests these effects may be small, although they may have some bearing on overestimated heat contents in 1978 and 1979.

Finally, the model was developed and tested with data from Lake Ontario. It is therefore encouraging that the model has performed well for Lake Erie. These results provide confidence that the model has captured the essential physics and is numerically stable.

5.3. LONG-TERM VARIATIONS

Figures 5.5 and 5.6 illustrate the annual variation of hydrometeorological variables, radiation, and energy balance components for Lake Erie and Lake Ontario, respectively, for the period 1953-1983. Trends are observed for some of the variables, while other variables display little or no trend. The best documented trend has been the decrease of air temperatures since the late 1940's. Figures 5.5 and 5.6

demonstrate decreasing air temperatures over both lakes since 1953. The decrease is not consistent and several years (1953, 1955, 1959, 1964, 1973, 1975, and 1983) stand out as years with well-above average (for 1953- 1983 period) annual temperatures. The decrease in annual temperatures appears to have halted near 1965 and fluctuate for approximately the next ten years. Air temperatures over both lakes then begin increasing. Since 1978, mean annual air temperatures have risen 2.3 °C over Lake Erie and 1 °C over Lake Ontario. By 1983, mean annual temperatures were well above the 31 year average and close to values observed near the beginning of the study period.

Dew point temperatures and surface water temperatures closely mirror the changes that have occurred in air temperatures during this time. Since 1978, annual surface water temperatures have increased for both lakes, although the increase has been more moderate for Lake Ontario than for Lake Erie. In this same period, however, dew point temperatures have increased by the same amount for both lakes.

Annual variation of Bowen ratio appears erratic over Lake Ontario, with largest values occuring between 1968 and 1980. Over Lake Erie, annual Bowen ratios appear to be inversely proportional to mean annual temperature.

Annual variations in cloudiness appear to be the same over lakes, with a very small increase over this period. There appears to be little variation in annual mean visibility over Lake Ontario. Lake Erie visibilities fluctuate about the 31 year mean until approximately 1970, after which time visibilities begin increasing. Since 1972, annual mean visibility has increased by nearly 3 km. The value for 1983, 12.7 km, is close to values observed for Lake Ontario (13.1 km).

Wind speed has varied similarly over both lakes. Values increased between 1953 and 1958 and then began slowly decreasing until 1976. Wind speeds for 1976 are amongst the highest values observed for both lakes during the 31 year period. Wind speeds have decreased since 1977. By 1983, annual wind speeds had

Figure 5.5 - Annual Variation of Hydrometeorological Variables, Radiation, and Energy Balance Components for Lake Erie, 1953 - 1983. Mean values for 1953-1983 period shown by thin dashed line.

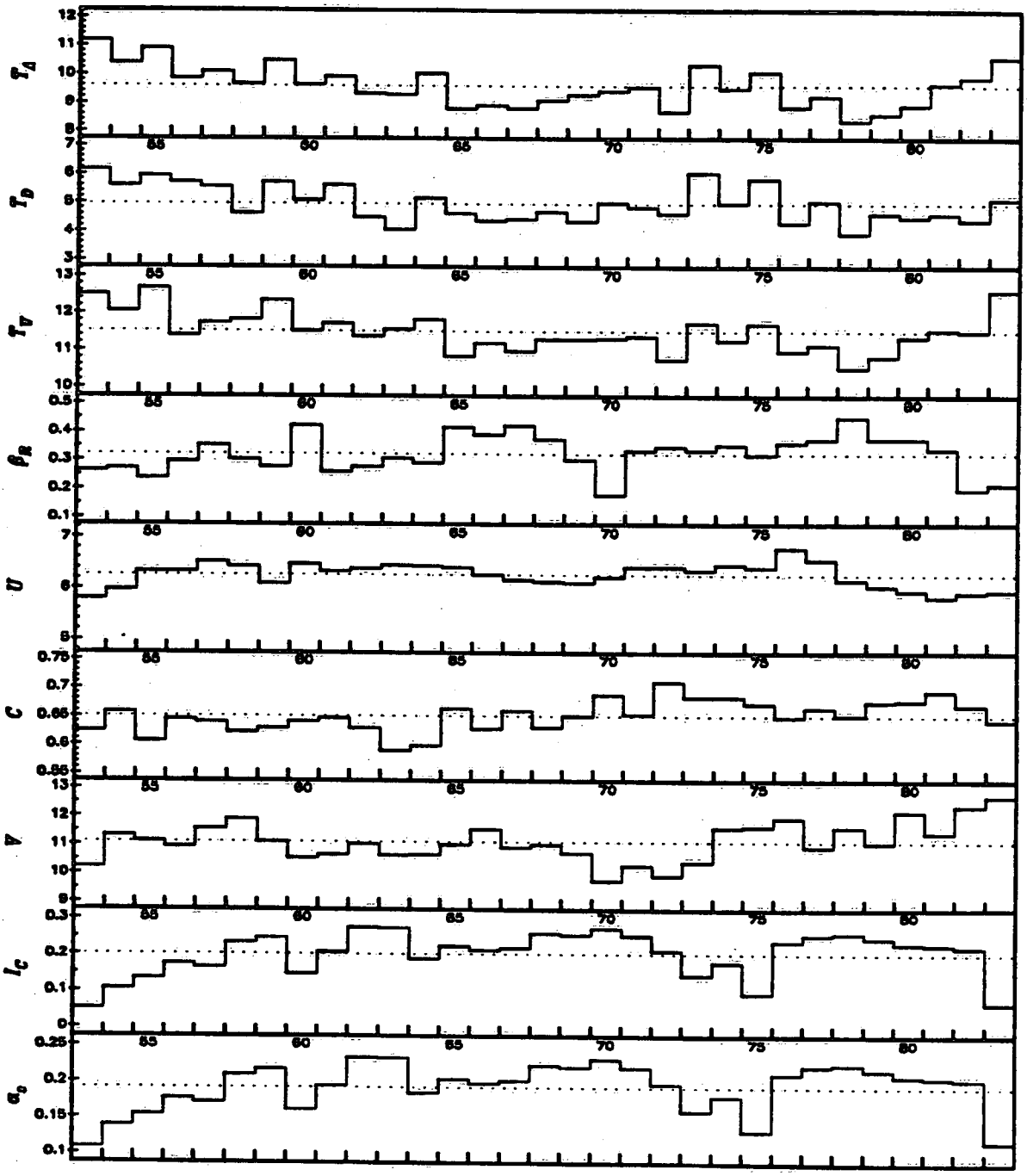

decreased close to low values observed in the early 1950's.

Ice concentrations have varied inversely with air temperatures. Thus, there has been a slow, but steady, increase in annual mean ice concentrations over Lake Erie

Figure 5.5 - Annual Variation of Hydrometeorological Variables, Radiation, and Energy Balance Components for Lake Erie, 1953 - 1983. Mean values for 1953-1983 period shown by thin dashed line.

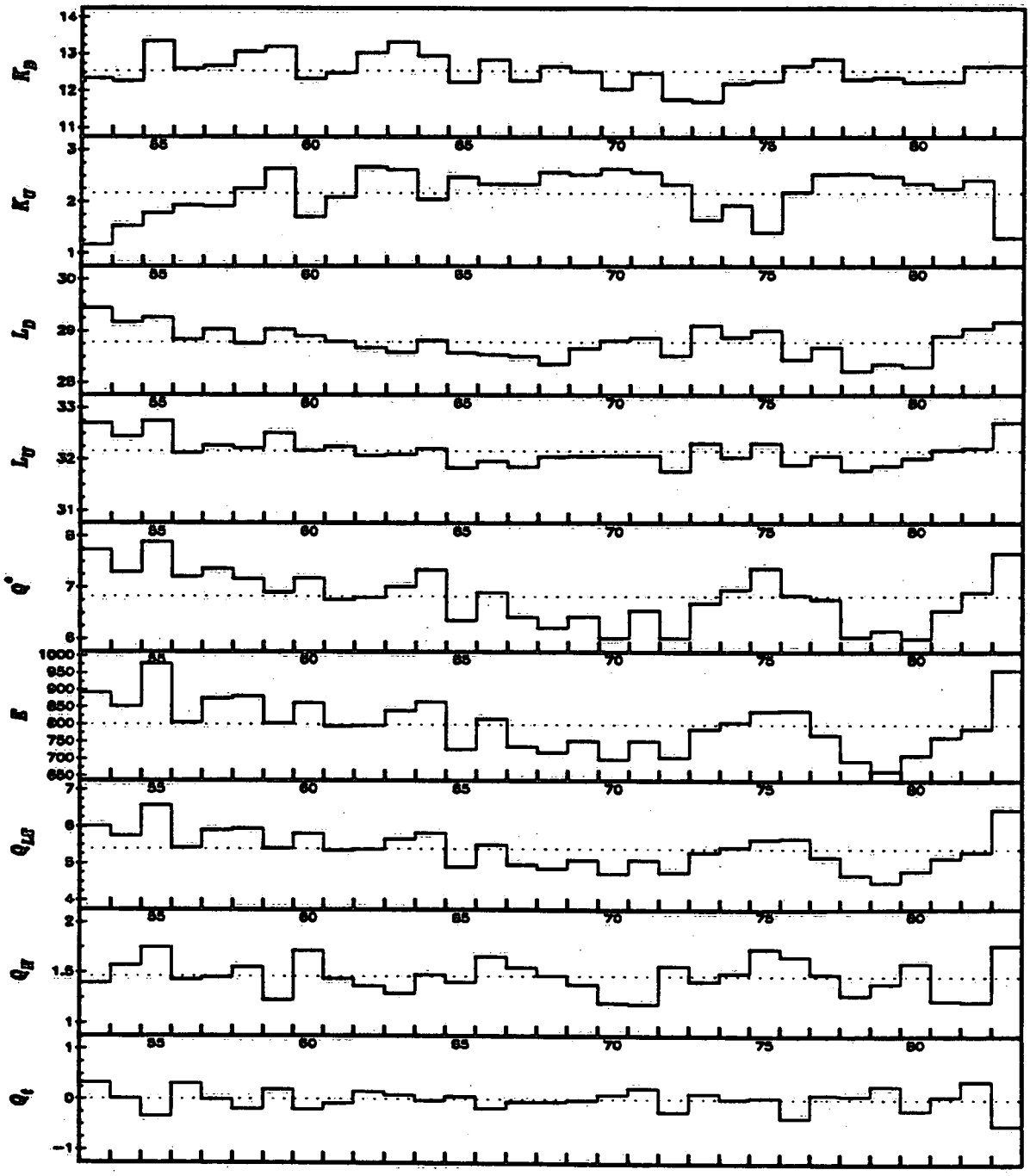

which apparently culminated in 1970. Ice concentrations then decrease dramatically to 1975 (to low values observed in the early 1950's) and then increase rapidly to near record values in 1978. Values decrease slowly thereafter and especially in

Figure 5.6 - Annual Variation of Hydrometeorological Variables, Radiation, and Energy Balance Components for Lake Ontario, 1953 - 1983. Mean values for 1953-1983 shown by thin dashed line.

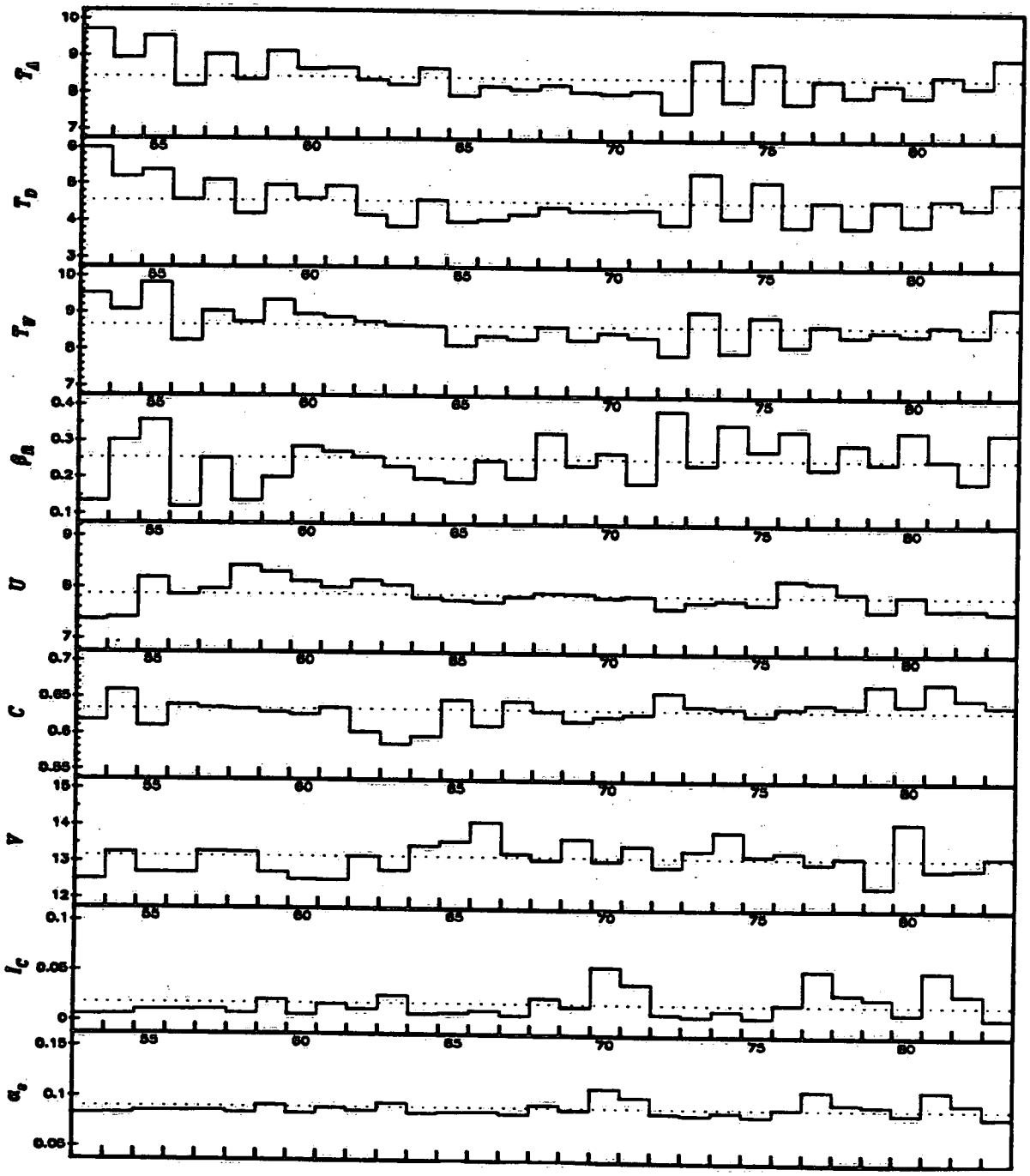

1983 when there is a large decrease associated with the record warmth of 1983. This pattern is also observed for Lake Ontario. Surface albedo is directly proportional to ice concentrations, and thus annual variation in surface albedo and

Figure 5.6 - Annual Variation of Hydrometeorological Variables, Radiation, and Energy Balance Components for Lake Ontario, 1953 - 1983. Mean values for 1953-1983 shown by thin dashed line.

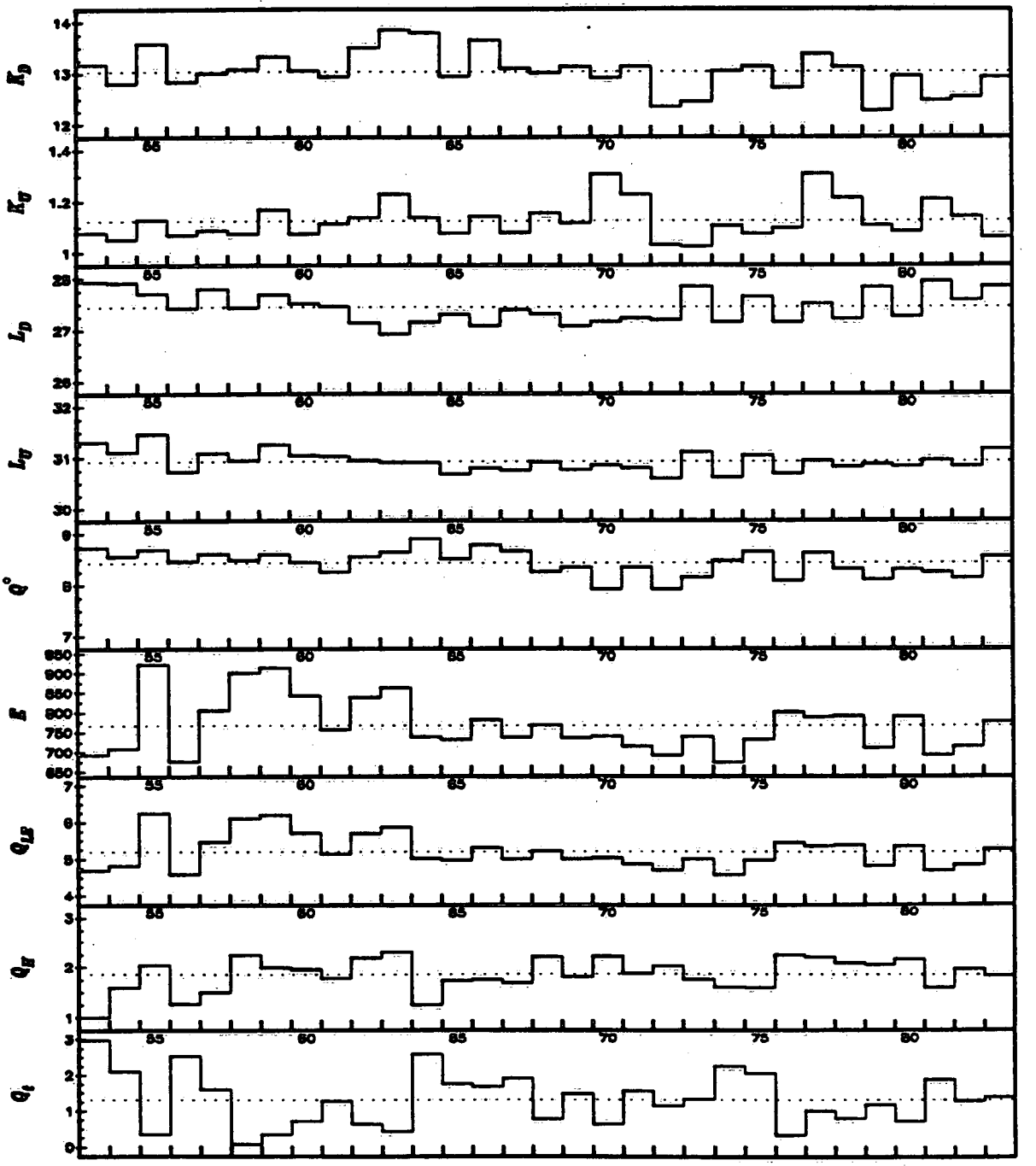

reflected shortwave radiation is almost identical to that for ice concentrations.

Incoming shortwave radiation appears to fluctuate around the 31 year period mean from 1953 to 1963 and then begins to slowly decrease thereafter. This pat-

tern is observed for both lakes. The decrease appears to have halted in 1973 for Lake Erie and 1972 for Lake Ontario. The decrease appears to be related to increasing cloudiness over this period of time. The decrease, 1.6 MJ m^{-2} day^{-1}, is the same for both lakes. Incoming shortwave radiation receipts have increased over Lake Erie since 1972, mostly as a result of increased visibility. Incoming shortwave radiation receipts have fluctuated about the 31 year mean value for Lake Ontario, although the results suggest a steady increase since 1979.

Incoming longwave receipts have generally declined from 1953 to approximately 1970 after which time receipts begin increasing. The decrease prior to 1970 amounts to approximately 1 MJ m^{-2} day^{-1}, and is slightly more than half the decrease in incoming shortwave radiation. This may be the result of increasing cloudiness which has reduced, at least partially, the effect of decreased temperatures. Incoming longwave fluxes have generally increased since 1970, with values in 1983 close to, or equalling, the large values observed near the beginning of the study period. The upward emitted longwave flux, being directly proportional to surface water temperature, varies in almost the same manner as the latter.

The net effect of changes in radiative fluxes is summarized by variations in net radiation. For Lake Ontario, annual variations in net radiation are small, rarely exceeding 0.3 MJ m^{-2} day^{-1}. Variations are much larger over Lake Erie, amounting to approximately 0.8 MJ m^{-2} day^{-1}. Net radiation over Lake Erie appears to respond much more closely to changes in air temperature. For example, annual net radiation decreases by 1.4 MJ m^{-2} day^{-1} between 1975 and 1978 when the corresponding change in annual mean air temperature is 1.8 °C. In contrast, the corresponding temperature change over Lake Ontario during the same time period is 0.8 °C while net radiation decreases by only 0.3 MJ m^{-2} day^{-1}.

Annual variations in latent heat transfer closely follow variations in net radiation. Thus, evaporation and latent heat fluxes have generally decreased from the

large values observed for the 1950's until approximately 1972 (Lake Erie) and 1974 (Lake Ontario). Thereafter, latent heat fluxes display minor fluctuations, with increased values near 1975 when wind speeds increase. Sensible heat fluxes are proportional to both the Bowen ratio and latent heat fluxes. The net effect is one in which sensible heat fluxes, for both lakes, fluctuate on a time period of approximately three (Lake Erie) to five (Lake Ontario) years with little or no trend over the 31 year period.

The net effect of annual variations in radiation and turbulent fluxes is one where annual surface heat fluxes are approximately balanced for Lake Erie over periods ranging from three to five years, while Lake Ontario has recorded a small gain over the 31 year period. These results suggest that lake heat content is a strongly conservative property of the lake system and resilient to thirty year period variations in hydrometeorological variables.

Several years emerge as distinctly different from average conditions. Figure 5.4 illustrates these years for Lake Erie. These years include: 1953, 1955, 1959, 1982, and 1983. These years are notable for the well-above average heat contents compared to normal. These years are similar in that above-average heat contents were recorded during summer months. The winters of 1953/54, 1954/55, 1963/64, 1973/74, 1979/80, and 1982/83, also emerge as unusually mild winters with well-above heat contents. Some abnormally cold years with well-below average heat contents are also observed. These include the summer months of 1963, 1965, 1971, 1972, and 1976. The winter periods of 1961/62, 1969/70, 1976/77, 1977/78, 1978/79, and 1981/82, are notable for winters with below average heat contents. These deviations from average conditions are remarkable for length of time over which they occur, lasting anywhere from four to six months. These variations in heat content are clearly different from the synoptic effects on, for example, evaporation described by Quinn and den Hartog (1981).

These longer-term variations suggest a persistence of certain synoptic events. Three of these events have been examined in further detail for Lake Erie. These include: (i) June to October, 1983, (ii) November, 1982, to April, 1983, and (iii) June to September, 1972. The first two periods represent above normal lake heat contents during summer months and winter months, respectively. The third period represents below normal lake heat contents during summer.

Figure 5.7 illustrates five-day mean values of selected hydrometeorological variables (thick line) and corresponding mean (1953-1983) five-day values (thin line). Throughout this period, air (and dew point) temperatures are well above average values, ranging from 2 to 4 °C above average. Atmospheric pressure is above average for most of the time, while wind speeds and cloudiness are both below average. This combination suggests extended anticyclonic weather arising from a poleward displacement of the Bermuda anticyclone. In this situation, both incoming shortwave and longwave radiation are well above normal. Throughout much of June and July, net radiation averaged 4 to 5 MJ m^{-2} day^{-1} above average, and was near normal, or slightly above normal, throughout the remainder of the period.

The Bowen ratio was generally below average during this period, and was frequently negative, especially during June and July indicating sensible heat transfer to the lake surface. Latent heat fluxes are also observed to be below average. The average deviation throughout much of the June to August period is approximately 2 to 4 MJ m^{-2} day^{-1}. The combination of increased radiative receipt, reduced loss of latent heat, and (a small) gain of sensible heat results in above average surface heat flux. Surface heat flux is found to be above average through most of June, the first half of July, and most of August and early September. The average deviation is modest, approximately 3 MJ m^{-2} day^{-1}, but extended over a long period of time amounts to a large heat gain by the lake.

Figure 5.8 illustrates five-day means for hydrometeorological variables from

Figure 5.7 - Five-Day Mean Air Temperatures, Dew Point Temperatures, Surface Water Temperatures, Wind Speed, Cloudiness, Net Radiation, Latent, Sensible, and Surface Heat Flux, for Lake Erie, 1 June, 1983- 31 October, 1983 (thick line) and Corresponding Long-Term (1953-1983) Values (thin lines).

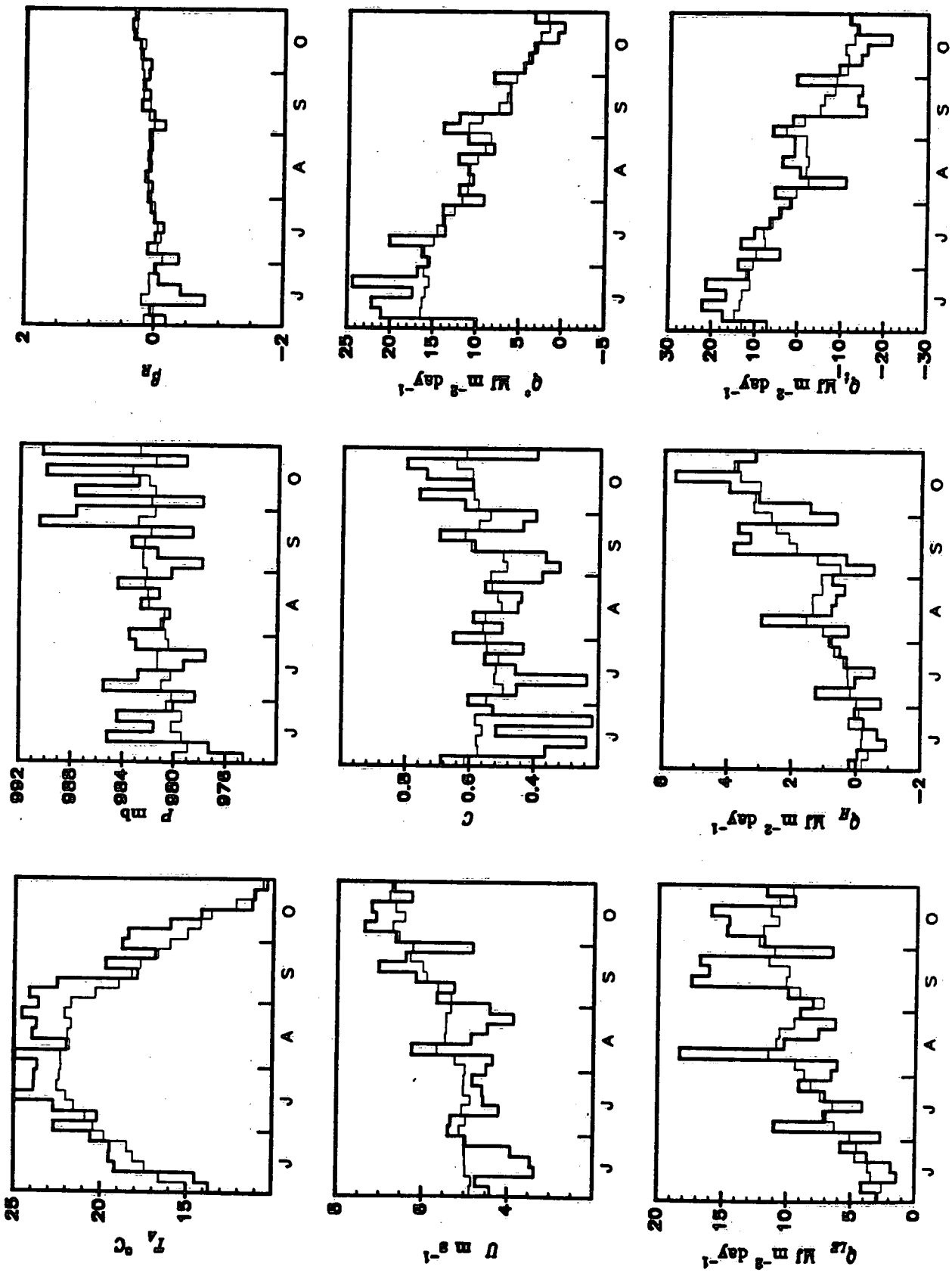

Figure 5.8 - Five-Day Mean Air Temperatures, Dew Point Temperatures, Surface Water Temperatures, Wind Speed, Cloudiness, Net Radiation, Latent, Sensible, and Surface Heat Flux, for Lake Erie, 1 November, 1982 - 30 April, 1983 (thick line) and Corresponding Long-Term (1953-1983) Values (thin line).

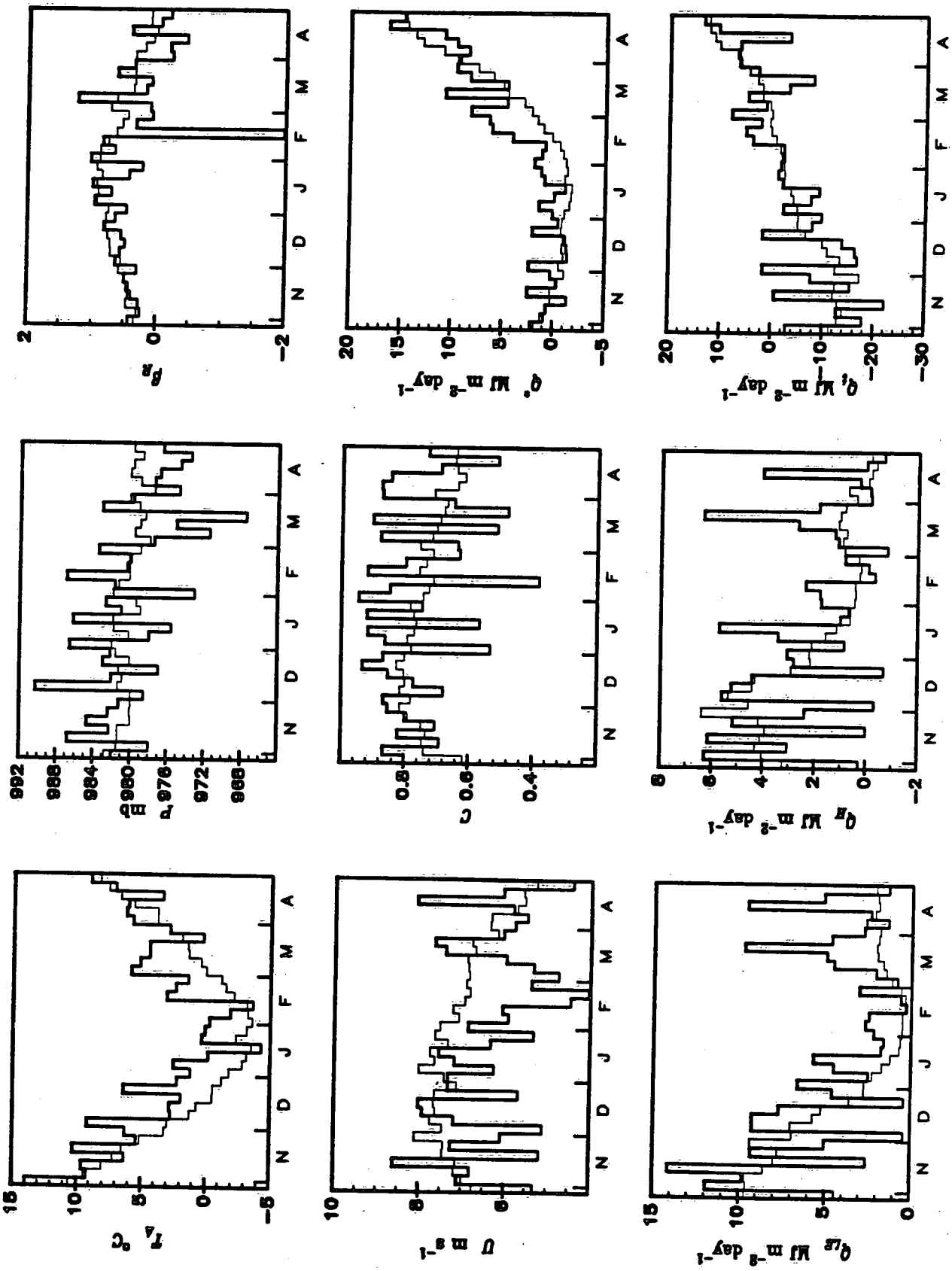

November, 1982, to April, 1983. This period is notable in that it coincides with one of the most intense and longest lasting El Nino events on record (Ramage, 1987). Like most El Nino events, the event of 1982/83 began in early December, but unlike most occurrences lasted much longer, in this case until mid-April. Air temperature (and dew point temperature) averaged 2 to 10 °C above average, and was below average (approximately 1 °C) on only three occasions from the beginning of November to the middle of April.

The distribution of atmospheric pressure illustrates several intense cyclonic events, following a more poleward than normal path, were largely responsible for warm air advection into the Great Lakes basin. Some of the above average temperatures, however, with clearly associated with the poleward extension of the Bermuda anticyclone. It is these conditions that resulted in a Bowen ratio average value of -2 during February. Bowen ratios were below normal throughout most of the period, as were wind speeds, especially from mid-January to mid-March, when they averaged 2 to 3 m s^{-1} below average.

Cloudiness was above average throughout much of the period. Net radiation was above average for most of the period, and in fact, was positive for most of November, December, and January, when it is normally negative. Most of the gain in net radiation can be attributed to increased incoming longwave radiation, which increased in response to both increased cloudiness and atmospheric temperatures.

The combined effect of below average Bowen ratios, reduced wind speeds, and positive net radiation, resulted in greatly reduced latent and sensible heat losses from the lake surface. In fact, on a number of occasions in November and December, the lake was actually gaining sensible heat from the atmosphere. The net effect on the surface heat flux was to greatly reduce the heat loss at the surface. The effect was most notable during November and December and from mid- February to mid-March, when heat losses were as much as 12 MJ m^{-2} day^{-1} below average.

On one-third of the days in December, the lake experienced a net heat gain, although the gain was small, generally less than 1 MJ m^{-2} day^{-1}. This value may be compared with an average daily loss of -12 MJ m^{-2} day^{-1} for December for the 31 year period.

Figure 5.9 illustrates extended, below normal, heat contents that existed over Lake Erie during the summer months of 1972. In many ways, meteorological conditions over Lake Erie during this time period were very similar to those over Lake Ontario during IFYGL. Thus, air temperatures averaged well below average from early June to mid-July and from the third week of July to the third week of August. Five-day mean air temperatures exceeded average values on only three occasions from the beginning of June to the middle of September, and never by more than 0.5 °C. Throughout much of this period, air temperatures averaged 2 to 4 °C below average, which is similar to results obtained over Lake Ontario (Phillips and Almazan, 1981).

The overall synoptic pattern for these summer months was characterized by the polar vortex over Baffin Island with a mean trough to Lake Ontario. The resulting wind flow was described as weak westerlies (Phillips and Almazan, 1981). Except for two exceptions in June, mean wind speed was below normal for most of June and July. The remnants of Hurricane Agnes, on 21 June, was the only major cyclonic event of the summer (mean pressure, 968 mb). There is relatively little variation in surface pressure, suggesting relatively little movement of the trough. Cloudiness was well above average, especially during June, and from the middle of July to the middle of August.

The above average cloudiness accounted for a well-below average net radiation, which was reduced through reduction of incoming shortwave radiation. The increased cloudiness partially offset the reduction in incoming longwave radiation due to lower air temperatures. The reduction in net radiation is observed to be

Figure 5.9 - Five-Day Mean Air Temperatures, Dew Point Temperatures, Surface Water Temperatures, Wind Speed, Cloudiness, Net Radiation, Latent, Sensible, and Surface Heat Flux, for Lake Erie, 1 June, 1972 - 30 September, 1972 (thick line) and Corresponding Long-Term (1953-1983) Values (thin line).

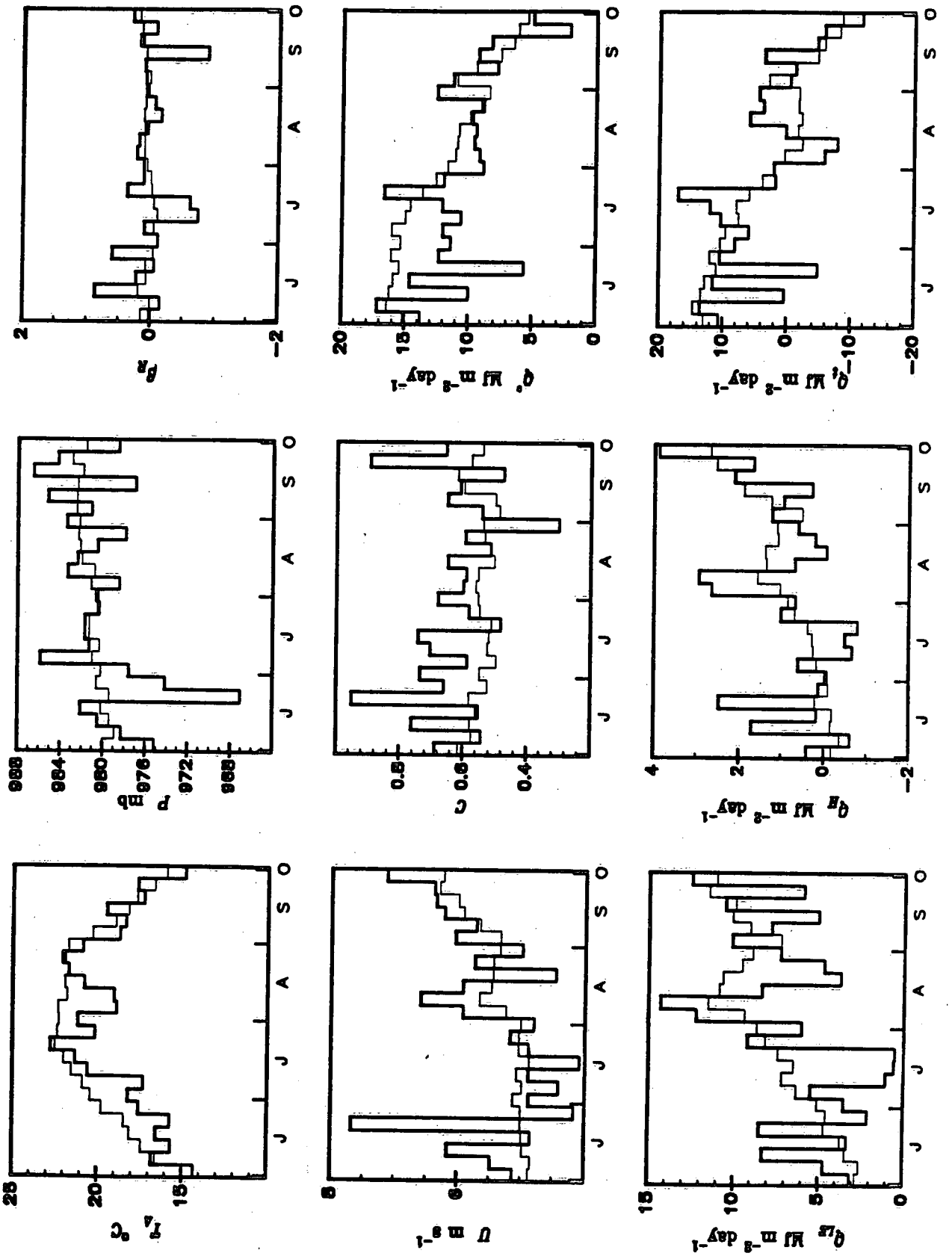

large: five-day mean values were reduced by 5 to 12 MJ m^{-2} day^{-1} from the beginning of June to the middle of August.

Latent heat losses were generally above average during June, as were sensible heat fluxes, largely as a result of above average wind speeds, especially during the passage of Hurricane Agnes. Wind speeds were below normal throughout much of July, with the result that the latent heat flux was well below average values, by approximately 6 MJ m^{-2} day^{-1}. There was a slight gain (approximately 1 MJ m^{-2} day^{-1}) by the lake of sensible heat from the atmosphere. The reduction in latent and sensible heat losses reduced the impact of a below average radiative receipt. Nevertheless, the surface heat flux was below average through all of June and much of July and August. On approximately one third of the days of June, when surface heat flux averages approximately 14 MJ m^{-2} day^{-1}, the surface heat flux was close to zero or negative.

5.4. COMPARISONS WITH OTHER STUDIES

There are few studies of the long-term surface energy balance of the lower Great Lakes. Derecki (1975) applied the water balance method and two variants of the mass transfer approach (*MT*-I and *MT*-II) to estimate monthly evaporation totals for Lake Erie for the period 1950-1968. Yu and Brutsaert (1969), using meteorological data from Toronto and Rochester and a mass transfer procedure, estimated monthly evaporation totals for Lake Ontario for the period 1872 to 1965. Schertzer (1987) applied what is essentially Derecki's *MT*-I approach for Lake Erie for the period 1967-1982, although calculations were not performed for the months of December through March. These four studies overlap with the present study and permit comparisons of evaporation estimates.

Figures 5.10 and 5.11 compare monthly evaporation estimates from the present study with Derecki's *MT*-I (Fig. 5.10) and *MT*-II (Fig.5.11) estimates for the period 1953 to 1968, while Fig. 5.12 compares evaporation estimates from the present

study with those of Yu and Brutsaert for Lake Ontario for the period 1953 to 1965. Figure 5.13 summarizes the comparisons for mean monthly values for the respective time periods. The studies are similar in that evaporation is determined from variants of the mass transfer method. The major differences lie in: (i) the number of stations from which data was used to estimate mean meteorological conditions over the lake, (ii) determination of surface water temperature, (iii) incorporation of atmospheric stability effects, and (iv) evaluation of net radiation.

Derecki's (1975) *MT*-II approach consisted of surface water temperatures derived from water intakes at Erie and Lake Avon, Ohio, with adjustments to overlake conditions. Derecki observes that "the average temperature from these two stations was considered to be sufficiently representative of the whole lake by Powers *et.al.*, (1959)". The time period associated with this average is not given, nor are any comparisons between estimated and measured surface water temperatures. The number of meteorological stations used in Derecki's study and the present study is the same, while overlake wind speeds were scaled by Lamire's (1961) monthly wind ratios for March through October and Richards and Fortin's wind ratios for November through February. The mass transfer results shown in Fig. 5.10 is based on Harbeck's (1962) mass transfer coefficient where the need for adjustment of humidity values is eliminated. Richards and Fortin's monthly scaling ratios for wind speed during the autumn and winter months (October through February) are large: they range from 1.94 in February to 2.09 in November. These values are considerably larger than used in the present study and must have considerable impact on evaporation estimates. Derecki considered effects of atmospheric stability on wind ratios (with values from Richards *et.al.*, 1966), but elected to not include stability effects on the basis that evaporation estimates using monthly wind ratios gave better results.

Derecki's *MT*-I approach is similar to the *MT*-II approach, except that the mass

Figure 5.10 - Comparison of Monthly Evaporation Estimates from Present Study (thin line) with Derecki's (1975) *MT*-II Approach (thick line) for Lake Erie, 1953 - 1968.

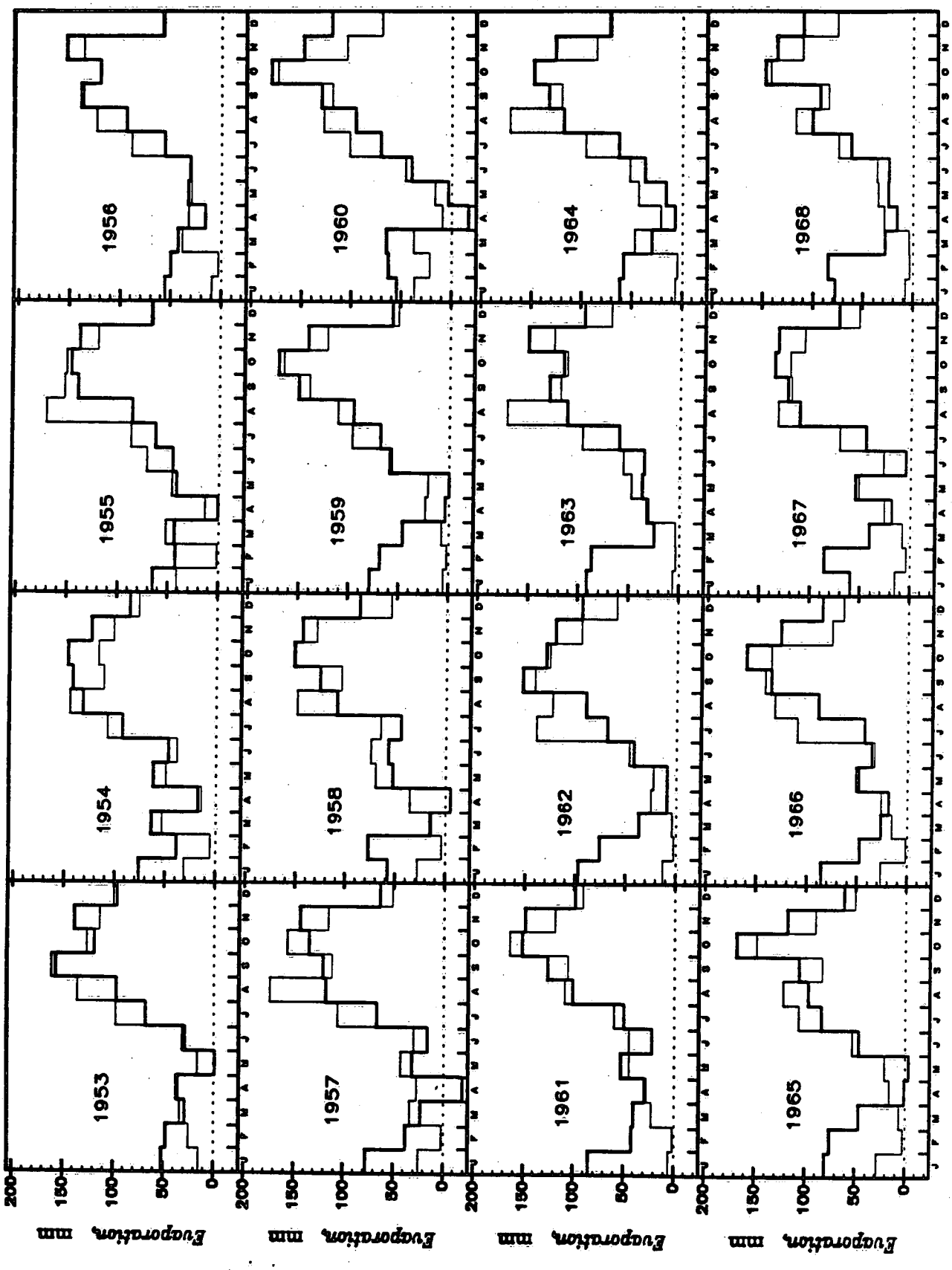

Figure 5.11 - Comparison of Monthly Evaporation Estimates from Present Study (thin line) with Derecki's (1975) *MT*-I Approach (thick line) for Lake Ontario, 1953-1965.

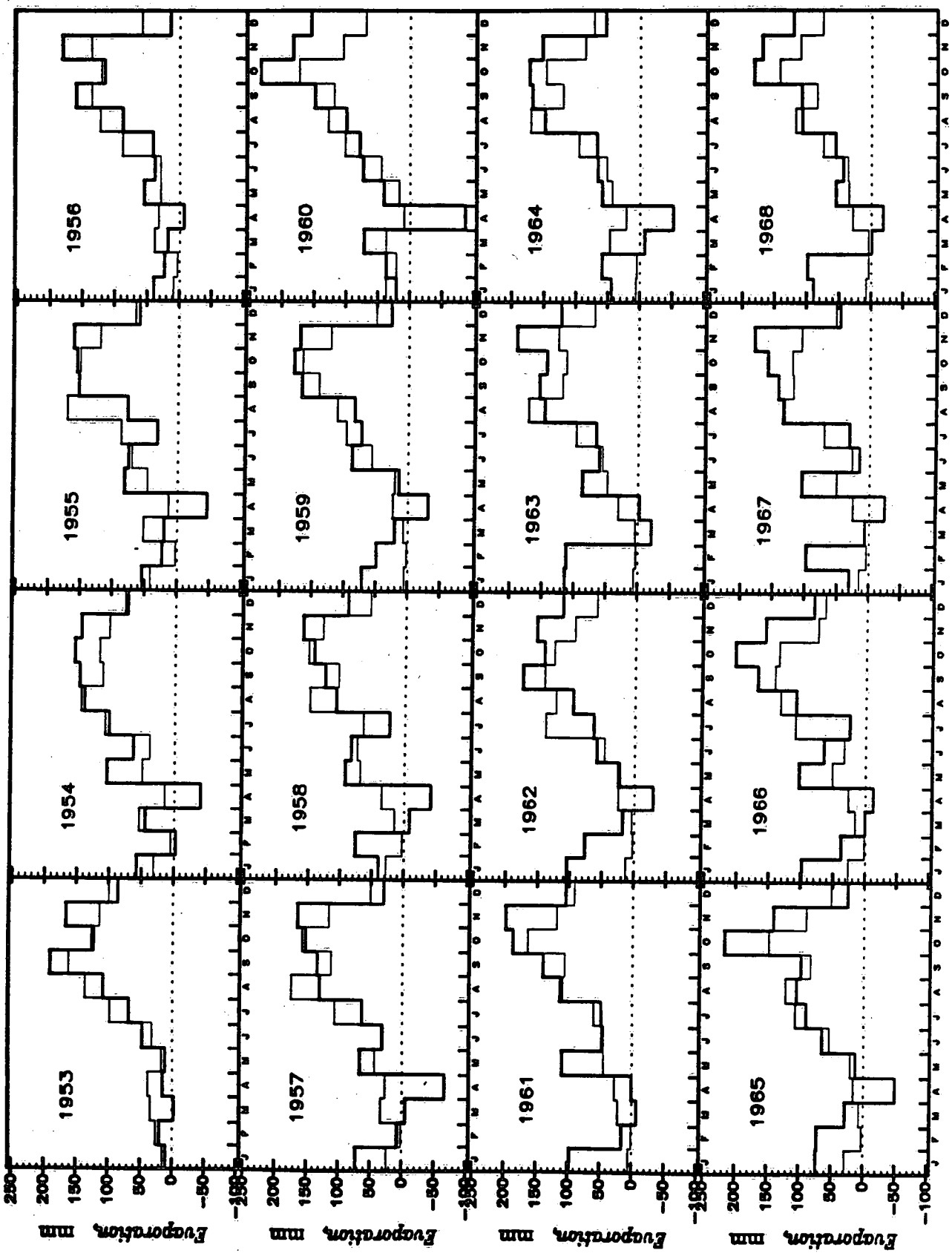

transfer coefficient is that determined for Lake Hefner, while overlake vapour pressures are scaled by Richards and Fortin (1962) monthly humidity ratios. Like the *MT*-II approach, wind speeds are scaled by Lamire's (1961) monthly wind ratio's, while wind ratios for the winter months (November through February) are from Richards and Fortin (1962). The difference between the present study and Derecki's study thus amounts to differences in scaling overlake meteorological variables, treatment of atmospheric stability, and evaluation of surface water temperature and net radiation.

Figure 5.10 illustrates that differences in monthly evaporation estimates occur at approximately three times of the year. The first period occurs during January and February, when Derecki's estimates are much larger than those from the present study. They differ by approximately 50 mm in each month. Almost all of this difference can be accounted for by the neglect of the effect of ice in Derecki's study: his results resemble evaporation from Lake Ontario, which is largely ice-free during winter.

The second major difference occurs during July and August, when estimates from the present study are approximately 40 mm larger than estimates from Derecki's study. The third difference occurs during the high evaporation months of November and December, when estimates from the study average 10 to 30 mm less than estimates by Derecki. Much of this difference must lie in the offsetting effects of atmospheric stability and Lemire's monthly wind scaling ratios. Application of monthly wind ratios cannot faithfully replicate individual monthly evaporation because no allowance for possible differences in meteorological conditions for a given month can be taken into account. Monthly wind ratios implicitly assume that differences among same months are minor. Section 5.3 demonstrated that this is not necessarily true, and deviations in climatic means for same months can be considerable. The agreement between the high evaporation months of September and

October is, however, good. As Fig. 5.10 illustrates the agreement can be quite good during some years, but not necessarily in all years. We suspect, although we can not demonstrate this conclusively, that evaporation estimates derived from application of monthly wind ratios may prove suitable when averaged over a sufficiently long number of years, e.g. 20 to 30.

Figure 5.11 illustrates the comparison between monthly evaporations totals and Derecki's *MT*-I approach for the same time period. The agreement between these results and the present study is slightly better, and demonstrates the improvement from including humidity ratios even if they are only monthly values. The large differences between evaporation totals for July and August (Fig. 5.10) have been reduced substantially. The agreement has also improved for December, March, and June. The difference for April is much larger, with Derecki's approach predicting a mean condensation of 30 mm over this time period compared to a mean evaporation of less than 20 mm from the present study. This is a sizeable difference. Examination of five-day means for Lake Erie evaporation does indicate frequent, but small, condensation occurring during the early spring months but never as large as predicted by Derecki's approach.

This difference could arise from the combination of errors in wind speed and values of monthly humidity ratios. Derecki observes that the wind and humidity ratios are both based on limited overlake data, although evaporation estimates agree with calculations from the water balance approach. This statement, too, must be qualified. Derecki has shown that evaporation estimates derived from the water balance are extremely sensitive to values of inflow and outflow of water into the lake. Errors as small as one percent in inflow/outflow values can result in changes in evaporation estimates as large as 70 percent. These errors must be largest during spring when snowmelt is largest. While the uncertaintly of springtime evaporation totals can be reduced by considering monthly time periods in the water bal-

ance approach, it must still be large. One approach that might be applied to resolve these differences would be to evaluate lake heat content on the basis of these evaporation estimates. Lake Erie surface heat fluxes are close to zero on an annual basis and this provides a rigorous test for evaporation estimates.

Figure 5.12 illustrates evaporation estimates from the present study and Yu and Brutsaert's (1969) study. Their approach is almost identical to that described for Derecki's mass transfer method (*MT*-II). Overlake wind speeds and humidity were scaled by monthly scaling ratios given by Richards *et.al.*, (1966), while surface water temperatures were estimated from Millar's (1952) tabulation of mean monthly surface water temperatures. These values were "corrected" for individual months by temperature data from water intakes at Hamilton, Ontario, and Rochester, New York. No error estimates of this approach are given by these authors. They simply assume that these errors are sufficiently small to be negligible. Effects of atmospheric stability are not explicity taken into account, except as expressed by Richards *et.al.*, monthly scaling ratios.

Figure 5.12 illustrates the evaporation estimates. It shows many of the same features as Figs. 5.10 and 5.11, namely, that there is considerable variation for given months. The major difference is that the two evaporation estimates compare favorably during the January to May period. The present study yields a small condensation during both May and June, while Yu and Brutsaert observe condensation during May only. Their estimated evaporation for July is higher than for the present study by approximately 30 mm. The estimates agree during August and September, but are consistently different during the October to December period, when Yu and Brutsaert's estimates average 30 mm less per month. It is likely that this difference arises from the application of monthly wind ratios as described above. There is another possibility. Harbeck's mass transfer coefficient was developed from studies over water resevoirs in the western United States. The coefficient may produce rea-

Figure 5.12 - Comparison of Monthly Evaporation Estimates from Present Study (thin line) with Estimates from Yu and Brutsaert (1969) (thick line) for Lake Ontario, 1953 - 1965.

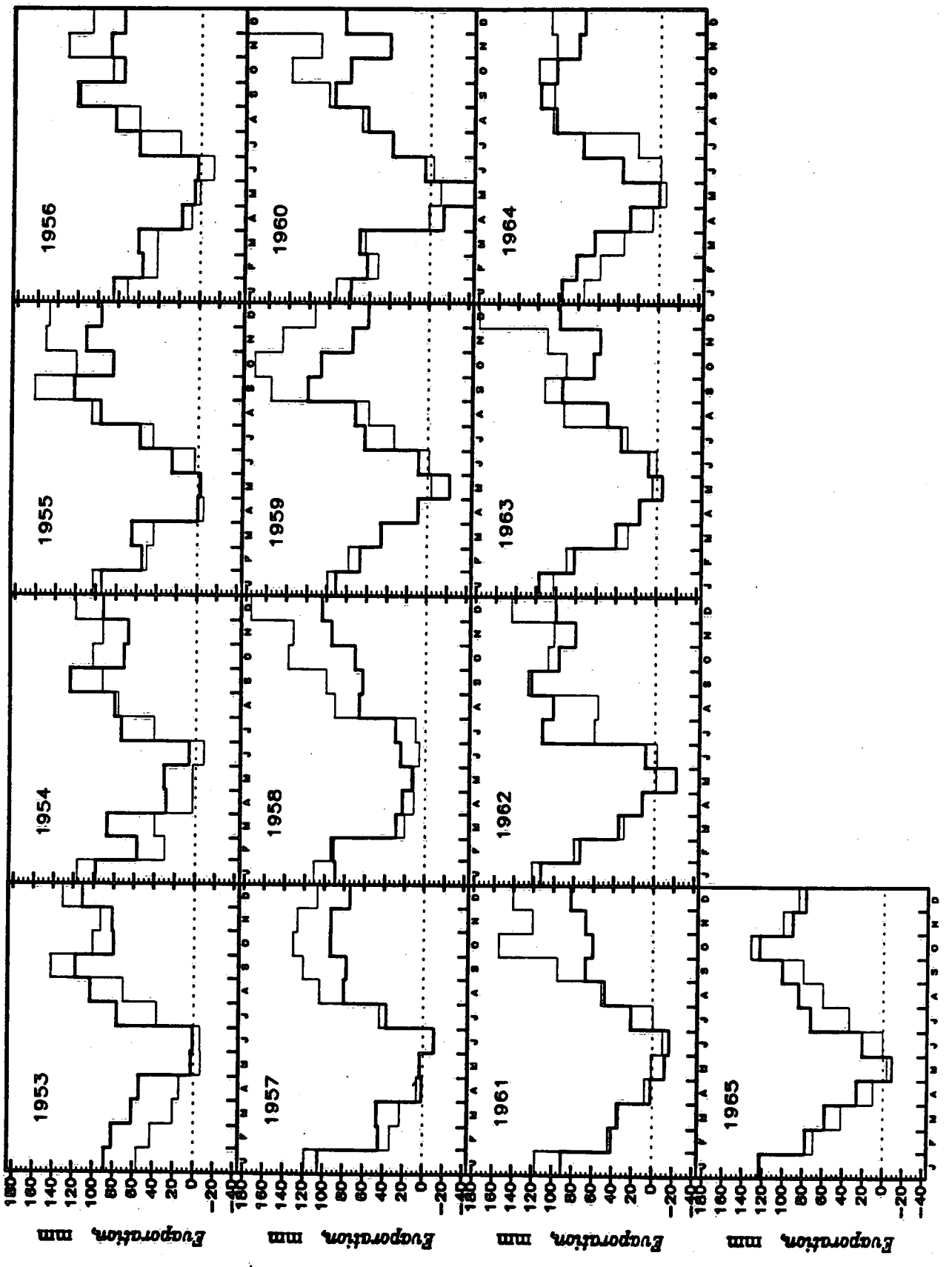

sonable estimates for Lake Ontario during the late winter months, but there can be little guarantee that it will provide valid estimates at other times.

Schertzer (1987) applied what is essentially Derecki's *MT*-I approach to evaluate surface energy balance components for Lake Erie for the period 1967 to 1982. This study did not consider the months of December through March. There is one major refinement in this study, namely, the availability of surface water temperatures, although interpolation was necessary for days between ship and *ART* surveys. Nevertheless, the availability of surface water temperatures, as opposed to values based on water intakes and (largely dubious) correction factors, removes a major source of uncertainty in surface energy balance calculations. Unfortunately, values for individual years were not tabulated, so that only comparisons of mean monthly values could be made.

These comparisons are shown in Fig. 5.13(d), while mean monthly comparisons for Derecki's results are shown in Fig. 5.13 (a) (*MT*-I) and (b) (*MT*-II), and Yu and Brutsaert's results are shown in Fig. 5.13(c). The symbol and error bars in Fig. 5.13(d) illustrates mean, +1, and -1 standard deviation for monthly evaporation totals from 1967 to 1982. Corresponding results from the present study are shown by the thin and thick lines. The application of surface water temperatures has resulted in excellent agreement between Schertzer's results and results from the present study for July and August. There is still a large disgreement between evaporation estimates during April while the agreement during the high evaporation months of September through November can only be described as poor.

Net radiation estimates, averaged over this time period, are small and cannot account for these differences, except in individual months, while differences in surface water temperature are likely to be small. This leaves overlake scaling functions and atmospheric stability as the possible source for the disagreements.

Figure 5.13 - Comparison of Mean Monthly Evaporation Estimates from the Present Study (thin line) with Estimates from Derecki (1975) for Lake Erie, 1953-1968, (a) [*MT*-I] and (b) [*MT*-II], Yu and Brutsaert (1969) for Lake Ontario, 1953-1965, (c), and Schertzer (1987) for Lake Erie, 1967-1982, (d). In Figure (d), Schertzer's mean values shown by symbol, while error bars represent +1 and -1 standard deviations, while mean values from present study shown by thick line with upper and lower thin lines denoting +1 and -1 standard deviations.

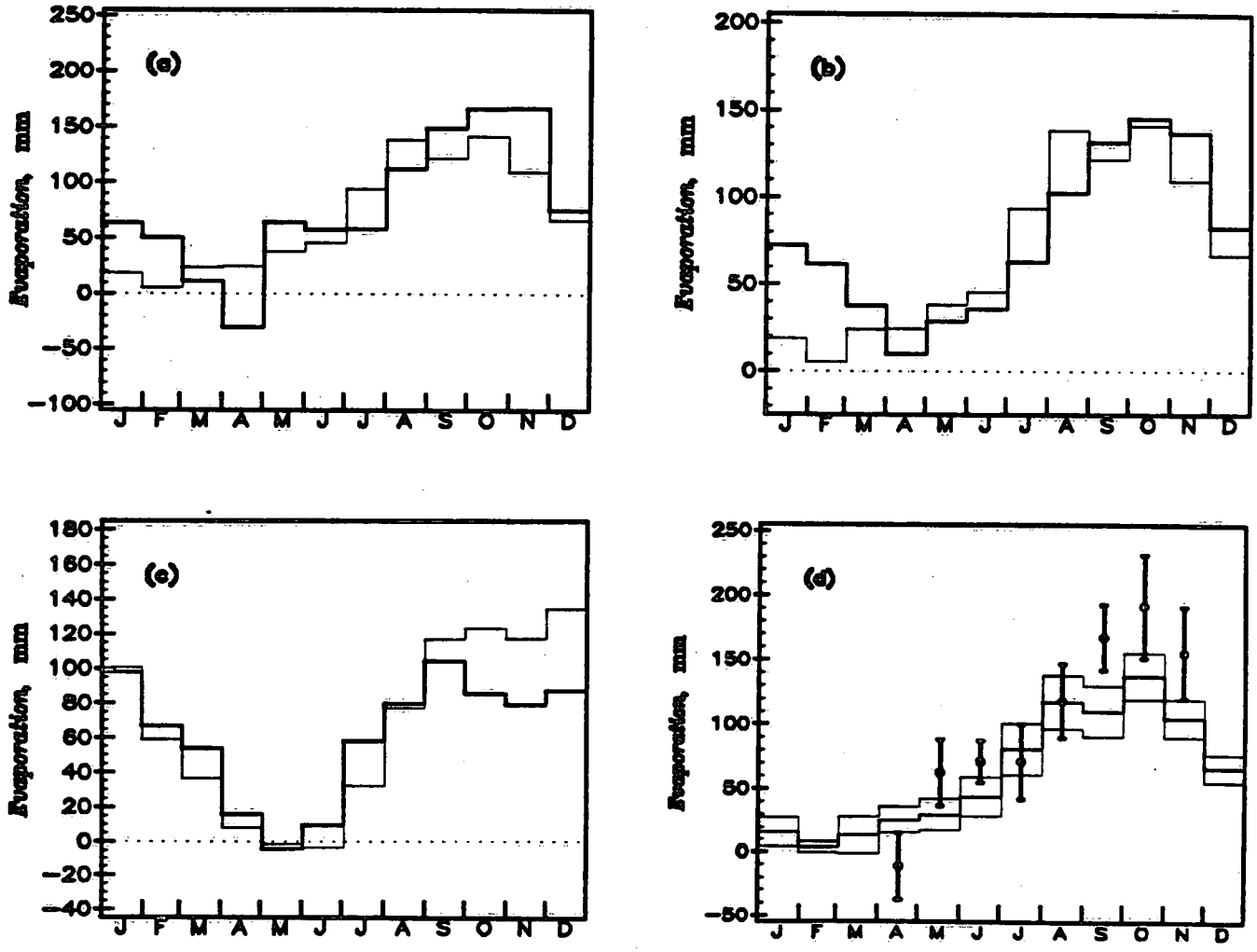

There are two possible ways of interpreting Fig. 5.13(d). First, values for over-lake scaling functions applied in the present study may be in error, with much of

the error arising during very stable and very unstable conditions. Over Lake Erie, these will occur during March through May (for very stable conditions) and during September through November (for very unstable conditions). In the present study, these events are given values derived from statistical analyses. There is no real functional relationship between overlake conditions and overlake scaling functions, although the impact on wind speeds is reduced because the bulk evaporation coefficent is determined as a function of wind speed.

The second possibility is that the mass transfer coefficient and/or scaling ratios for overlake data, as applied in Derecki's and Schertzer's study, were inappropriate. First, the value of the mass transfer coefficient used was that for Lake Hefner. Quinn and den Hartog (1981) have shown that application of the Lake Hefner mass transfer coefficient to Lake Ontario during IFYGL resulted in an evaporation overestimate of approximately 20 percent compared to recommended values, with largest overestimates generally occurring during the autumn months when evaporation rates are largest. This might account for large evaporation totals over Lake Erie during the autumn months.

Second, monthly wind ratios, as noted by Derecki, are based on limited overlake data, while values derived from data over Lake Ontario may not be strictly applicable to Lake Erie, as assumed in the present study. Nevertheless, wind ratios applied by Schertzer and Derecki for Lake Erie, especially during the autumn and winter months, are large: they average 2.0 during these months. While these values may be fairly representative of storm events and very unstable conditions, most autumn and winter months are not dominated by these events in a statistical sense. This is evident from Phillips and Irbe's (1976) detailed analyses of paired land-lake meteorological data. Presumably, good agreement between the two approaches arises when a large frequency of days within a given month can be classified as very unstable. These circumstances lead to largest wind speeds in the present study,

and hence good agreement with wind speeds predicted from Richards and Fortins monthly wind speed ratios. Unfortunately, this hypothesis cannot be examined here, as Schertzer provides only statistical summaries of monthly evaporation estimates.

These comparisons serve to emphasize that evaporation estimates derived from application of monthly scaling ratios should be considered with caution. They may yield good estimates when meteorological conditions in a given month are close to average values predicted by the scaling ratios for that month. Over the lower Great Lakes, however, few months are like the average for that month.

We thus leave the reasons for differences in evaporation estimates depicted in Fig. 5.13 as unresolved. Figure 5.13 illustrates that these differences are neither trivial nor easily reconciled. Carefully designed numerical experiments with benchmark results will be required to resolve these differences.

6. SUMMARY AND CONCLUSIONS

The study objectives were to develop a physical model to estimate daily components of the radiation and energy balances at a lake surface from a limited data base and apply the model to the lower Great Lakes. The data base consists of hourly meteorological data recorded at shoreline stations. The overall thrust of model development was to replace, where possible, empirical and/or site-specific formulations with physically-based models to achieve general application while providing confidence in numerical estimates. Each of the model components was tested with data collected over Lake Ontario during IFYGL and compared with results from previous radiation and energy balance studies over Lake Ontario.

Model development focussed on three aspects: radiation receipt, evaporation rates, and ice cover. Net radiation was estimated from the sum of net shortwave and net longwave radiation fluxes. The shortwave model is a true radiative transfer model and marks the first time that such a model has been applied to evaluate shortwave radiation receipts in a boundary-layer study. Comparison of model estimates with measured values shows the model can estimate daily totals of incoming shortwave radiation that are within, or close to, the range of values measured on most days during IFYGL. Largest differences between model estimates and measured values were observed on days with predominantly thin, high-altitude clouds, e.g. Cirro-Stratus combinations. Maximum differences between model estimates and measured values on such days amounted to thirty percent of measured values. The impact of high-altitude clouds on surface radiation receipt was much less when low clouds were present.

Estimates of longwave radiation were obtained from a variant of Beer's law that incorporates effects of clouds, aerosols, and atmospheric gases on incoming longwave radiation. Estimates of daily totals of incoming longwave radiation were usually within 2 to 3 MJ m^{-2} day^{-1} of measured values, which is within the uncertainty of

incoming longwave measurements on most days. In general, largest errors in estimates of incoming longwave radiation were observed for mostly clear days. The model underestimated incoming longwave fluxes in these circumstances. These underestimates may result from: (i) underestimated overlake air temperatures, (ii) inaccurate specification of reference height for mean atmospheric temperature for emission of radiation and/or inaccurate specification of vertical temperature profile for a mostly clear atmosphere, and (iii) neglect of multiple scattering effects. Specification of reference height and vertical temperature profile is likely the most important consideration. This study assumed a reference height ranging from 200 m (winter) to 300 m (summer) as recommended by Paltridge and Platt (1976). If the reference height was changed to 50 m, as recommended by van Ulden and Holtslag (1985), mean atmospheric temperature for emission would increase by approximately 2.5 °C. This temperature increase would be sufficient to bring clear-sky longwave radiation estimates to within instrumental uncertainty of measured values on most days. This hypothesis should be investigated in future research.

The evaporation model is a variant of the mass transfer approach. The key improvement is the replacement of the Lake Hefner value for the mass transfer coefficient with a formulation that includes a dependency on wind speed (Quinn and den Hartog, 1981). Although this formulation is strictly applicable to neutral conditions, atmospheric stability is incorporated through scaling of overlake wind speeds. This approach resulted in evaporation estimates for Lake Ontario during IFYGL that compare very favourably with values recommended by the IFYGL Energy Balance Panel. Estimated daily Bowen ratios were found to compare favourably with values tabulated by Pinsak and Rodgers (1981).

A simple model of ice extent, based on the cumulative freezing degree day concept, provided acceptable estimates of ice heat flux due to ice formation and decay. Although the heat transfer associated with ice formation and decay is small, ice extent

is important because of the high albedo for shortwave radiation and the effect of ice in reducing evaporation rates. Comparison of mean ice extent derived from a 31 year simulation for Lake Ontario and Lake Erie with tabulated values of Assel *et al.* (1983) showed good agreement.

The model was applied to produce a 31 year simulation of daily radiation and energy balance components for Lake Erie and Lake Ontario. Daily lake heat contents were obtained from the product of estimated surface heat flux and lake surface area. Heat content estimates were compared with measured heat contents for both lakes for the period 1967-1982 when vertical temperature surveys conducted from ship cruises permitted direct evaluation of heat content. Estimated and measured heat contents showed excellent agreement on most days, usually within the accuracy of heat content measurements.

Examination of annual surface heat flux values, obtained from summing daily estimates, reveals that annual surface heat fluxes are not balanced on an annual basis. For Lake Erie, surface heat flux appears to be balanced over periods ranging from three to six years. Lake Ontario appears to be gaining heat, although the gains are small and within the uncertainty of measured heat contents.

Comparison of computed monthly evaporation totals with previous studies displayed some interesting comparisons and suggests avenues for future research. These may be briefly outlined as follows. First, there are a variety of ways for scaling overland meteorological data to estimate overlake conditions. These methods should be examined rigorously with benchmark heat contents collected for Lake Ontario during IFYGL. This is important, not only from the viewpoint of accuracy of overlake meteorology, but also in understanding why different models predict closely in some months but not in others.

Second, there are several ways of incorporating atmospheric stability into overlake data and it is not at all clear which approach performs best in combination with

the method for scaling overlake variables.

Third, and perhaps most importantly, future research should examine improvements in estimating surface water temperature. This is the crucial variable in energy balance studies over lakes. It arises in estimation of overlake meteorological variables, Bowen ratio, and incoming and emitted longwave radiation. Thus, almost all components of the model require a knowledge of surface water temperature. One crucial aspect of model development should be incorporation of effects of (colder) upwelled water.

APPENDIX A - List of Symbols

Variables are dimensionless, except where noted. Bold-face quantities represent vector-matrix quantities.

UPPER CASE ROMAN

A	Coefficient matrix for linear system of equations defining diffuse radiation fluxes in a vertically inhomogeneous atmosphere.
C	fractional cloudiness
C_o	duration (hours) of overcast
C_E	bulk evaporation coefficient
CT	clock time (hours)
D	diffuse radiation flux (MJ m^{-2} day^{-1}), D-statistic
D_C	cloud depth (m)
D_H	depth of haze layer (m)
D_o	day of winter season (= 1 on 1 November).
E	evaporation rate (mm day^{-1})
E_{mb}	mean bias error
E_{rms}	root mean square error
E_t	equation of time (radians)
E_{xt}	extinction coefficient (km^{-1})
F_D	downward diffuse flux (W m^{-2})
F_U	upward (reflected) diffuse radiation at the ground surface (W m^{-2})
H	length of daylight period (hours)
$H_{½}$	length of half-daylight period (radians)
I_{max}	maximum ice concentration (fraction of lake surface area)
I_{min}	minimum ice concentration (fraction of lake surface area)
I_n	normal ice concentration (fraction of lake surface area)
I_o	solar constant (1370 W m^{-2})
$I(\tau,\mu,\phi)$	intensity of diffuse radiation at a point in the atmosphere (W $m^{-2}sr^{-1}$)
K_D	total incoming shortwave radiation at the ground surface

	(MJ m^{-2} day^{-1})
L	latent heat of vapourization (MJ kg^{-3})
L_C	longwave radiation emitted from cloud base
$L_{C,H}$	net incoming longwave radiation emitted by cloud and aerosol (W m^{-2})
L_D	total incoming longwave radiation at the ground surface (MJ m^{-2} day^{-1})
L_o	incoming clear-sky longwave radiation (W m^{-2})
L_p	standard longitude (degrees) for time zone of station (75°W for this study)
L_r	reflected longwave radiation (MJ m^{-2} day^{-1})
L_s	station longitude (degrees)
L_U	(upward) emitted longwave radiation by ground surface (MJ m^{-2} day^{-1})
LAT	local apparent time (true sun time) (hours)
M	mass transfer coefficient
ND	aerosol number density (particles cm^{-3})
P	atmospheric pressure (mb) (also denoted as p - see below)
P_k	Legendre Polynomial of order k
P_o	layer ozone amount (atm-cm)
P_W	layer water vapour amount (g cm^{-2})
Q_l	minimum (lake) heat content (J)
Q_u	maximum (lake) heat content (J)
Q'	lake heat content scaled to [-1, 1]
Q_t	surface heat flux (MJ m^{-2} day^{-1})
Q_H	sensible heat flux (MJ m^{-2} day^{-1})
Q_{LE}	latent heat flux (MJ m^{-2} day^{-1})
Q_M	minor heat flux terms (MJ m^{-2} day^{-1})
Q^*	net radiation (MJ m^{-2} day^{-1})
R	gas constant for air (287 $Jkg^{-1}K^{-1}$)
R_W	ratio of overlake to overland wind speeds (ms^{-1})
R^*	(normalized) radius vector (radians)

S	direct-beam radiation flux (MJ m^{-2} day^{-1})
S_o	duration (hours) of the daylight period that sky is cloud-free
T	temperature (°C, K)
T_A, T_a	air temperature (°C, K)
T_B	cloud-base temperature (K)
T_d	dew point temperature (°C)
T_K	ice-surface temperature (273.15 K)
T_r	reference temperature in wing-scaling approximation for absorption of radiation by water vapour
T_S	lake surface temperature (K) (ice-water combination)
T_W	surface water temperature (°C)
T'	scaled ([-1, 1]) air temperature
$\bar{T}$	mean temperature (°C, K)
U_a	wind speed at level a above lake surface (ms^{-1})
U_8	wind speed (ms^{-1}) at $z = 8m$
U_G	amount of absorbing gas in an atmospheric layer
U_R	relative humidity (percent)
V	visibility (km)
W	cloud liquid water content (gm^{-2})
W_c	equivalent condensed water corresponding to cloud depth D_c (g kg^{-1})
Z	solar zenith angle (degrees)

LOWER CASE ROMAN

b	right-hand side vector in system of linear equations defining diffuse radiation fluxes for a vertically inhomogeneous atmosphere.
c_p	specific heat of air (1005 J kg^{-1} K^{-1})
c	(column) vector of unknowns in system of linear equations defining diffuse radiation fluxes for a vertically inhomogeneous atmosphere
d_n	day of year (0 on 1 January; 364 on 31 December)
e	ambient atmospheric vapour pressure (mb)
e_a	atmospheric vapour pressure at a level a above lake surface (mb)

e_s	saturation vapour pressure (mb)
f_P	fraction of Planck curve within window wavelengths (8 μm - 12 μm)
f_S	fractional truncation of scattering phase function in the *Delta–M* method.
g	gravitational acceleration (9.8 m s^{-2}) or asymmetry factor
g_B	bulk layer asymmetry factor
g'	scaled (*Delta–M* method) asymmetry factor
h	hour angle (degrees)
i_d	ice depth (m)
k	constant in expression for Bowen ratio
$k_\nu(p,T)$	spectral gaseous absorption coefficient as a function of pressure and temperature
l	latitude (degrees)
p	atmospheric pressure (mb)
p_r	reference pressure (300 mb) in the wing-scaling approximation for absorption by water vapour
p_l	fraction of lake surface area covered by ice
$p(\mu,\phi;\mu',\phi')$	scattering phase function
q_a	ambient specific humidity at a level a above lake surface (kg kg^{-1})
q_s	saturation specific humidity ($kg\,kg^{-1}$)
t_D	number of seconds in a day
t_D'	constant, = 0.622 t_D
w	weight factors for Gaussian quadrature, weight factors in the wing-scaling approximation for absorption of radiation by water vapour
z	height or altitude (m)

UPPER CASE GREEK

Γ	dry adiabatic lapse rate (-9.8 °C km^{-1})
Γ_s	saturated adiabatic lapse rate (°C km^{-1})
ΔT	generally, temperature difference (°C, K)
ΔT_a	overland air temperature - overwater air temperature

ΔT_d	overland dew point - overwater dew point (°C)
ΔT_{B-T}	temperature difference between cloud base and cloud top (°C)
$(\Sigma f_D)_{max}$	maximum cumulative freezing degree days on a given day of the winter season D_o
$(\Sigma f_D)_{min}$	minimum cumulative freezing degree days
$(\Sigma f_D)_n$	normal cumulative freezing degree days

LOWER CASE GREEK

α_s	surface albedo
β_R	Bowen ratio
γ	environmental lapse rate (–6.5 °C km^{-1})
ϵ	ratio of gas constant for dry air to water vapour (= 0.622)
ϵ_s	surface emissivity
ϵ_C	cloud emissivity
ϵ_H	aerosol (haze) emissivity
θ	zenith angle (degrees)
θ_o	day of year expressed in radians
λ	(positive) eigenvalue, or wavelength (μm)
μ	generally, cosine (zenith angle)
μ_o	cosine (solar zenith angle)
$\bar{\mu}_{o,C}$	cosine of (mean) solar zenith angle for overcast portion of the day
$\bar{\mu}_{o,S}$	cosine of (mean) solar zenith angle for clear portion of the day.
ν	frequency of radiation
πF_o	incident top-of-the-atmosphere shortwave radiation (W m^{-2})
ρ	generally, density
ρ_I	density of ice (916 kgm^{-3})
ρ_s	density of water (kgm^{-3})
σ	Stefan-Boltzmann constant (5.67×10^{-8}W m^{-2} K^{-4})
τ	generally, optical depth
τ_H	aerosol (haze) optical depth

τ_B	bulk (layer) optical depth
τ_R	Rayleigh scattering optical depth
$\tau_{C,IR}$	cloud optical depth for the near infrared band of shortwave radiation
$\tau_{C,V}$	cloud optical depth for the visible band of shortwave radiation
τ'	*Delta–M* scaled optical depth
ψ	scattering angle (degrees)
ϕ	generally, azimuth angle
ϕ_o	azimuth angle of the solar beam
ω	(scattering) phase function moments
$\tilde{\omega}_o$	single scattering albedo
$\tilde{\omega}_{oB}$	bulk (layer) single scattering albedo
$\tilde{\omega}_o'$	*Delta–M* scaled single scattering albedo

APPENDIX B - Spectral Data for *Delta–D_2* Model

TABLE B.1 - Band Limits, Incident Radiation, and Absorbers for *Delta–D_2* Model.

Band	Spectral Limits (μm)	Incident Radiation W m^{-2}	Absorber
1	0.20 - 0.83	799.1	Ozone
2	0.83 - 3.80	550.7	Water Vapour

TABLE B.2 - Spectral Weights w and Absorption Coefficients k for Water Vapour (g^{-1} cm^2) and Ozone ($(atm–cm)^{-1}$) in the *Delta–D_2*model.

Band	Interval	Weights, w, Dimensionless	Absorption Coefficient, k
1	1	0.1889376	0.0
	2	0.1530344	0.0046545
	3	0.4792264	0.0453514
	4	0.1350144	0.1151237
	5	0.0188087	0.8960393
	6	0.0070454	5.371737
	7	0.0069078	21.22268
	8	0.0041797	67.33543
	9	0.0068452	221.0945
2	1	0.2081286	2.23873E-5
	2	0.1281448	2.23873E-4
	3	0.1652784	2.23873E-3
	4	0.1788882	2.23873E-2
	5	0.1538072	2.23873E-1
	6	0.0991907	2.23873
	7	0.0475173	2.23873E+1
	8	0.0150750	2.23873E+2
	9	0.0039158	2.23873E+3

APPENDIX C

Coefficients for Estimating Saturation Vapour Pressure

TABLE C.1 - Coefficients for Estimating Saturation Vapour Pressure e_s (mb). [Pruppacher and Klett, 1980].

$$e_s = a_0 + T(a_1 + T(a_2 + T(a_3 + T(a_4 + T(a_5 + a_6 T)))))$$

with T (°C) and e_s in mb.

$$a_0 = 6.107799961 \times 10^{0}$$
$$a_1 = 4.436518521 \times 10^{-1}$$
$$a_2 = 1.428945805 \times 10^{-2}$$
$$a_3 = 2.650648471 \times 10^{-4}$$
$$a_4 = 3.031240396 \times 10^{-6}$$
$$a_5 = 2.034080948 \times 10^{-8}$$
$$a_6 = 6.136820929 \times 10^{-11}$$

Range of Validity: -50 °C to +50 °C (for water).

APPENDIX D - Optical Properties of Clouds and Aerosols

TABLE D.1 - Band-Average Values of Single Scattering Albedo and Asymmetry Factor for Clouds and Normalized Rayleigh Scattering Optical Depths.

Band	Spectral Limits μm	$\tilde{\omega}_o$	g	τ_o
Visible	0.20 - 0.83	0.9999	0.8689	0.19295
Near Infrared	0.83 - 3.80	0.8203	0.8936	0.0048235

TABLE D.2 - Coefficients for Estimating Aerosol Emissivity (ϵ_H) at 11 μm as a Function of Relative Humidity.

a_0	a_1	a_2	a_3	a_4	a_5	rhlim
-0.24300	-0.20551e-2	0.81030e-1	0.16252	-0.47488e-1	-0.12591	99.0

ϵ_H may be evaluated with the following FORTRAN code:

```
  xrh = amin1(rh, rhlim)
  srh = (2.0*xrh - rhlim)/rhlim
  hazem = srh*a(5)
  do 1 j = 5,1,-1
1 hazem = (hazem + a(j))*srh
  hazem = 10.0**(hazem + a(0))
```

where -hazem- represents ϵ_H and -rh- is the relative humidity (percent).

TABLE D.3 - Coefficients for Estimating Fraction of Planck Function.

a_i	8.3 μm – 12.8 μm	9.4 μm – 9.9 μm	8.97 μm – 9.17 μm
a_0	.26721	.30074e-1	.11547e-1
a_1	.10942	.16638e-1	.78395e-2
a_2	-.68153e-1	-.74495e-2	-.24480e-2
a_3	-.14258e-2	-.15143e-2	-.10605e-2

TABLE D.4 - Coefficients for Estimating Asymmetry Factor at Infrared Wavelengths

a_0	a_1	a_2	a_3	a_4	a_5	rhlim
-.19851	.62111e-1	.98930e-1	-.10799e-2	-.34113e-1	.16006e-1	99.0

FORTRAN code for evaluating infrared asymmetry factor is identical to that given in TABLE D.2.

TABLE D.5 - Monthly Values of Thickness of Aerosol Layer (km) and Cloud Depths (m).

Month	Aerosol Layer (km)	Cloud Depth (m)
January	0.20	225
February	0.20	225
March	0.35	250
April	0.35	250
May	0.50	275
June	0.50	275
July	0.50	300
August	0.50	300
September	0.35	275
October	0.35	275
November	0.20	250
December	0.20	250

APPENDIX E

Coefficients for Estimating Atronomical Parameters

TABLE E.1 - Coefficients for Estimating Astronomical Parameters R^* (Normalized Radius Vector), E_t (Equation of Time), and δ (Solar Declination). From Spencer (1971).

a_i	R^*	E_t	δ
a_0	1.000110	0.000075	0.006918
a_1	0.034221	0.001868	-0.399912
a_2	0.001280	-0.032077	0.070257
a_3	0.000719	-0.014615	-0.006758
a_4	0.000077	-0.040849	0.000907
a_5			-0.002697
a_6			0.001480

APPENDIX F

Coefficents for Estimating Surface Water Temperatures

TABLE F.1 - Coefficients for Estimating Surface Water Temperature (°C) from Total Lake Heat Content Q (EJ).

a_i	Ontario	Lake Erie (lakewide)	Lake Erie west basin	Lake Erie central basin	Lake Erie east basin
Warming Phase					
x_l	4.0 EJ	2.0 EJ	0.2 EJ	2.0 EJ	0.75 EJ
x_u	56.0 EJ	42.4 EJ	2.4 EJ	28.0 EJ	12.0 EJ
a_0	0.82643e+01	0.13724e+02	0.14832e+02	0.14280e+02	0.15161e+02
a_1	0.15407e+02	0.12236e+02	0.11734e+02	0.11487e+02	0.15818e+02
a_2	0.75194e+01	-.17184e+01	0.35468e+01	-.10608e+01	-.25469e+01
a_3	-.50768e+01	-.73865e+00	0.45731e+01	0.25846e+01	-.84817e+01
a_4	-.56839e+01	-.14363e+01	-.81691e+01	-.75174e+00	-.37557e+00
a_5	-.51098e+00	0.00000e+00	-.51634e+01	-.31538e+01	0.39948e+01
Cooling Phase					
x_l	4.0 EJ	2.0 EJ	0.2 EJ	2.0 EJ	0.75 EJ
x_u	56.0 EJ	42.4 EJ	2.4 EJ	28.0 EJ	12.0 EJ
a_0	0.36163e+02	0.18809e+02	0.10579e+01	0.13006e+02	0.53041e+01
a_1	0.19963e+02	0.18270e+02	0.12109e+01	0.11966e+02	0.43129e+01
a_2	0.56224e+01	0.10396e+01	0.10952e-01	0.13132e+01	0.32590e+00
a_3	0.39791e+01	0.12633e+01	-.54137e+00	0.21834e+01	0.19230e+01
a_4	-.14835e+02	-.22080e+01	0.34588e+00	-.78715e+00	-.21486e+00
a_5	-.23086e+01	0.00000e+00	0.24897e-01	-.11266e+01	-.13190e+01

EJ denotes exa (10^{18}) Joules.

Surface water temperature may be obtained by the following FORTRAN 77 code. Let variable -q- represent total lake heat content (EJ). Let variable -tw- represent surface water temperature (°C).

```
*
*          scale -q- to the interval [-1, +1]
*
      qpr = (2*q - x_l - x_u)/(x_u - x_l)
      tw = a(5)*qpr + a(4)
      do 1 j = 3,1,-1
    1 tw = tw*qpr + a(j)
      tw = tw + a(0)
```

The above code assumes the coefficients have been stored in an array -a- dimensioned as: dimension a(0:5)

TABLE F.2 - Coefficients for Estimating Total Lake Heat Content Q (EJ) from Daily Mean Surface Water Temperature (°C)

a_i	Lake Ontario	Lake Erie lakewide	Lake Erie west basin	Lake Erie central basin	Lake Erie east basin
Warming Phase					
x_l	0.2°C	0.2°C	0.2°C	0.2°C	0.2°C
x_u	24.0°C	24.0°C	24.0°C	24.0°C	24.0°C
a_0	0.36163e+2	0.18809e+2	0.10579e+1	0.13006e+2	0.53041e+1
a_1	0.19963e+2	0.18270e+2	0.12109e+1	0.11966e+2	0.43129e+1
a_2	0.56224e+1	0.10396e+1	0.10952e-1	0.13132e+1	0.32590
a_3	0.39791e+1	0.12633e+1	-0.54137	0.21834e+1	0.19230e+1
a_4	-0.14835e+2	-0.22080e+1	0.34588	-0.78715	-0.21486
a_5	-0.23086e+1	0.0	0.24897e-1	-0.11266e+1	-0.13190e+1
Cooling Phase					
x_l	0.2 °C	0.2 °C	0.2 °C	0.2 °C	0.2 °C
x_u	24.0°C	24.0°C	24.0°C	24.0°C	24.0°C
a_0	0.48147e+2	0.24345e+2	0.11112e+1	0.15562e+2	0.72691e+1
a_1	0.78752e+1	0.21845e+2	0.10060e+1	0.14617e+2	0.60597e+1
a_2	0.13206e+1	-0.54089e+1	-0.21496	0.39205e-1	0.98320
a_3	0.30410e+2	-0.11124e+1	0.14084	-0.11531e-1	-0.56904e+1
a_4	-0.29281e+2	-0.35103e+1	0.18906	-0.24354e+1	-0.34716e+1
a_5	-0.23910e+2	0.0	-0.15333	-0.99768	0.58219e+1

EJ denotes exa (10^{18}) Joules.

Values of Q (EJ) obtained in same manner as described in TABLE F.1, except that Q is the independent variable and must be first scaled to the interval [-1, +1] with scale parameters x_l and x_u.

APPENDIX G - Mean Daily Surface Water Temperature

TABLE G.1 - Coefficients for Estimating Mean Daily Surface Water Temperatures (°C) from Julian Day for Lake Ontario, Lake Erie, and Basins of Lake Erie.

a_i	Lake Ontario	Lake Erie lakewide	Lake Erie west basin	Lake Erie central basin	Lake Erie east basin
x_l	-27.0	-46.0	-46.0	-46.0	-46.0
x_u	385.0	486.0	486.0	486.0	486.0
a_0	0.80687e+1	0.80339e+1	0.82985e+1	0.80765e+1	0.77241e+1
a_1	0.45313e+1	0.13207	0.73451e-1	0.14442	0.13607
a_2	-0.82138e+1	-0.12429e+2	-0.13960e+2	-0.12472e+2	-0.11505e+2
a_3	-0.10205e+2	-0.46734e+1	-0.77306	-0.47287e+1	-0.66188e+1
a_4	0.50333e+1	0.14905e+2	0.16454e+2	0.14972e+2	0.13985e+2
a_5	0.63675e+1	0.24774e+1	0.74508	0.24699e+1	0.33434e+1
a_6	-0.13872e+1	-0.59669e+1	-0.62509e+1	-0.58893e+1	-0.59795e+1
a_7	-0.39342e+1	-0.14051e+1	-0.11553e+1	-0.15000e+1	-0.13210e+1
a_8	0.12666	0.27684e+1	0.28398e+1	0.25877e+1	0.32154e+1
a_9	0.22003e+1	-0.49606	0.20994	-0.56877	-0.51692
a_{10}	-0.18160	-0.98244	-0.18352	-0.83773	-0.19092e+1
a_{11}	-0.11911e+1	0.63489	-0.18616	0.80162	0.64314
a_{12}	0.99835e-2	0.35397e-3	-0.81433	-0.50919e-2	0.44718
a_{13}	0.26826	-0.15105	0.20263e-1	-0.19075	-0.62935e-1
a_{14}	-0.73768	0.31140	0.34955	0.30950	0.40840

Mean daily surface water temperatures may be evaluated as follows. Let variable -jday- represent the Julian day for which surface water temperature is desired. Let variable -tw- represent the surface water temperature. Surface water temperature (°C) may then be determined from the following FORTRAN 77 code.

```
*
*       scale -jday- to interval [-1, +1]
*
      daynot = (2*jday - x_l - x_u)/(x_u - x_l)
*
      tw = a(0) + a(1)*daynot
      pm2 = 1.0
      pm1 = daynot
      do 1 j = 2,14
        n = j - 1
        p = ((n + n - 1)*daynot*pm1 - n*pm2)/(n + 1)
        tw = tw + a(j)*p
        pm2 = pm1
        pm1 = p
    1 continue
```

APPENDIX H - Ice Concentration Data

TABLE H.1 - Maximum, Mean, and Minimum Cumulative Freezing Degree Days (Σf_D) and Corresponding Ice Concentration (I) for Selected Days of the Winter Season (D_o) for Lake Ontario.

Date	D_o	I_{min} (%)	I_n (%)	I_{max} (%)	$(\Sigma f_D)_{min}$ °C	$(\Sigma f_D)_n$ °C	$(\Sigma f_D)_{max}$ °C
1 Nov	1	0.0	0.0	0.0	0.0	0.5	1
15 Nov	15	0.2	0.5	1.0	1	1	3
1 Dec	31	0.4	1.0	3.0	2	8	44
15 Dec	45	0.8	2.0	17.0	22	42	130
1 Jan	62	1.0	8.0	28	44	102	217
15 Jan	76	0.0	7.0	52.0	48	172	356
1 Feb	93	5.0	19.0	84.0	65	262	517
15 Feb	107	5.0	24.0	91.0	91	350	644
1 Mar	121	2.0	10.0	51.0	117	407	739
15 Mar	135	0.8	6.0	28.0	135	432	783
1 Apr	152	0.4	2.0	18.0	96	408	739
15 Apr	166	0.2	0.5	1.0	46	341	687
30 Apr	181	0.0	0.0	0.0	0	231	596

TABLE H.2 - Maximum, Mean, Minimum Cumulative Freezing Degree Days (Σf_D) and Corresponding Ice Concentrations (I) for Selected Days of the Winter Season (D_o) for Lake Erie.

Date	D_o	I_{min} (%)	I_n (%)	I_{max} (%)	$(\Sigma f_D)_{min}$ °C	$(\Sigma f_D)_n$ °C	$(\Sigma f_D)_{max}$ °C
1 Nov	1	0.0	0.0	0.0	0	0	0
15 Nov	15	1.0	1.0	1.0	1	2	3
1 Dec	31	0.2	2.0	3.0	2	6	44
15 Dec	45	0.4	9.0	64.0	3	30	91
1 Jan	62	0.6	36.0	100.0	22	73	200
15 Jan	76	0.8	65.0	100.0	9	122	309
1 Feb	93	1.0	90.0	100.0	44	185	478
15 Feb	107	2.0	90.0	100.0	48	249	593
1 Mar	121	1.0	64.0	99.0	52	286	630
15 Mar	135	0.8	26.0	94.0	56	287	604
1 Apr	152	0.4	10.0	84.0	22	244	534
15 Apr	166	0.2	3.0	17.0	1	175	500
30 Apr	181	0.0	0.0	0.0	0	88	326

APPENDIX I - Minor Energy Balance Terms

TABLE I.1 - Average Daily Values of Minor Energy Balance Terms Q_M for Lake Ontario and Lake Erie (MJ m^{-2} day^{-1}).

Month	Lake Ontario	Lake Erie
January	0.40	0.38
February	0.40	0.29
March	0.40	0.13
April	-0.19	0.38
May	-0.19	-0.46
June	-0.19	-0.13
July	-0.19	0.13
August	-0.19	0.25
September	-0.19	0.25
October	0.40	0.46
November	0.40	0.46
December	0.40	0.46

REFERENCES

Abramowitz, M. and I. A. Stegun, 1972: *Handbook of Mathematical Functions*, Dover, New York, 1046 pp.

Almazan, J.A., 1980: Surface Wind, Ch. 2 of *IFYGL Atlas - Lake Ontario Summary Data*, C.F. Jenkins (editor). Published by National Oceanic and Atmospheric Admisnistration, Great Lakes Environmental Research Laboratory, U.S. Department of Commerce, Ann Arbor, Michigan, 48104, pp.26 - 67.

Almazan, J.A., and R.L. Pickett, 1980: Water Temperature, Ch. 11 of *IFYGL - Lake Ontario Summary Data*, C.F. Jenkins (editor). Published by National Oceanic and Atmospheric Administration, Great Lakes Environmental Research Laboratory, U.S. Department of Commerce, Ann Arbor, Michigan, 48104, pp.200- 244.

Angstrom, A., 1924: Solar and Terrestrial Radiation, *Quart. J. Roy. Meteorol. Soc.*, **50**, 121-126.

Angstrom, A., 1956: On Computation of Global Radiation from the Records of Sunshine, *Archiv. Geophys.*, **3**, 555-556.

Atwater, M.A., and J.T. Ball, 1974: Cloud Cover and the Radiation Budget, Volume I (CEM Report Number 4130-513a), IFYGL Contract No. 2-35353, The Center for the Environment and Man, Inc., Hartford, Connecticut, 06120, 111 pages.

Assel, R.A., F.H. Quinn, G.A. Leshkevich, and S.J. Bolsenga, 1983: *Great Lakes Ice Atlas*, published by the Great Lakes Environmental Research Laboratory, Ann Arbor, Michigan, 48104, 115 pages.

Bergstrom, R.W., and R. Viskanta, 1972: *Theoretical Study of the Thermal Structure and Dispersion and Dispersion in Polluted Urban Atmospheres*, School of Mechanical Engineering Report, Purdue University, West Lafayette, Indiana, 187 pages.

Boyce, F.M., W.J. Moody, and B.L. Killins, 1977: *Heat Content of Lake Ontario and Estimates of Average Surface Heat Fluxes during IFYGL*, , Technical Bulletin No. 101, Inland Waters Directorate, Canada Centre for Inland Waters, Burlington, Ontario, 120 pages.

Braslau, N. and J. V. Dave, 1972: *Effects of Aerosols on the Transfer of Solar Energy through Realistic Model Atmospheres. Part 1: Non-Absorbing Aerosols*, Report RC4114, IBM Technical Journal, Watson Research Center, Yorkton Heights, New York, U.S.A.

Brunt, D., 1932: Notes on Radiation in the Atmosphere, *Quart. J. Roy. Meteorol. Soc.*, **58**, 389-420.

Brutsaert, W., 1975: On a Derivable Formula for Longwave Radiation from Clear Skies, *Water Resour. Res.*, **11**, 742-744.

Chandrasekhar, S., 1950: *Radiative Transfer*, Dover Publications,Inc., (Dover Reprint, 1960), 393 pages.

Chou, M. D. and A. Arking, 1981: An Efficient Method for Computing the Absorption of Solar Radiation by Water Vapour, *J. Atmos. Sci.*, **40** , 116-138.

Dalrymple, G.J., and M.H. Unsworth, 1978: Longwave Radiation at the Ground: IV. Comparison of Measurement and Calculation of Radiation from Cloudless Skies, *Quart. J. R. Met. Soc.*, **104**, 989-997.

Davies, J.A., 1965: Estimation of Insolation for West Africa, *Quart. J. Roy. Meteorol. Soc.*, **91**, 359-363.

Davies, J.A., P.J. Robinson and M. Nunez, 1971: Field Determinations of Surface Emissivity and Temperature for Lake Ontario, *J. Appl. Meteorol.*, **10**, 811-819.

Davies, J.A. and W.M. Schertzer, 1974: *Canadian Radiation Measurements and Surface Radiation Balance Estimates for Lake Ontario during IFYGL*, Department of Geography, McMaster University, Hamilton, Ontario, 77 p.

Davies, J.A., 1980: *Models for Estimating Incoming Solar Irradiance*, Report prepared for Atmospheric Environment Canada under Department of Supply and Services (Canada) Contract No. OSU79-00163, Department of Geography, McMaster University, Hamilton, Ontario, 100 pages.

Derecki, J. A., 1975: *Evaporation from Lake Erie*, NOAA Technical Report ERL 342-GLERL 3, U.S. Department of Commerce, National Oceanic and Atmospheric Administration, Environmental Research Laboratories, Boulder, Colorado, 84 pp.

Driedger, H.L., and A.J.W. Catchpole, 1970: Estimation of Solar Radiation Receipt from Sunshine Duration at Winnipeg, *Meteorol. Mag.*, **99**, 285-291.

Elder, F.C., F.M. Boyce and J.A. Davies, 1974: Preliminary Energy Budget of Lake Ontario for the Period May through November, 1972 (IFYGL), *Proceedings of the 17th Conference on Great Lakes Research*, 1974, pp.713-724.

Fouquart, Y. and B. Bonnel, 1980: Computations of Solar Heating in the Earth's Atmosphere - A New Parameterization, *Cont. Atmos. Phys.*, **53**, 35-62.

Hansen, J.E., 1969: Exact and Approximate Solutions for Multiple Scattering in Cloudy and Hazy Atmospheres, *J. Atmos. Sci.*, **26**, 478-487.

Hansen, J.E. and L.D.Travis, 1974: Light Scattering in Planetary Atmospheres, *Space Sci. Rev.*, **16**, 527-610.

Harbeck, G.E., Jr., 1962: A Practical Field Technique for Measuring Reservoir Evaporation Utilizing Mass Transfer Theory, *U.S. Geol. Surv. Profess. Paper 272-E.*

Henderson-Sellers, B. 1986: Calculating the Surface Energy Balance for Lake and Reservoir Modeling: A Review, *Rev. Geophys.*, **24**, 625-649.

Holland, J.Z., W. Chen, J.A. Almazan, and F.C. Elder, 1981: Atmospheric Boundary Layer, in *IFYGL - The International Field Year for the Great Lakes*, edited by E.J. Aubert and T.L. Richards, National Oceanic and Atmospheric Administration, Great Lakes Research Laboratory, U.S. Department of Commerce, Ann Arbor, Michigan, 48104, pp. 109-168.

Houghton, J.T., 1986: *The Physics of Atmospheres*, second edition, Cambridge University Press, Cambridge, 271 pp.

Hunt, G.E., 1973: Radiative Properties of Terrestrial Clouds at Visible and Infrared Thermal Window Wavelengths, *Quart. J. R. Met. Soc.*, **99**, 346-369.

Idso, S.B., 1981: A Set of Equations for Full Spectrum and 8-14 μm and 10.5-12.5 μm Thermal Radiation from Cloudless Skies, *Water Resour. Res.*, **17**, 295-304.

Idso, S.B., and R.D. Jackson, 1969: Thermal Radiation from the Atmosphere, *J. Geophys. Res.*, **74**, 5397-5403.

Issacson, and H.B. Keller, 1966: *Analysis of Numerical Methods*, John Wiley and Sons, New York, 541 pp.

Joseph, J. H., W. J. Wiscombe and J. A. Weinman, 1976: The Delta-Eddington Approximation for Radiative Flux Transfer, *J. Atmos. Sci.*, **33**, 2452-2459.

Kimura, K., and D.G. Stephenson, 1969: *Solar Radiation on Cloudy Days*, Research Paper No. 418, Division of Building Research, National Research Council of Canada, Ottawa, 8 pages.

Kondrat'yev, K. Ya., 1965: *Radiative Heat Exchange in the Atmosphere*, Pergamon Press, Oxford, 411 pages.

Labs, D. and H. Neckel, 1968: The Radiation of the Solar Photosphere from 2000 A to 100 μm, *Z. Astrophys.*, **69**, 1-73.

Laevastu, T., 1960: Factors Affecting the Temperature of the Surface Layers of the Sea, *Societas Scientiarum Fennica, Commentationes Physico-Mathematicae*, **25**, 136 pages.

Lam, D.C.L., W.M. Schertzer, and A.S. Fraser, 1983: *Simulation of Lake Erie Water Quality Responses to Loading and Weather Variations*, National Water Research Institute, Inland Waters Directorate, Canada Centre for Inland Waters, Burlington, Ontario, Scientific Series Number 134, 310 pp.

Latimer, J.R., 1971: *Radiation Measurement*, International Field Year for the Great Lakes, Technical Manual Series No. 2 (reprint 1978), published by The Secretariat, Canadian National Committee for the International Hydrological Decade, No. 8 Building, Carling Ave., Ottawa, Ontario.

Leighton, H. G., 1978: *A Parameterized Model for the Interaction of Solar Radiation with the Atmosphere Including Aerosol*, Final Report (Contract OSU77-00063), Atmospheric Environment Service, Downsview, Canada.

Lemire,F., 1961: *Winds on the Great Lakes*, CIR-3560,TEC-380, Can. Dept. of Transport, Metropolitan Branch.

Lenoble, J.(ed.), 1977: *Standard Procedures to Compute Atmospheric Radiative Transfer in a Scattering Atmosphere*. Vol. 1, International Association of Meteorology and Atmospheric Physics (IAMAP), Radiation Commission, National Center for Atmospheric Research, Boulder, Colorado, U.S.A.

Liou, K. N., 1973: A Numerical Experiment of Chandrasekhar's Discrete Ordinate Method for Radiative Transfer. Application to Hazy and Cloudy Atmospheres, *J. Atmos. Sci.*, **30**, 1303-1326.

Liou, K.N., 1980: *An Introduction to Atmospheric Radiation*, Academic Press, New York, 392 pp.

Mateer, C.L., 1955: A Preliminary Estimate of the Average Insolation in Canada, *Canad. J. Agric. Sci.*, **35**, 579-594.

Matveev, L.T., 1965, *Fundamentals of General Meteorology: Physics of the Atmosphere*. Published by Gidrometeorologichesko Izdatel'stvo, Leningrad. Translation by Isreal Program for Scientific Translations, 1967, IPST Cat. No. 1993, 699 pp.

Matveev, L.T., 1984, Cloud Dynamics, D. Reidel Publishing Co., Dordrecht, 340 pp.

McClatchey, R. et.al., 1972: *Optical Properties of the Atmosphere*, Third Edition, AFCRL-72-0497, Air Force Cambridge Research Laboratories, Hanscombe, Mass., U.S.A., 107 pp.

Millar, F.G., 1952: Surface Water Temperatures on the Great Lakes, *J. Fish. Res. Board of Canada*, **9**, p329-376.

McIntosh, D.H. and A.S. Thom, *Essentials of Meteorology*, Wykeham Publications (London) Ltd., 1969, 239 pages.

Monteith, J.L., 1973: *Principles of Environmental Physics*, Edward Arnold Limited (publishers), 241 pages.

Neiburger, M., 1949: Reflection, Absorption, and Transmission of Insolation by Stratus Clouds, *J. Meteor.*, **6**, 98-104.

Paltridge, G.W. and C.M.R. Platt, 1976: *Radiative Processes in Meteorology and Climatology*, Elsevier, New York, 318 pp.

Phillips, D.W., 1978: Evaluation of Evaporation from Lake Ontario during IFYGL by a

Modified Mass Transfer Equation, *Water Resour. Res,* **(2)**, 197-205.

Phillips, D.W., and G.J. Irbe, 1976: *A Comparison of Mass Transfer Estimates of Evaporation from Lake Ontario during IFYGL,* Technical Memoranda (TEC 838), Environment Canada, 4905 Dufferin St, Downsview, Ont., 27 pp.

Phillips, D.W., and Irbe, 1978: *Lake to Land Comparison of Wind, Temperature, and Humidity on Lake Ontario during the International Field Year for the Great Lakes (IFYGL),* CLI-2-77, Atmospheric Environment Service, Downsview, Ontario, Canada, 51 pp.

Phillips, D.W., and Almazan, J., 1983: Meteorological Analyses, Ch.1 of: *IFYGL - The International Field Year for the Great Lake,* ed. by E.J.Aubert and T.L.Richards, NOAA Great Lakes Environmental Research Laboratory, Ann Arbor, Michigan, 1981.

Pinsak, A.P., and G.K. Rodgers, 1981: Energy Balance, Ch. 6 of *IFYGL - The International Field Year for the Great Lakes,* edited by E.J. Aubert and T.L. Richards. Published by the National Oceanic and Atmospheric Administration, Great Lakes Environmental Research Laboratory, U.S. Department of Commerce, Ann Arbor, Michigan, 48104, pp. 169-198.

Powers, C.F., D.L.Jones and J.C.Ayers, 1959: *Sources of Hydrographic and Meteorological Data on the Great Lakes,* Great Lakes Research Division Special Report 8, 183 pp. University of Michigan, Ann Arbor.

Pruppacher, H.R., and J.D. Klett, 1980: *Microphysics of Clouds and Precipitation,* D. Reidel Publishing Company, Dordrecht, 714 pages.

Quinn, F.H., 1978: An Improved Aerodynamic Evaporation Technique for Large Lakes with Application to the IFYGL, *Water Resour. Res.,* **15(4)**, 935-940.

Quinn, F.H., and G. den Hartog, 1981: Evaporation Synthesis, Ch.7 of *IFYGL - The International Field Year for the Great Lakes,* ed. E.J. Aubert and T.L.Richards, NOAA Great Lakes Environmental Research Laboratory, Ann Arbor, Michigan, 1981,pp. 241-246.

Ramage, C.S., 1987: Necessary and Sufficient Conditions and El Nino, in: *Toward Understanding Climate Change,* The J.O. Fletcher Lectures on Problems and Prospects of Climate Analysis and Forecasting, edited by Uwe Radok, Westview Press, Boulder, 200 pp.

Raschke, E., 1978: *Terminology and Units of Radiation Quantities and Measurements,* Radiation Commission, International Association of Meteorology and Atmospherics (IAMAP), Published at the National Center for Atmospheric Research, Boulder, Colorado, U.S.A., 80307, 17 pp.

Richards, T.L., and J.P.Fortin, 1962: *An Evaluation of the Lake-Land Vapour Pressure Relationship for the Great Lakes,* Publ.**9**, Great Lakes Res. Div., University of Michigan, pp.103-110.

Richards, T.L., H.Dragert, and D.R.McIntyre, 1966: Influence of Atmospheric Stability and Overwater Fetch on Winds over the Lower Great Lakes, *Mon. Weather Rev.,* **94**, 448-453.

Richards, T.L., and J.G. Irbe, 1969: Estimates of Monthly Evaporation Losses from the Great Lakes 1950 to 1968 Based on the Mass Transfer Technique, *Proceedings of the Conference on Great Lakes Research,* **12**, p.469.

Rouse, W.R., D. Noad, and J. McCutcheon, 1973: Radiation, Temperature, and Atmospheric Emissivities in a Polluted Urban Atmosphere at Hamilton, Ontario, *J. Appl. Met.,* **12**, 798-807.

Satterlund, D.R., 1979: An Improved Equation for Estimating Longwave Radiation from the Atmosphere, *Water Resour. Res.,* **15**, 1649-1650.

Sawchuk, A.M., 1983: *Development and Application of the Delta–D_M Method for Computing Shortwave Radiative Fluxes in a Vertically Inhomogeneous Atmosphere*, Ph.D. Thesis, McMaster University, Hamilton, Ontario, 138 pages.

Schaller, E., 1979: A Delta-Two Stream Approximation in Radiative Flux Calculations, *Cont. Atmos. Phys.*, **52**, 17-26.

Schertzer, W.M., and Sawchuk, A.M., 1985: *Summary of Water Surface Temperature Observations for Lake Ontario (1966-1984) and Lake Erie (1967- 1982)*, NWRI Contribution Number 85-159, Canada Centre for Inland Waters, Burlington, Ont., Canada, 49 pp.

Schertzer, W.M., 1987: Heat Balance and Heat Storage Estimates for Lake Erie , *J. Great Lakes Res.*, **13(4)**, 454-467.

Schmetz, J.E., E. Raschke and H. Fimpel, 1981: Solar and Thermal Radiation in Maritime Stratocumulus Clouds, *Cont. Atmos. Phys.*, **54**, 442-452.

Selby, J.E.A., and R.A. McClatchey, 1975: *Atmospheric Transmittance from 0.25 to 28.5 μm: Computer Code LOWTRAN 4*, Report AFCRL-TR-75-0255, Air Force Cambridge Laboratories, Hanscombe, Mass., U.S.A.

Shettle, E.P. and R.W. Fenn, 1979: *Models for the Aerosols of the Lower Atmosphere and the Effects of Humidity Variations on their Optical Properties*, Air Force Geophysics Laboratory, Hanscombe, Mass., U.S.A.

Slingo, A., and H.M. Schrecker, 1981: On the Shortwave Radiative Properties of Stratiform Water Clouds, *Quart. J. Roy. Met. Soc.*, **108**, 407-426.

Slingo, A., S. Nicholls and J. Schmetz, 1982: Aircraft Observations of Marine Stratocumulus during JASIN, *Quart. J. Roy. Met. Soc.*, **109**, 833-856.

Spencer, J.W., 1971: Fourier Series Representations of the Position of the Sun, *Search*, **2**, 172.

Stephens, G.L., 1978a: Radiation Profiles in Extended Water Clouds, Part I: Theory, *J. Atmos. Sci.*, **35**, 2111-2122.

Stephens, G.L., 1978b: Radiation Profiles in Extended Water Clouds, Part II: Parameterization Schemes, *J. Atmos. Sci.*, **35**, 2123-2132.

Swinbank, W.C., 1963: Longwave Radiation from Clear Skies, *Quart. J. Roy. Meteorol. Soc.*, **89**, 339-348.

Timanovskaya, R.G., and Ye. M. Feygel'son, 1972: Some Parameters of Cumulus Clouds Observed by Photographs of the Sky and from Ground Actinometric Measurements, in *Heat Transfer in the Atmosphere*, edited by Ye. M. Feygel'son and L.R.Tsvang. Published by "Nauka" Press, Moscow, 1972. NASA Technical Transl Technical Translation (TT F-790), National Technical Information Service, Springfield, Virginia, U.S.A., 22151, pp. 138-145.

Welch, R., and Zdunkowski, W., 1976: A Radiative Model of the Polluted Atmospheric Boundary Layer, *J. Atmos. Sci.*, **33**, 2170-2184.

Willmott, C.J., 1981: On the Validation of Models, *Phys. Geog.*, **2**.

Wiscombe, W.J., 1977a: *The Delta-Eddington Approximation for a Vertically Inhomogeneous Atmosphere*, Technical Note NCAR/TN-121, National Center for Atmospheric Research, Boulder, Colorado, U.S.A., 66 pp.

Wiscombe, W.J., 1977b: The Delta-M Method: Rapid Yet Accurate Radiative Flux Calculations for Strongly Asymmetric Phase Functions, *J. Atmos. Sci.*, **34**, 1408-1422.

Yu, S.L., and W. Brutsaert, 1969: Generation of an Evaporation Time Series for Lake Ontario, *Water Resour. Res.*, **5(4)**, 785-796.